Inference and Characterization of Planar Trajectories

Zhanglong Cao

a thesis submitted for the degree of

Doctor of Philosophy

at the University of Otago, Dunedin,

New Zealand.

All knowledge is, in the final analysis, history.
All sciences are, in the abstract, mathematics.
All judgments are, in their rationale, statistics.
– C. Radhakrishna Rao.

Abstract

Inference and characterization of planar trajectories have long been the focus of scientific and commercial research. Efficient algorithms for both precise and efficient trajectory reconstruction remain in high demand in a wide variety of applications.

Given time series GPS data of a moving object, trajectory reconstruction is the process of inferring the path between successive observation points. However, widely separated points and measurement errors can give rise to trajectories with sharp angles, which are not typical of a moving object. Smoothing spline methods can efficiently build up a more smooth trajectory. In conventional smoothing splines, the objective function is augmented with a penalty term, which has a single parameter that controls the smoothness of reconstruction. Adaptive smoothing splines extend the single parameter to a function that can vary, hence the degree of smoothness can be different regions. A new method named the V-spline is proposed, which incorporates both location and velocity information but penalizes excessive accelerations. In the application of interest, the penalty term is also dependent on a known operational state of the object. The V-spline includes a parameter that controls the degree to which the velocity information is used in the reconstruction. In addition, the smoothing penalty adapts the observations are irregular in time. An extended cross-validation technique is used to find all spline parameters.

It is known that a smoothing spline can be thought of as the posterior mean of a Gaussian process regression in a certain limit. By constructing a reproducing kernel Hilbert space with an appropriate inner product, the Bayesian form of the V-spline is derived when the penalty term is a fixed

constant instead of a function. An extension to the usual generalized cross-validation formula is utilized to find the optimal V-spline parameters.

In on-line trajectory reconstruction, smoothing methods give way to filtering methods. In most algorithms for combined state and parameter estimation in state-space models either estimate the states and parameters by incorporating the parameters in the state-space, or marginalize out the parameters through sufficient statistics. Instead of these approaches, an adaptive Markov chain Monte Carlo algorithm is proposed. In the case of a linear state-space model and starting with a joint distribution over states, observations, and parameters, an MCMC sampler is implemented with two phases. In the learning phase, a self-tuning sampler is used to learn the parameter mean and covariance structure. In the estimation phase, the parameter mean and covariance structure informs the proposed mechanism and is also used in a delayed-acceptance algorithm, which greatly improves sampling efficiency. Information on the resulting state of the system is indicated by a Gaussian mixture. In the on-line mode, the algorithm is adaptive and uses a sliding window approach by cutting off historical data to accelerate sampling speed and to maintain applicable acceptance rates. This algorithm is applied to the joint state and parameters estimation in the case of irregularly sampled GPS time series data.

Acknowledgements

First of all, I am so grateful to my primary supervisor Dr. Matthew Parry for offering me this opportunity to take part in the collaborative project with the Physics department, and to work with him and other talented researchers. His extensive knowledge of statistics and physics leads me in the right way and encourages me throughout this difficult project. His passionate at exploring the unknown world of science motivated me and will motivate me to go further and deeper in the area of developing and implementing statistical models.

Secondly, I would like to appreciate my co-supervisor Professor David Bryant for his great help in my research progress and careful reading of the manuscript. He offered me extraordinary supports during the time when Matthew was overseas. His guidance and expert advice inspire me and lit my way in finding a different method.

A special gratitude goes out to the Ministry of Business, Innovation and Employment for supporting my research. This project would have been impossible without their generous fundings. Additionally, many thanks to TracMap company for providing GPS data set, which is the base stone of all the work.

Moreover, I want to thank all the support staff at Mathematics and Statistics Department for their great job, including Lenette, Marguerite, Leanne, Chris and Greg, and give many thanks to my office mates and friends, including but not limited to Paula, Chuen Yan, Johannes, Vivian, Juan, Bob and his family, Freddy and his family, for their friendship and accompanying me is the last three years. We had enjoyable and unforgettable experiences together.

Finally, last but by no means least, I will thank my parents for their wise counsel and encouragements to me for studying overseas, and my beloved wife Yingying for all her love and support, and my daughter Anyang, who was born in my second year of study. Being her father is the greatest accomplishment of my life.

Thanks for all your encouragements!

Contents

List of Tables

List of Figures

Chapter 1

Introduction

1.1 Background

The *Global Positioning System* (abbreviated as GPS) is a space-based navigation system consisting of a network of 24 satellites placed in space in six different 12-hour orbital paths (Agrawal and Zeng, 2015), so that at least five of them are in view from every point on the globe (Kaplan and Hegarty, 2005; Bajaj *et al.*, 2002). A GPS device receives signals from these satellites and triangulates its location in terms of longitude, latitude, and elevation. GPS is the most widely known location-sensing system providing an excellent framework for determining geographic positions (Hightower and Borriello, 2001). Offered free of charge and accessible worldwide, GPS has a vast number of applications, including aircraft tracking, vehicle navigation, robot localization, surveying, astronomy, and so on.

GPS units in vehicles typically record position, speed, and direction of travel. With this information, a target tracking system becomes available and useful. Such a tracking system can be used to reduce costs by knowing in real-time the current location of a vehicle, such as a truck or a bus (Chadil *et al.*, 2008), with applications to Intelligent Transportation Systems (ITS) (McDonald, 2006). It can also be used to measure real-time traffic data and to identify congestion areas. In farming applications, a tracking system allows the location and operational status of farm vehicles to be monitored remotely.

Given time series data from a vehicle-mounted GPS unit, an important question is how to infer the trajectory of the vehicle. This is known as trajectory reconstruction and is the motivating question of this thesis.

1.2 The Problem

Two keys issues for reconstruction are (i) how to handle observations that are inherently noisy measurements of the truth, and (ii) how to interpolate appropriately between observation times.

GPS units in vehicles provide y_t, noisy measurements of the actual position x_t, and v_t, noisy measurements of the actual velocity u_t, for a sequence of times $t \in T$. These data may also be augmented with information on operating characteristics of the vehicle, b_t. The trajectory reconstruction problem is the problem of estimating x_s, for an arbitrary time s, given a subset of the observations $\{y_t, v_t, b_t \mid t \in T\}$. Note that in this definition of trajectory reconstruction, we are not explicitly interested in estimating u_s.

The *TracMap* company, located in New Zealand and USA, produces GPS display units to aid precision farming in agriculture, horticulture and viticulture. Operational data is collected and sent by these units to a remote server for further analysis. An example of position data, which has been subsampled at irregular time points, is given in Figure 1.1.

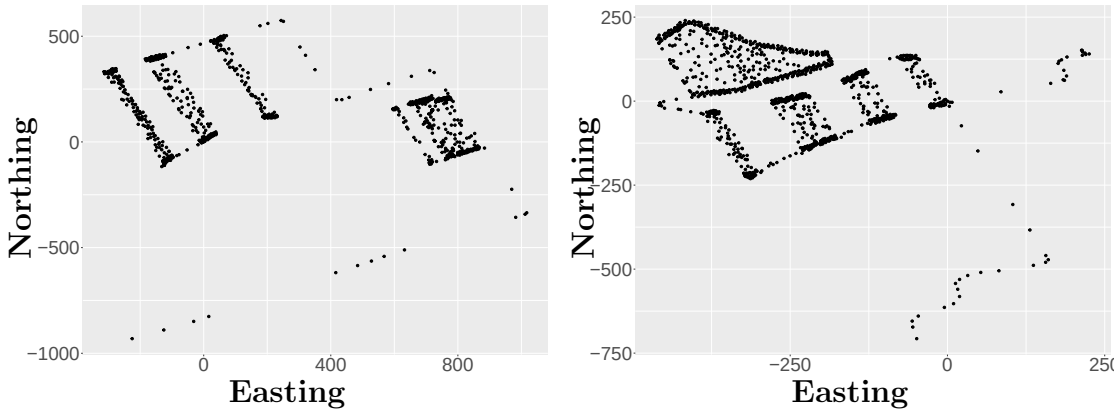

Figure 1.1: Examples of GPS data. Observed positions y_t are shown. In trajectory reconstruction, the y_t are combined with velocity information v_t and operating characteristics b_t to infer actual positions x_s, for times of interest s.

1.3 Smoothing Spline Based Reconstruction

Smoothing spline approaches are natural solutions to trajectory reconstruction, see e.g. Eubank (2004) and Durbin and Koopman (2012) for details.

Some form of interpolation is an obvious approach to trajectory reconstruction. The simplest method, piecewise linear interpolation, connects successive locations by straight lines. Clearly, this interpolation implies abrupt changes in velocity at the join points. Smooth trajectories are more common in real life applications. A single polynomial function that is defined on the entire interval, such as Bézier curve, is not as flexible as a piecewise combination of polynomials, each of which is defined on a subinterval. The polynomials are joined at the endpoints of their subintervals – these endpoints are termed *knots*. This kind of piecewise polynomial interpolation is called a *spline*.

A number of splines are commonly in use, see Chapter 5 of Hastie *et al.* (2009) for discussions. The B-spline, short for basis spline, gives a closed-form expression for the trajectory with continuous second derivatives and goes through the points smoothly while ignoring outliers (Komoriya and Tanie, 1989; Ben-Arieh *et al.*, 2004). It is flexible and has minimal support with respect to a given degree, smoothness, and domain partition. Once the knots are given, it is easy to compute the B-spline recursively for any desired degree of the polynomial (De Boor *et al.*, 1978; Cox, 1982). An attractive feature of the B-spline is its flexibility for univariate regression and its appealing simplicity of the method is explained in (Dierckx, 1995; Eilers and Marx, 1996). Gasparetto and Zanotto (2007) use a fifth-order B-spline to compose the overall trajectory. Almost every spline can be represented as a B-spline.

Another widely used spline is the piecewise cubic spline, which is continuous on an interval $[a, b]$ and has continuous first and second derivatives (Wolberg, 1988). Let $f(t)$ denote a trajectory reconstruction, i.e. the location of the vehicle at time t. For the piecewise cubic spline,

$$f(t) = d_j(t - t_j)^3 + c_j(t - t_j)^2 + b_j(t - t_j) + a_j, \tag{1.1}$$

on the subinterval $[t_j, t_{j+1})$ with given coefficients d_j, c_j, b_j and a_j, $j = 1, 2, \ldots, K$. The coefficients are chose in such a way that f and its first and second derivatives are continuous at each knot t_j. If the second derivative of f is zero at a and b, f is said to be a *natural cubic spline* and these conditions are called the *natural boundary conditions* (Green and Silverman, 1993).

Given observations (t_i, y_i), $i = 1, \ldots, n$ $(n \geq K)$, one can use regression methods to estimate $f(t)$. Specifically, let $y_i = f(t_i) + \varepsilon_i$ with random errors $\{\varepsilon_i\}_{i=1}^n \sim N(0, \sigma^2)$. In the case of the natural cubic spline, where $f \in C^{(2)}[a, b]$, this leads to a standard linear parametric model (Kim and Gu, 2004).

However, a parametric approach only captures features contained in the preconceived class of functions and increases model bias (Yao *et al.*, 2005). To improve the performances, nonparametric methods have been developed. Rather than giving specified parameters, it is desired to reconstruct f from the data $y(t_i) \equiv y_i$ itself (Craven and Wahba, 1978). The estimates of polynomial smoothing splines appear as a solution to the following minimization problem: find $\hat{f} \in C^{(m)}[a, b]$ that minimizes the penalized residual sum of squares:

$$\text{RSS} = \sum_{i=1}^{n} (y_i - f(t_i))^2 + \lambda \int_a^b \left(f^{(m)}\right)^2 dt, \tag{1.2}$$

for a pre-specified value $\lambda(> 0)$ (Aydin and Tuzemen, 2012). In the above equation, the first term is the residual sum squares controlling the lack of fit. The second term is the roughness penalty weighted by a smoothing parameter λ, which varies from 0 to $+\infty$ and establishes a trade-off between interpolation and a straight line fit in the following way:

$$\begin{cases} \lambda = 0 & f \text{ can be any function that interpolates the data} \\ \lambda = +\infty & \text{the simple least squares line fit since no second derivative can be tolerated} \end{cases}$$

(Hastie *et al.*, 2009).

Hence, the cost of the equation (1.2) is determined not only by its goodness-of-fit to the data quantified by the residual sum of squares but also by its roughness (Schwarz, 2012). The motivation of the roughness penalty term is from a formalization of a mechanical device: if a thin piece of flexible wood, called a spline, is bent to the shape of the curve g, then the leading term in the strain energy is proportional to $\int f''^2$ (Green and Silverman, 1993).

1.4 Parameter Selection

As discussed in the previous section, the determination of an optimal smoothing parameter λ in the interval $(0, +\infty)$ was found to be an underlying complication and the fundamental idea of nonparametric smoothing is to let the data choose the amount of smoothness, which consequently decides the model complexity (Gu, 1998). Various studies for selecting an appropriate smoothing parameter are developed and compared in literatures. Most of these methods are focusing on data driven criteria, such as cross-validation (CV), generalized cross-validation (GCV) (Craven and Wahba, 1978)

and generalized maximum likelihood (GML) (Wahba, 1985) and recently developed methods, such as improved Akaike information criterion (AIC) (Hurvich *et al.*, 1998), exact risk approaches (Wand and Gutierrez, 1997) and so on. See e.g. Craven and Wahba (1978); Härdle *et al.* (1988); Härdle (1990); Wahba (1990); Green and Silverman (1993); Cantoni and Ronchetti (2001); Aydın *et al.* (2013) for details.

A classical parameter selection method is *cross-validation* (CV). The idea behind this method can be traced back to 1930s (Larson, 1931). Because in most applications, only a limited amount of data is available. Thus, an idea is to split this data set into two subgroups, one of which is used for training the model and the other one is used to evaluate its statistical performance. The sample used in evaluation is considered as "new data" as long as data is i.i.d. .

A single data split yields a validation estimate of the risk and averaging over several splits yields a cross-validation estimate (Arlot and Celisse, 2010). Because of the assumption that data are identically distributed, and training and validation samples are independent, CV methods are widely used in parameter selection and model evaluation.

For example, a k-fold CV splits the data into k roughly equal-sized parts. For the kth part, we fit the model to the other $k-1$ parts of the data, and calculate the prediction error of the fitted model when predicting the kth part of the data. A detailed procedure is given by Wahba and Wold (1975): suppose we have n paired data $(t_1, y_1), \ldots, (t_n, y_n)$. Run a k-fold CV according to the following Algorithm 1.1. Mathematically, we denote the CV score as

$$\mathrm{CV}(\hat{f}, \lambda) = \frac{1}{n} \sum_{i}^{n} \left(y_i - \hat{f}^{-k(i)}(t_i, \lambda) \right)^2, \tag{1.3}$$

where $\hat{f}^{(-k)}(t)$ denotes the fitted function computed with the k-th part of the data removed. Typical choices for k are 5 and 10 (Hastie *et al.*, 2009). The function $\mathrm{CV}(\hat{f}, \lambda)$ provides an estimate of the test error curve, and the tuning parameter λ that minimizes it will be the optimal solution.

A special case of k-fold CV is setting $k = n$, which is known as *leave-one-out cross-validation*. In this scenario, the CV function takes each of the data out and calculate the errors of $\hat{f}^{(-i)}$ from the remaining $n-1$ points. In fact, with the property that taking one point out does not affect the estimation, the fitting of a smoothing spline allows us to implement CV methods without hesitation.

As an improvement of CV, the GCV algorithm was proposed to calculate the trace of the estimation matrix $A(\lambda)$ instead of calculating individual elements for linear fitting under squared error loss, in which way it provides further computational savings.

Algorithm 1.1: k-fold Cross-Validation

1 Initialization: Remove the first data t_1 and last date t_n from the data set.
2 Split the rest data $t_2, \ldots, t_{n-1}$ into k groups by: for $i = 1, \ldots, k$, the ith Group $G_i = \{t_{i+1}, t_{i+1+k}, t_{i+1+2k}, \cdots\}$.
3 Guess a value λ^*.
4 **while** *CV score is not optimized* **do**
5 **for** $i = 1, \ldots, k$ **do**
6 Delete the ith group of data. Fit a smoothing spline to the first data (t_1, y_1), the rest $k-1$ groups of data set and the last data (t_n, y_n) with λ^*.
7 Compute the sum of squared deviations s_i of this smoothing spline from the deleted ith group data points.
8 **end**
9 Add the sums of squared deviations from steps 5 to 8 and divide it by k to achieve a cross-validation score of λ^*, that is $s = \frac{1}{k}\sum_{i=1}^{k} s_i$.
10 Vary λ systematically and repeat steps 5 to 9 until CV shows a minimum.
11 **end**

Suppose we have a solution $\hat{f} = A(\lambda)y$ with a given λ, for many linear fittings, the CV score is

$$\mathrm{CV} = \frac{1}{n}\sum_{i=1}^{n}\left(y_i - \hat{f}^{(-i)}(t_i)\right)^2 = \frac{1}{n}\sum_{i=1}^{n}\left(\frac{y_i - \hat{f}(t_i)}{1 - A_{ii}}\right)^2, \tag{1.4}$$

where A_{ii} is the ith diagonal element of $A(\lambda)$. Then, the GCV approximation score is

$$\mathrm{GCV} = \frac{1}{n}\sum_{i=1}^{n}\left(\frac{y_i - \hat{f}(t_i)}{1 - \mathrm{tr}(A)/n}\right)^2. \tag{1.5}$$

In smoothing problems, GCV can also alleviate the tendency of cross-validation to under-smooth (Hastie *et al.*, 2009).

Rather than λ being constant, a new challenge is posed that the smoothing parameter becomes a function $\lambda(t)$ and is varying in domains. The structure of this penalty function controls the complexity of each domain and the whole final model. Donoho *et al.* (1995) introduce adaptive splines and a method to calculate piecewise parameters and Liu and Guo (2010) give an improved formula for this method. They proposed an approximation to the penalty function with an indicator and extended the generalized likelihood to the adaptive smoothing spline. This will be another interesting research topic.

Overall, almost every technique found in the scientific literatures on the reconstruction and trajectory planning problem is based on the optimization of objective functions or parameter selections, such as the objective function (1.2) and cross-validation approaches (Gasparetto and Zanotto, 2007).

1.5 Bayesian Filtering

Smoothing spline algorithms have several advantages in inferring and characterizing planar trajectories, particularly in reconstruction. However, subject to the property that smoothing splines require the solution of a global problem that involves the entire set of points to be interpolated, it might not be suitable for on-line estimation or instant updating (Biagiotti and Melchiorri, 2013). It is the time to use Bayesian filtering to implement on-line/instant estimation and prediction.

The word *filtering* refers to the methods for estimating the state of a time-varying system, which is indirectly observed through noisy measurements. A Bayes filter is a general probabilistic approach to infer an unknown probability density function recursively over time using incoming measurements and a mathematical process model. The concept *optimal estimation* refers to some criteria that measure the optimality in specific sense (Anderson and Moore, 1979). For example, the mean of the posterior distribution $\hat{x}_t = \mathrm{E}[x_t \mid y_{1:t}]$ that minimizes the loss function $J_t = \mathrm{E}[x_t - \hat{x}_t]^2$, or least mean squared errors, maximum likelihood approximation and so on. See e.g. Chen (2003); Särkkä (2013) for discussions. Hence, an optimal *Bayesian filtering* uses the Bayesian way of formulating optimal filtering by meeting some statistical criteria.

It is no doubt that in a conventional target tracking system, the most common method is the standard Kalman filter, which is a recursive solution to the discrete data linear filtering problem.

Kalman Filter

In a discrete-time linear system, the optimal Bayesian solution coincides with the least squares solution. The successful optimal one was given by Kalman (1960), the famous *Kalman filter*. It is a set of mathematical equations that provides an efficient computational means to estimate the state of a process in a recursive way by minimizing the mean of the squared errors (Bishop and Welch, 2001).

The Kalman filter recursively updates the estimated state by computing from the previous estimation and a new observation. Without the need for storing the entire past

observed data, the Kalman filter computes more efficient than computing the estimate directly from the entire past observed data at each step of the filtering process (Haykin, 2001).

A detailed Kalman filter and its variants can be found in (Chen, 2003; Rhodes, 1971; Kailath, 1981; Sorenson, 1985). Tusell (2011) gives a review of some R packages, which are used to fit data with Kalman filter methods. Besides, it is also shown that the Kalman filter can be derived within a Bayesian framework and reduces to a maximum posterior probability (MAP) solution, and can be easily extended to ML solution (Haykin, 2001; Guzzi, 2016).

Consider the following model

$$\begin{array}{ccccccccccc} \cdots & \rightarrow & x_{t-1} & \rightarrow & x_t & \rightarrow & x_{t+1} & \rightarrow & \cdots & & \text{truth} \\ \cdots & & \downarrow & & \downarrow & & \downarrow & & \cdots & & \\ \cdots & & y_{t-1} & & y_t & & y_{t+1} & & \cdots & & \text{observation} \end{array} \tag{1.6}$$

in which $x_t = F(x_{t-1}) + \varepsilon_x$ is the true hidden state propagating through the transition matrix F and $y_t = G(x_t) + \varepsilon_y$ is the observation measured by the measurement matrix G of the system, where ε_x and ε_y can be viewed as white noise random sequences with unknown statistics in the discrete-time domain.

To estimate the filtering state x_t from $y_{1:t} = \{y_1, \ldots, y_t\}$, Bayesian wants to maximize the posterior $p(x_t \mid y_{1:t})$ by marginalizing out all the previous measurements. Given the joint distribution of $p(x_t, x_{t-1}, y_{1:t})$, Kalman filter supposes the expectation $\hat{x}_{t-1}$ and its variance S_{t-1} are known and passing through the system by $\hat{x}_t = F\hat{x}_{t-1}$ and $S_t = FS_{t-1}F^\top + Q_t$, here Q_t is the covariance of ε_x. Because of the log-likelihood function is written in such way: $\ln p(x_t \mid y_{1:t}) \propto -\frac{1}{2}(y_t - Gx_t)^\top R_t^{-1}(y_t - Gx_t) - \frac{1}{2}(x_t - \hat{x}_{t-1})^\top S_{t-1}^{-1}(x_t - \hat{x}_{t-1})$, and R_t is the covariance of ε_y. As a result, the solution is

$$\hat{x}_t = \left(G^\top R_t^{-1} G + S_{t-1}^{-1}\right)^{-1} \left(G^\top R_t^{-1} y_t + S_{t-1}^{-1}\hat{x}_{t-1}\right). \tag{1.7}$$

Additionally, by setting $S_t^{-1} = G^\top R_t^{-1} G + S_{t-1}^{-1}$, the recursive estimation of covariance matrix is $S_t = S_{t-1} - K_t G S_{t-1}$, and $K_t = S_{t-1}G^\top (R_t + GS_{t-1}G^\top)^{-1}$ is named Kalman gain matrix. Consequently, the recursive estimation is

$$\hat{x}_t = \hat{x}_{t-1} + K_t(y_t - G\hat{x}_{t-1}). \tag{1.8}$$

Further, compared with the filtering distribution $p(x_t \mid y_{1:t})$, the prediction distribution is trying to find an n-steps later distribution $p(x_{t+n} \mid y_{1:t})$ from the current state, and the smoothing distribution is to find the distribution $p(x_k \mid y_{1:t})$ of a specific state x_k in the past for any k, where $1 < k < t$.

However, Kalman filter has a limitation that it does not apply to general non-linear model and non-Gaussian distributions. For a non-linear system, one can use the extended Kalman filter (EKF), which is widely used for solving nonlinear state estimation applications (Gelb, 1974; Bar-Shalom and Li, 1996). The EKF uses Taylor expansion to construct linear approximations of nonlinear functions, therefore the state transition f and observation g do not have to be linear but to be differentiable. However, in the EKF process, these approximations can incur large errors in the true posterior mean and covariance of the transformed random variable (Wan and Van Der Merwe, 2000).

Alternatively, the unscented Kalman filter (UKF) is a derivative-free method (Wan and Van Der Merwe, 2000; György *et al.*, 2014). It uses the Kalman filter to create a normal distribution that approximates the result of a non-linear transformation numerically by seeing what happens to a few deliberately chosen points. The unscented transform is used to recursively estimate the equation (1.8), where the state random variable is re-defined as the concatenation of the original state and noise variables. By contrast, Kalman filter does not require numerical approximations.

The performances of EKF and UKF are compared in a few references regarding to different kinds of aspects, such as (Chandrasekar *et al.*, 2007; LaViola, 2003; St-Pierre and Gingras, 2004). There is not an overall conclusion that which one performs better.

Limited to its property, Kalman filter is tied up for a dynamic system, where the parameters and noise variances are unknown. In some dynamic systems, the variances are obtained based on the system identification algorithm, correlation method, and least squares fusion criterion. To solve this issue, a self-tuning weighted measurement fusion Kalman filter is proposed by Ran and Deng (2010). Likewise, a new adaptive Kalman filter will be another choice (Oussalah and De Schutter, 2001).

However, when the target maneuver occurs, Kalman filtering accuracy will be reduced or even diverged due to the model mismatch and noise characteristics that cannot be known exactly (Liu *et al.*, 2014). Additionally, Kalman filter based methods require the state vector contains pre-specified coefficients during the whole approximation procedure and are within the bounded definition range determined at the beginning (Jauch *et al.*, 2017).

A more generic algorithm is investigated in the following section.

Monte Carlo Filter

Monte Carlo filter is a class of Monte Carlo approaches (Chen, 2003). The power of these approaches is that they can numerically and efficiently handle integration and

optimization problems.

The important advantage of Monte Carlo is that a large number of posterior moments can be estimated at a reasonable computational effort and that estimates of the numerical accuracy of these results are obtained in a simple way (Kloek and Van Dijk, 1978). *Sequential Monte Carlo* method uses Monte Carlo approaches to estimate and to compute recursively. One of the attractive merits is in the fact that they allow on-line estimation by combining the powerful Monte Carlo sampling methods with Bayesian inference at an expense of reasonable computational cost (Chen, 2003).

For example, consider the model (1.6) with parameter θ. The likelihood approximation is $p(y_t \mid y_{1:t-1}, \theta)$ and can be written by

$$p(y_t \mid y_{1:t-1}, \theta) = \int p(y_t \mid x_t, \theta) p(x_t \mid y_{1:t-1}, \theta) dx_t = \mathrm{E}[y_t \mid x_t, \theta]. \tag{1.9}$$

The standard Monte Carlo algorithm is trying to compute the integration by drawing N independent samples $x_t^{(i)}$ from $p(x_t \mid y_{1:t-1}, \theta)$ first and then, by adding them up, to approximate the integration for large N in the following way

$$\mathrm{E}\left[y_t \mid x_t, \theta\right] \approx \frac{1}{N} \sum_i p(y_t \mid x_t^{(i)}, \theta), \tag{1.10}$$

(Kalos and Whitlock, 2008).

In terms of getting good samples of $x_t^{(i)}$, which can be used for representing $p(y_t \mid x_t^{(i)}, \theta)$, an importance sampling method was devised. The idea of this method is by assigning weights $w_t^{(i)}$ to samples, the most important ones are evaluated for computing the integral. Further, sequential importance sampling (SIS) allows a sequential update of the importance weights by

$$w_t^{(i)} \propto w_{t-1}^{(i)} \frac{p\left(y_t \mid x_t^{(i)}\right) p\left(x_t^{(i)} \mid x_{t-1}^{(i)}\right)}{q\left(x_t^{(i)} \mid x_{t-1}^{(i)}, y_t\right)} \tag{1.11}$$

with an appropriate chosen *proposal distribution* $q(x_t \mid x_{t-1}, y_t)$. It is also called *importance density* or *important function* (Chen, 2003).

Nevertheless, the SIS makes samples skewed that only a few samples have proper weights as time increases and most of them have small but positive weights. This phenomenon is often called *weight degeneracy* or *sample impoverishment* (Green, 1995; Berzuini *et al.*, 1997).

Besides the SIS processes, a resampling step, also known as a selection step, is trying to eliminate the samples with small weights and duplicate the samples with

large weights in a principled way (Rubin, 2004; Tanner and Wong, 1987). This method is named *sampling and importance resampling* (SIR). Suppose samples with associated weights are $\left\{x_t^{(i)}, w_t^{(i)}\right\}$, a resampling step is executed by generating new samples $\tilde{x}_t^{(i)}$ according to normalized weights $\tilde{w}_t^{(i)}$. It is pointed out that the resampling step does not prevent weights degeneracy but improve further calculation.

The common feature of SIS and SIR is that both of these methods are based on importance sampling and updating samples weights recursively. The difference is that in SIR, the resampling step is always performed. Whereas, in SIS, the resampling is only taken when needed.

Particle filter (PF) is the most successful application of importance sampling with resampling algorithm. It randomly generates a cloud of points and push these points through the computation process. It is a recursive implementation of the Monte Carlo approaches (Doucet and Johansen, 2009).

A generic PF generates N uniformly weighted random measurements $\left\{x_{t-1}^{(i)}, \frac{1}{N}\right\}$ first at time $t-1$. Once a new observation y_t comes into the system, the weights will be updated recursively by involving the likelihood function $p(y_t \mid x_t^{(i)})$ and propagation function $p(x_t^{(i)} \mid x_{t-1}^{(i)})$. In fact, it is the SIS step. To monitor how bad is the weight degeneracy, a suggested measurement *effective sample size* is introduced in (Kong *et al.*, 1994). It is the reciprocal of the sum of squared weights in the form of

$$N_{\text{ess}} = \frac{1}{\sum_{i=1}^{N} \left(w_t^{(i)}\right)^2}. \tag{1.12}$$

If the N_{ess} is less than a predefined threshold, the resampling procedure is executed and the set of particles remains the same size N.

However, the PF sampling and resampling methods may cause practical problems. Such as high weighted particles have been selected many times and lead to the loss of diversity. This problem is known as sample impoverishment, in which way the particles are not representative. The improvements of particle filter's performance have been devoted by (Carpenter *et al.*, 1999; Godsill *et al.*, 2001; Stavropoulos and Titterington, 2001; Doucet *et al.*, 2011).

Apparently, Bayesian filtering has become a broad topic involving many scientific areas that a comprehensive survey and detailed treatment seems crucial to cater the ever growing demands of understanding this important field for many novices, though it is noticed by the author that in the literature there exist a number of excellent tutorial papers on particle filters and Monte Carlo filters (Chen, 2003; Doucet *et al.*, 2000; Chen *et al.*, 2012; Doucet *et al.*, 2000).

1.6 Markov Chain Monte Carlo Methods

Schemes exist to counteract sample impoverishment, which incurs in particle filter (Ristic *et al.*, 2004). One approach is to consider the states for the particles to be predetermined by the forward filter and then to obtain the smoothed estimates by recalculating the particles' weights via a recursion from the final to the first time step (Godsill *et al.*, 2000). Another approach is to use a *Markov chain Monte Carlo* (MCMC) move step (Carlin *et al.*, 1992). MCMC refers to constructing Markov chains that move in the unobserved quantity space and produce a sequence samples from the posterior distribution. After the chain has been run long enough, the sequence is considered as an approximation to the posterior distribution (Kokkala, 2016).

MCMC methods are a set of powerful stochastic algorithms that allow us to solve most of these Bayesian computational problems when the data are available in batches (Andrieu *et al.*, 1999; Green, 1995; Andrieu *et al.*, 2001). They are based on sampling from probability distributions based on a Markov chain. If samples are unable to be drawn directly from a distribution $\pi(x)$, we can construct a Markov chain of samples from another distribution $\hat{\pi}(x)$ that is equilibrium to $\pi(x)$. If the chain is long enough, these samples of the chain can be used as a basis for summarizing features of $\pi(x)$ of interest (Smith and Roberts, 1993). This is a crucial property. See e.g. Cappé *et al.* (2009); Liu (2008) for details.

Metropolis-Hastings Algorithm

The *Metropolis-Hastings* (MH) algorithm is an important class of MCMC algorithms (Smith and Roberts, 1993; Tierney, 1994; Gilks *et al.*, 1995). Given essentially a probability distribution $\pi(\cdot)$ (the target distribution), MH algorithm provides a way to generate a Markov chain $x_1, x_2, \ldots, x_t$, who has the target distribution as a stationary distribution, for the uncertain parameters x requiring only that this density can be calculated at x. Suppose that we can evaluate $\pi(x)$ for any x. The transition probabilities should satisfy the detailed balance condition

$$\pi\left(x^{(t)}\right) q\left(x', x^{(t)}\right) = \pi\left(x'\right) q\left(x^{(t)}, x'\right), \tag{1.13}$$

which means that the transition from the current state $\pi\left(x^{(t)}\right)$ to the new state $\pi\left(x'\right)$ has the same probability as that from $\pi\left(x'\right)$ to $\pi\left(x^{(t)}\right)$. In sampling method, drawing x_i first and then drawing x_j should have the same probability as drawing x_j and then drawing x_i. However, in most situations, the details balance condition is not satisfied.

Therefore, a function $\alpha(x, y)$ is introduced for satisfying

$$\pi(x')\, q\left(x', x^{(t)}\right) \alpha\left(x', x^{(t)}\right) = \pi\left(x^{(t)}\right) q\left(x^{(t)}, x'\right) \alpha\left(x^{(t)}, x'\right). \tag{1.14}$$

In this way, a tentative new state x' is generated from the proposal density $q\left(x'; x^{(t)}\right)$ and it is then accepted or rejected according to acceptance probability

$$\alpha = \frac{\pi(x')}{\pi\left(x^{(t)}\right)} \frac{q\left(x^{(t)}, x'\right)}{q\left(x', x^{(t)}\right)}. \tag{1.15}$$

If $\alpha \geq 1$, then the new state is accepted. Otherwise, the new state is accepted with probability α.

A simple mechanic proposing algorithm is *random walk Metropolis-Hastings* (RM MH). It is easy to implement and symmetric under the exchange of the initial and proposed points.

Besides, modified Metropolis-Hastings algorithms, such as the delayed-rejection MH, multiple-try MH and reversible-jump MH algorithms have been studied by Tierney and Mira (1999); Liu *et al.* (2000); Green (1995).

Adaptive MCMC Algorithm

Metropolis-Hastings algorithm is widely used in statistical inference, to sample from complicated high-dimensional distributions. Typically, this algorithm has parameters that must be tuned in each new situation to obtain reasonable mixing times, such as the step size in a random walk Metropolis (Mahendran *et al.*, 2012). Tuning of associated parameters such as proposal variances is crucial to achieving efficient mixing, but can also be difficult.

Adaptive MCMC methods have been developed to automatically adjust these parameters, such as (Andrieu and Thoms, 2008; Girolami and Calderhead, 2011; Atchade *et al.*, 2009; Roberts and Rosenthal, 2009). One of the most successful adaptive MCMC algorithms is introduced by Haario *et al.* (2001), where, based on the random walk Metropolis algorithm, the covariance of the proposal distribution is calculated using all of the previous states. For instance, with an adaptive MCMC chain $x_0, x_1, \ldots, x_t$, the proposal x' is from $N(\cdot \mid x_t, R_t)$, where R_t is the covariance matrix determined by the spatial distribution of the state $x_0, x_1, \ldots, x_t$.

Even though the adaptive Metropolis algorithm is non-Markovian, the establishment was verified that the adaptive MCMC algorithm indeed has the correct ergodic properties.

A Bayesian optimization for adaptive MCMC was proposed by Mahendran *et al.* (2012). The author proposed adaptive strategy consists of two phases: adaptation and sampling. In the first phase, Bayesian optimization is used to construct a randomized policy. After that, in the second phase, a mixture of MCMC kernels selected according to the learned randomized policy is used to explore the target distribution.

Further investigation in the use of adaptive MCMC algorithms to automatically tune the Markov chain parameters can be found at (Roberts and Rosenthal, 2009).

Other Monte Carlo Algorithms

The *Hamiltonian Monte Carlo* (HMC), devised by Duane *et al.* (1987) as hybrid Monte Carlo, uses Hamiltonian dynamics to produce distant proposals for the Metropolis algorithm in order to avoid slow exploration of the state-space that results from the diffusive behavior of simple random walk proposals (Neal, 2011). In practice, the HMC sampler is more efficient for sampling in high-dimensional distributions than MH.

The key feature of HMC is the Hamiltonian system equation as follows:

$$H(x, v) = U(x) + K(v), \tag{1.16}$$

which is consisting of potential energy $U(x)$ with a d-dimensional momentum vector (position) x and kinetic energy function $K(v) = \frac{v^\top M^{-1} v}{2}$ with a d-dimensional momentum vector (velocity) v. To propose $\{x', v'\}$, HMC uses the leapfrog method, which is based on Euler's method and modified Euler's method, to increase the proposing accuracy (Betancourt, 2017). It is accepted with the probability

$$\alpha = \min\left\{\exp[H(x, v) - H(x', v')], 1\right\}. \tag{1.17}$$

Compared with MH sampler, the HMC has a higher efficiency in most of the high-dimensional cases. It is incorporating not only with energy $U(x)$ but also with a gradient. In this way, HMC explores a larger area and converges to balance faster.

The *Zig-Zag Monte Carlo* uses a continuous-time piecewise zig-zag process to increase the sampling efficiency (Bierkens and Roberts, 2016). It is an application of the Curie-Weiss model in high dimension and provides a practically efficient sampling scheme for sampling in the big data regime with some remarkable properties (Turitsyn *et al.*, 2011; Bierkens and Duncan, 2017).

Given a target density $\pi(\cdot)$, the Zig-Zag process $f(x, \theta)$ is defined in a $d \otimes 2$ space $\mathcal{E}$. x is in the d-dimensional topological subspace and θ is in a binary discrete $\{-1, 1\}_d$ subspace denoting the flipping statues. The switching rate $\lambda(x, \theta)$ agrees with the target

distribution $\pi(\cdot)$ in a certain way and is defined as $\lambda(x,\theta) = \max\{0, \theta U'(x)\} + \gamma(x)$, where $U'(x) = \lambda(x,\theta) - \lambda(x,-\theta)$. Then, the Zig-Zag operator L is

$$Lf(x,\theta) = \theta \partial f_x + \lambda(x,\theta)[f(x,-\theta) - f(x,\theta)], \tag{1.18}$$

for all $(x,\theta) \in \mathcal{E}$.

Thereafter, the obtained sequence of the Zig-Zag process is used to approximate expectations with respect to $\pi(\cdot)$ according to the law of large numbers. The application of Zig-Zag process in big data scheme and some properties are given in (Bierkens and Duncan, 2017).

The t-walk given by Christen and Fox (2010) is a self-adjusting MCMC algorithm that requires no tuning and has been shown to provide good results in many cases of up to 400 dimensions. Because of the t-walk is not adaptive, it does not require new restricting conditions but only the log of the posterior and two initial points (Blaauw and Christen, 2011).

Given a posterior distribution $\pi(\cdot)$, the new objective function $f(x,x')$ is the product of $\pi(x)\pi(x')$ from $X \otimes X$. The new proposal (y,y') is given by

$$(y,y') = \begin{cases} (x, h(x',x)) & \text{with probability } 0.5 \\ (h(x',x), x') & \text{with probability } 0.5 \end{cases} \tag{1.19}$$

where $h(x,x')$ is a preselected proposing strategy. In each iteration, only one of the two chains x and x' moves according to a random walk. For example, suppose in the first step the x stays the same but y' is proposed from $q(\cdot \mid x, x')$, then the acceptance ratio is

$$\frac{\pi(y')}{\pi(x')} \frac{q(x' \mid y', x)}{q(y' \mid x', x)}. \tag{1.20}$$

After a few iterations, there are two dual and coupled chains obtained. Hence, the t-walk is a kind of multiple chain approach.

Four recommendations for the choices of $h(x,x')$ including a scaled random walk, referred to *the walk move*, *traverse move*, *hop moves* and *blow moves* are given in (Christen and Fox, 2010). The t-walk is now available in a complete set of computer packages, including *R*, *Python*. It is convenient for researchers to go a deeper implementation.

1.7 Original Contributions and Thesis Outline

The original contributions presented in this thesis are:

(i) An adaptive spline-based approach to trajectory reconstruction called the V-spline. The V-spline incorporates velocity information and a piecewise constant penalty term, and has been developed to handle irregularly sampled data.

(ii) The reconstructed trajectory can be understood as an element of a reproducing kernel Hilbert space. The approach of (Gu, 2013) is extended to allow for a piecewise constant penalty term and the V-spline is shown to be the posterior mean of a particular Gaussian process.

(iii) A fast on-line algorithm for trajectory reconstruction, based on Markov chain Monte Carlo, is developed for simultaneous parameter and state estimation in the context of a linear state space model. This approach is simpler to implement than particle methods that rely on sufficient statistics.

In Chapter 2, an adaptive smoothing V-spline method, which is based on *Hermite spline* basis functions, is proposed to obtain a reconstruction of f and f' from noisy data $y_{1:n}$ and $v_{1:n}$. Instead of minimizing the residuals of $f(t_i) - y_i$ only, the residuals of $f'(t_i) - v_i$ with a new parameter γ are consisted in the new objective function. A modified leave-one-out cross-validation algorithm is used for find the optimal parameters. Numerical simulation and real data implementation are given after theoretical methodology.

In Chapter 3, the Bayesian estimation form of the V-spline is given. It is proved that the Bayes estimate is corresponding to a V-spline in the reproducing kernel Hilbert space $\mathcal{C}^{(2)}_{\text{p.w.}}[0,1]$, where the second-derivative is piecewise-continuous. An extended GCV is used to find the optimal parameters for the Bayes estimate.

In Chapter 4, a comprehensive overview of existing methods for sequential state and parameter inference is given. Basic concepts and popular algorithms of sequential state estimation are discussed in the second section. Furthermore, the algorithms for combined state and parameter estimation are brought into a separate section. A numerical comparison of different methods is given at the end of this chapter.

In Chapter 5, a random walk Metropolis-Hastings algorithm in the learning phase is utilized to learn the mean and the covariance of the parameters space. After that, the information is implemented in the estimation phase, where an adaptive Delayed-Acceptance Metropolis-Hastings algorithm is proposed for estimating the posterior distribution of combined state and parameter. To remain a high running efficiency, a sliding window approach, in which way historical data is cut off when new observations

come into the data stream, is used to improve the sampling speed. This algorithm is applied to irregularly sampled time series data and implemented in real GPS data set.

The proof of theorems, details of equation calculations, and results of simulation studies are all presented in appendices. For details, the Appendix A includes V-spline related theorems, lemmas, calculations and figures. In Appendix B, the proposed adaptive sequential MCMC related works and outcomes are illustrated, including details of the recursive form calculation, tables and figures of parameters comparison and so on.

A spin-off outcome is presented in Appendix C. It is a data simplification method used for reducing the size of a data set and saving storage costs without losing important information.

Chapter 2

Adaptive Smoothing V-Spline for Trajectory Reconstruction

2.1 Introduction

GPS devices are widely used for tracking individuals and vehicles. The position and velocity of moving objects are determined by GPS units and can be used in batch and on-line estimation of trajectories.

The use of GPS receivers for obtaining trajectory information is carried out for a wide variety of reasons. The *TracMap* company, located in New Zealand and USA, produces GPS display units to aid precision farming in agriculture, horticulture and viticulture. With these units, operational data is collected and sent to a remote server for further analysis. GPS units also guide drivers of farm vehicles to locations on the farm that require specific attention and can indicate the location of potential hazards.

Given a sequence of position vectors in a tracking system, the simplest way of constructing the complete trajectory of a moving object is by connecting positions with a sequence of lines, known as line-based trajectory representation (Agarwal *et al.*, 2003). Vehicles with an omnidirectional drive or a differential drive can actually follow such a path in a drive-and-turn fashion, though it is highly inefficient (Gloderer and Hertle, 2010) and this kind of non-smooth motion can cause slippage and over-actuation (Magid *et al.*, 2006). By contrast, most vehicles typically follow smooth trajectories without sharp turns.

Several methods have been investigated to solve this issue. One of them uses the minimal length path that is continuously differentiable and consists of line segments or arcs of circles, with no more than three segments or arcs between successive positions

(Dubins, 1957). This method is called Dubins curve and has been extended to other more complex vehicle models but is still limited to line segments and arcs of circles (Yang and Sukkarieh, 2010). However, there are still curvature discontinuities at the junctions between lines and arcs, leading to yaw angle errors (Wang *et al.*, 2017).

Spline methods have been developed to overcome these issues and to construct smooth trajectories. Magid *et al.* (2006) propose a path-planning algorithm based on splines. The main objective of the method is the smoothness of the path, not a shortest or minimum-time path. A curve-based method uses a parametric cubic function $P(t) = a_0 + a_1 t + a_2 t^2 + a_3 t^3$ to obtain a spline that passes through any given sequence of joint position-velocity paired points $(y_1, v_1), (y_2, v_2), \ldots, (y_n, v_n)$ (Yu *et al.*, 2004). More generally, a B-spline gives a closed-form expression for the trajectory with continuous second derivatives and goes through the points smoothly while ignoring outliers (Komoriya and Tanie, 1989; Ben-Arieh *et al.*, 2004). It is flexible and has minimal support with respect to a given degree, smoothness, and domain partition. Gasparetto and Zanotto (2007) use fifth-order B-splines to compose the overall trajectory, allowing one to set kinematic constraints on the motion, expressed as the velocity, acceleration, and jerk. In computer (or computerized) numerical control (CNC), Erkorkmaz and Altintas (2001) presented a quintic spline trajectory generation algorithm connecting a series of reference knots that produces continuous position, velocity, and acceleration profiles. Yang and Sukkarieh (2010) proposed an efficient and analytical continuous curvature path-smoothing algorithm based on parametric cubic Bézier curves. Their method can fit ordered sequential points smoothly.

However, a parametric approach only captures features contained in the preconceived class of functions (Yao *et al.*, 2005) and increases model bias. To avoid this, nonparametric methods have been developed. Rather than giving specified parameters, it is desired to reconstruct the trajectory $f(t)$ from the data $y(t_i) \equiv y_i$, $i = 1, \ldots, n$, (Craven and Wahba, 1978). Smoothing spline estimates of $f(t)$ appear as a solution to the following minimization problem: find $\hat{f} \in \mathcal{C}^{(2)}[a, b]$ that minimizes the penalized residual sum of squares:

$$\text{RSS} = \sum_{i=1}^{n} (y_i - f(t_i))^2 + \lambda \int_a^b (f''(t))^2 \, dt \tag{2.1}$$

for a pre-specified value $\lambda > 0$ (Aydin and Tuzemen, 2012). In equation (2.1), the first term is a residual sum of squares and penalizes lack of fit. The second term is a roughness penalty term weighted by a smoothing parameter λ, which varies from 0 to $+\infty$ and establishes a trade-off between interpolation and a straight line. The

roughness penalty term is a formalization of a mechanical device: if a thin piece of flexible wood, called a spline, is bent to the shape of the curve f, then the leading term in the strain energy is proportional to $\int f''^2 dt$ (Green and Silverman, 1993). The reconstruction cost, equation (2.1), is determined not only by its goodness-of-fit to the data quantified by the residual sum of squares but also by its roughness (Schwarz, 2012). For a given λ, minimizing equation (2.1) will give the best compromise between smoothness and goodness-of-fit. Notice that the first term in equation (2.1) depends only on the values of f at $t_i, i = 1, \ldots, n$. Green and Silverman (1993) show that the function that minimizes the objective function for fixed values of $f(t_i)$ is a cubic spline: an interpolation of points via a continuous piecewise cubic function, with continuous first and second derivatives. The continuity requirements uniquely determine the interpolating spline, except at the boundaries (Sealfon *et al.*, 2005).

Zhang *et al.* (2013) propose Hermite interpolation on each interval to fit position, velocity and acceleration with kinematic constraints. Their trajectory formulation is a combination of several cubic splines on every interval or, alternatively, is a single function found by minimizing

$$\lambda \sum_{i=1}^{n} |y_i - f(t_i)|^2 + (1 - \lambda) \int |f''(t)|^2 dt, \tag{2.2}$$

where p is a smoothing parameter (Castro *et al.*, 2006).

A conventional smoothing spline is controlled by one single parameter, which controls the smoothness of the spline on the whole domain. A natural extension is to allow the smoothing parameter to vary as a function of the independent variable, adapting to the change of roughness in different domains (Silverman, 1985; Donoho *et al.*, 1995). The objective function is now of the form

$$\sum_{i=1}^{n} (y_i - f(t_i))^2 + \int \lambda(t) \left(f''(t)\right)^2 dt. \tag{2.3}$$

Similar to the conventional smoothing spline problem, one has to choose the penalty function $\lambda(t)$. The fundamental idea of nonparametric smoothing is to let the data choose the amount of smoothness, which consequently decides the model complexity (Gu, 1998). When λ is constant, most methods focus on data-driven criteria, such as cross-validation (CV), generalized cross-validation (GCV) (Craven and Wahba, 1978) and generalized maximum likelihood (GML) (Wahba, 1985). Allowing the smoothing parameter to be a function poses additional challenges, though Liu and Guo (2010) were able to extend GML to adaptive smoothing splines.

In this chapter, an adaptive smoothing spline named the V-spline is proposed that uses modified Hermite spline basis functions to obtain a reconstruction of f and f' from noisy paired position data $\mathbf{y} = \{y_1, \ldots, y_n\}$ and velocity data $\mathbf{v} = \{v_1, \ldots, v_n\}$. Rather than just using residuals of $f(t_i) - y_i$, the extra residuals of $f'(t_i) - v_i$ and a new parameter γ are included in the objective function. The parameter γ controls the degree to which the velocity information is used in the reconstruction. In this way, the V-spline keeps a balance between position and velocity. An advanced cross-validation formula is given for the V-spline parameters. It is shown that the new spline performs well on simulated signal data *Blocks*, *Bumps*, *HeaviSine* and *Doppler* (Donoho and Johnstone, 1994). Finally, an application of the V-spline to a set of 2-dimensional real data is given.

2.2 V-Spline

In the nonparametric regression, consider n paired time series points $\{t_1, y_1, v_1\}$, ..., $\{t_n, y_n, v_n\}$, such that $a = t_0 < t_1 < t_2 < \cdots < t_n < t_{n+1} = b$, y is the position information and v indicates its velocity. As in (Silverman, 1985) and (Donoho *et al.*, 1995), we use a positive penalty function $\lambda(t)$ in the following objective function.

For a function $f : [a, b] \mapsto \mathbb{R}$ and $\gamma > 0$, define the objective function

$$J[f] = \frac{1}{n}\sum_{i=1}^{n}\left(f(t_i) - y_i\right)^2 + \frac{\gamma}{n}\sum_{i=1}^{n}\left(f'(t_i) - v_i\right)^2 + \sum_{i=0}^{n}\int_{t_i}^{t_{i+1}} \lambda(t) f''(t)^2 dt, \qquad (2.4)$$

where γ is the parameter that weights the residuals between $\mathbf{f}'$ and $\mathbf{v}$. We make the simplifying assumption that $\lambda(t)$ is a piecewise constant and adopts a constant value λ_i on interval (t_i, t_{i+1}) for $i = 1, \ldots, n-1$.

Theorem 1. *For $n \geq 2$, the objective function $J[f]$ is uniquely minimized by a cubic spline, piecewise on the intervals $[t_i, t_{i+1})$, $i = 1, \ldots, n-1$, and linear on $[a, t_1]$ and $[t_n, b]$.*

A further minimizer of (2.4) is called a *V-spline*, coming from the incorporation with velocity information and applications on vehicle and vessel tracking. The proof of Theorem 1 is in Appendix A.2.

2.2.1 Constructing Basis Functions

To construct basis functions cooperating with position and velocity, it is recommended to use the cubic Hermite spline (Hermite, 1863), by which the combination of

heading and speeding at both registration points are treated at two points (Hintzen *et al.*, 2010). The following equation describes the cubic Hermite spline on interval $[0, 1]$

$$f(s) = \left(2s^3 - 3s^2 + 1\right) y_0 + \left(s^3 - 2s^2 + s\right) v_0 + \left(-2s^3 + 3s^2\right) y_1 + \left(s^3 - s^2\right) v_1. \quad (2.5)$$

For an arbitrary interval $[t_i, t_{i+1})$, one can replace s with $(t - t_i)/(t_{i+1} - t_i)$ and the cubic spline basis functions are

$$h_{00}^{(i)}(t) = \begin{cases} 2\left(\frac{t-t_i}{t_{i+1}-t_i}\right)^3 - 3\left(\frac{t-t_i}{t_{i+1}-t_i}\right)^2 + 1 & t_i \le t < t_{i+1} \\ 0 & \text{otherwise} \end{cases}, \quad (2.6)$$

$$h_{10}^{(i)}(t) = \begin{cases} \frac{(t-t_i)^3}{(t_{i+1}-t_i)^2} - 2\frac{(t-t_i)^2}{t_{i+1}-t_i} + (t - t_i) & t_i \le t < t_{i+1} \\ 0 & \text{otherwise} \end{cases}, \quad (2.7)$$

$$h_{01}^{(i)}(t) = \begin{cases} -2\left(\frac{t-t_i}{t_{i+1}-t_i}\right)^3 + 3\left(\frac{t-t_i}{t_{i+1}-t_i}\right)^2 & t_i \le t < t_{i+1} \\ 0 & \text{otherwise} \end{cases}, \quad (2.8)$$

$$h_{11}^{(i)}(t) = \begin{cases} \frac{(t-t_i)^3}{(t_{i+1}-t_i)^2} - \frac{(t-t_i)^2}{t_{i+1}-t_i} & t_i \le t < t_{i+1} \\ 0 & \text{otherwise} \end{cases}. \quad (2.9)$$

Consequently, the cubic Hermite spline $f^{(i)}(t)$ on an arbitrary interval $[t_i, t_{i+1})$ with two successive points $P_i = \{t_i, y_i, v_i\}$ and $P_{i+1} = \{t_{i+1}, y_{i+1}, v_{i+1}\}$ is expressed as

$$f^{(i)}(t) = h_{00}^{(i)}(t) y_i + h_{10}^{(i)}(t)\left(t_{i+1} - t_i\right) v_i + h_{01}^{(i)}(t) y_{i+1} + h_{11}^{(i)}(t)\left(t_{i+1} - t_i\right) v_{i+1}. \quad (2.10)$$

To construct basis function for a V-spline on the entire interval $[a, b]$, the new basis functions are defined in such way, that $N_1 = h_{00}^{(1)}$, $N_2 = h_{10}^{(1)}$, and for all $i = 1, 2, \ldots, n-2$,

$$N_{2i+1}(t) = h_{01}^{(i)}(t) + h_{00}^{(i+1)}(t), \quad (2.11)$$

$$N_{2i+2}(t) = h_{11}^{(i)}(t) + h_{10}^{(i+1)}(t), \quad (2.12)$$

and

$$N_{2n-1}(t) = \begin{cases} h_{01}^{(n-1)}(t) & \text{if } t < t_n \\ 1 & \text{if } t = t_n \end{cases}, \quad (2.13)$$

$$N_{2n}(t) = h_{11}^{(n-1)}(t). \quad (2.14)$$

Any f in the function space can be represented in the form of

$$f = \sum_{k=1}^{2n} N_k(t)\theta_k, \tag{2.15}$$

where $\{\theta_k\}_{k=1}^{2n}$ are parameters.

2.2.2 Computing V-Spline

Basis functions have been defined in the previous subsection, therefore the V-spline $f(t)$ on $[a, b]$, where $a \leq t_1 < t_2 < \cdots < t_{n-1} < t_n \leq b$, can be found by minimizing the objective function (2.4), which is corresponding to

$$nJ[f](\theta, \lambda, \gamma) = (\mathbf{y} - B\theta)^\top (\mathbf{y} - B\theta) + \gamma (\mathbf{v} - C\theta)^\top (\mathbf{v} - C\theta) + n\theta^\top \mathbf{\Omega}_\lambda \theta, \tag{2.16}$$

where $\{B\}_{ij} = N_j(t_i)$, $\{C\}_{ij} = N_j'(t_i)$ and $\left\{\Omega_{2n}^{(i)}\right\}_{jk} = \int_a^b \lambda(t) N_j''(t) N_k''(t) dt$. After substituting the series observation $t_1, \ldots, t_n$ into the basis function, one can get $N_1(t_1) = 1, N_1(t_2) = 0, \ldots, N_{2i-1}(t_i) = 1, N_{2i}(t_i) = 0, \ldots, N_{2n-1}(t_n) = 1, N_{2n}(t_n) = 0$; and into its first derivative, one will get $N_1'(t_1) = 0, N_1'(t_2) = 1, \ldots, N_{2i-1}'(t_i) = 0, N_{2i}'(t_i) = 1, \ldots, N_{2n-1}'(t_n) = 0, N_{2n}'(t_n) = 1$. That means the matrices B and C in the equation (2.16) are $n \times 2n$ dimensional and the elements are

$$B = \{B\}_{ij} = \begin{cases} 1, & j = 2i - 1 \\ 0, & \text{otherwise} \end{cases} \tag{2.17}$$

$$C = \{C\}_{ij} = \begin{cases} 1, & j = 2i \\ 0, & \text{otherwise} \end{cases} \tag{2.18}$$

where $i = 1, \ldots, n$, $j = 1, \ldots, 2n$ and $k = 1, \ldots, 2n$. The i-th $\Omega^{(i)}$ on the interval $[t_i, t_{i+1}]$ is a $2n \times 2n$ matrix and $\Omega^{(n)}$ does not exist. The detailed structure of Ω is in Appendix A.1. As a result, the penalty term is a bandwidth four matrix written in such a way:

$$\mathbf{\Omega}_\lambda = \sum_{i=1}^{n-1} \lambda_i \Omega^{(i)}. \tag{2.19}$$

By taking derivatives of equation (2.16) with respect to θ, one can achieve

$$\left(B^\top B + \gamma C^\top C + n\mathbf{\Omega}_\lambda\right) \hat{\theta} = \left(B^\top \mathbf{y} + \gamma C^\top \mathbf{v}\right). \tag{2.20}$$

Therefore, the solution is

$$\hat{\theta} = \left(B^\top B + \gamma C^\top C + n\mathbf{\Omega}_\lambda\right)^{-1} \left(B^\top \mathbf{y} + \gamma C^\top \mathbf{v}\right) \tag{2.21}$$

a generalized ridge regression. Consequently, the fitted smoothing spline is given by $\hat{f}(t) = \sum_{k=1}^{2n} N_k(t)\hat{\theta}_k$.

A smoothing spline with parameters $\lambda(t)$ and γ is an example of a linear smoother (Hastie *et al.*, 2009). This is because the estimated parameters in equation (2.21) are a linear combination of y_i and v_i. Denote by $\hat{\mathbf{f}}$ and $\hat{\mathbf{f}}'$ the $2n$ vector of fitted values $\hat{f}(t_i)$ and $\hat{f}'(t_i)$ at the training points t_i. Then

$$\begin{aligned}\hat{\mathbf{f}} =& B\left(B^\top B + \gamma C^\top C + n\boldsymbol{\Omega}_\lambda\right)^{-1}\left(B^\top \mathbf{y} + \gamma C^\top \mathbf{v}\right) \\ =& \mathbf{S}_{\lambda,\gamma}\mathbf{y} + \gamma \mathbf{T}_{\lambda,\gamma}\mathbf{v}\end{aligned} \tag{2.22}$$

$$\begin{aligned}\hat{\mathbf{f}}' =& C\left(B^\top B + \gamma C^\top C + n\boldsymbol{\Omega}_\lambda\right)^{-1}\left(B^\top \mathbf{y} + \gamma C^\top \mathbf{v}\right) \\ =& \mathbf{U}_{\lambda,\gamma}\mathbf{y} + \gamma \mathbf{V}_{\lambda,\gamma}\mathbf{v}\end{aligned} \tag{2.23}$$

The fitted $\hat{\mathbf{f}}$ and $\hat{\mathbf{f}}'$ are linear in $\mathbf{y}$ and $\mathbf{v}$, and the finite linear operators $\mathbf{S}_{\lambda,\gamma}, \mathbf{T}_{\lambda,\gamma}, \mathbf{U}_{\lambda,\gamma}$ and $\mathbf{V}_{\lambda,\gamma}$ are known as the smoother matrices. One consequence of this linearity is that the recipe for producing $\hat{\mathbf{f}}$ and $\hat{\mathbf{f}}'$ from $\mathbf{y}$ and $\mathbf{v}$, do not depend on $\mathbf{y}$ and $\mathbf{v}$ themselves; $\mathbf{S}_{\lambda,\gamma}, \mathbf{T}_{\lambda,\gamma}, \mathbf{U}_{\lambda,\gamma}$ and $\mathbf{V}_{\lambda,\gamma}$ depend only on $t_i, \lambda(t)$ and γ.

Suppose in a traditional least squares fitting, B_ξ is $N \times M$ matrix of M cubic-spline basis functions evaluated at the N training points x_i, with knot sequence ξ and $M \ll N$. Thus the vector of fitted spline values is given by

$$\hat{\mathbf{f}} = B_\xi\left(B_\xi^\top B_\xi\right)^{-1} B_\xi \mathbf{y} = \mathbf{H}_\xi \mathbf{y} \tag{2.24}$$

Here the linear operator $\mathbf{H}_\xi$ is a symmetric, positive semidefinite matrices, and $\mathbf{H}_\xi\mathbf{H}_\xi = \mathbf{H}_\xi$ (idempotent) (Hastie *et al.*, 2009). In our case, it is easily seen that $\mathbf{S}_{\lambda,\gamma}, \mathbf{T}_{\lambda,\gamma}, \mathbf{U}_{\lambda,\gamma}$ and $\mathbf{V}_{\lambda,\gamma}$ are symmetric, positive semidefinite matrices as well. Additionally, by Cholesky decomposition

$$\left(B^\top B + \gamma C^\top C + n\boldsymbol{\Omega}_\lambda\right)^{-1} = \mathbf{R}\mathbf{R}^\top, \tag{2.25}$$

it is easy to prove that $\mathbf{T}_{\lambda,\gamma} = B\mathbf{R}\mathbf{R}^\top C^\top$ and $\mathbf{U}_{\lambda,\gamma} = C\mathbf{R}\mathbf{R}^\top B^\top$, then we will have $\mathbf{T}_{\lambda,\gamma} = \mathbf{U}_{\lambda,\gamma}^\top$. When $\lambda = \gamma = 0$, the matrix $\mathbf{S}_{\lambda_0,\gamma_0} = B\left(B^\top B\right)^{-1} B^\top$ is idempotent.

Corollary 1. *If $f(t)$ is the V-spline on the entire interval $[t_1, t_n]$, for sufficient cases of a piecewise constant $\lambda(t)$ and parameter γ, $f(t)$ has the following property:*

(i) if $\gamma \neq 0$, then f and f' are continuous, f'' is piecewise linear but not continuous at knots;

(ii) if $\gamma = 0$, the same as above;

(iii) *if $\lambda(t)$ is not only piecewise constant but constant on the entire interval and $\gamma \neq 0$, the same as above;*

(iv) *if $\lambda(t)$ is not only piecewise constant but constant and $\gamma = 0$, then f, f' are continuous, f'' is piecewise linear and continuous at knots.*

The proof of the Corollary 1 is in Appendix A.3.

2.2.3 Adjusted Penalty Term and Parameter Function

The polynomial in cubic Hermite spline form consists of two points with two positions and two velocities. Suppose there are two points $P_1 = \{t_1, y_1, v_1\}$ and $P_2 = \{t_2, y_2, v_2\}$ on the an arbitrary interval $[t_1, t_2]$. For sake of simplicity, by assuming $t_1 = 0$ and $y_1 = 0$, one can achieve a simple cubic Hermite spline from equation (2.10)

$$f(t) = \left\{ \left(s^3 - 2s^2 + s\right) v_1 + \left(-2s^3 + 3s^2\right) \frac{\Delta d_1}{\Delta T_1} + \left(s^3 - s^2\right) v_2 \right\} \Delta T_1, \tag{2.26}$$

where $s = \frac{t}{\Delta T_1}$. Thus, the second derivative of f is

$$f''(t) = \frac{1}{\Delta T_1} \left\{ 6 \left(\varepsilon_1 + \varepsilon_2\right) s - 2 \left(2\varepsilon_1 + \varepsilon_2\right) \right\}, \tag{2.27}$$

where $\varepsilon_1 = v_1 - \bar{v}$, $\varepsilon_2 = v_2 - \bar{v}$ and $\bar{v}$ is the average velocity $\Delta d_1 / \Delta T_1$. Hence, the penalty term $\lambda \int_{t_1}^{t_2} \left(f''(t)\right)^2 dt = \lambda \int_0^1 \left(f''(s)\right)^2 \Delta T_1 ds$. Being more explicit, the penalty term becomes

$$\lambda \int_0^1 \left(\frac{f''(s)}{\Delta T_1} \right)^2 \Delta T_1 ds = \lambda \frac{\left(2\varepsilon_1 + \varepsilon_2\right)^2 + 3\varepsilon_2^2}{\Delta T_1}. \tag{2.28}$$

Given a constant $\lambda = \frac{(\Delta T_1)^3}{(\Delta d_1)^2} \eta$, the penalty term (2.28) becomes

$$\begin{aligned} \eta \frac{\left(\Delta T_1\right)^2}{\left(\Delta d_1\right)^2} \left(\left(2\varepsilon_1 + \varepsilon_2\right)^2 + 3\varepsilon_2^2 \right) &= \eta \frac{\left(2\varepsilon_1 + \varepsilon_2\right)^2 + 3\varepsilon_2^2}{\bar{v}^2} \\ &\sim \left(\frac{\text{discrepancy in velocity}}{\text{average velocity}} \right)^2, \end{aligned} \tag{2.29}$$

which will be enormous with large measured errors in velocity v_1 or v_2 comparing to average velocity $\bar{v}$.

With noise-free observations, the cubic Hermite spline effectively reconstructs the trajectory between two successive points. However, in real life application, the measurements are coming with errors. Imagine the situation that a vehicle stays unchanged in its positions between a long time gap ΔT. Due to the noise, the velocities v_1 and v_2

are non-zeros and heading to different directions. Cooperating with velocity, the Hermite spline basis function reconstructs the trajectory that starts from the first point along the direction of v_1 and ends at the second point at direction of v_2. It returns a wiggle between the two points, however, there should be a straight line. Or after a long break, where ΔT is extremely large, the velocity becomes worthless. The vehicle can be anywhere during such a long time. In this scenario, we are expecting that the vehicle is following a straight line path. See Figure 2.1.

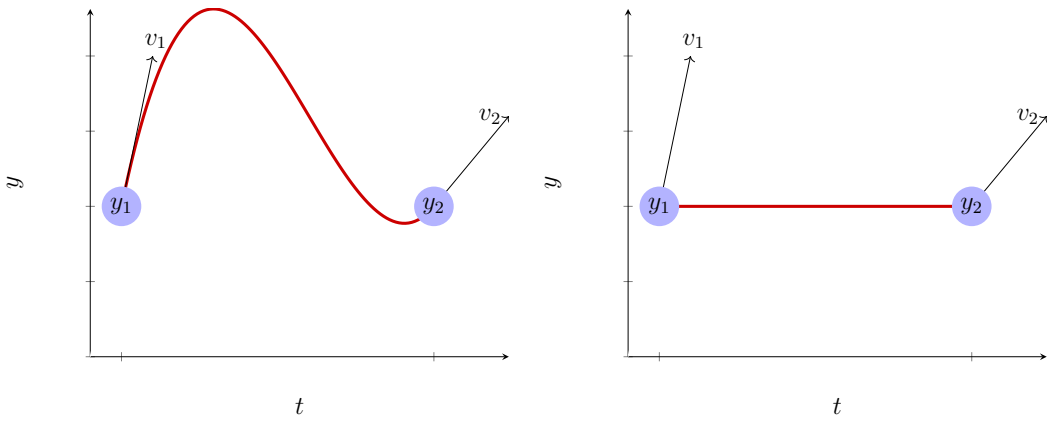

(a) cubic Hermite spline reconstruction (b) straight line reconstruction

Figure 2.1: Comparing reconstructions of cubic Hermite spline and straight line. On the left side, a genuine cubic Hermite spline is cooperating with noisy velocities. Even though the vehicle is not moving, the reconstruction is following the directions of P_1 and P_2 and gives a wiggle between the two points. On the right side, it is an expected reconstruction between two not-moving points after a long time gap.

We address this issue by introducing an adjusted penalty term $\frac{(\Delta T_i)^3}{(\Delta d_i)^2}$ found in equation (2.29) to the penalty function $\lambda(t)$, in which the V-spline is penalized by its real differences of Δd_i and ΔT_i for each interval $[t_i, t_{i+1}]$. With this term, either the measurement in velocity becomes unreliable comparing to average speed or after a long time gap, the adjusted penalty term will works on the penalty function and forces it to return a straight line rather than a curve on this particular domain. From the physical point of view, the term is the reciprocal of the product of velocity and acceleration. Either velocity or acceleration goes to zero, the vehicle should either stop, which returns a straight line through time on y axis, or keep moving with the same speed, which returns a linear interpolation instead of a curved path.

Therefore, the final form of the penalty function $\lambda(t, \eta)$ is piecewise constant having

the following form on each interval

$$\lambda_i = \frac{(\Delta T_i)^3}{(\Delta d_i)^2}\eta, \tag{2.30}$$

where η is an unknown parameter and $t_i \leq t < t_{i+1}$, $i = 1, \ldots, n-1$. Eventually, in the objective function, there are two unknown parameters: η controlling the curvature of V-spline on different domains and γ controlling the residuals of velocity. The piecewise constant function $\lambda(t, \eta)$ is using a data driven method to model the penalty function in the adaptive V-splines.

2.3 Parameter Selection and Cross-Validation

The problem of choosing the smoothing parameter is ubiquitous in curve estimation, and there are two different philosophical approaches to this question. The first one is to regard the free choice of smoothing parameter as an advantageous feature of the procedure. The other one is to find the parameter automatically by the data (Green and Silverman, 1993). We prefer the latter one and use data to train our model and find the best parameters. The most well-known method for this is cross-validation.

Assuming that mean of the random errors is zero, the true regression curve $f(t)$ has the property that, if an observation y is taken away at a point t, the value $f(t)$ is the best predictor of y in terms of returning a least value of $(y - f(t))^2$.

Now, focus on an observation y_i at point t_i as being a new observation by omitting it from the set of data, which are used to estimate $\hat{f}$. Denote by $\hat{f}^{(-i)}(t, \lambda)$ the estimated function from the remaining data, where λ is the smoothing parameter. Then $\hat{f}^{(-i)}(t, \lambda)$ is the minimizer of

$$\frac{1}{n}\sum_{j \neq i}(y_j - f(t_j))^2 + \lambda \int (f''(t))^2 dt, \tag{2.31}$$

and can be quantified by the cross-validation score function

$$\mathrm{CV}(\lambda) = \frac{1}{n}\sum_{i=1}^{n}\left(y_i - \hat{f}^{(-i)}(t_i, \lambda)\right)^2. \tag{2.32}$$

The basis idea of the cross-validation is to choose the value of λ that minimizes $\mathrm{CV}(\lambda)$ (Green and Silverman, 1993).

Through the equation (2.24), it is known that the value of the smoothing spline $\hat{f}$ depends linearly on the data $y_1, \ldots, y_n$. Define the matrix $A(\lambda)$, which is a map vector of observed values y_i to predicted values $\hat{f}(t_i)$. Then we have

$$\hat{\mathbf{f}} = A(\lambda)\mathbf{y} \tag{2.33}$$

and the following lemma.

Lemma 1. *(Green and Silverman, 1993) The cross-validation score satisfies*

$$CV(\lambda) = \frac{1}{n}\sum_{i=1}^{n}\left(\frac{y_i - \hat{f}(t_i)}{1 - A_{ii}(\lambda)}\right)^2 \tag{2.34}$$

where $\hat{f}$ is the spline smoother calculated from the full data set $\{(t_i, y_i)\}$ with smoothing parameter λ.

For a V-spline and its objective function, there are two parameters η, as is shown in (2.30), and γ to be estimated for. Therefore, $\hat{f}^{(-i)}(t, \eta, \gamma)$ is the minimizer of

$$\frac{1}{n}\sum_{j\neq i}\left(y_j - f(t_j)\right)^2 + \frac{\gamma}{n}\sum_{j\neq i}\left(v_j - f'(t_j)\right)^2 + \int \lambda(t,\eta)\left(f''\right)^2 dt, \tag{2.35}$$

and the cross-validation score function is

$$\mathrm{CV}\left(\lambda(t,\eta),\gamma\right) = \frac{1}{n}\sum_{i=1}^{n}\left(y_i - \hat{f}^{(-i)}\left(t_i,\eta,\gamma\right)\right)^2. \tag{2.36}$$

Additionally, it is known that the parameter $\hat{\theta}$ in equation (2.21) is the solution, $\hat{\mathbf{f}}$ and $\hat{\mathbf{f}}'$ have linear forms depending on $\mathbf{y}$ and $\mathbf{v}$, shown in equations (2.22) and (2.23), from Lemma 1, we can prove the following theorem:

Theorem 2. *The cross-validation score of a V-spline satisfies*

$$CV(\eta,\gamma) = \frac{1}{n}\sum_{i=1}^{n}\left(\frac{\hat{f}(t_i) - y_i + \gamma\frac{T_{ii}}{1-\gamma V_{ii}}(\hat{f}'(t_i) - v_i)}{1 - S_{ii} - \gamma\frac{T_{ii}}{1-\gamma V_{ii}}U_{ii}}\right)^2 \tag{2.37}$$

where $\hat{f}$ is the V-spline smoother calculated from the full data set $\{(t_i, y_i, v_i)\}$ with smoothing parameter η and γ.

The proof of Theorem 2 follows immediately from a lemma, and gives an expression for the deleted residuals $y_i - \hat{f}^{(-i)}(t_i)$ and $v_i - \hat{f}'^{(-i)}(t_i)$ in terms of $y_i - \hat{f}(t_i)$ and $v_i - \hat{f}'(t_i)$ respectively.

Lemma 2. *Given fixed η to $\lambda(t,\eta)$, γ and i, denote $\mathbf{f}^{(-i)}$ by the vector with components $f_j^{(-i)} = \hat{f}^{(-i)}\left(t_j,\eta,\gamma\right)$, $\mathbf{f}'^{(-i)}$ by the vector with components $f_j'^{(-i)} = \hat{f}'^{(-i)}\left(t_j,\eta,\gamma\right)$, and define vectors $\mathbf{y}^*$ and $\mathbf{v}^*$ by*

$$\begin{cases} y_j^* = y_j & j \neq i \\ y_i^* = \hat{f}^{(-i)}(t_i) & \textit{otherwise} \end{cases} \tag{2.38}$$

$$\begin{cases} v_j^* = v_j & j \neq i \\ v_i^* = \hat{f}'^{(-i)}(t_i) & \textit{otherwise} \end{cases} \tag{2.39}$$

Then

$$\hat{\mathbf{f}}^{(-i)} = S\mathbf{y}^* + \gamma T\mathbf{v}^* \tag{2.40}$$

$$\hat{\mathbf{f}}'^{(-i)} = U\mathbf{y}^* + \gamma V\mathbf{v}^* \tag{2.41}$$

2.4 Simulation Study

In this section, we give extensive comparison of methods for regularly sampled time series data followed by simulation of irregularly sampled data. The examination is based on the ability of reconstructing four functions derived from *Blocks*, *Bumps*, *Heavi-Sine* and *Doppler*, which were used in (Donoho and Johnstone, 1994, 1995; Abramovich *et al.*, 1998) because of their caricature features in imaging, spectroscopy and other scientific signal processing. Notice that the Blocks and Bumps functions have infinite first derivatives, and cannot be inferred by V-splines. Hence, we use these functions, denoted by $g(t)$, as models of velocity rather than position.

If the original function $g(t)$ is treated as the velocity function of some function $f(t)$, then $f'(t) = g(t)$. By setting initial position $f(t_0) = y_0 = 0$ and acceleration $a_0 = 0$, one can calculate the position data with the following formula:

$$f(t_{i+1}) = f(t_i) + (g(t_i) + g(t_{i+1}))\,\frac{t_{i+1} - t_i}{2}. \tag{2.42}$$

Further, we add some i.i.d. zero-mean ε noise to them

$$\begin{aligned} y_i &= f(t_i) + \varepsilon_f, \\ v_i &= g(t_i) + \varepsilon_g, \end{aligned} \tag{2.43}$$

where $\varepsilon_f \sim N(0, \sigma_f/SNR)$, $\varepsilon_g \sim N(0, \sigma_g/SNR)$ and $i = 0, \ldots, n$. A random seed was fixed to ensure repeatability. The noise is i.i.d. zero-mean Gaussian distributed with standard deviation regarding to signal-to-noise ratio (SNR), which specifies the ratio of the standard deviation of the function to the standard deviation of the simulated errors. Explicitly, if the standard deviation of the true signal f is σ_f, the simulated data will be $f + \varepsilon$, where the simulated error $\varepsilon \sim N(0, \sigma_f/SNR)$. The value of SNR can be chosen 7 or 3.

2.4.1 Regularly Sampled Time Series Data

A set of regularly sampled time series data has equal time difference between each pair of successive points. For example, denoted by $\Delta T_i = t_{i+1} - t_i$ for $i = 1, \ldots, n-1$, then $\Delta T_1 = \cdots = \Delta T_{n-1}$.

Following Nason (2010), we fix $n = 1024$ in the simulation. To compare the performance of the proposed method, a few competitors are attending this competition. For wavelet transform reconstructions, we use the threshold policy of *sure* and *BayesThresh* with levels $l = 4, \ldots, 9$ (Donoho and Johnstone, 1995; Abramovich *et al.*, 1998). A semi-parametric regression model with spatially adaptive penalized splines (*P-spline*) is added in comparison (Krivobokova *et al.*, 2008; Ruppert *et al.*, 2003).

In the V-spline, there are two parameters η and γ to optimize. To evaluate the performance of the velocity term in objective function (2.4) and the adjusted penalty term in (2.30), the parameter γ is set as 0 in one reconstruction of V-spline, whose objective function and solution become

$$J[f]_{\gamma=0} = \frac{1}{n}\sum_{i=1}^{n}\left(f(t_i) - y_i\right)^2 + \sum_{i=0}^{n}\int_{t_i}^{t_{i+1}} \lambda(t) f''(t)^2 dt, \tag{2.44}$$

and

$$\hat{\theta}_{\gamma=0} = \left(B^\top B + n\Omega_\lambda\right)^{-1} B^\top \mathbf{y}. \tag{2.45}$$

In another reconstruction, the adjusted penalty term in (2.30) is removed and the model is denoted by "V-spline without APT".

Numerical Examples

Figure 2.2 to 2.5 display the original (velocity), generated position, wavelet with two different threshold methods, P-spline and three kinds of V-spline fitted functions. The parameters λ and γ of a V-spline are automatically selected with the formula (2.37) by optim function in *R* (Nelder and Mead, 1965).

By comparing the results, we can see that all these methods can rebuild up the skeleton of generated trajectory. *Wavelet(sure)* method has more wiggles in interior interval than *Wavelet(BayesThresh)* does, and the latter one becomes fluctuation near boundary knots. *P-spline* gives a smoother fit than wavelets, but the drawback is lack of specific details. V-spline without velocity loses some information, as can be seen from *Blocks* and *Bumps* where there should be a straight line. V-spline without adjusted penalty term gets over-fitting when the direction changes more frequently than normal, although it catches specific feature in *HeaviSine*. The proposed V-spline performs much better than other methods and returns the near-true trajectory reconstructions.

Figure 2.6 shows the estimated penalty values $\lambda(t, \eta) = \frac{(\Delta T)^3}{(\Delta d)^2}\eta$ at SNR=7. The figures in the left column illustrate the values of the penalty term at different intervals, the figures in the right column are the observations and reconstructed trajectory. The

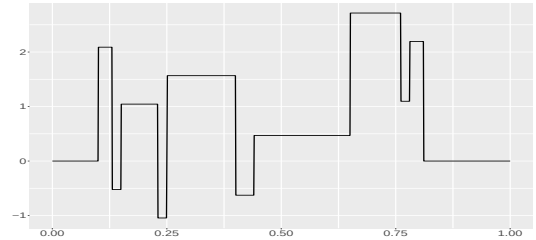

(a) The *Blocks* function

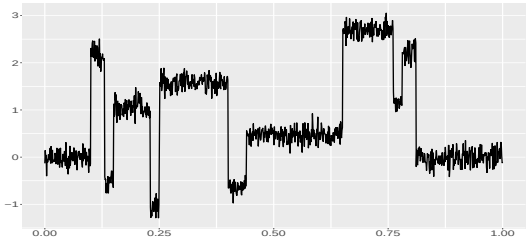

(b) Noisy *Blocks* at SNR=7

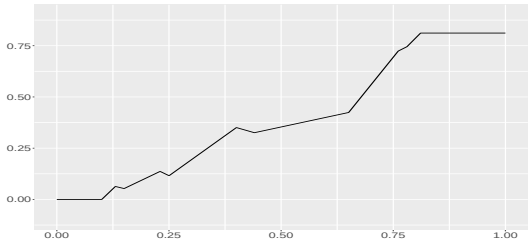

(c) Generated positions

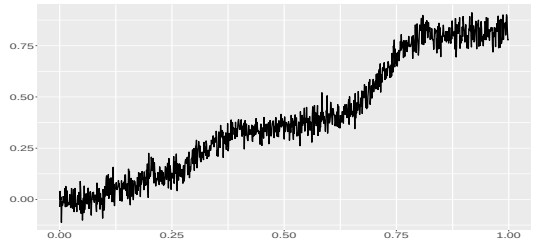

(d) Noisy position at SNR=7

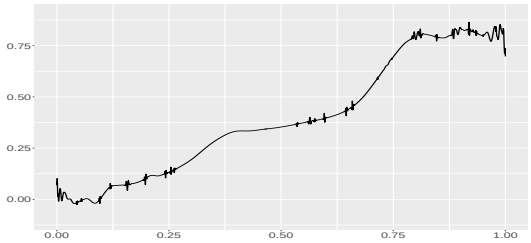

(e) Reconstruction from Wavelet by sure threshold

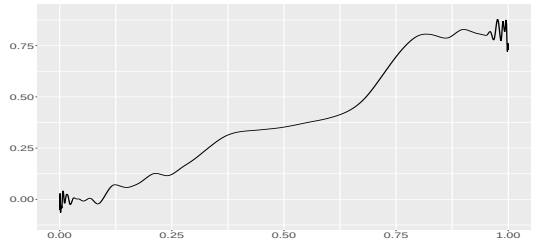

(f) Reconstruction from Wavelet by BayesThresh approach

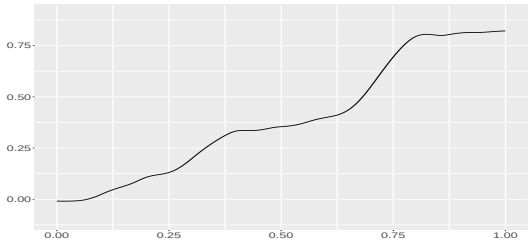

(g) Reconstruction by P-spline

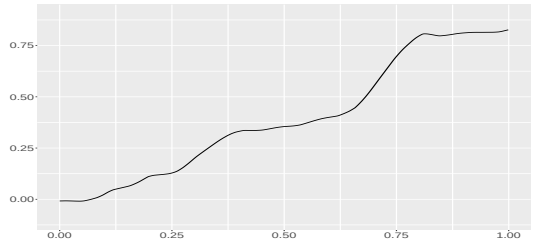

(h) Reconstruction by V-spline setting $\gamma = 0$

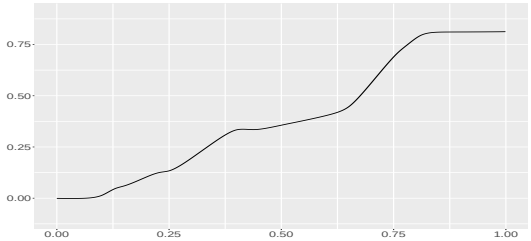

(i) Reconstruction by V-spline with conventional penalty term

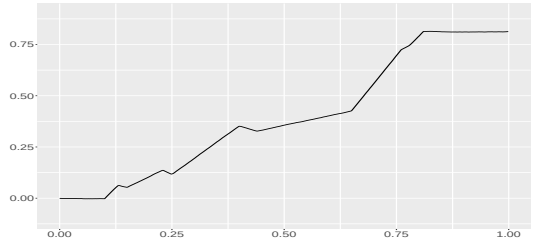

(j) Reconstruction by the proposed V-spline

Figure 2.2: Numerical example: *Blocks*. Comparison of different reconstruction methods with simulated data.

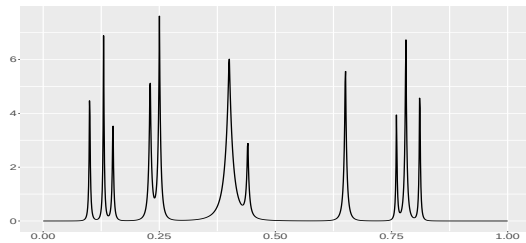

(a) True *Bumps* function

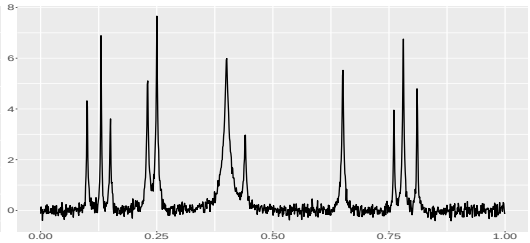

(b) Noisy *Bumps* at SNR=7

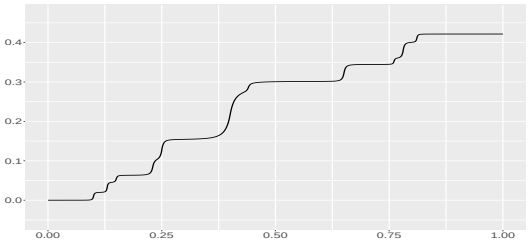

(c) Generated positions

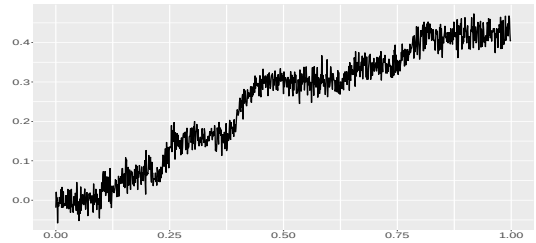

(d) Noisy position at SNR=7

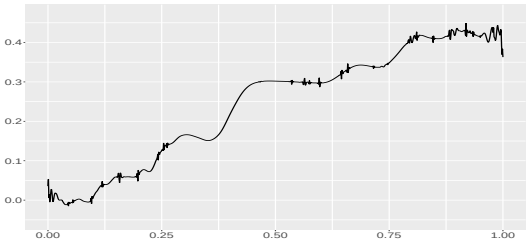

(e) Reconstruction from Wavelet by sure threshold

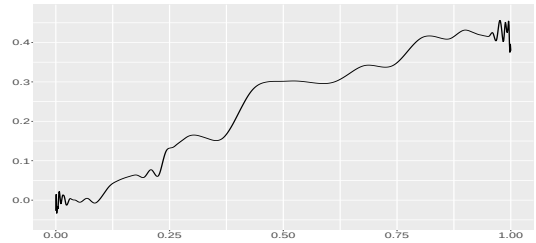

(f) Reconstruction from Wavelet by BayesThresh approach

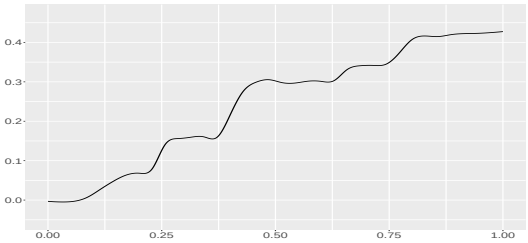

(g) Reconstruction by P-spline

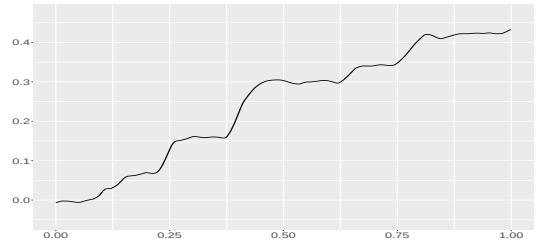

(h) Reconstruction by V-spline setting $\gamma = 0$

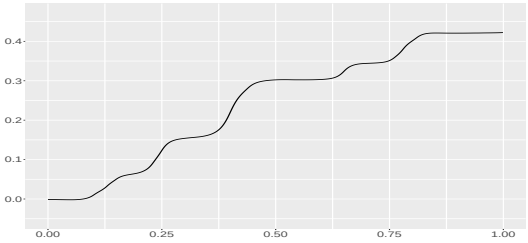

(i) Reconstruction by V-spline with conventional penalty term

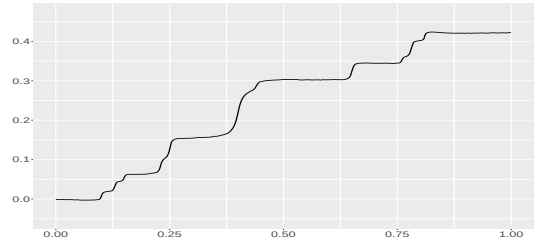

(j) Reconstruction by the proposed V-spline

Figure 2.3: Numerical example: *Bumps*. Comparison of different reconstruction methods with simulated data.

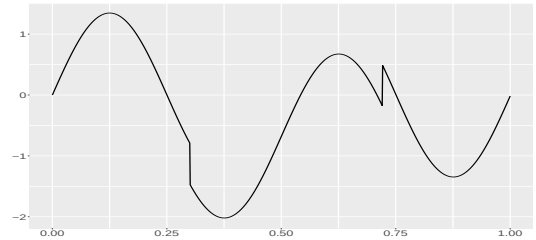

(a) True *HeaviSine* function

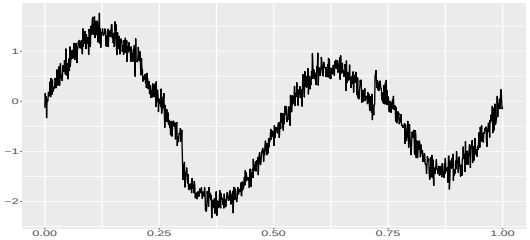

(b) Noisy *HeaviSine* at SNR=7

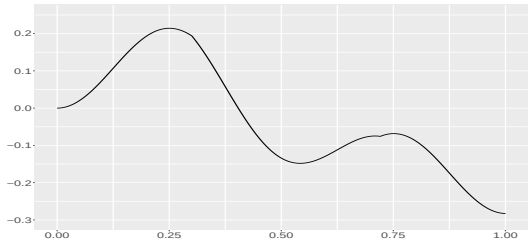

(c) Generated positions

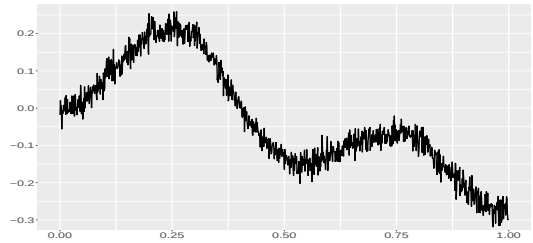

(d) Noisy position at SNR=7

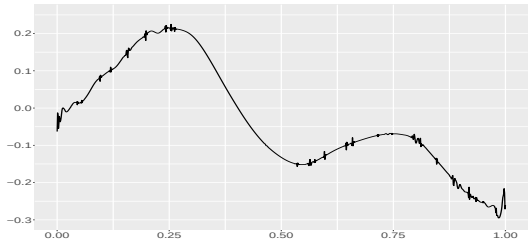

(e) Reconstruction from Wavelet by sure threshold

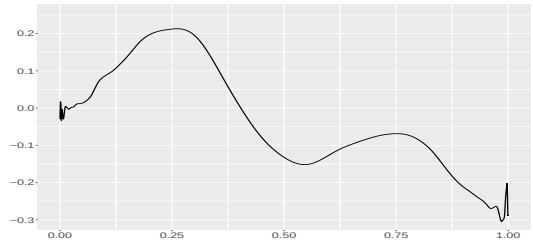

(f) Reconstruction from Wavelet by BayesThresh approach

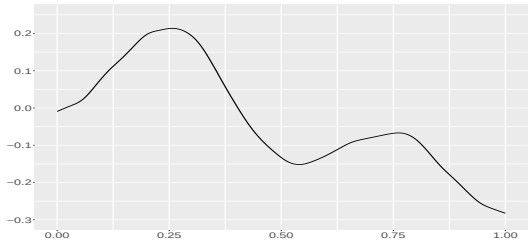

(g) Reconstruction by P-spline

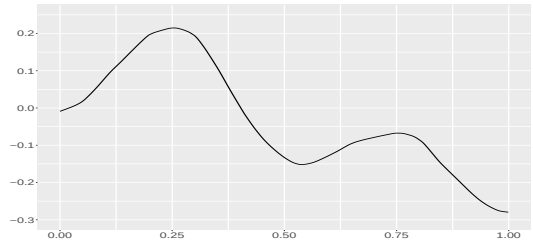

(h) Reconstruction by V-spline setting $\gamma = 0$

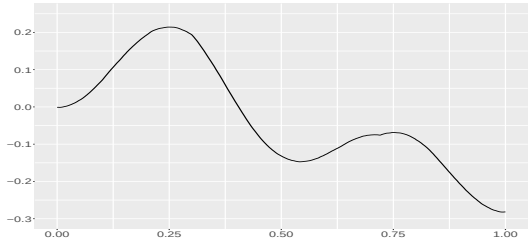

(i) Reconstruction by V-spline with conventional penalty term

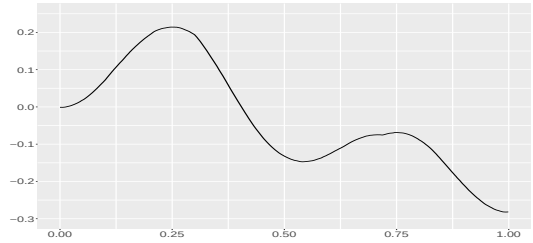

(j) Reconstruction by the proposed V-spline

Figure 2.4: Numerical example: *HeaviSine*. Comparison of different reconstruction methods with simulated data.

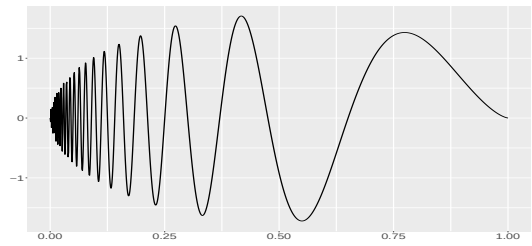

(a) True *Doppler* function

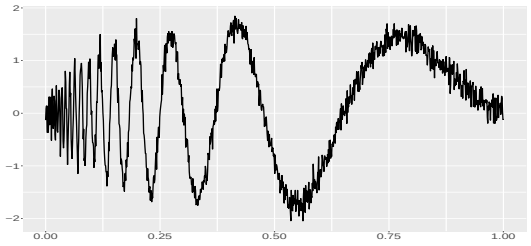

(b) Noisy *Doppler* at SNR=7

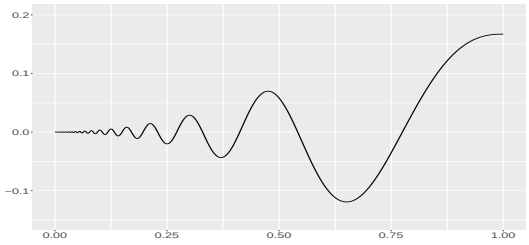

(c) Generated positions

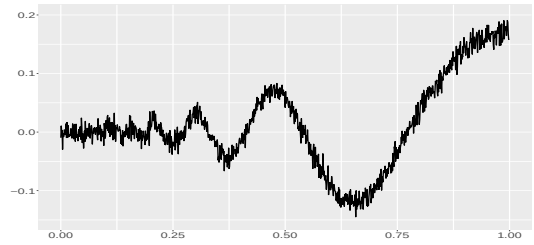

(d) Noisy position at SNR=7

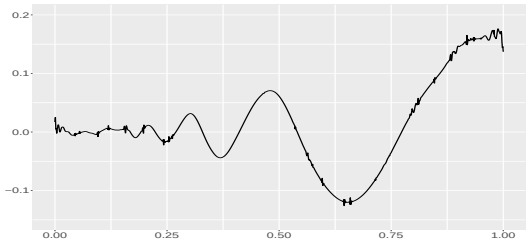

(e) Reconstruction from Wavelet by sure threshold

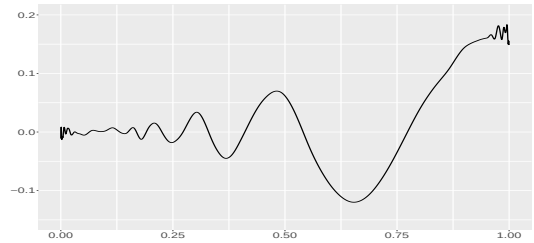

(f) Reconstruction from Wavelet by BayesThresh approach

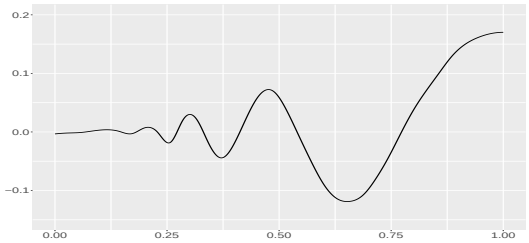

(g) Reconstruction by P-spline

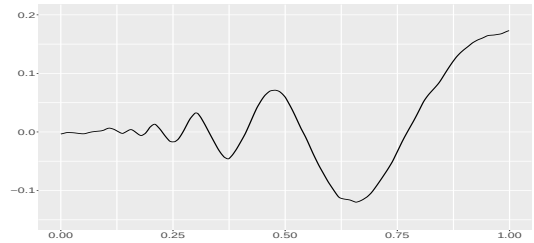

(h) Reconstruction by V-spline setting $\gamma = 0$

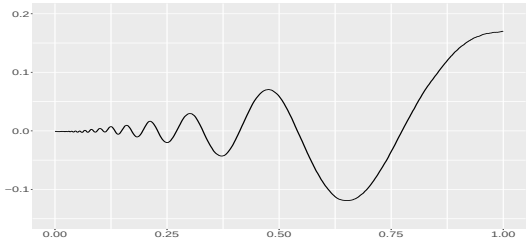

(i) Reconstruction by V-spline with conventional penalty term

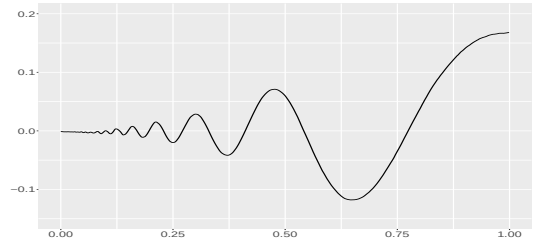

(j) Reconstruction by the proposed V-spline

Figure 2.5: Numerical example: *Doppler*. Comparison of different reconstruction methods with simulated data

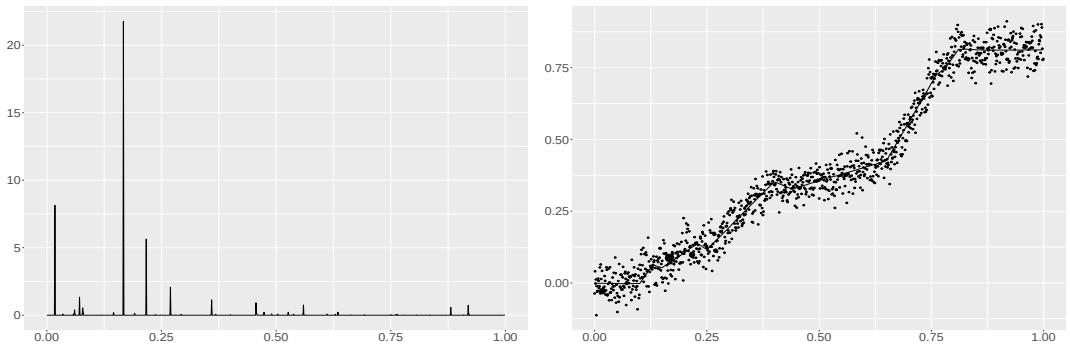

(a) Distribution of the penalty values in reconstructed *Blocks*

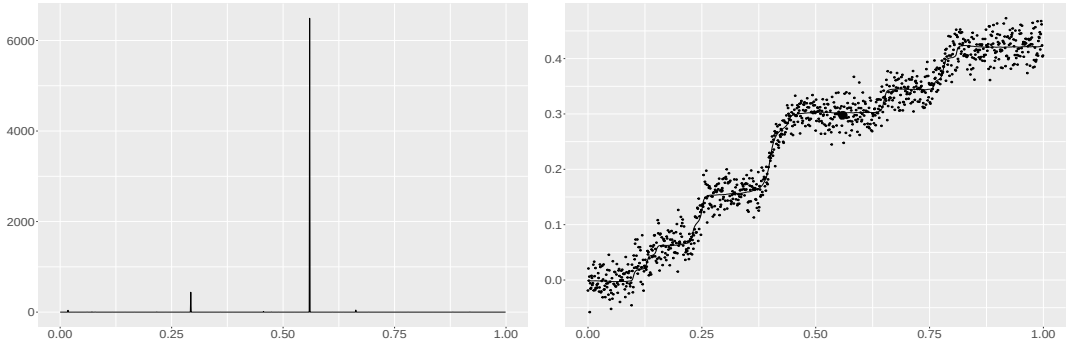

(b) Distribution of the penalty values in reconstructed *Bumps*

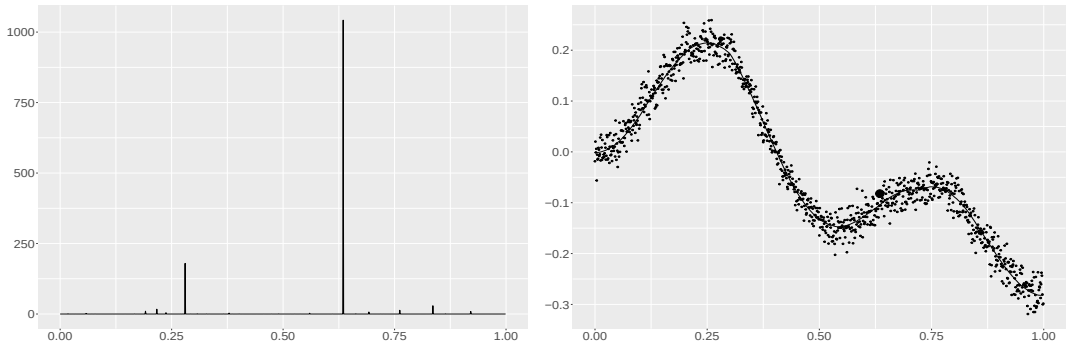

(c) Distribution of the penalty values in reconstructed *HeaviSine*

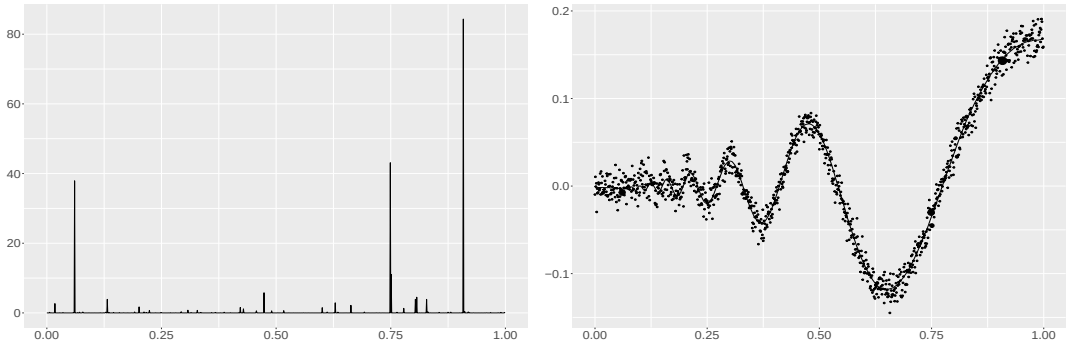

(d) Distribution of the penalty values in reconstructed *Doppler*

Figure 2.6: Distribution of the penalty values $\lambda(t, \eta)$ in V-spline. Figures on the left side indicate the values varying in intervals. On the right side, these values are projected into reconstructions. The bigger the blacks dots present, the larger the penalty values are.

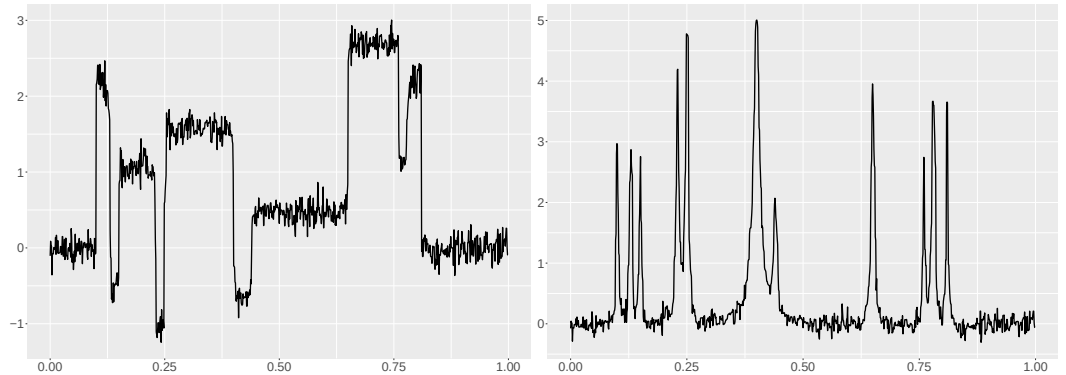

(a) Estimated *Blocks* (b) Estimated *Bumps*

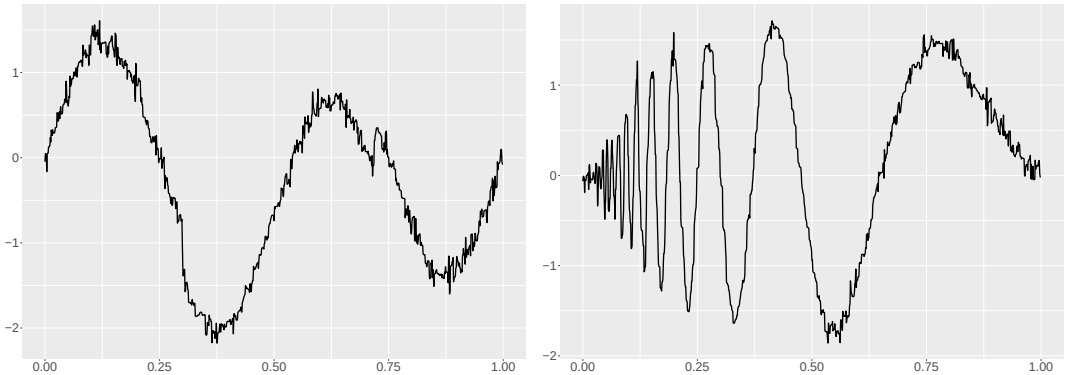

(c) Estimated *HeaviSine* (d) Estimated *Doppler*

Figure 2.7: Estimated velocity functions by V-spline. The velocity is generated from the original simulation functions by equation (2.42)

bigger black dots present larger penalty values. It can be seen that $\lambda(t, \eta)$ adapts to the smoothness pattern of position and will be large where a long time gap may occur. The details of how this penalty function works will be explained in next subsection. Figure A.1 illustrates the reconstructions of V-spline at SNR=3.

Figure 2.7 demonstrates the estimated velocity functions. By taking the first derivative of fitted V-spline, it is simple to get the original four velocity functions. The fittings of velocity are not as smooth as that of position, because we only care about the smoothness of position rather than velocity in our cross-validation formula (2.37). However, velocity information does help us in reconstructing the trajectory.

Evaluation

To examine the performance of the V-spline, we conduct a evaluation by comparing the mean squared errors and true mean squared errors, which are respectively calculated

Table 2.1: MSE. Mean squared errors of different methods. The numbers in bold indicate the least error among these methods under the same level. The difference is not significant.

MSE (10^{-4})	SNR	V-spline	$VS_{\gamma=0}$	$VS_{APT=0}$	P-spline	W(sure)	W(Bayes)
Blocks	7	16.53	15.99	16.69	16.14	**15.39**	16.68
	3	89.79	**87.64**	89.94	88.27	98.35	90.24
Bumps	7	4.40	4.19	4.55	4.33	**4.18**	4.59
	3	23.93	**23.19**	24.10	23.55	26.23	23.74
HeaviSine	7	4.16	4.01	4.16	4.02	**3.79**	4.19
	3	22.63	**22.19**	22.65	22.02	23.53	22.07
Doppler	7	1.15	**1.07**	1.10	1.15	**1.07**	1.13
	3	6.27	**5.94**	6.28	6.05	6.85	6.29

with the following formulas:

$$\text{MSE} = \frac{1}{n}\sum_{i=1}^{n}\left(y_i - \hat{f}_{\eta,\gamma}(t_i)\right)^2, \tag{2.46}$$

$$\text{TMSE} = \frac{1}{n}\sum_{i=1}^{n}\left(f(t_i) - \hat{f}_{\eta,\gamma}(t_i)\right)^2. \tag{2.47}$$

The results are shown in Tables 2.1 and 2.2. All of these methods have good performances in fitting noisy data. The differences of mean squared error between these methods are not significant, as can be seen from Table 2.1. The proposed method is not the best among these simulations according to MSE. However, from Table 2.2, V-spline returns the smallest true mean squared errors. The difference is significant, that means the reconstruction from V-spline is closer to the true trajectory.

Residual Analysis

The simulated data is generated by equations (2.43) and the SNRs are set at 7 and 3 separately to compare the performances of different algorithms. All of the algorithms can reconstruct the true trajectory from noisy data and return acceptable MSE values, though V-spline returns the least TMSE in most of the circumstances.

Table 2.3 is comparing the capability of V-spline in retrieving the true SNR. The measurements are generated from f and g with predefined SNR. The V-spline reconstructs the true trajectory and retrieves the SNR value, both of which are close to the truth.

Table 2.2: TMSE. True mean squared errors of different methods. The numbers in bold indicate the least error among these methods under the same level. The proposed V-spline returns the smallest TMSE among all the methods under the same level except for *Doppler* with SNR=7. The differences are significant.

TMSE (10^{-6})	SNR	V-spline	$\text{VS}_{\gamma=0}$	$\text{VS}_{\text{APT}=0}$	P-spline	W(sure)	W(Bayes)
Blocks	7	**1.75**	54.25	28.68	54.76	201.02	182.12
	3	**16.44**	152.5	30.76	171.59	1138.08	712.36
Bumps	7	**1.64**	23.44	21.10	24.21	71.71	69.26
	3	**8.51**	77.78	37.12	77.52	330.77	238.79
HeaviSine	7	**1.53**	7.80	1.56	9.54	55.37	44.88
	3	**8.21**	33.56	8.49	34.26	240.72	110.49
Doppler	7	1.51	6.67	**1.08**	8.26	14.87	12.01
	3	**8.10**	22.14	8.25	19.95	81.48	50.33

Table 2.3: Retrieved SNR. V-spline effectively retrieves the SNR, which is calculated by $\sigma_{\hat{f}}/\sigma_{(\hat{f}-y)}$.

SNR	predefined value	generated f	V-spline $\hat{f}$
Blocks	7	6.9442	6.9485
	3	2.9761	2.9817
Bumps	7	6.9442	6.9548
	3	2.9761	2.9953
HeaviSine	7	6.9442	6.9207
	3	2.9761	2.9706
Doppler	7	6.9442	6.8757
	3	2.9761	2.9625

Further analysis in Figures A.2 and A.3 shows that the residuals from V-splines are independent.

2.4.2 Irregularly Sampled Time Series Data

A set of irregularly sampled time series data has different time differences between each pair of successive points. The distribution of ΔT_i is not uniform.

In this section, it is shown that the proposed V-spline has the ability to reconstruct the true trajectory even though the data is irregularly sampled. With the same functions that are used in the previous section, we firstly generate the simulation data of length $n = 1024$. Then we draw a length of 512 subsequence with indices $1, 3, \ldots, 1023$ from the mother data set for regularly sampled points and another 512 random indices for irregularly sampled points. See Figure 2.8.

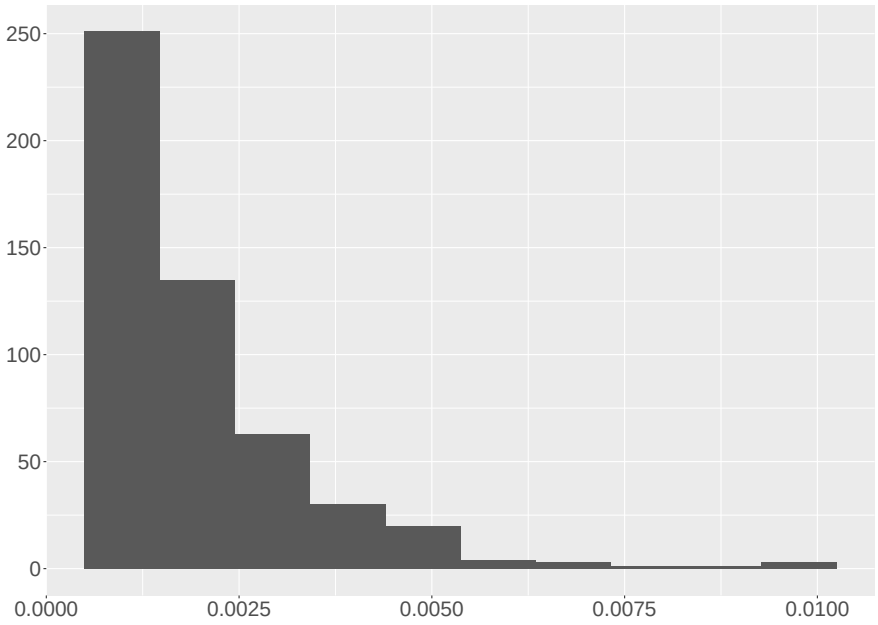

Figure 2.8: Histogram of ΔT for irregularly sampled data

The reconstructions of regularly and irregularly sampled data are very competitive.

Table 2.4: Retrieved SNR of reconstructions from regularly and irregularly sampled data

SNR	Regularly	Irregularly
Blocks	7.0479	6.8692
Bumps	7.0241	7.1937
HeaviSine	7.2367	6.8793
Doppler	6.8692	7.3645

Table 2.5: MSE and TMSE of reconstructions from regularly and irregularly sampled data

	MSE $\times 10^{-4}$		TMSE $\times 10^{-6}$	
	Regularly	Irregularly	Regularly	Irregularly
Blocks	8.0260	8.3358	3.5197	10.8596
Bumps	2.1374	2.0203	1.6662	6.2586
HeaviSine	2.0232	2.1272	1.1275	1.1077
Doppler	0.5251	0.5219	1.0101	1.7832

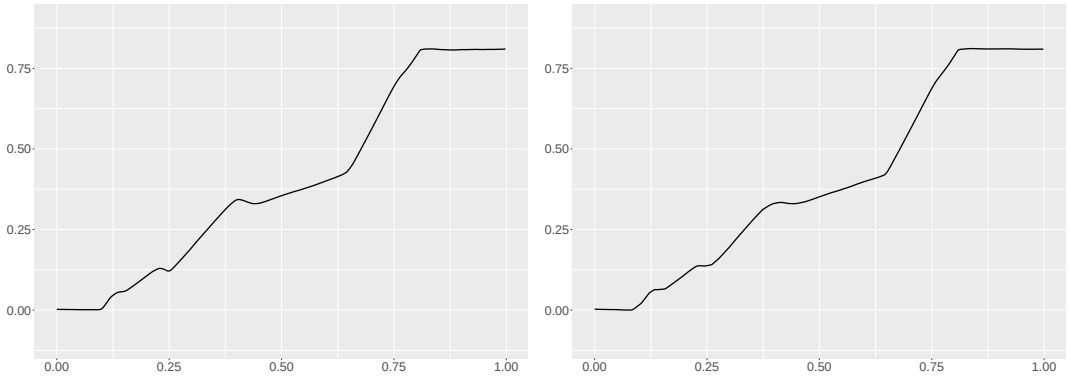

(a) Reconstruction of *Blocks* from regularly and irregularly sampled data

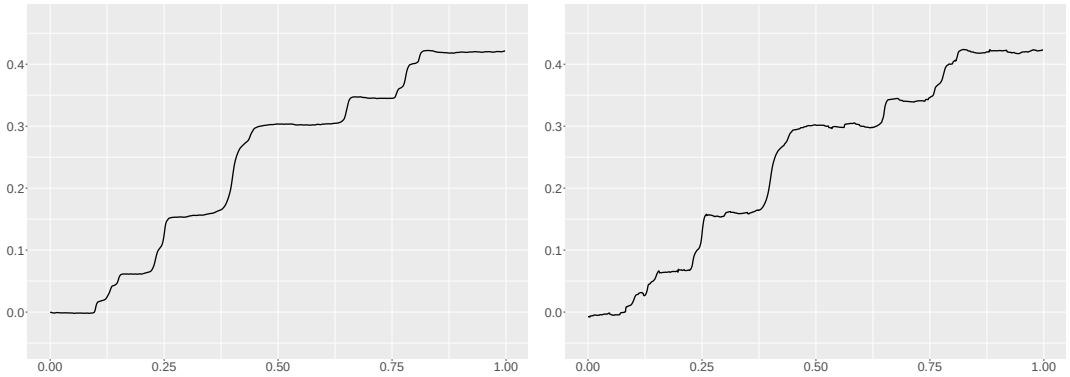

(b) Reconstruction of *Bumps* from regularly and irregularly sampled data

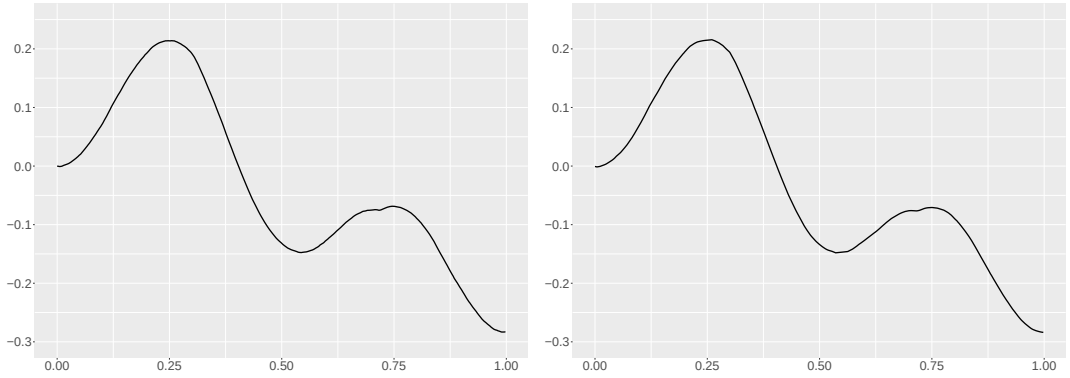

(c) Reconstruction of *HeaviSine* from regularly and irregularly sampled data

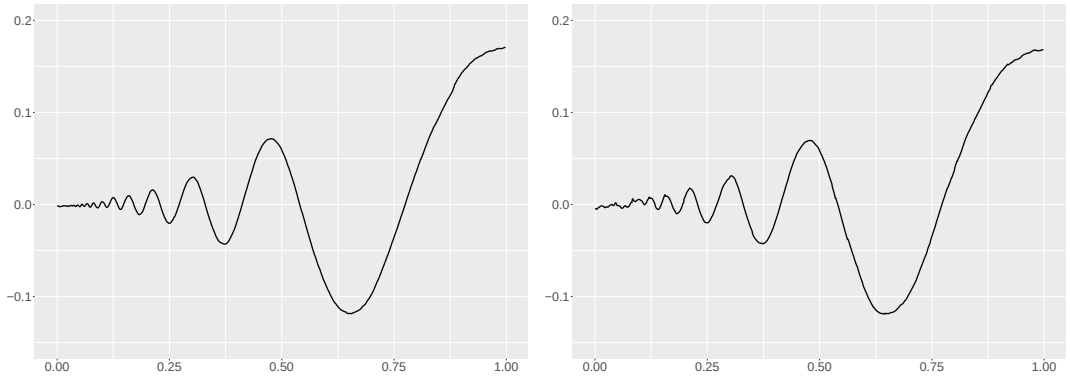

(d) Reconstruction of *Doppler* from regularly and irregularly sampled data

Figure 2.9: Comparison of regularly and irregularly sampled data

2.5 Inference of Tractor Trajectories

In the real life application, the movement of vehicles or tractors has complicated features. The velocity of a moving object looks like a combination of the original bumps and blocks functions: it is a turbulent waves fluctuating around zero. In this section, we apply the proposed V-spline to real data set, which is recorded by a GPS unit mounted on a tractor. The original data set contains the information about time marks, longitude, latitude, velocity, bearing (in degrees, heading to North) and boom status. The data is not regularly recorded and the time difference has a high variance.

In a two or higher d-dimensional curve nonparametric regression, consider the general form of a length n time series data points $\{t_1, p_1, s_1\}, \ldots, \{t_n, p_n, s_n\}$, such that $a \leq t_1 < t_2 < \cdots < t_n \leq b$, p_i and s_i are d-dimensional vectors contain position and velocity information at time i respectively. The positive piecewise constant function $\lambda(t) = \lambda_i$ on each interval $t_i \leq t < t_{i+1}, t_0 = a, t_{n+1} = b$. Then function $f : [a, b] \mapsto \mathbb{R}^d$ with $\gamma > 0$ is a V-spline in the d-dimensional space if it is the solution to the generic form of the objective function:

$$J[f] = \frac{1}{n}\sum_{i=1}^{n}\|f(t_i) - p_i\|_d^2 + \frac{\gamma}{n}\sum_{i=1}^{n}\|f'(t_i) - s_i\|_d^2 + \sum_{i=0}^{n}\lambda_i \int_{t_i}^{t_{i+1}} \|f''(t)\|_d^2 dt. \qquad (2.48)$$

Particularly, GPS data is recorded in two directions, easting and northing. In this situation $d = 2$. Hence, in the following application, we split the 2-dimensional function $f(x, y)$ into two sub-functions $f_x(t)$ on x-axis (easting direction) and $f_y(t)$ on y-axis (northing direction) with respect to time t. Compared with other parameters, choosing time t to be the parameter has some advantages: (i) the expressions of all the constraints are simpler (Zhang *et al.*, 2013); (ii) it can be simply applied from 2-dimension to 3-dimension by adding an extra z-axis, such as altitude. Without loss of generality, a data set in a higher dimensional space can be projected into several sub-spaces, such as $p = \{x, y, z, \ldots\}$ and $s = \{u, v, w, \ldots\}$.

Thereafter, we convert the longitude and latitude information from a 3D sphere to 2D surface first by *Universal Transverse Mercator coordinate system* (UTM) and then project the speed s into u and v on x-axis and y-axis respectively by

$$u = s \cdot \sin\left(\omega \frac{\pi}{180}\right), \qquad (2.49)$$

$$v = s \cdot \cos\left(\omega \frac{\pi}{180}\right), \qquad (2.50)$$

where ω is bearing in degrees. Boom status is tagged as 0 if it is not operating and 1 if it is. Time marks are transformed by subtracting the first mark, in which way the

time starts from 0. Time duplicated data, caused by errors, have been removed from the data set[1]. For the convenience of comparing with wavelet algorithm, we choose the first 512 out of 928 rows of data. The original measurements are plotted in Figure 2.10.

In order to fit the real data, we bring the parameter η_d to our model. Then, we are now having three parameters η_d and η_u regarding boom status and γ controlling velocity residuals. The criteria of a good fitting are that it can catch more information, recognize time gaps between two points where tractor stops and return a smaller MSE.

2.5.1 1-Dimensional Trajectory Reconstruction

We treat x and y position separately and compare how the velocity information and the adjusted penalty term of equation (2.30) work in our model. All parameters in fitted V-spline are automatically selected by cross-validation by equation (2.37). Figure 2.11 and Figure 2.12 compare the results of fitted methods on x and y axes. P-spline gives over-fitting on x axis reconstruction and not applicable on y axis due to errors. Wavelet(sure) misses some key points at corners when a tractor tries to turn around. V-spline without adjusted penalty term presents less fitting at time gap knots, where time marks keep increasing while position stays the same and velocity is 0. If we take the last knot p_k before and the first knot p_{k+1} after the time gap, Hermite spline basis will use y_k, v_k, y_{k+1} and v_{k+1} to build up a cubic spline, even though the velocity information is not useful. That is why we got a curve rather than a straight line. Wavelet(BayesThresh), V-spline without velocity and proposed V-spline give acceptable results.

Table 2.6 illustrates the MSE of all methods on both x and y axes. The proposed V-spline returns the least errors among all methods.

The penalty function of the proposed V-spline is

$$\lambda(t) = b\frac{(\Delta T)^3}{(\Delta d)^2}\eta_d + (1-b)\frac{(\Delta T)^3}{(\Delta d)^2}\eta_u, \text{ where } \begin{cases} b = 1 & \text{if boom is operating} \\ b = 0 & \text{if boom is not operating} \end{cases} \tag{2.51}$$

To explain the differences more clearly, we take $\lambda(t)$ in our demonstration. Figure 2.13 indicates that at turning points and long time gap knots, the adjusted penalty term will lead $\lambda(t)$ to large values, which forces the spline to be a straight line between two

[1]In some cases, further data simplification to remove spurious or non-informative observations may be warranted. In Appendix C, we introduce a new data simplification method for vehicle trajectories which compares favorably with Douglas-Peucker algorithm.

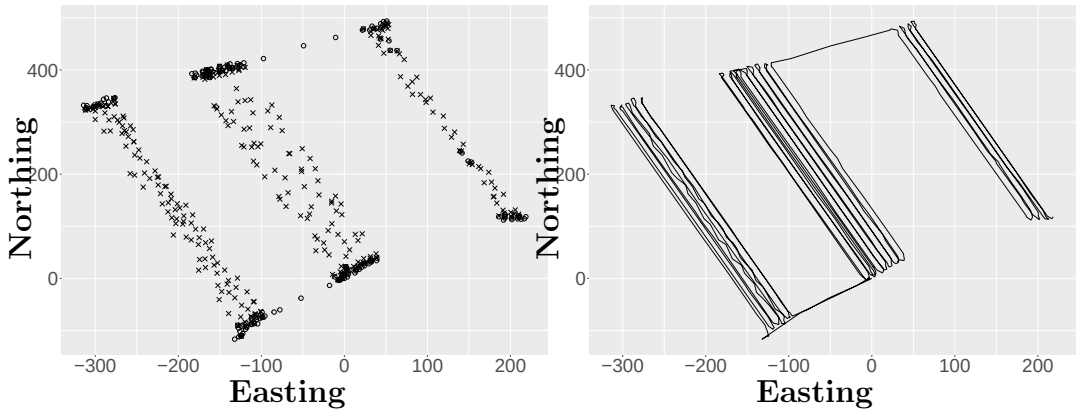

(a) Original positions

(b) Line-based trajectory

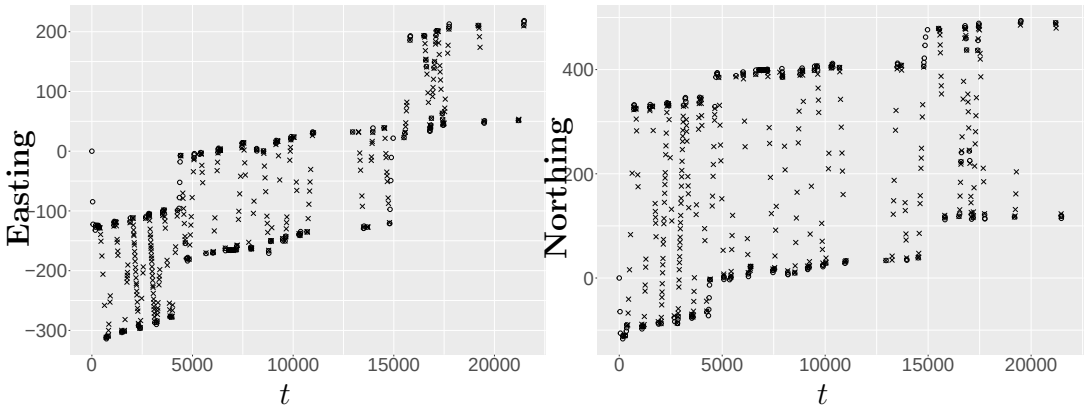

(c) Original positions on easting direction (x-axis)

(d) Original positions on northing direction (y-axis)

Figure 2.10: Original data points. Figure 2.10a is the original positions recorded by GPS units. Circle points means the boom is not operating; cross points means it is operating. Figure 2.10b is the line-based trajectory by simply connecting all points sequentially with straight lines. Figure 2.10c is the original x position. Figure 2.10d is the original y positions.

Table 2.6: Mean squared error. V-spline returns smallest errors among all these methods. P-spline was unable to reconstruct the y trajectory as the original data set contains 0 Δ_y.

MSE	V-spline	$VS_{\gamma=0}$	$VS_{APT=0}$	P-spline	W(sure)	W(Bayes)
x	**0.2046**	0.2830	0.3298	2860.5480	256.0494	6.2959
y	**0.0020**	0.3062	0.3115	*NA*	1960.2220	19.3330

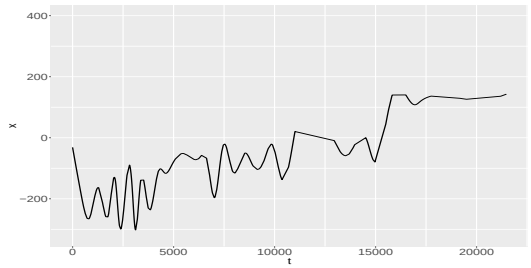

(a) Reconstruction by P-spline

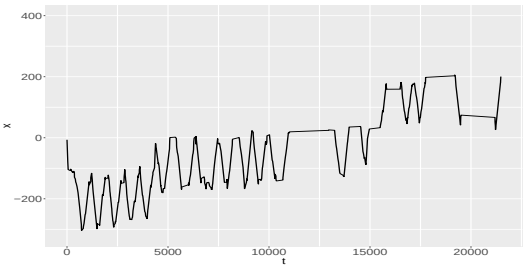

(b) Reconstruction by wavelet (*sure*)

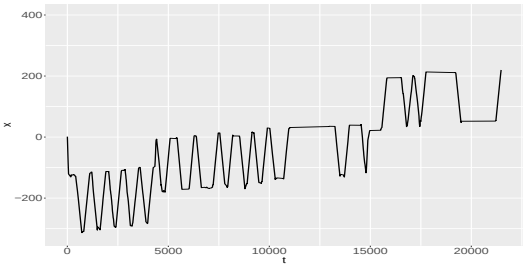

(c) Reconstruction by wavelet (*Bayes*)

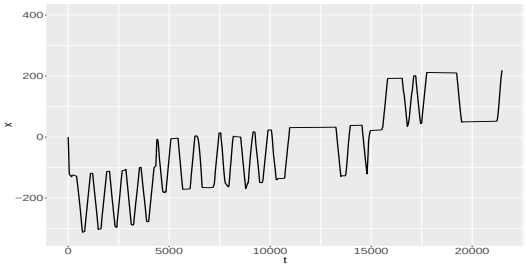

(d) Reconstruction by V-spline setting $\gamma = 0$

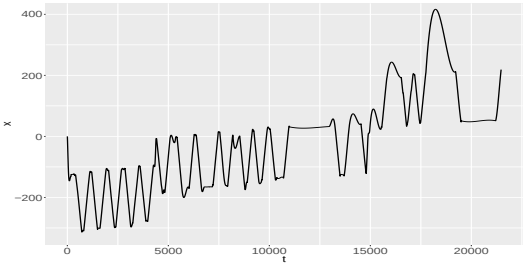

(e) Reconstruction by V-spline setting with conventional penalty term

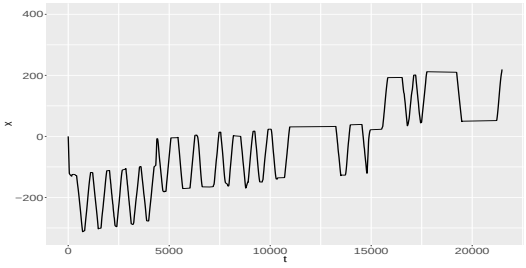

(f) Reconstruction by proposed V-spline

Figure 2.11: Fitted data points on x axis. Figure 2.11a Fitted by P-spline, which gives over-fitting on these points and misses some information. Figure 2.11b Fitted by wavelet (*sure*) algorithm. At some turning points, it gives over-fitting. Figure 2.11c Fitted by wavelet (*BayesThresh*) algorithm. It fits better than (*sure*) and the result is close to the proposed method. Figure 2.11d Fitted by V-spline without velocity information. The reconstruction is good to get the original trajectory. Figure 2.11e Fitted by V-spline without adjusted penalty term. It gives less fitting at boom-not-operating points because of a large time gap. Figure 2.11f Fitted by proposed method. It fits all data points in a good way.

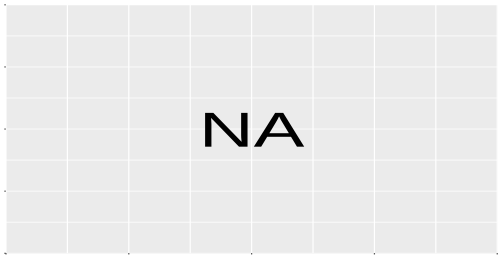

(a) Not available for P-spline

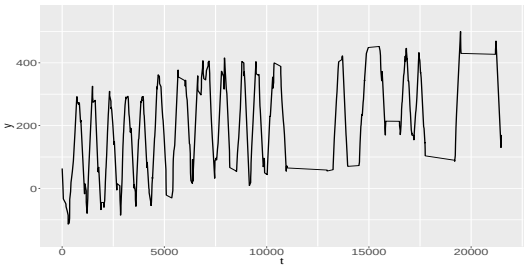

(b) Reconstruction by wavelet (*sure*)

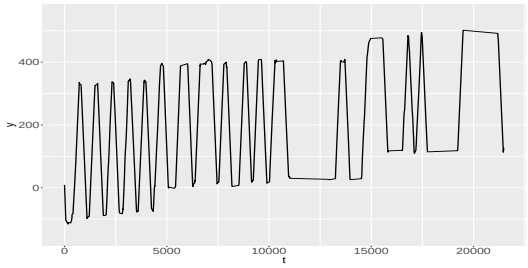

(c) Reconstruction by wavelet (*Bayes*)

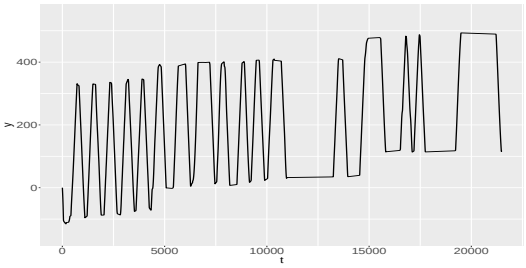

(d) Reconstruction by V-spline setting $\gamma = 0$

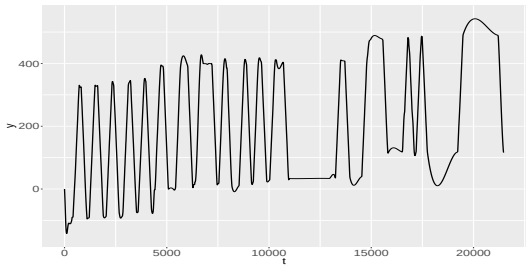

(e) Reconstruction by V-spline setting with conventional penalty term

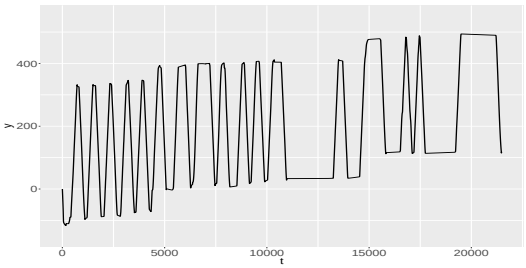

(f) Reconstruction by proposed V-spline

Figure 2.12: Fitted data points on y axis. Figure 2.12a Fitted P-spline is not applicable on y axis as the matrix is not invertible. Figure 2.12b Fitted by wavelet (*sure*) algorithm. At some turning points, it gives over-fitting. Figure 2.12c Fitted by wavelet (*BayesThresh*) algorithm is much better than wavelet (*sure*). Figure 2.12d Fitted by V-spline without velocity information. The reconstruction is good to get the original trajectory. Figure 2.12e Fitted by V-spline without adjusted penalty term. It gives less fitting at boom-not-operating. Figure 2.12f Fitted by proposed method. It fits all data points in a good way.

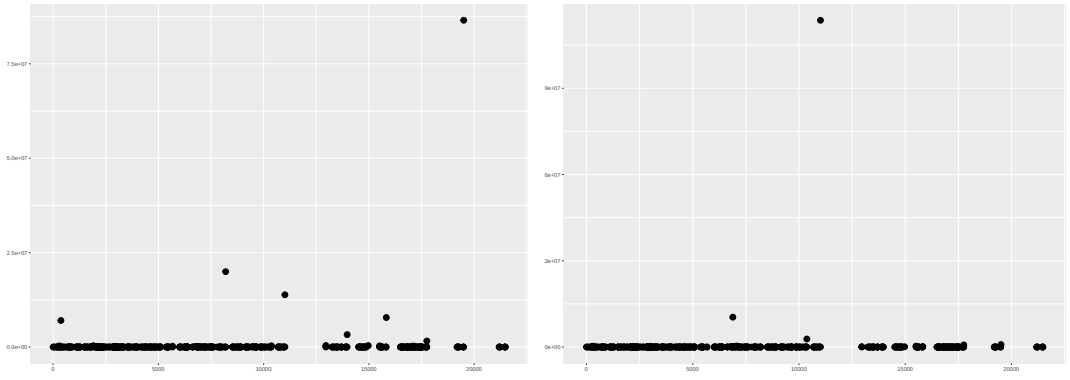

(a) Distribution of the penalty term on x and y

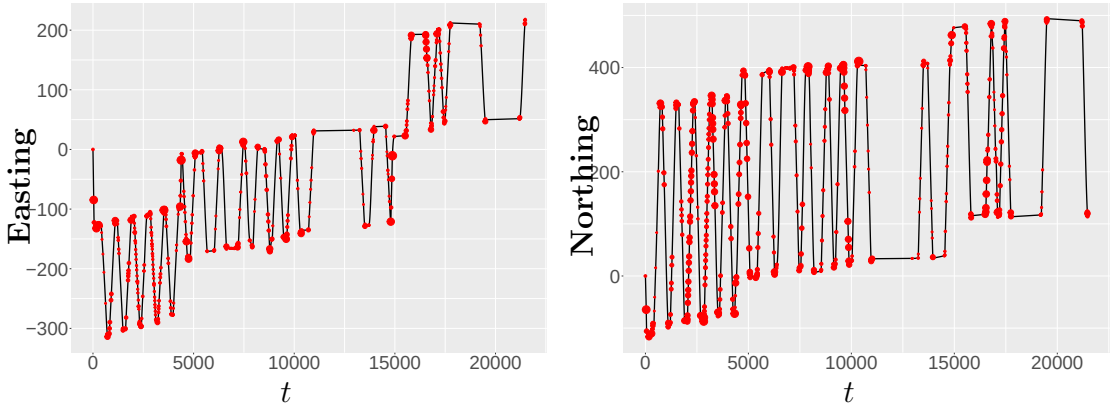

(b) Reconstruction on easting (x) and northing (y) directions separately.

Figure 2.13: The penalty value $\lambda(t)$ of the V-spline on x and y axes. Red dots are the measurements $\mathbf{y}$. The bigger red dots in Figure 2.13b indicate larger penalty values at the points. It can be seen that most of large penalty values occur at turnings, where the tractor likely slows down and takes breaks.

knots. It can be seen in Figure 2.13b clearly. Histogram plots of $\lambda(t)$ show that most of the penalty values are small, which allows the V-spline to go as closer as possible to the observed points. Only a few of penalty values are large, so that V-spline gives a straight line at tricky points.

The 1-dimensional reconstruction gets the best fittings $\hat{f}_x$ and $\hat{f}_y$ on x and y axes separately by using different penalty values, denoted as $\eta_{d,x}$, $\eta_{u,x}$, $\eta_{d,y}$, $\eta_{u,y}$, γ_x and γ_y. The final reconstruction is the combination of $\hat{f}_x$ and $\hat{f}_y$. It is shown in Figure 2.14.

2.5.2 2-Dimensional Trajectory Reconstruction

In a 2-dimensional trajectory reconstruction, different from combined 1-dimensional reconstruction, we use the same parameters λ_d, λ_u and γ for both x and y axes. The

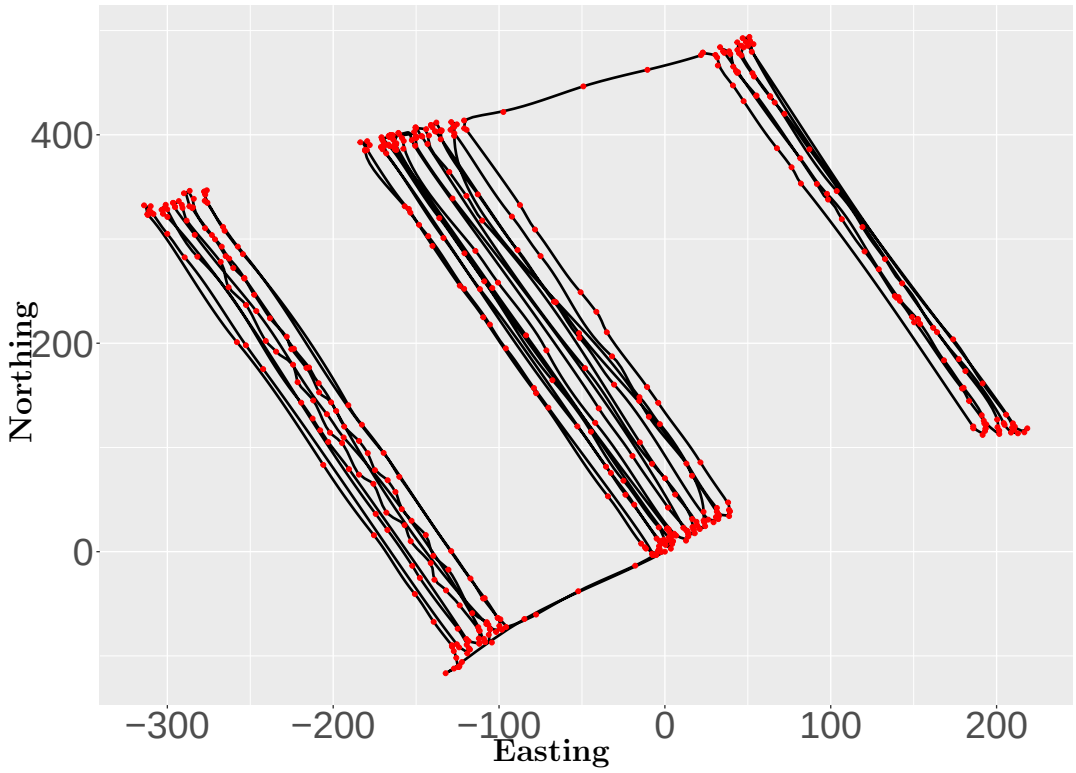

Figure 2.14: Combined reconstruction on easting (x) and northing (y) directions. Red dots are the measurements. The bigger size indicates larger penalty value at that point.

overall best parameters return the least cross-validation score on all axes. Explicitly, it is calculated by the following formula

$$\mathrm{CV} = \mathrm{CV}_x + \mathrm{CV}_y. \tag{2.52}$$

In the adjusted penalty term, Δd is the Euclidean distance $\Delta_d(p_1, p_2) = \sqrt{(\Delta x)^2 + (\Delta y)^2}$ between two positions on the 2D surface. Similar to 1-dimensional reconstruction, the velocity information keeps trajectory in the right direction and the penalty term makes sure that the crazy curve will disappear between long-time-gap points. Figure 2.15 demonstrates the complete 2D reconstruction of the whole data set.

The penalty function $\lambda(t)$ of a 2-dimensional reconstruction is shared by x and y axes and presented in Figure 2.16. The complete penalty term is

$$n\theta_x^\top \Omega_{\eta_d,\eta_u} \theta_x + n\theta_y^\top \Omega_{\eta_d,\eta_u} \theta_y. \tag{2.53}$$

Similarly, most of the large penalty values appear at long-time-gap knots and turning points. A histogram plot of penalty function shows that most of the values are small and only a couple of them are large.

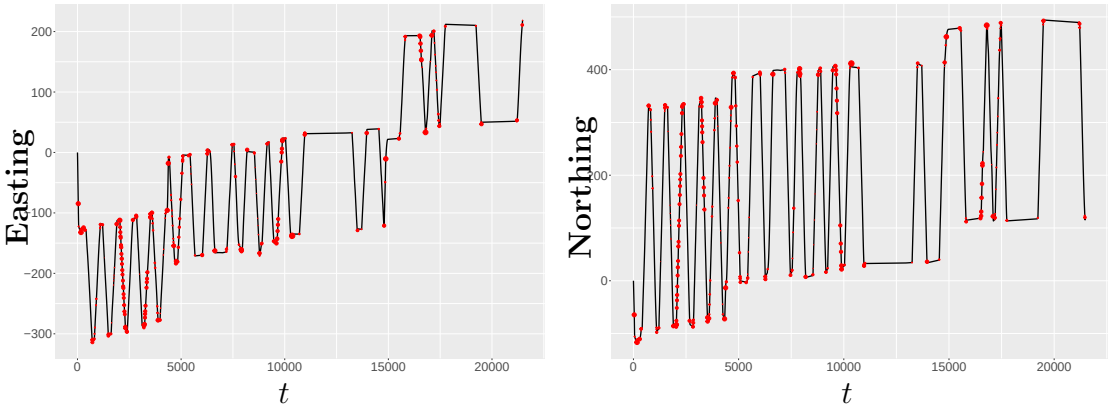

(a) 2-dimensional reconstruction on easting (x) and northing (y) directions separately.

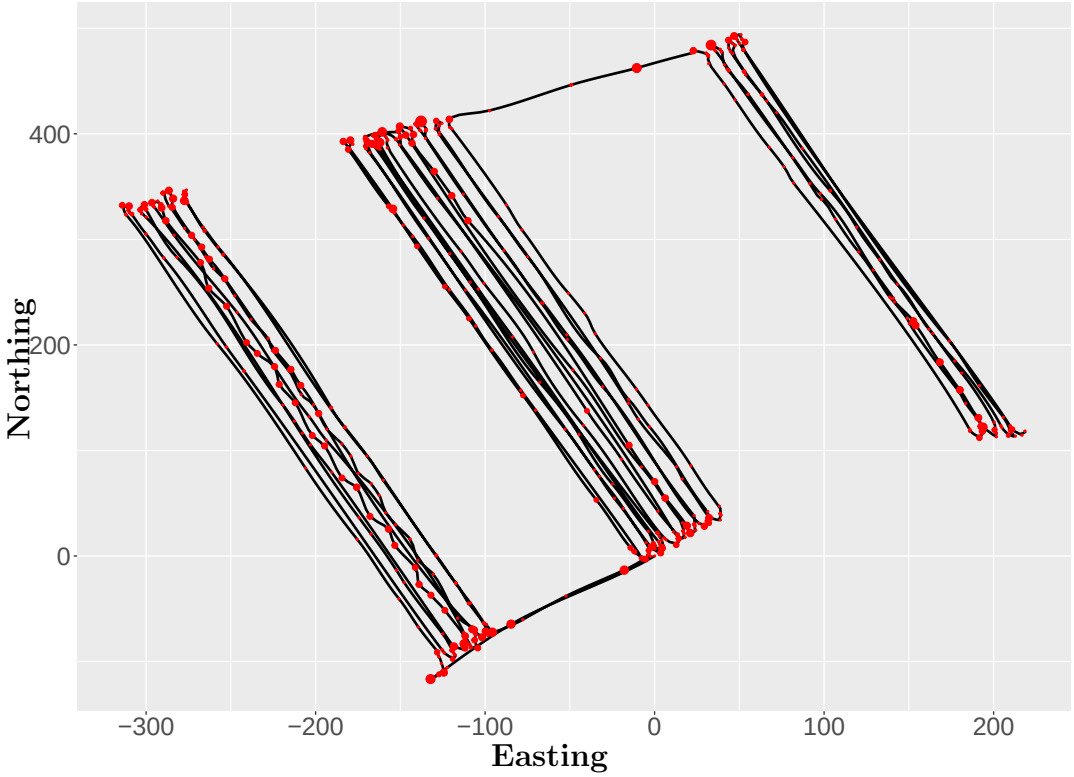

(b) Combined 2-dimensional reconstruction.

Figure 2.15: 2-dimensional reconstruction. Larger dots indicate bigger values of penalty function $\lambda(t)$.

The following Figure 2.17 is a complete reconstruction from the whole observed data set $\{x, u, y, v\}$. The overall reconstruction gives a smoothing path that goes through each measurement and avoids curvatures at turning points.

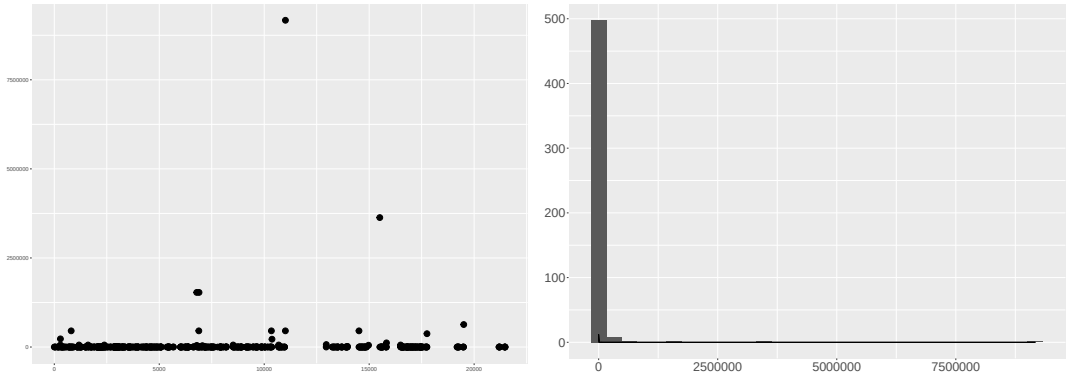

Figure 2.16: Penalty value of $\lambda(t)$ in 2-dimensional reconstruction.

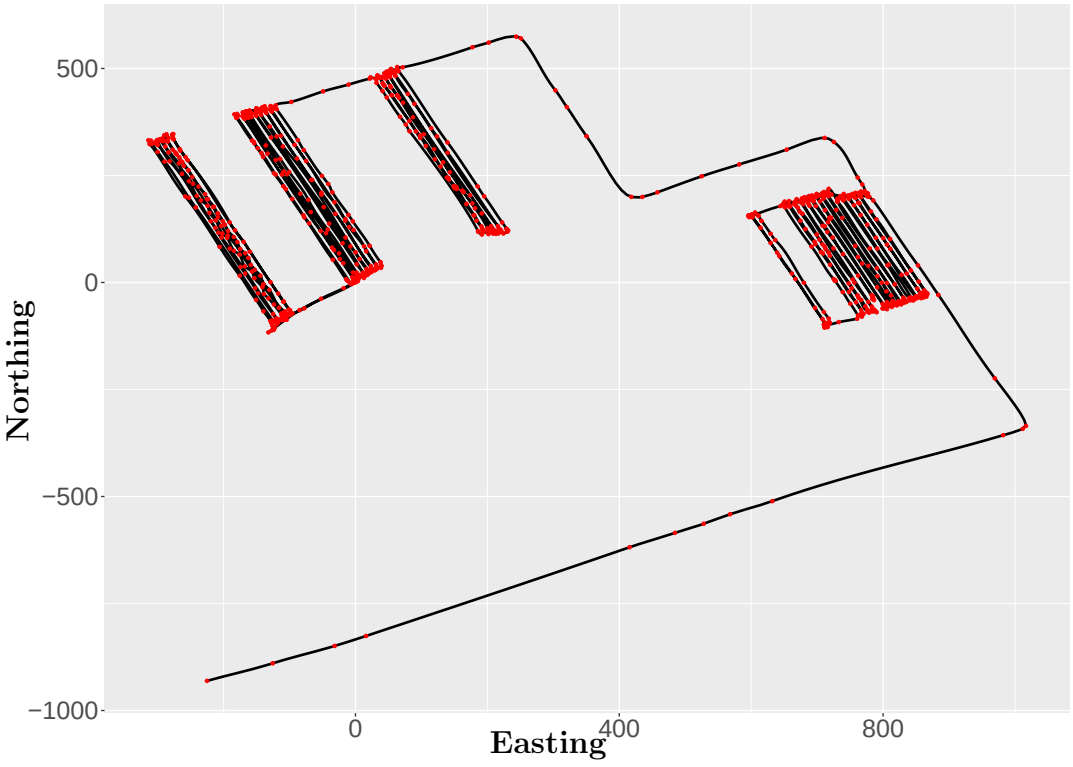

Figure 2.17: A complete 2-dimensional reconstruction on both easting and northing directions. Red dots are the measurements.

2.6 Conclusion and Discussion

In this chapter, a V-spline model is proposed to solve the objective function, which is consisting of both position and velocity information. The adjusted penalty function adapts to complicated curvatures. In a d-dimensional space, V-spline can be projected into sub-spaces with respect to t and combined each solution together as a final. This method performs better when we know the position and velocity information than

other methods.

Additionally, the reconstruction of a V-spline contains $4 \times (n-1)$ parameters if we have n knots. By adding $2 \times (n-2)$ constraints, the original function, and its first derivative are continuous at each interior knots, the degrees of freedom will be $4 \times (n-1) - 2 \times (n-2) = 2n$. Because there are n position and n velocity points, we do not need to specify more parameters or add more constraints to the model.

In our experimental studies, the MSE of the V-spline were neither significantly better or worse than other methods. However, its true MSE was significantly less.

In parameter selection, the cross-validation only focuses on the errors of f ignoring that in f'. So the reconstruction of f' is not as smooth as that of f, which does not affect trajectory reconstruction. A drawback of V-spline is that the computing time in finding local minimal CV score is more than B-spline. If there is an efficient way to compute matrix inverse, the calculation speed will be much faster. So in the simulation and application studies, we try to optimize our coding to make it run as faster as possible.

Another potential application of V-spline is to vessel monitoring system. The system is a fisheries surveillance that allows environmental and fisheries regulatory organization to track and monitor the activities of fishing vessels. The system calculates the position of the moving object and sends a data report to shore-side users. This information includes time, latitude and longitude positions. However, due to weak signals, the tracking system may lose useful information. The V-spline can help to reconstruct the whole trajectory for a fishery vessel and to analyze its behavior. For example, a larger penalty value indicates stops on the sea inferring that the vessel is casting nets; a smaller penalty value indicates the vessel is moving normally.

After all, there is a wide range of applications for V-spline in real life. A future work is to implement V-spline on-line for instant estimation and to make it run faster.

Chapter 3

V-Spline as Bayes Estimate

3.1 Introduction

A Hilbert space is a real or complex inner product space with respect to the distance function induced by the inner product (Dieudonné, 2013). In particular, the Hilbert space $\mathcal{L}_2[0,1]$ is the set of square integrable functions $f(t) : [0,1] \mapsto \mathbb{R}$, where all functions satisfy

$$\mathcal{L}_2[0,1] = \left\{ f : \int_0^1 f^2 dt < \infty \right\} \tag{3.1}$$

with an inner product $\langle f, g \rangle = \int_0^1 fg dt$.

Consider a regression problem with observations modeled as $y_i = f(t_i) + \varepsilon_i$, $i = 1, \ldots, n$, where $\varepsilon_i \sim N(0, \sigma^2)$ are i.i.d. Gaussian noise and $f \in \mathcal{C}^{(m)}[0,1] = \{f : f^{(m)} \in L_2[0,1]\}$. The classic nonparametric or semi-parametric regression is a function that minimizes the following penalized sum of squares functional

$$\frac{1}{n} \sum_{i=1}^{n} \left(y_i - f(t_i)\right)^2 + \lambda \int_0^1 \left(f^{(m)}\right)^2 dt, \tag{3.2}$$

where the first term is the lack of fit of f to the data. The parameter λ in the second term is a fixed smoothing parameter controlling the trade-off between over-fitting and bias (Hastie *et al.*, 2009). The minimizer f_λ of the above equation resides in an n-dimensional space and the computation in multivariate settings is generally of the order $\mathrm{O}\left(n^3\right)$ (Kim and Gu, 2004). Schoenberg (1964) shows that a piecewise polynomial smoothing spline of degree $2m-1$ provides an aesthetically satisfying method for estimating f if $\mathbf{y}$ cannot be interpolated exactly by some polynomial of degree less than m. For instance, when $m = 2$, a piecewise cubic smoothing spline provides a

powerful tool to estimate the above nonparametric function, in which the penalty term is $\int f''^2 dt$ (Hastie and Tibshirani, 1990).

Further, Wahba (1978) shows that a Bayesian version of this problem is to take a Gaussian process prior $f(t_i) = a_0 + a_1 t_i + \cdots + a_{m-1} t_i^{m-1} + x_i$ on f with $x_i = X(t_i)$ being a zero-mean Gaussian process whose mth derivative is scaled white noise, $i = 1, \ldots, n$ (Speckman and Sun, 2003). The extended Bayes estimates f_λ with a "partially diffuse" prior is exactly the same as the spline solution. Heckman and Woodroofe (1991) show that if prior distribution of the vector $\mathbf{f} = (f(t_1), \ldots, f(t_n))^\top$ is unknown but lies in a known class Ω, the estimator $\hat{f}$ is found by minimizing the $\max \mathrm{E}[\hat{f} - f]^2$. Branson *et al.* (2017) propose a Gaussian process regression method that acts as a Bayesian analog to local linear regression for sharp regression discontinuity designs. It is no doubt that one of the attractive features of the Bayesian approach is that, in principle, one can solve virtually any statistical decision or inference problem. Particularly, one can provide an accuracy assessment for $\hat{f} = \mathrm{E}(f \mid \mathbf{y})$ using posterior probability regions (Cox, 1993).

Based on the correspondence between nonparametric regression and Bayesian estimation, Craven and Wahba (1978) propose an generalized cross-validation estimate for the minimizer f_λ. The estimate $\hat{\lambda}$ is the minimizer of the function where the trace of matrix $A(\lambda)$ in (2.33) is incorporated. It is also possible to establish an optimal convergence property for the estimator when the number of observations in a fixed interval tends to infinity (Wecker and Ansley, 1983). A highly efficient algorithm to optimize generalized cross-validation and generalized maximum likelihood scores with multiple smoothing parameters via the Newton method was proposed by Gu and Wahba (1991). This algorithm can also be applied to maximum likelihood estimation and restricted maximum likelihood estimation. The behavior of the optimal regularization parameter in different regularization methods was investigated by Wahba and Wang (1990).

In this chapter, it is proved that the V-spline can be estimated by a Bayesian approach in a certain reproducing kernel Hilbert space. An extended GCV is used to find the optimal parameters for the V-spline.

3.2 Polynomial Smoothing Splines on $[0, 1]$ as Bayes Estimates

A polynomial smoothing spline of degree $2m - 1$ is a piecewise polynomial of the same degree on each interval $[t_i, t_{i+1})$, $i = 1, \ldots, n-1$, and the first $2m - 2$ derivatives

are continuous at the knots. For instance, when $m = 2$, a piecewise cubic smoothing spline is a special case of the polynomial smoothing spline providing a powerful tool to estimate the above nonparametric function (3.2) in the space $\mathcal{C}^{(2)}[0,1]$, where the penalty term is $\int f''^2 dt$ (Hastie and Tibshirani, 1990; Wang, 1998). If a general space $\mathcal{C}^{(m)}[0,1]$ is equipped with an appropriate inner product, it can be made into a reproducing kernel Hilbert space.

3.2.1 Polynomial Smoothing Spline

A spline is a numeric function that is piecewise-defined by polynomial functions, which possesses a high degree of smoothness at the places where the polynomial pieces connect (known as knots) (Judd, 1998; Chen, 2017). Suppose we are given observed data $(t_1, y_1), (t_2, y_2), \ldots, (t_n, y_n)$ in the interval $[0,1]$, satisfying $0 < t_1 < t_2 < \cdots < t_n < 1$, a piecewise polynomial function $f(t)$ can be obtained by dividing the interval into contiguous intervals $(t_1, t_2), \ldots, (t_{n-1}, t_n)$ and represented by a separate polynomial on each interval. For any continuous $f \in \mathcal{C}^{(m)}[0,1]$, it can be represented in a linear combination of basis functions $h_m(t)$ as $f(t) = \sum_{m=1}^{M} \beta_m h_m(t)$, where β_m are coefficients (Ellis *et al.*, 2009). It is just like every vector in a vector space can be represented as a linear combination of basis vectors.

A smoothing polynomial spline is uniquely the smoothest function that achieves a given degree of fidelity to a particular data set (Whittaker, 1922). In deed, the minimizer of function (3.2) is the curve estimate $\hat{f}(t)$ over all spline functions $f(t)$ with $m-1$ continuous derivatives fitting observed data in the space $\mathcal{C}^{(m)}[0,1]$. In fact, Kimeldorf and Wahba (1971, 1970) prove that the minimizer f_λ of function (3.2) has the following form

$$f(t) = \sum_{\nu=1}^{m} d_\nu \phi_\nu(t) + \sum_{i=1}^{n} c_i R_1(t, t_i). \tag{3.3}$$

where $\{\phi_\nu(t)\}$ is a set of basis functions of space $\mathcal{H}_0$ and $R(\cdot,\cdot)$ is the reproducing kernel in $\mathcal{H}_1$.

Additionally, the coefficients c_i and d_ν might be changed when different ϕ_ν and R_1 are used, but the function estimate remains the same regardless of the choices of ϕ_ν and R_1 (Gu, 2013).

3.2.2 Reproducing Kernel Hilbert Space on $[0, 1]$

For any $f \in \mathcal{C}^{(m)}[0, 1]$, its standard Taylor expansion is

$$f(t) = \sum_{\nu=0}^{m-1} \frac{t^\nu}{\nu!} f^{(\nu)}(0) + \int_0^1 \frac{(t-u)_+^{m-1}}{(m-1)!} f^{(m)}(t)dt, \tag{3.4}$$

where $(\cdot)_+ = \max\{0, \cdot\}$. With an inner product

$$\langle f, g\rangle = \sum_{\nu=0}^{m-1} f^{(\nu)}(0)g^{(\nu)}(0) + \int_0^1 f^{(m)}(t)g^{(m)}(t)dt, \tag{3.5}$$

the representer is

$$R_s(t) = \sum_{\nu=0}^{m-1} \frac{s^\nu}{\nu!}\frac{t^\nu}{\nu!} + \int_0^1 \frac{(s-u)_+^{m-1}}{(m-1)!}\frac{(t-u)_+^{m-1}}{(m-1)!}du \triangleq R_0(s, t) + R_1(s, t). \tag{3.6}$$

It is easy to prove that $R(s, t)$ is non-negative and is reproducing kernel, by which $\langle R(s, t), f(t)\rangle = \langle R_s(t), f(t)\rangle = f(s)$. Additionally, $R_s^{(\nu)}(0) = s^\nu/\nu!$ for $\nu = 0, \ldots, m - 1$.

Before moving on to further steps, we are now introducing the following two theorems.

Theorem 3. *(Aronszajn, 1950) Suppose R is a symmetric, positive definite kernel on a set X. Then, there is a unique Hilbert space of functions on X for which R is a reproducing kernel.*

Theorem 4. *(Gu, 2013) If the reproducing kernel R of a space $\mathcal{H}$ on domain X can be decomposed into $R = R_0 + R_1$, where R_0 and R_1 are both non-negative definite, $R_0(x, \cdot), R1(x, \cdot) \in \mathcal{H}$, for $\forall x \in X$, and $\langle R_0(x, \cdot), R_1(y, \cdot)\rangle = 0$, for $\forall x, y \in X$, then the spaces $\mathcal{H}_0$ and $\mathcal{H}_1$ corresponding respectively to R_0 and R_1 form a tensor sum decomposition of $\mathcal{H}$. Conversely, if R_0 and R_1 are both nonnegative definite and $\mathcal{H}_0 \cap \mathcal{H}_1 = \{0\}$, then $\mathcal{H} = \mathcal{H}_0 \oplus \mathcal{H}_1$ has a reproducing kernel $R = R_0 + R_1$.*

According to Theorem 3, the Hilbert space associated with $R(\cdot)$ can be constructed as containing all finite linear combinations of the form $\sum a_i R(t_i, \cdot)$, and their limits under the norm induced by the inner product $\langle R(s, \cdot), R(t, \cdot)\rangle = R(s, t)$. As for Theorem 4, it is easy to verify that R_0 corresponds to the space of polynomials $\mathcal{H}_0 = \left\{f : f^{(m)} = 0\right\}$ with an inner product $\langle f, g\rangle_0 = \sum_{\nu=0}^{m-1} f^{(\nu)}(0)g^{(\nu)}(0)$ and R_1 corresponds to the orthogonal complement of $\mathcal{H}_0$, that is $\mathcal{H}_1 = \left\{f : f^{(\nu)}(0) = 0, \nu = 0, \ldots, m-1, \int_0^1 (f^{(m)})^2 dt < \infty\right\}$ with an inner product $\langle f, g\rangle_1 = \int_0^1 f^{(m)}g^{(m)}dt$.

3.2.3 Polynomial Smoothing Splines as Bayes Estimates

Because it is possible to interpret the smoothing spline regression estimator as a Bayes estimate when the mean function $r(\cdot)$ is given an improper prior distribution (Wahba, 1990; Berlinet and Thomas-Agnan, 2011). Therefore, one can find that the posterior mean of f on $[0,1]$ with a vague improper prior is the polynomial smoothing spline of the objective function (3.2).

Consider $f = f_0 + f_1$ on $[0,1]$, with f_0 and f_1 having independent Gaussian priors with zero means and covariances satisfying

$$\mathrm{E}[f_0(s)f_0(t)] = \tau^2 R_0(s,t) = \tau^2 \sum_{\nu=0}^{m-1} \frac{s^\nu}{\nu!}\frac{t^\nu}{\nu!}, \tag{3.7}$$

$$\mathrm{E}[f_1(s)f_1(t)] = bR_1(s,t) = b\int_0^1 \frac{(s-u)_+^{m-1}}{(m-1)!}\frac{(t-u)_+^{m-1}}{(m-1)!}, \tag{3.8}$$

where R_0 and R_1 are from (3.6). Because of the observations are normally distributed as $y_i \sim N(f(t_i), \sigma^2)$, then the joint distribution for $\mathbf{y} = \{y_1, \ldots, y_n\}$ and $f(t)$ is normal with zero mean and the following covariance matrix

$$\mathrm{Cov}(f, \mathbf{y}) = \begin{bmatrix} bQ + \tau SS^\top + \sigma^2 I & b\xi + \tau^2 S\phi \\ b\xi^\top + \tau^2\phi^\top S^\top & bR_1(t,t) + \tau^2\phi^\top\phi \end{bmatrix}, \tag{3.9}$$

where $\{Q_{i,j}\}_{n\times n} = R_1(t_i, t_j)$, $\{S_{i,\nu}\}_{n\times m} = t_i^{\nu-1}/(\nu-1)!$, $\{\xi_{i,1}\}_{n\times 1} = R_1(t_i, t)$ and $\{\phi_{\nu,1}\}_{m\times 1} = t^{\nu-1}/(\nu-1)!$. Consequently, the posterior is

$$\begin{aligned} \mathrm{E}[f(t) \mid \mathbf{y}] &= \left(b\xi^\top + \tau\phi^\top s^\top\right)\left(bQ + \tau^2 SS^\top + \sigma^2 I\right)^{-1}\mathbf{y} \\ &= \xi^\top\left(Q + \rho SS^\top + n\lambda I\right)^{-1}\mathbf{y} + \phi^\top\rho S^\top\left(Q + \rho SS^\top + n\lambda I\right)^{-1}\mathbf{y}, \end{aligned} \tag{3.10}$$

where $\rho = \tau^2/b$ and $n\lambda = \sigma^2/b$. Furthermore, by denoting $M = Q + n\lambda I$, Gu (2013) gives that, when $\rho \to \infty$, the posterior mean is in the form $\mathrm{E}[f(t) \mid y_{1:n}] = \xi^\top\mathbf{c} + \phi^\top\mathbf{d}$ with coefficients

$$\mathbf{c} = \left(M^{-1} - M^{-1}S\left(S^\top M^{-1}S\right)^{-1}S^\top M^{-1}\right)\mathbf{y}, \tag{3.11}$$

$$\mathbf{d} = \left(S^\top M^{-1}S\right)^{-1}S^\top M^{-1}\mathbf{y}. \tag{3.12}$$

Theorem 5. *(Gu, 2013) The polynomial smoothing spline of* (3.2) *is the posterior mean of $f = f_0 + f_1$, where f_0 diffuses in span $\{t^{\nu-1}, \nu = 1, \ldots, m\}$ and f_1 has a Gaussian process prior with mean zero and a covariance function*

$$bR_1(s,t) = b\int_0^1 \frac{(s-u)_+^{m-1}}{(m-1)!}\frac{(t-u)_+^{m-1}}{(m-1)!}, \tag{3.13}$$

for $b = \sigma^2/n\lambda$.

Remark: Equation (3.7) can be obtained from equation (3.3) if we assume $d_\nu \sim N(0, \tau^2 I_{m\times m})$. Therefore the limit of $\rho = \frac{\tau^2}{b} \to \infty$ indicates a diffuse prior for the coefficients $\mathbf{d}$.

3.2.4 Gaussian Process Regression

Gaussian processes are the extension of multivariate Gaussian to infinite-sized collections of real value variables, any finite number of which have a joint Gaussian distribution (Rasmussen and Williams, 2006). Gaussian process regression is a probability distribution over functions. It is fully defined by its mean $m(t)$ and covariance $K(s,t)$ function as

$$m(t) = \mathrm{E}[f(t)] \tag{3.14}$$

$$K(s,t) = \mathrm{E}[(f(s) - m(s))\,(f(t) - m(t))], \tag{3.15}$$

where s and t are two variables. A function f distributed as such is denoted in form of

$$f \sim GP\left(m(t), K(s,t)\right). \tag{3.16}$$

Usually the mean function is assumed to be zero everywhere.

Given a set of input variables $\mathbf{t} = \{t_1, \ldots, t_n\}$ for function $f(t)$ and the output $\mathbf{y} = f(\mathbf{t}) + \varepsilon$ with i.i.d. Gaussian noise ε of variance σ_n^2, we can use the above definition to predict the value of the function $f_* = f(t_*)$ at a particular input t_*. As the noisy observations becoming

$$\mathrm{Cov}(y_p, y_q) = K(t_p, t_q) + \sigma_n^2 \delta_{pq} \tag{3.17}$$

where δ_{pq} is a Kronecker delta which is one if and only if $p = q$ and zero otherwise, the joint distribution of the observed outputs $\mathbf{y}$ and the estimated output f_* according to prior is

$$\begin{bmatrix} \mathbf{y} \\ f_* \end{bmatrix} \sim N\left(0, \begin{bmatrix} K(\mathbf{t},\mathbf{t}) + \sigma_n^2 I & K(\mathbf{t}, t_*) \\ K(t_*, \mathbf{t}) & K(t_*, t_*) \end{bmatrix}\right). \tag{3.18}$$

The posterior distribution over the predicted value is obtained by conditioning on the observed data

$$f_* \mid \mathbf{y}, \mathbf{t}, t_* \sim N\left(\bar{f}_*, \mathrm{Cov}(f_*)\right) \tag{3.19}$$

where

$$\bar{f}_* = \mathrm{E}\left(f_* \mid \mathbf{y}, \mathbf{t}, t_*\right) = K(t_*, \mathbf{t})\left(K(\mathbf{t},\mathbf{t}) + \sigma_n^2\right)^{-1}\mathbf{y}, \tag{3.20}$$

$$\mathrm{Cov}(f_*) = K(t_*, t_*) - K(t_*, \mathbf{t})\left(K(\mathbf{t},\mathbf{t}) + \sigma_n^2 I\right)^{-1} K(\mathbf{t}, t_*). \tag{3.21}$$

Therefore it can seen that the Bayesian estimation of a smoothing spline is a special format of Gaussian process regression with diffuse prior and the covariance matrix $R(s,t)$.

3.3 V-Spline as Bayes Estimate

Recall the definition of V-spline that is introduced in Section 2.2. It is the solution to the objective function (2.4), where an extra term for $f'(t) - v$ and an extra parameter γ are incorporated. The penalty parameter $\lambda(t)$ is a function varying on different domains. If $\lambda(t) = \lambda$ is constant and $\gamma = 0$, the V-spline degenerate to a conventional cubic smoothing spline consisting of a set of given basis functions.

However, the Bayes estimate for a polynomial smoothing spline requires fixed interval on $[0,1]$ and the penalty parameter is constant. For the first constraint, without loss of generality, an arbitrary interval $[a,b]$ can be transformed to $[0,1]$. For the second constraint, it is assumed that $\lambda(t)$ stays the same constant in each subinterval of $[0,1]$ and name the solution "trivial V-spline". In this section, we still use "V-spline" for sake of simplicity.

In the following, we are going to prove that this kind of trivial V-spline is corresponding to Bayes estimate in a particular reproducing kernel Hilbert space.

3.3.1 Reproducing Kernel Hilbert Space $\mathcal{C}^{(2)}_{\text{p.w.}}[0,1]$

The space $\mathcal{C}^{(m)}[0,1] = \left\{f : f^{(m)} \in L_2[0,1]\right\}$ is a set of functions f whose mth derivatives are square integrable on the domain $[0,1]$. For a V-spline, it only requires $m = 2$. In fact, its second derivative is piecewise linear but is not necessarily continuous at the knots. Besides, if and only if $\lambda(t)$ is constant and $\gamma = 0$, the second derivative is piecewise linear and continuous at the knots. Here we are introducing the space

$$\mathcal{C}^{(2)}_{\text{p.w.}}[0,1] = \{f : f'' \in L_2[0,1], f, f' \text{ are continuous and } f'' \text{ is piecewise linear}\},$$

in which the second derivative of any function f is not necessarily continuous.

Given a sequence of paired data $\{(t_1, y_1, v_1), \ldots, (t_n, y_n, v_n)\}$, the the minimizer of

$$J[f] = \frac{1}{n}\sum_{i=1}^{n}(y_i - f(t_i))^2 + \frac{\gamma}{n}\sum_{i=1}^{n}(v_i - f'(t_i))^2 + \lambda\int_0^1 f''^2 dt \tag{3.22}$$

in the space $\mathcal{C}^{(2)}_{\text{p.w.}}[0,1]$ is a V-spline. Equipped with an appropriate inner product

$$\langle f, g\rangle = f(0)g(0) + f'(0)g'(0) + \int_0^1 f''(t)g''(t)dt, \tag{3.23}$$

the space $\mathcal{C}^{(2)}_{\text{p.w.}}[0,1]$ is made a reproducing kernel Hilbert space. In fact, the representer $R_s(\cdot)$ is

$$R_s(t) = 1 + st + \int_0^1 (s-u)_+(t-u)_+ du. \tag{3.24}$$

It can be seen that $R_s(0) = 1, R_s'(0) = s$, and $R_s''(t) = (s-t)_+$. The two terms of the reproducing kernel $R(s,t) = R_s(t) \triangleq R_0(s,t) + R_1(s,t)$, where

$$R_0(s,t) = 1 + st \tag{3.25}$$

$$R_1(s,t) = \int_0^1 (s-u)_+(t-u)_+ du \tag{3.26}$$

are both non-negative definite themselves.

According to Theorem 4, R_0 can correspond the space of polynomials $\mathcal{H}_0 = \{f : f'' = 0\}$ with an inner product $\langle f, g\rangle_0 = f(0)g(0) + f'(0)g'(0)$, and R_1 corresponds the orthogonal complement of $\mathcal{H}_0$

$$\mathcal{H}_1 = \left\{ f : f(0) = 0, f'(0) = 0, \int_0^1 f''(t)^2 dt < \infty \right\} \tag{3.27}$$

with inner product $\langle f, g\rangle_1 = \int_0^1 f''g'' dt$. Thus, $\mathcal{H}_0$ and $\mathcal{H}_1$ are two subspaces of the $\mathcal{C}^{(2)}_{\text{p.w.}}[0,1]$, and the reproducing kernel is $R_s(\cdot) = R_0(s,\cdot) + R_1(s,\cdot)$.

Define a new notation $\dot{R}(s,t) = \frac{\partial R}{\partial s}(s,t) = \frac{\partial R_0}{\partial s}(s,t) + \frac{\partial R_1}{\partial s}(s,t) = t + \int_0^s (t-u)_+ du$. Obviously $\dot{R}_s(t) \in \mathcal{C}^{(2)}_{\text{p.w.}}[0,1]$. Additionally, we have $\dot{R}_s(0) = 0, \dot{R}_s'(0) = \frac{\partial \dot{R}_s}{\partial t}(0) = 1$, and $\dot{R}_s''(t) = \begin{cases} 0 & s \le t \\ 1 & s > t \end{cases}$. Then, for any $f \in \mathcal{C}^{(2)}_{\text{p.w.}}[0,1]$, we have

$$\langle \dot{R}_s, f\rangle = \dot{R}_s(0)f(0) + \dot{R}_s'(0)f'(0) + \int_0^1 \dot{R}_s'' f''(u) du = f'(0) + \int_0^t f''(u) du = f'(t). \tag{3.28}$$

It can be seen that the first term $\dot{R}_0 = t \in \mathcal{H}_0$, and the space spanned by the second term $\dot{R}_1 = \int_0^s (t-u)_+ du$, denoted as $\dot{\mathcal{H}}$, is a subspace of $\mathcal{H}_1$, and $\dot{\mathcal{H}} \ominus \mathcal{H}_1 \neq \emptyset$. Given the sample points $t_j, j = 1, \ldots, n$, in equation (3.22) and noting that the space

$$\mathcal{A} = \left\{ f : f = \sum_{j=1}^n \alpha_j R_1(t_j, \cdot) + \sum_{j=1}^n \beta_j \dot{R}_1(t_j, \cdot) \right\} \tag{3.29}$$

is a closed linear subspace of $\mathcal{H}_1$. Then, we have a new space $\mathcal{H}_* = \dot{\mathcal{H}} \cup \mathcal{A}$. Thus, the two new sub spaces in $\mathcal{C}^{(2)}_{\text{p.w.}}[0,1]$ are $\mathcal{H}_0$ and $\mathcal{H}_*$.

For any $f \in \mathcal{C}^{(2)}_{\text{p.w.}}[0,1]$, it can be written as

$$f(t) = d_1 + d_2 t + \sum_{j=1}^n c_j R_1(t_j, t) + \sum_{j=1}^n b_j \dot{R}_1(t_j, \cdot) + \rho(t) \tag{3.30}$$

where $\mathbf{d} = \{d_1, d_2\}, \mathbf{c} = \{c_j\}$ and $\mathbf{b} = \{b_j\}$, $j = 1, \ldots, n$, are coefficients, and $\rho(t) \in \mathcal{H}_1 \ominus \mathcal{H}_*$. Thus, by substituting to the equation (3.22), it can be written as

$$\begin{aligned} nJ[f] = &\sum_{i=1}^{n} \left(y_i - d_1 - d_2 t - \sum_{j=1}^{n} c_j R_1(t_j, t_i) - \sum_{j=1}^{n} b_j \dot{R}_1(t_j, t_i) - \rho(t_i) \right)^2 \\ &+\gamma \sum_{i=1}^{n} \left(v_i - d_2 - \sum_{j=1}^{n} c_j R_1'(t_j, t_i) - \sum_{j=1}^{n} b_j \dot{R}_1'(t_j, t_i) - \rho'(t_i) \right)^2 \\ &+n\lambda \int_0^1 \left(\sum_{j=1}^{n} c_j R_1''(t_j, t) + \sum_{j=1}^{n} b_j \dot{R}_1''(t_j, t) + \rho''(t) \right)^2 dt \end{aligned} \tag{3.31}$$

Because of orthogonality, $\rho(t_i) = \langle R_1(t_i, \cdot), \rho \rangle = 0$, $\rho'(t_i) = \langle \dot{R}_1(t_i, \cdot), \rho' \rangle = 0$, $i = 1, \ldots, n$. By denoting that

$$\begin{aligned} S = \{S_{ij}\}_{n\times 2} = \begin{bmatrix} 1 & t_i \end{bmatrix}, \quad Q = \{Q_{ij}\}_{n\times n} = R_1(t_j, t_i), \quad P = \{P_{ij}\}_{n\times n} = \dot{R}_1(t_j, t_i), \\ S' = \left\{S_{ij}'\right\}_{n\times 2} = \begin{bmatrix} 0 & 1 \end{bmatrix}, \quad Q' = \left\{Q_{ij}'\right\}_{n\times n} = R_1'(t_j, t_i), \quad P' = \left\{P_{ij}'\right\}_{n\times n} = \dot{R}_1'(t_j, t_i). \end{aligned}$$

and noting that $\int_0^1 R_1''(t_i, t) R_1''(t_j, t) dt = R_1(t_i, t_j)$, $\int_0^1 R_1''(t_i, t) \dot{R}_1''(t_j, t) dt = \int_0^v (t_i - t) dt = \dot{R}_1(t_j, t_i)$, and $\int_0^1 \dot{R}_1''(t_i, t) \dot{R}_1''(t_j, t) dt = \int_0^v 1 dt = \dot{R}_1'(t_i, t_j)$, where $v = \min\{t_i, t_j\}$, the above equation (3.31) can be written as

$$\begin{aligned} nJ[f] = &\left(\mathbf{y} - S\mathbf{d} - Q\mathbf{c} - P\mathbf{b}\right)^\top \left(\mathbf{y} - S\mathbf{d} - Q\mathbf{c} - P\mathbf{b}\right) \\ &+\gamma \left(\mathbf{v} - S'\mathbf{d} - Q'\mathbf{c} - P'\mathbf{b}\right)^\top \left(\mathbf{v} - S'\mathbf{d} - Q'\mathbf{c} - P'\mathbf{b}\right) \\ &+n\lambda \left(\mathbf{c}^\top Q\mathbf{c} + 2\mathbf{c}^\top P\mathbf{b} + \mathbf{b}^\top P'\mathbf{b}\right) + n\lambda \left(\rho, \rho\right). \end{aligned} \tag{3.32}$$

Note that ρ only appears in the third term and is minimized at $\rho = 0$. Hence, a V-spline resides in the space $\mathcal{H}_0 \oplus \mathcal{H}_*$ of finite dimension. Thus, the solution to (3.22) is computed via the minimization of the first three terms in (3.32) with respect to $\mathbf{d}$, $\mathbf{c}$ and $\mathbf{b}$.

3.3.2 Posterior of Bayes Estimates

In a general process, we know that $p(\mathbf{y}, \mathbf{v} \mid f) = N(f, \Gamma)$, where Γ is a covariance matrix. However, we are more interested in f given measurements, which is

$$p(f \mid \mathbf{y}, \mathbf{v}) \propto p(\mathbf{y}, \mathbf{v} \mid f) p(f), \tag{3.33}$$

where $f \sim GP(0, \Sigma)$ is a Gaussian process prior. In fact, the covariance matrix Σ is associated to the inner product $R(s, t)$.

Observing $y_i \sim N\left(f(t_i), \sigma^2\right)$ and $v_i \sim N\left(f(t_i), \frac{\sigma^2}{\gamma}\right)$, $i = 1, \ldots, n$, the joint distribution of $\mathbf{y}, \mathbf{v}$ and $f(t)$ is normal with mean zero and a covariance matrix can be found by the following

$$\begin{aligned}
\mathrm{E}[f(s)f(t)] &= \tau^2 R_0(s,t) + \beta R_1(s,t) & \mathrm{E}[f(s)f'(t)] &= \tau^2 R_0'(s,t) + \beta R_1'(s,t) \\
\mathrm{E}[f'(s)f(t)] &= \tau^2 \dot{R}_0(s,t) + \beta \dot{R}_1(s,t) & \mathrm{E}[f'(s)f'(t)] &= \tau^2 \dot{R}_0'(s,t) + \beta \dot{R}_1'(s,t) \\
\mathrm{E}[y_i, y_j] &= \tau^2 R_0(s_i,s_j) + \beta R_1(s_i,s_j) + \sigma^2\delta_{ij} & \mathrm{E}[v_i, v_j] &= \tau^2 \dot{R}_0'(s_i,s_j) + \beta \dot{R}_1'(s_i,s_j) + \frac{\sigma^2}{\gamma}\delta_{ij} \\
\mathrm{E}[v_i, y_j] &= \tau^2 \dot{R}_0(s_i,s_j) + \beta \dot{R}_1(s_i,s_j) & \mathrm{E}[y_i, v_j] &= \tau^2 R_0'(s_i,s_j) + \beta R_1'(s_i,s_j) \\
\mathrm{E}[y_i, f(s)] &= \tau^2 R_0(s_i,s) + \beta R_1(s_i,s) & \mathrm{E}[y_i, f'(s)] &= \tau^2 R_0'(s_i,s) + \beta R_1'(s_i,s) \\
\mathrm{E}[v_i, f(s)] &= \tau^2 \dot{R}_0(s_i,s) + \beta \dot{R}_1(s_i,s) & \mathrm{E}[v_i, f'(s)] &= \tau^2 \dot{R}_0'(s_i,s) + \beta \dot{R}_1'(s_i,s)
\end{aligned} \tag{3.34}$$

where $R_0(s,t)$ and $R_1(s,t)$ are taken from (3.25) and (3.26).

Therefore, by using a standard result on multivariate normal distribution (such as Result 4.6 in (Johnson and Wichern, 1992)), the posterior mean of $f(t)$ is seen to be

$$\begin{aligned}
\mathrm{E}[f \mid \mathbf{y}, \mathbf{v}] &= \begin{bmatrix} \mathrm{Cov}(\mathbf{y}, f) & \mathrm{Cov}(f, \mathbf{v}) \end{bmatrix} \begin{bmatrix} \mathrm{Var}(\mathbf{y}) & \mathrm{Cov}(\mathbf{y}, \mathbf{v}) \\ \mathrm{Cov}(\mathbf{v}, \mathbf{y}) & \mathrm{Var}(\mathbf{v}) \end{bmatrix}^{-1} \begin{bmatrix} \mathbf{y} \\ \mathbf{v} \end{bmatrix} \\
&= \begin{bmatrix} \tau^2\phi^\top S^\top + \beta\xi^\top & \tau^2\phi^\top S'^\top + \beta\psi^\top \end{bmatrix} \begin{bmatrix} \tau^2 SS^\top + \beta Q + \sigma^2 I & \tau^2 SS'^\top + \beta P \\ \tau^2 S'S^\top + \beta Q' & \tau^2 S'S'^\top + \beta P' + \frac{\sigma^2}{\gamma} I \end{bmatrix}^{-1} \begin{bmatrix} \mathbf{y} \\ \mathbf{v} \end{bmatrix} \\
&= \begin{bmatrix} \rho\phi^\top S^\top + \xi^\top & \rho\phi^\top S'^\top + \psi^\top \end{bmatrix} \begin{bmatrix} \rho SS^\top + Q + n\lambda I & \rho SS'^\top + P \\ \rho S'S^\top + Q' & \rho S'S'^\top + P' + \frac{n\lambda}{\gamma} I \end{bmatrix}^{-1} \begin{bmatrix} \mathbf{y} \\ \mathbf{v} \end{bmatrix} \\
&= \left(\phi^\top \rho \begin{bmatrix} S \\ S' \end{bmatrix}^\top + \begin{bmatrix} \xi^\top & \psi^\top \end{bmatrix} \right) \left(\rho \begin{bmatrix} S \\ S' \end{bmatrix}^\top \begin{bmatrix} S \\ S' \end{bmatrix} + \begin{bmatrix} Q + n\lambda I & P \\ Q' & P' + \frac{n\lambda}{\gamma} I \end{bmatrix} \right)^{-1} \begin{bmatrix} \mathbf{y} \\ \mathbf{v} \end{bmatrix} \\
&\triangleq \phi^\top \rho T^\top \left(\rho T^\top T + M\right)^{-1} \begin{bmatrix} \mathbf{y} \\ \mathbf{v} \end{bmatrix} + \begin{bmatrix} \xi^\top & \psi^\top \end{bmatrix} \left(\rho T^\top T + M\right)^{-1} \begin{bmatrix} \mathbf{y} \\ \mathbf{v} \end{bmatrix}
\end{aligned} \tag{3.35}$$

where ϕ is 2×1 matrix with entry 1 and t, ξ is $n \times 1$ matrix with ith entry $R(t_i, t)$, $T^\top = \begin{bmatrix} S^\top & S'^\top \end{bmatrix}$ and ψ is $n \times 1$ matrix with ith entry $\dot{R}(t_i, t)$, $\rho = \tau^2/\beta$ and $n\lambda = \sigma^2/\beta$.

Lemma 3. *Suppose M is symmetric and nonsingular and T is of full column rank.*

$$\lim_{\rho\to\infty} \left(\rho TT^\top + M\right)^{-1} = M^{-1} - M^{-1}T\left(T^\top M^{-1} T\right)^{-1} T^\top M^{-1}, \tag{3.36}$$

$$\lim_{\rho\to\infty} \rho T^\top \left(\rho TT^\top + M\right)^{-1} = \left(T^\top M^{-1} T\right)^{-1} T^\top M^{-1}. \tag{3.37}$$

Setting $\rho \to \infty$ in equation (3.35) and applying Lemma 3, the posterior mean

$\mathrm{E}(f(t) \mid \mathbf{y}, \mathbf{v})$ is $\hat{f} = \phi^\top \mathbf{d} + \xi^\top \mathbf{c} + \psi^\top \mathbf{b}$, with the coefficients given by

$$\mathbf{d} = \left(T^\top M^{-1} T\right)^{-1} T^\top M^{-1} \begin{bmatrix} \mathbf{y} \\ \mathbf{v} \end{bmatrix}, \tag{3.38}$$

$$\begin{bmatrix} \mathbf{c} \\ \mathbf{b} \end{bmatrix} = \left(M^{-1} - M^{-1} T \left(T^\top M^{-1} T\right)^{-1} T^\top M^{-1}\right) \begin{bmatrix} \mathbf{y} \\ \mathbf{v} \end{bmatrix}, \tag{3.39}$$

where $T = \begin{bmatrix} S \\ S' \end{bmatrix}$ and $M = \begin{bmatrix} Q + n\lambda I & P \\ Q' & P' + \frac{n\lambda}{\gamma} I \end{bmatrix}$.

It is easy to verify that $\mathbf{d}, \mathbf{c}, \mathbf{b}$ are the solutions to

$$\begin{cases} S^\top (S\mathbf{d} + Q\mathbf{c} + P\mathbf{b} - \mathbf{y}) + \gamma S'^\top \left(S'\mathbf{d} + P^\top \mathbf{c} + P'\mathbf{b} - \mathbf{v}\right) = 0, \\ Q (S\mathbf{d} + (Q + n\lambda I)\mathbf{c} + P\mathbf{b} - \mathbf{y}) + P \left(\gamma S'\mathbf{d} + \gamma P^\top \mathbf{c} + (\gamma P' + n\lambda I)\mathbf{b} - \gamma \mathbf{v}\right) = 0, \\ P^\top (S\mathbf{d} + (Q + n\lambda I)\mathbf{c} + P\mathbf{b} - \mathbf{y}) + P' \left(\gamma S'\mathbf{d} + P^\top \mathbf{c} + (\gamma P' + n\lambda I)\mathbf{b} - \gamma \mathbf{v}\right) = 0. \end{cases} \tag{3.40}$$

Finally we obtain the following theorem:

Theorem 6. *The smoothing V-spline of* (3.22) *is the posterior mean of* $f = f_0 + f_1 + \dot{f}_1$, *where* f_0 *diffuses in span* $\{1, t\}$ *and* f_1, $\dot{f}_1$ *have Gaussian process priors with mean zero and covariance functions*

$$\mathrm{Cov}\,(f_1, f_1) = \beta R_1(s,t) = \beta \int_0^1 (s-u)_+ (t-u)_+ \, du, \tag{3.41}$$

$$\mathrm{Cov}\left(\dot{f}_1, f_1\right) = \beta \dot{R}_1(s,t) = \beta \int_0^s (t-u)_+ \, du, \tag{3.42}$$

$$\mathrm{Cov}\left(\dot{f}_1, \dot{f}_1\right) = \beta \dot{R}'_1(s,t) = \beta \min\{s,t\}, \tag{3.43}$$

for $\beta = \sigma^2/n\lambda$.

3.4 Bayes Estimate for Non-trivial V-Spline

For a sequence $0 = t_0 < t_1 < \cdots < t_n < t_{n+1} = 1$ on the interval $[0,1]$ in the reproducing kernel Hilbert space $\mathcal{C}^{(2)}_{\text{p.w.}}[0,1]$, define an inner product

$$\langle f, g \rangle = f(0)g(0) + f'(0)g'(0) + \sum_{i=0}^{n} w_i \int_{t_i}^{t_{i+1}} f''(t) g''(t) dt, \tag{3.44}$$

where $w_i > 0$, $i = 0, \ldots, n$. The representer is

$$R_s(t) = 1 + st + \sum_{i=0}^{n} w_i^{-1} \int_{t_i}^{t_{i+1}} (s-u)_+ (t-u)_+ du, \tag{3.45}$$

having the following properties

$$R_s'(t) = s + \sum_{i=0}^{n} w_i^{-1} \int_{t_i}^{t_{i+1}} (s-u)_+ \Theta(t-u) du, \tag{3.46}$$

$$\dot{R}_s(t) = t + \sum_{i=0}^{n} w_i^{-1} \int_{t_i}^{t_{i+1}} \Theta(s-u)(t-u)_+ du, \tag{3.47}$$

$$R_s''(t) = \sum_{i=0}^{n} w_i^{-1} \int_{t_i}^{t_{i+1}} (s-u)_+ \delta(t-u) du, \tag{3.48}$$

and $R_s(0) = 1$, $R_s'(0) = s$. The function $\Theta(t-u)$ is the Heaviside function and $\delta(t-u)$ is the Dirac delta function.

Further, $R(\cdot)$ and $\dot{R}(\cdot)$ on $[0,1]$ have the following properties

$$\begin{aligned}
\langle R_s, f \rangle &= R_s(0)f(0) + R_s'(0)f'(0) + \sum_{i=0}^{n} w_i \int_{t_i}^{t_{i+1}} R_s''(u) f''(u) du \\
&= f(0) + sf'(0) + \sum_{i=0}^{n} w_i \int_{t_i}^{t_{i+1}} \sum_{j=0}^{n} w_j^{-1} \int_{t_j}^{t_{j+1}} (s-u)_+ \delta(v-u) du f''(v) dv \\
&= f(0) + sf'(0) + \sum_{i=0}^{n} \int_{t_i}^{t_{i+1}} (s-u)_+ f''(u) du \\
&= f(s)
\end{aligned} \tag{3.49}$$

$$\begin{aligned}
\langle \dot{R}_s, f \rangle &= \dot{R}_s(0)f(0) + \dot{R}_s'(0)f'(0) + \sum_{i=0}^{n} w_i \int_{t_i}^{t_{i+1}} \dot{R}_s''(u) f''(u) du \\
&= f'(0) + \sum_{i=0}^{n} w_i \int_{t_i}^{t_{i+1}} \sum_{j=0}^{n} w_j^{-1} \int_{t_j}^{t_{j+1}} \Theta(s-u) \delta(v-u) du f''(v) dv \\
&= f'(0) + \sum_{i=0}^{n} \int_{t_i}^{t_{i+1}} \Theta(s-u) f''(u) du \\
&= f'(s)
\end{aligned} \tag{3.50}$$

Define the two terms of the reproducing kernel $R(s,t) = R_s(t) = R_0(s,t) + R_1(s,t)$, where

$$R_0(s,t) = 1 + st \tag{3.51}$$

$$R_1(s,t) = \sum_{i=0}^{n} w_i^{-1} \int_{t_i}^{t_{i+1}} (s-u)_+ (t-u)_+ du \tag{3.52}$$

are both non-negative definite themselves. For R_0 there corresponds the space of polynomials $\mathcal{H}_0 = \{f : f'' = 0\}$ with an inner product $\langle f, g \rangle = f(0)g(0) + f'(0)g'(0)$,

and for R_1 there corresponds a sequence of orthogonal spaces $\mathcal{H}^{(i)}$

$$\mathcal{H}^{(i)} = \{f : f(0) = 0, f'(0) = 0, \int_{t_i}^{t_{i+1}} f''(t)^2 dt < \infty\}$$

and $\mathcal{H}_1 = \oplus_{i=1}^{n-1} \mathcal{H}^{(i)}$. The inner product through the entire space $\mathcal{H}_1$ is $\langle f, g\rangle = \sum_{i=1}^{n-1} w_i \int_{t_i}^{t_{i+1}} f''(t)g''(t)dt$.

Given a sequence of paired sampling points $\{s_i, y_i, v_i\}, i = 1, \ldots, n$ on the interval $[s_1, s_n]$, it can be transformed to $\{t_i, y_i, v_i\}$ on the interval $[0, 1]$, where $0 = t_0 < t_1 < \cdots < t_n < t_{n+1} = 1$. The objective function of a V-spline on $[0, 1]$ is

$$J[f] = \frac{1}{n}\sum_{i=1}^{n} (y_i - f(t_i))^2 + \frac{\gamma}{n}\sum_{i=1}^{n} (v_i - f'(t_i))^2 + \sum_{i=0}^{n} \lambda_i \int_{t_i}^{t_{i+1}} f''(t)^2 dt. \tag{3.53}$$

Any $f \in \mathcal{C}^{(2)}_{\text{p.w.}}[0, 1]$ can be written as

$$f(t) = d_1 + d_2 t + \sum_{j=1}^{n} c_j R_1(t_j, t) + \sum_{j=1}^{n} b_j \dot{R}_1(t_j, t) + \rho(t) \tag{3.54}$$

Thus, by substituting to the equation (3.53), it can be written as

$$\begin{aligned} nJ[f] = &\left(y_i - d_1 - d_2 t_i - \sum_{j=1}^{n} c_j R_1(t_j, t_i) - \sum_{j=1}^{n} b_j \dot{R}_1(t_j, t_i) - \rho(t_i)\right)^2 \\ &+\gamma \sum_{i=1}^{n} \left(v_i - d_2 - \sum_{j=1}^{n} c_j R_1'(t_j, t_i) - \sum_{j=1}^{n} b_j \dot{R}_1'(t_j, t_i) - \rho'(t_i)\right)^2 \\ &+n \sum_{i=0}^{n} \lambda_i \int_{t_i}^{t_{i+1}} \left(\sum_{j=1}^{n} c_j R_1''(t_j, t) + \sum_{j=1}^{n} b_j \dot{R}_1''(t_j, t) + \rho''(t)\right)^2 dt. \end{aligned} \tag{3.55}$$

Because of orthogonality, $\rho(t_i) = \langle R_1(t_i, \cdot), \rho\rangle = 0$, $\rho'(t_i) = \langle \dot{R}_1(t_i, \cdot), \rho'\rangle = 0$, $i = 1, \ldots, n$. For further use, we need to notice the property of the inner product and R_1 satisfy

$$\langle R_1(s, \cdot), \dot{R}_1(t, \cdot)\rangle = R_1'(s, t) \tag{3.56}$$

$$\langle \dot{R}_1(s, \cdot), \dot{R}_1(t, \cdot)\rangle = \dot{R}_1'(s, t) \tag{3.57}$$

By denoting the matrices $\{S\}_{ij} = (t_i)^{j-1}$, $j = 1, 2$, $\{Q\}_{ij} = R_1(t_j, t_i)$, $\{P\}_{ij} = \dot{R}_1(t_j, t_i)$ and $\{P'\}_{ij} = \dot{R}_1'(t_j, t_i)$, the above equation (3.55) becomes the matrix form

$$\begin{aligned} nJ[f] = &(\mathbf{y} - S\mathbf{d} - Q\mathbf{c} - P\mathbf{b})^\top (\mathbf{y} - S\mathbf{d} - Q\mathbf{c} - P\mathbf{b}) \\ &+\gamma (\mathbf{v} - S'\mathbf{d} - Q'\mathbf{c} - P'\mathbf{b})^\top (\mathbf{v} - S'\mathbf{d} - Q'\mathbf{c} - P'\mathbf{b}) \\ &+n\Lambda \left(\mathbf{c}^\top Q\mathbf{c} + 2\mathbf{c}^\top P\mathbf{b} + \mathbf{b}^\top P'\mathbf{b}\right) + n\Lambda(\rho, \rho), \end{aligned} \tag{3.58}$$

where $\lambda_i = \Lambda w_i$.

Thus, the solution to (3.53) is computed via the minimization of the first three terms in (3.58) with respect to **d**, **c** and **b**.

Therefore, the calculation goes through the same process in Section 3.3.2 and the following theorem is obtained.

Theorem 7. *The smoothing V-spline of* (3.53) *is the posterior mean of* $f = f_0 + f_1 + \dot{f}_1$, *where* f_0 *diffuses in span* $\{1, t\}$ *and* f_1, $\dot{f}_1$ *have Gaussian process priors with mean zero and covariance functions*

$$\mathrm{Cov}\left(f_1, f_1\right) = \beta R_1\left(s,t\right) = \beta \sum_{i=0}^{n} w_i^{-1} \int_{t_i}^{t_{i+1}} \left(s-u\right)_+ \left(t-u\right)_+ du, \tag{3.59}$$

$$\mathrm{Cov}\left(\dot{f}_1, f_1\right) = \beta \dot{R}_1\left(s,t\right) = \beta \sum_{i=0}^{n} w_i^{-1} \int_{t_i}^{t_{i+1}} \Theta\left(s-u\right) \left(t-u\right)_+ du, \tag{3.60}$$

$$\mathrm{Cov}\left(\dot{f}_1, \dot{f}_1\right) = \beta \dot{R}_1'\left(s,t\right) = \beta \sum_{i=0}^{n} w_i^{-1} \int_{t_i}^{t_{i+1}} \Theta\left(s-u\right) \Theta\left(t-u\right) du, \tag{3.61}$$

for $\beta = \sigma^2 / n\Lambda$.

3.5 V-Spline with Correlated Random Errors

In most of the studies on polynomial smoothing splines, the random errors are assumed being independent. By contrast, observations are often correlated in applications, such as time series data and spatial data. It is known that the correlation greatly affects the selection of smoothing parameters, which are critical to the performance of smoothing spline estimates (Wang, 1998). The presence of correlation between the errors, if ignored, causes the commonly used automatic tuning parameter selection methods, such as cross-validation and generalized cross-validation (GCV), to break down or underestimate the parameters (Opsomer *et al.*, 2001).

Diggle and Hutchinson (1989) extend GCV for choosing the degree of smoothing spline to accommodate an autocorrelated error sequence, by which the smoothing parameter and autocorrelation parameters are estimated simultaneously. Kohn *et al.* (1992) propose an algorithm to evaluate the cross-validation functions, whose autocorrelated errors are modeled by an autoregressive moving average. Wang (1998) extend GML and unbiased risk (UBR), other than GCV, to estimate the smoothing parameters and correlation parameters simultaneously. In this section, we explore the extended GCV for V-spline with correlated errors.

First of all, consider observations $y = f(t) + \varepsilon_1$ and $v = f'(t) + \varepsilon_2$, where $\varepsilon_1 \sim N(0, \sigma^2 W^{-1})$, $\varepsilon_2 \sim N\left(0, \frac{\sigma^2}{\gamma} U^{-1}\right)$ with variance parameter σ^2. The V-spline $\hat{f}$ with correlated errors in space $\mathcal{C}^{(2)}_{p.w}[0,1]$ is the minimizer of

$$J[f] = \frac{1}{n}(\mathbf{y} - \mathbf{f})^\top W (\mathbf{y} - \mathbf{f}) + \frac{\gamma}{n}(\mathbf{v} - \mathbf{f}')^\top U (\mathbf{v} - \mathbf{f}') + \lambda \int_0^1 (f'')^2 \, dt. \tag{3.62}$$

Because $f = \sum_{i=1}^{2n} \theta_i N_i(t)$ is a linear combination of basis functions, extended to the solution with covariance matrices, the parameter is found as

$$\hat{\theta} = \left(B^\top W B + \gamma C^\top U C + n\Omega_\lambda\right)^{-1} \left(B^\top W \mathbf{y} + \gamma C^\top U \mathbf{v}\right). \tag{3.63}$$

Furthermore, in Gaussian process regression, the covariance matrix with correlated variances becomes $M = \begin{bmatrix} Q + n\lambda W & P \\ Q' & P' + \frac{n\lambda}{\gamma} U \end{bmatrix}$ and the rest stays the same.

Recall the leave-one-out cross-validation score of a V-spline,

$$\text{LOOCV}(\lambda, \gamma) = \frac{1}{n} \sum_{i=1}^{n} \left(\frac{\hat{f}(t_i) - y_i + \frac{\gamma T_{ii}}{1 - \gamma V_{ii}} (\hat{f}'(t_i) - v_i)}{1 - S_{ii} - \frac{\gamma T_{ii}}{1 - \gamma V_{ii}} U_{ii}} \right)^2. \tag{3.64}$$

Followed by the approximation $S_{ii} \approx \frac{1}{n}\text{tr}(S)$, $T_{ii} \approx \frac{1}{n}\text{tr}(T)$, $U_{ii} \approx \frac{1}{n}\text{tr}(U)$ and $V_{ii} \approx \frac{1}{n}\text{tr}(V)$ (Syed, 2011), the GCV for the V-spline will be

$$\text{GCV}(\lambda, \gamma) = \frac{1}{n} \sum_{i=1}^{n} \left(\frac{\hat{f}(t_i) - y_i + \frac{\gamma \text{tr}(T)/n}{1 - \gamma \text{tr}(V)/n} (\hat{f}'(t_i) - v_i)}{1 - \text{tr}(S)/n - \frac{\gamma \text{tr}(T)/n}{1 - \gamma \text{tr}(V)/n} \text{tr}(U)/n} \right)^2, \tag{3.65}$$

which may provide further computational savings since it requires finding the trace rather than the individual diagonal entries of the hat matrix. Hence, it can be written in the form of

$$\text{GCV}(\lambda, \gamma) = \frac{\left(\hat{\mathbf{f}} - \mathbf{y}\right)^\top \left(\hat{\mathbf{f}} - \mathbf{y}\right) + \frac{2\text{tr}(\gamma T)}{\text{tr}(I - \gamma V)} \left(\hat{\mathbf{f}} - \mathbf{y}\right)^\top \left(\hat{\mathbf{f}}' - \mathbf{v}\right) + \left(\frac{\text{tr}(\gamma T)}{\text{tr}(I - \gamma V)}\right)^2 \left(\hat{\mathbf{f}}' - \mathbf{v}\right)^\top \left(\hat{\mathbf{f}}' - \mathbf{v}\right)}{\left(\text{tr}(I - S - \frac{\text{tr}(\gamma T)}{\text{tr}(I - \gamma V)} U)\right)^2}. \tag{3.66}$$

A natural extension to the above GCV for V-spline with correlated errors is

$$\text{GCV}(\lambda, \gamma) = \frac{\left(\hat{\mathbf{f}} - \mathbf{y}\right)^\top W \left(\hat{\mathbf{f}} - \mathbf{y}\right) + \frac{2\text{tr}(\gamma T)}{\text{tr}(I - \gamma V)} \left(\hat{\mathbf{f}} - \mathbf{y}\right)^\top W^{1/2} U^{\top 1/2} \left(\hat{\mathbf{f}}' - \mathbf{v}\right) + \left(\frac{\text{tr}(\gamma T)}{\text{tr}(I - \gamma V)}\right)^2 \left(\hat{\mathbf{f}}' - \mathbf{v}\right)^\top U \left(\hat{\mathbf{f}}' - \mathbf{v}\right)}{\left(\text{tr}\left(I - S - \frac{\text{tr}(\gamma T)}{\text{tr}(I - \gamma V)} U\right)\right)^2}. \tag{3.67}$$

The GCV is used for finding the unknown constant parameter λ, instead of a piecewise constant $\lambda(t)$ at different intervals, and the parameter γ. The structures of covariance matrices W and U are assumed known. If the errors are independent, in which way W and U become identity matrices, the solution $\hat{f}$ degenerates to a conventional V-spline with constant λ through over the entire interval $[0, 1]$.

3.6 Conclusion

In this chapter, we take a review of the work that has been done for the correspondence between polynomial smoothing spline and the Bayes estimates. With improper priors, the two methods correspond to each other. In fact, the smoothing spline is a particular case of Gaussian process regression. By following the work done by Gu (2013), we find the Bayes estimate of a V-spline if the penalty parameter $\lambda(t)$ is piecewise constant. Additionally, we give the formula of GCV for V-splines with correlated errors on y and v.

Compared with the V-spline, which is proposed in Chapter 2, the advantage of its Bayes estimate is that there are numerous sampling algorithms for parameter selection. The Bayes estimate does not require to pick a bunch of basis functions and, in some way, is more robust than V-splines.

Chapter 4

An Overview of On-line State and Parameter Estimation

4.1 Introduction

With data acquisition becoming easier, cheaper and faster, the challenges of "big data" are becoming ubiquitous. Classical methods for estimation and prediction, such as MCMC, are more suitable in batch mode. However, for data streams, more robust and efficient on-line methods are required. Approaches, such as Kalman filter and Sequential Monte Carlo, for on-line updating and estimation have been well studied in scientific literature and have been applied in real world applications.

The state-space model, which is a popular class of time series models, has found numerous of applications in fields as diverse as statistics, ecology, econometrics, engineering and environmental sciences (Cappé *et al.*, 2009; Doucet *et al.*, 2011; Elliott *et al.*, 1995; Cargnoni *et al.*, 1997). The state-space model allows us to establish complex linear and nonlinear Bayesian representations of time series patterns (Vieira and Wilkinson, 2016).

In this chapter, we review state-space models and a number of filtering methods for combined state and parameter estimation that have been proposed in the literature. They are then compared to the method described and developed in Chapter 5.

State-Space Model

State-space models are models that rely on the concept of state variables. If we describe a system as an operator mapping from the space of inputs to the space of

outputs, then we may need the entire input-output history of the system together with the planned input in order to compute the future output values (Hangos *et al.*, 2006). Alternatively, a sequential method builds on past data and the initial conditions by incorporating new information when it arrives. A generic state-space model consists of two sets of equations: state equation and output equation. The state equation describes the evolution of the true input and state variables sequentially as a function and passes the variable one after one, generally, with some noise. The output equation catches the input values and interprets it out by an algebraic equation. A general state-space model has the following form

$$\text{State equation } x_t = G_t(x_{t-1}) + w_t, \tag{4.1}$$

$$\text{Output equation } y_t = F_t(x_t) + \varepsilon_t \tag{4.2}$$

with an initial state x_0, where w_t and ε_t are noise terms. x_t are true status variables and y_t are output values. Many researchers have been interested in this model and its application because of its good property. It can be used to model univariate or multivariate time series and can be applied to a system that exhibits non-stationarity, structural changes, and irregular patterns (Petris *et al.*, 2009).

The most simple and important system is given by Gaussian linear state-space models, also known by dynamic linear models (DLM), which defines a very general class of non-stationary time series models. First of all, the model is linear, that means G_t and F_t are linear processes and satisfy linearity property. Secondly, it is specified by a normal prior distribution for the p-dimensional state vector at initial state $t = 0$,

$$x_0 \sim N_p(m_0, C_0)$$

and two independent zero-mean normal distributed noise $\epsilon_t \sim N_p(0, V_t)$ and $w_t \sim N_p(0, W_t)$ (Petris *et al.*, 2009). The celebrated Kalman filter is a particular algorithm that is used to solve state-space models in the linear case. This was first derived by Kalman (1960).

The assumption Markovian keeps the current state x_t only depending on the previous one step x_{t-1} and the observed y_t depending on x_t. A state-space is shown in the diagram (1.6) in Chapter 1.

In applications, the process functions G_t and F_t contain one or more unknown parameters that need to be estimated (De Jong, 1988) and the goal is to estimate the true states on sequential observations $y_1, \ldots, y_t$. Then it becomes to estimate the joint density of $p(x_{1:t}, \theta \mid y_{1:t})$, where $x_{1:t} = \{x_1, x_2, \ldots, x_t\}$ are the hidden states and $y_{1:t} = \{y_1, y_2, \ldots, y_t\}$ are the observed outcomes and θ is a set of unknown parameters.

Contents

In this chapter, an overview of existing methods for sequential state and parameter inference is given with discussions and a numerical study. In Section 4.2, the concepts and popular algorithms of sequential state estimation are introduced. These algorithms are the fundamental of advanced methods. In Section 4.3, we will have a look at on-line algorithms that can estimate both unknown state and parameter in different ways. In Section 4.4, a numerical study is to analyze and compare the performances of these methods, including the proposed Algorithm 5.2 in Section 5.5.

4.2 State Estimation Filters

Vehicle tracking system uses the GPS data to enable users to locate their vehicles with ease and in a convenient manner (Pham *et al.*, 2013). One the most important problems in this tracking system is state estimation (Toloei and Niazi, 2014). A general approach uses the system functional form to perform the state estimation with the assumption that all parameters are known. Indeed, two aspects of the functional form that mainly affect the analysis of such systems: (i) is the system model linear or non-linear in the state, and (ii) is the noise modeled as a random variable or a non-random bounded variable.

The following sections, we explore state filters that are not restricted by assumptions of linearity and may be applied to non-Gaussian noise models.

4.2.1 Sequential Monte Carlo Method

The use of *Monte Carlo* methods for filtering can be traced back to the pioneering contributions of (Handschin and Mayne, 1969; Handschin, 1970). These researchers tried to use an importance sampling paradigm to approximate the target distributions and. Later on, an importance sampling algorithms were implemented sequentially in the filtering context. This algorithm is named *sequential importance sampling*, often abbreviated SIS, and has been known since the early 1970s. Limited by the power of computers and suffering from sample impoverishment or weight degeneracy, the SIS did not develop well until 1993. Gordon *et al.* (1993) use this a technique based on sampling and importance sampling methods to find the best state estimation. A particle filter algorithm was proposed to allow rejuvenation of the set of samples by duplicating the samples with high importance weights and, on the contrary, removing samples with

low weights (Cappé *et al.*, 2009). Since then, sequential Monte Carlo (SMC) methods have been applied in many different fields including but not limited to computer vision, signal processing, control, econometrics, finance, robotics, and statistics (Doucet *et al.*, 2011; Ristic *et al.*, 2004).

In the state-space model, a generic particle filter estimates the posterior distribution of the hidden states using the observation measurement process. The filtering problem is to estimate sequentially the values of the hidden states x_t given the values of the observation process $y_{1:t}$ at any time t. In another word, it is to find the value of $p(x_t \mid y_{1:t})$. The process is divided into two steps: prediction and updating. In the prediction step, the assumption of Markov chain is the current status x_t only depends on the previous one x_{t-1}. Then we can calculate the probability of x_t by

$$\begin{aligned} p(x_t \mid y_{1:t-1}) &= \int p(x_t, x_{t-1} \mid y_{1:t-1}) dx_{t-1} \\ &= \int p(x_t \mid x_{t-1}, y_{1:t-1}) p(x_{t-1} \mid y_{1:t-1}) dx_{t-1} \\ &= \int p(x_t \mid x_{t-1}) p(x_{t-1} \mid y_{1:t-1}) dx_{t-1}. \end{aligned} \tag{4.3}$$

Continuously, in the updating phase, $p(x_t \mid y_{1:t})$ is easily found, as long as $p(x_t \mid y_{1:t-1})$ is known, by

$$\begin{aligned} p(x_t \mid y_{1:t}) =& \frac{p(y_t \mid x_t, y_{1:t-1}) p(x_t \mid y_{1:t-1})}{p(y_t \mid y_{1:t-1})} \\ =& \frac{p(y_t \mid x_t) p(x_t \mid y_{1:t-1})}{p(y_t \mid y_{1:t-1})}, \end{aligned} \tag{4.4}$$

where $p(y_t \mid y_{1:t-1}) = \int p(y_t \mid x_t) p(x_t \mid y_{1:t-1}) dx_t$ is the normalization (Arulampalam *et al.*, 2002).

Imagine that the state-space is partitioned as many parts, in which the particles are filled according to some probability measure. The higher probability, the denser the particles are concentrated. Suppose the particles $x_k^{(1)}, \ldots, x_k^{(N)}$ at time k are drawn from the target probability density function $p(\cdot \mid y_{1:t})$, then for any function of interest $f(x)$ these particles are used to estimate its expectation,

$$\mathrm{E}[f(x)] = \int_a^b f(x) p(x \mid y_{1:t}) dx. \tag{4.5}$$

The posterior distribution or density is empirically represented by a weighted sum of samples $x_k^{(1)}, \ldots, x_k^{(N)}$

$$p(x_k \mid y_{1:t}) \approx \hat{p}(x_k \mid y_{1:t}) = \frac{1}{N} \sum_{i=1}^{N} \delta \left(x_k - x_k^{(i)} \right). \tag{4.6}$$

Hence, a continuous variable is approximated by a discrete one with a random support. When N is sufficiently large, $\hat{p}(x_k \mid y_{1:t})$ is treated by particle filter as the true posterior $p(x_k \mid y_{1:t})$. By this approximation, the expectation of $f(x)$ at time k is

$$\begin{aligned} \mathrm{E}[f(x_k)] &\approx \int f(x_k)\hat{p}(x_k \mid y_{1:t})dx_k \\ &= \frac{1}{N}\sum_{i=1}^{N}\int f(x_k)\delta(x_k - x_k^{(i)})dx_k \\ &= \frac{1}{N}\sum_{i=1}^{N} f\left(x_k^{(i)}\right). \end{aligned} \tag{4.7}$$

The expectation is the mean of the status of all particles $x_k^{(1)}, \ldots, x_k^{(N)}$.

However, the posterior distribution is unknown and impossible to sample from the true posterior. To solve this issue, some sampling methods are investigated in the following sections.

4.2.2 Importance sampling

It is common to sample from an easy-to-implement distribution, the so-called proposal distribution $q(x \mid y)$, hence

$$\begin{aligned} \mathrm{E}[f(x)] &= \int f(x_t)\frac{p(x_t \mid y_{1:t})}{q(x_t \mid y_{1:t})}q(x_t \mid y_{1:t})dx_t \\ &= \int f(x_t)\frac{p(x_t)p(y_{1:t} \mid x_t)}{p(y_{1:t})q(x_t \mid y_{1:t})}q(x_t \mid y_{1:t})dx_t \\ &= \int f(x_t)\frac{w_t(x_t)}{p(y_{1:t})}q(x_t \mid y_{1:t})dx_t, \end{aligned} \tag{4.8}$$

where $w_t(x_t) = \frac{p(x_t)p(y_{1:t}|x_t)}{q(x_t|y_{1:t})} \propto \frac{p(x_t|y_{1:t})}{q(x_t|y_{1:t})}$. Because of $p(y_{1:t}) = \int p(y_{1:t} \mid x_t)p(x_t)dx_t$, the above equation can be rewritten as

$$\begin{aligned} \mathrm{E}[f(x)] &= \frac{1}{p(y_{1:t})}\int f(x_t)W_t(x_t)q(x_t \mid y_{1:t})dx_t \\ &= \frac{\int f(x_t)w_t(x_t)q(x_t \mid y_{1:t})dx_t}{\int p(y_{1:t} \mid x_t)p(x_t)dx_t} \\ &= \frac{\int f(x_t)w_t(x_t)q(x_t \mid y_{1:t})dx_t}{\int w_t(x_t)q(x_t \mid y_{1:t})dx_t} \\ &= \frac{\mathrm{E}_{q(x_t|y_{1:t})}[w_t(x_t)f(x_t)]}{\mathrm{E}_{q(x_t|y_{1:t})}[w_t(x_t)]}. \end{aligned} \tag{4.9}$$

To solve the above equation, we can use Monte Carlo method by drawing samples $\left\{x_t^{(i)}\right\}$ from $q(x_t \mid y_{1:t})$ and get its expectation, which is approximated by

$$\begin{aligned} \mathrm{E}[f(x_t)] &\approx \frac{\frac{1}{N}\sum_{i=1}^{N} w_t\left(x_t^{(i)}\right) f\left(x_t^{(i)}\right)}{\frac{1}{N}\sum_{i=1}^{N} w_t\left(x_t^{(i)}\right)} \\ &= \sum_{i=1}^{N} \tilde{w}_t\left(x_t^{(i)}\right) f\left(x_t^{(i)}\right), \end{aligned} \tag{4.10}$$

where $\tilde{w}_t\left(x_t^{(i)}\right) = \frac{w_t\left(x_t^{(i)}\right)}{\sum_{i=1}^{N} w_t\left(x_t^{(i)}\right)}$ is factorized weight. Each particle has its own weighted value, so the overall expectation is a weighted mean. However, the drawback of this method is that the computation is expensive. A smarter way is to update $w_t^{(i)}$ recursively. Suppose the proposal distribution

$$q(x_{0:t} \mid y_{1:t}) = q(x_{0:t-1} \mid y_{1:t-1}) q(x_t \mid x_{0:t-1}, y_{1:t}), \tag{4.11}$$

then the recursive form of the posterior distribution is

$$\begin{aligned} p(x_{0:t} \mid y_{1:t}) &= \frac{p(y_t \mid x_{0:t}, y_{1:t-1}) p(x_{0:t} \mid y_{1:t-1})}{p(y_t \mid y_{1:t-1})} \\ &= \frac{p(y_t \mid x_{0:t}, y_{1:t-1}) p(x_t \mid x_{0:t-1}, y_{1:t-1}) p(x_{0:t-1} \mid y_{1:t-1})}{p(y_t \mid y_{1:t-1})} \\ &= \frac{p(y_t \mid x_t) p(x_t \mid x_{t-1}) p(x_{0:t-1} \mid y_{1:t-1})}{p(y_t \mid y_{1:t-1})} \\ &\propto p(y_t \mid x_t) p(x_t \mid x_{t-1}) p(x_{0:t-1} \mid y_{1:t-1}), \end{aligned} \tag{4.12}$$

the recursive form of the weights are

$$\begin{aligned} w_t^{(i)} &\propto \frac{p\left(x_{0:t}^{(i)} \mid y_{1:t}\right)}{q\left(x_{0:t}^{(i)} \mid y_{1:t}\right)} \\ &= \frac{p\left(y_t \mid x_t^{(i)}\right) p\left(x_t^{(i)} \mid x_{t-1}^{(i)}\right) p\left(x_{0:t-1}^{(i)} \mid y_{1:t-1}\right)}{q\left(x_t^{(i)} \mid x_{0:t-1}^{(i)}, y_t\right) q\left(x_{0:t-1}^{(i)} \mid y_{1:t-1}\right)} \\ &= w_{t-1}^{(i)} \frac{p\left(y_t \mid x_t^{(i)}\right) p\left(x_t^{(i)} \mid x_{t-1}^{(i)}\right)}{q\left(x_t^{(i)} \mid x_{0:t-1}^{(i)}, y_t\right)}. \end{aligned} \tag{4.13}$$

4.2.3 Sequential Importance Sampling and Resampling

In practice, we are more interested in the current estimation $p(x_t \mid y_{1:t})$ instead of $p(x_{0:t} \mid y_{1:t})$. If

$$q(x_t \mid x_{0:t-1}, y_{1:t}) = q(x_t \mid x_{t-1}, y_t), \tag{4.14}$$

the importance weights $w_t^{(i)}$ can be updated recursively via

$$w_t^{(i)} \propto w_{t-1}^{(i)} \frac{p\left(y_t \mid x_t^{(i)}\right) p\left(x_t^{(i)} \mid x_{t-1}^{(i)}\right)}{q\left(x_t^{(i)} \mid x_{t-1}^{(i)}, y_t\right)}. \tag{4.15}$$

The problem of SIS filter is that the distribution of importance weights becomes more and more skewed as time increases. Hence, after several iterations, only few particles have non-zero importance weights. This phenomenon is called *weight degeneracy* or *sample impoverishment* (Doucet *et al.*, 2011).

The effective sample size N_{ess} is suggested to monitor how bad the degeneration is, which is defined as

$$N_{\text{ess}} = \frac{N}{1 + \text{Var}\left(w_t^{*(i)}\right)}, \tag{4.16}$$

where $w_t^{*(i)} = \frac{p\left(x_t^{(i)} | y_{1:t}\right)}{q\left(x_t^{(i)} | x_{t-1}^{(i)}, y_{1:t}\right)}$. The more difference of the biggest and smallest weights, the worse the degeneration is. In practice, the effective sample size is approximated by

$$\hat{N}_{\text{ess}} \approx \frac{1}{\sum_{i=1}^{N} \left(w_t^{(i)}\right)^2}. \tag{4.17}$$

If the value of N_{ess} is less than some threshold, some procedure should be used to avoid a worse degeneration. There are two ways one can do: choose an appropriate probability density function for importance sampling, or use resampling after SIS.

The idea of resampling is keeping the same size of particles, replacing the low weights particles with new ones. As discussed before,

$$p(x_t \mid y_{1:t}) = \sum_{i=1}^{N} w_t^{(i)} \delta\left(x_t - x_t^{(i)}\right). \tag{4.18}$$

After resampling, it becomes

$$\tilde{p}(x_t \mid y_{1:t}) = \sum_{j=1}^{N} \frac{1}{N} \delta\left(x_t - x_t^{(j)}\right) = \sum_{i=1}^{N} \frac{n_i}{N} \delta\left(x_t - x_t^{(i)}\right), \tag{4.19}$$

where n_i represents how many times the new particles $x_t^{(j)}$ were duplicated from$x_t^{(i)}$.

Then the process of SIS particle filter with resampling is summarized in following Algorithm 4.1.

In SIR, if we choose

$$q\left(x_t^{(i)} \mid x_{t-1}^{(i)}, y_t\right) = p\left(x_t^{(i)} \mid x_{t-1}^{(i)}\right), \tag{4.20}$$

Algorithm 4.1: Sampling and Importance Sampling

1 Initialization: Initialize particles at $t = 0$. For $i = 1, \ldots, N$, draw samples $\{x_0^{(i)}\}$ from $p(x_0)$.

2 **for** $t = 1, 2, \ldots, n$ **do**

3 Importance sampling: draw sample $\left\{\tilde{x}_t^{(i)}\right\}_{i=1}^{N}$ from $q(x_t \mid y_{1:t})$, calculate their weights $w_t^{(i)}$ and normalize them.

4 Resampling: Resample $\left\{\tilde{x}_t^{(i)}, \tilde{w}_t^{(i)}\right\}$ and get a new set $\left\{x_t^{(i)}, \frac{1}{N}\right\}$.

5 Output the status at time t: $\hat{x}_t = \sum_{i=1}^{N} \tilde{x}_t^{(i)} \tilde{w}_t^{(i)}$.

6 **end**

the weights become

$$\begin{aligned} w_t^{(i)} &\propto w_{t-1}^{(i)} \frac{p\left(y_t \mid x_t^{(i)}\right) p\left(x_t^{(i)} \mid x_{t-1}^{(i)}\right)}{q\left(x_t^{(i)} \mid x_{t-1}^{(i)}, y_t\right)} \\ &\propto w_{t-1}^{(i)} p\left(y_t \mid x_t^{(i)}\right). \end{aligned} \tag{4.21}$$

Because $w_{t-1}^{(i)} = \frac{1}{N}$, thus we have $w_t^{(i)} \propto p\left(y_t \mid x_t^{(i)}\right)$ and

$$w = \frac{1}{\sqrt{2\pi\Sigma}} \exp\left(-\frac{1}{2}(y_{\text{true}} - y)\Sigma^{-1}(y_{\text{true}} - y)\right). \tag{4.22}$$

However, SMC methods are suffering some drawbacks. At any time point $k(k < t)$, if $t-k$ is too large, the approximation to marginal $p(x_k \mid y_{1:t})$ is likely to be rather poor as the successive resampling steps deplete the number of distinct particle co-ordinates x_k (Andrieu *et al.*, 2010), which is also the difficulty of approximating $p(\theta, x_{1:t} \mid y_{1:t})$ with SMC algorithms (Andrieu *et al.*, 1999; Fearnhead, 2002; Storvik, 2002).

4.2.4 Auxiliary Particle Filter

The *auxiliary particle filter* (APF) is first introduced by Pitt and Shephard (1999) as an extension of SIR to perform inference in state-space model. The author uses the idea of stratification into particle filter to solve particle degeneracy by pre-selecting particles before propagation.

At each step, the algorithm draws a sample of the particle index i, which will be propagated from $t-1$ into the t, on the mixture in (4.10). These indexes are auxiliary variables only used as an intermediary step, hence the name of the algorithm (Pitt and

Shephard, 1999). Thus, the task becomes to sample from the joint density $p(x_t, i \mid y_{1:t})$. Define

$$p(x_t, i \mid y_{1:t}) \propto p(y_t \mid x_t) p\left(x_t \mid x_{t-1}^{(i)}\right) w_{t-1}^{(i)}, \tag{4.23}$$

and define $\mu_t^{(i)}$ as some characterization of $x_t \mid x_{t-1}$, which suggested by the author could be mean, mode, a sample and so on, then the joint density can be approximated by

$$\pi\left(x_t, i \mid y_{1:t}\right) \propto p\left(y_t \mid \mu_t^{(i)}\right) p\left(x_t \mid x_{t-1}^{(i)}\right) w_{t-1}^{(i)}, \tag{4.24}$$

with weights

$$w_t^{(i)} \propto \frac{p\left(y_t \mid x_t^{(i)}\right)}{p\left(y_t \mid \mu_t^{k(i)}\right)}. \tag{4.25}$$

This auxiliary variable based SIR requires only the ability to propagate and evaluate the likelihood, just as the original SIR suggested by Gordon *et al.* (1993).

The main idea behind the APF is modifying the original sequence of target distributions to guide particles in promising regions, can be extended outside the filtering framework (Johansen and Doucet, 2008). It is also recommended in the literature (Liu, 2008) that the particles can be resampled not according to the normalized weights $w_t^{\mathrm{SISR}}(x_{1:t}) = \frac{p(x_{1:t})}{p(x_{1:t-1})q(x_t|x_{1:t-1})}$ but according to a generic score function $w_t(x_{1:t}) > 0$ at time t

$$w_t(x_{1:t}) = g\left(w_t^{\mathrm{SISR}}(x_{1:t})\right), \tag{4.26}$$

where $g : \mathbb{R}^+ \mapsto \mathbb{R}^+$ is a monotonously increasing function, such as $g(x) = x^\alpha$, where $0 < \alpha \leq 1$.

4.2.5 Sequential Particle Filter

SMC method is effective for exploring the sequence of posteriors distribution $\pi(x_t \mid \theta) = p(x_t \mid y_{1:t}, \theta)$, where the static parameters are treated as known. An inference about π_{t-1} is used to draw an inference on π_t by SIS and resampling. Its interest is focusing on x_t instead of the whole path $x_{0:t}$, that is the filtering problem. However, this algorithm evolves weighting and resampling a population of N particles, $x_t^{(1)}, \ldots, x_t^{(N)}$, so that at each time t they are properly weighted samples from $\pi(x_t \mid \theta)$. Additionally, it is not practicable on huge size data sets, due to numerous iterations in the sampling process.

As a complementary solution, *sequential particle filter* method was proposed by Chopin (2002) in the first part of his doctorate thesis. Instead, sequential particle filter

uses preliminary explorations of partial distribution $\pi(\theta \mid y_{1:k})$ $(k < t)$. The concept is: an inference of $\pi(\theta)$ is drawn from the first k observations, named as learning phase, and it is updated through importance sampling to incorporate the following l observations, named as updating phase, (Chopin, 2002). This method is the *iterated batch importance sampling* (IBIS) algorithm, which is used for the recursive exploration of the sequence of the parameter posterior distributions $\pi(\theta)$. It updates a population of N particles for θ, $\theta^{(1)}, \ldots, \theta^{(N)}$, so that at each time t they are a properly weighted sample from $\pi(\theta)$. The algorithm includes occasional MCMC steps for rejuvenating the current population of particles of θ to prevent the number of distinct from decreasing over time.

In a batch mode, we are assuming that the parameter θ is static. When the first k observations become available, we can find the posterior distribution $\pi(\theta \mid y_{1:k})$. After that, with length of $l(< \infty)$ observations coming into data stream, the posterior becomes $\pi(\theta \mid y_{1:k+l})$ and it is likely to be similar with $\pi(\theta \mid y_{1:k})$. Hence, a set of proper re-weighted particles by the incremental weight is

$$\begin{aligned} w_{k,l}(\theta) &\propto \frac{\pi(\theta \mid y_{1:k+l})}{\pi(\theta \mid y_{1:k})} \\ &\propto \frac{p(y_{1:k+l} \mid \theta)}{p(y_{1:k} \mid \theta)} \\ &= p(y_{k+1:k+l} \mid y_{1:k}, \theta). \end{aligned} \tag{4.27}$$

Sequentially, the iterated batch importance sampling algorithm is in the following Algorithm 4.2.

Algorithm 4.2: Sequential Particle Filter

1 Initialization: General particles of θ_i and w_i, $i = 1, \ldots, N$.
2 **while** $k < t$ **do**
3 Re-weighting. Update the weights by $w_i^* = w_i \times w_{k,l}$, where $w_{k,l}(\theta_i) \propto p(y_{k+1:k+l} \mid y_{1:k}, \theta_i)$, $i = 1, \ldots, N$.
4 Resampling. Normalize θ_i and w_i^* to θ_i^* and $\frac{1}{N}$ according to $p(\theta_i^* = \theta_i) = \frac{w_i^*}{\sum w_i^*}$, $i = 1, \ldots, N$.
5 Propagating. Draw θ_i^m from $K_{k+l}(\theta_i^*)$, where K_{k+l} is a predefined transition kernel function with stationary distribution π_{k+l}.
6 Set $(\theta_i^m, \frac{1}{N})$ to (θ_i, w_i), $k + l$ to k.
7 **end**

The algorithm stops at $k = t$, where the particle system targets the distribution of interest $\pi(\theta \mid y_{1:t})$.

4.2.6 MCMC-Based Particle Algorithm

It is discussed that the sequential Monte Carlo approaches are powerful methodologies to cope with large data set recursively, but unfortunately, they are inefficient when apply to high dimensional problems (Septier *et al.*, 2009). An alternative set of powerful stochastic algorithms that allow us to solve most of Bayesian computational problems is MCMC method. However, as data set becomes larger and larger, it requires numerous computing in the process.

A natural extension is whether there exists a sequential MCMC method to diversify the degenerate particle population thus improving the empirical approximation for multi-target tracking or high dimensional space. Luckily, sequential approaches using MCMC method is proposed by Berzuini *et al.* (1997), who combines MCMC with importance resampling to sequentially update the posterior distribution. Other discussions, such as (Khan *et al.*, 2005; Golightly and Wilkinson, 2006; Pang *et al.*, 2008), use either resampling nor importance sampling.

As we discussed before, a filtering problem is to find the posterior distribution recursively, such as

$$p(x_t \mid y_{1:t}) \propto \int p(y_t \mid x_t) p(x_t \mid x_{t-1}) p(x_{t-1} \mid y_{1:t-1}) dx_{t-1}. \tag{4.28}$$

In particle filter, the posterior is approximated by particles $x_t^{(1)}, \ldots, x_t^{(N)}$ in equation (4.6). A MCMC procedure is designed using (4.6) as the target distribution with a proposal distribution of $q\left(x_t \mid x_t^{(i)}\right)$. Therefore, like MCMC, the desired approximation $\hat{p}(x_t \mid y_{1:t})$ is obtained by storing every accepted samples after the initial burn-in iterations (Septier *et al.*, 2009). The drawback is excessive computation occurs as the number of particles increases at each iteration.

To avoid this issue, an MCMC-based particle algorithm in (Pang *et al.*, 2008) considers the joint posterior distribution of x_t and x_{t-1}:

$$p(x_t, x_{t-1} \mid y_{1:t}) \propto p(y_t \mid x_t) p(x_t \mid x_{t-1}) p(x_{t-1} \mid y_{1:t-1}), \tag{4.29}$$

which becomes the new target distribution. At the ith sampling iteration, the joint x_k and x_{k-1} was proposed in a Metropolis-Hastings sampling step. After that, a refinement Metropolis-within-Gibbs step update x_k and x_{k-1} individually. Hence, the algorithm is summarized in Algorithm 4.3:

Algorithm 4.3: MCMC-Based Particle Algorithm

Initialization: Initialize particles $x_0^{(j)}, j = 1, \ldots, N$.

for $k = 1, \ldots, t$ **do**

  for $i = 1, \ldots, M$ **do**

    Propose $\left\{x_k^*, x_{k-1}^*\right\} \sim q_1\left(x_k, x_{k-1} \mid x_k^{(i-1)}, x_{k-1}^{(i-1)}\right)$.

    Accept $\left\{x_k^*, x_{k-1}^*\right\}$ with probability

    $\alpha_1 = \min\left\{1, \frac{p\left(x_k^*, x_{k-1}^* | y_{1:t}\right)}{p\left(x_k^{(i-1)}, x_{k-1}^{(i-1)} | y_{1:t}\right)} \frac{q_1\left(x_k^{(i-1)}, x_{k-1}^{(i-1)} | x_k^*, x_{k-1}^*\right)}{q_1\left(x_k^*, x_{k-1}^* | x_k^{(i-1)}, x_{k-1}^{(i-1)}\right)}\right\}$, where $p(\cdot \mid y_{1:t})$ is from equation (4.29)

    Propose $x_{k-1}^* \sim q_2\left(x_{k-1} \mid x_k^{(i)}, x_{k-1}^{(i)}\right)$

    Accept $x_{k-1}^{(i)} = x_{k-1}^*$ with probability

    $\alpha_2 = \min\left\{1, \frac{p\left(x_{k-1}^* | x_k^{(i)}, y_{1:t}\right)}{p\left(x_{k-1}^{(i)} | x_k^{(i)}, y_{1:t}\right)} \frac{q_2\left(x_{k-1}^{(i)} | x_{k-1}^*, x_k^{(i)}\right)}{q_2\left(x_{k-1}^* | x_k^{(i)}, x_{k-1}^{(i)}\right)}\right\}$.

    Propose $x_k^* \sim q_3\left(x_k \mid x_k^{(i)}, x_{k-1}^{(i)}\right)$.

    Accept $x_k^{(i)} = x_k^*$ with probability

    $\alpha_3 = \min\left\{1, \frac{p\left(x_k^* | x_{k-1}^{(i)}, y_{1:t}\right)}{p\left(x_k^{(i)} | x_{k-1}^{(i)}, y_{1:t}\right)} \frac{q_3\left(x_k^{(i)} | x_k^*, x_{k-1}^{(i)}\right)}{q_3\left(x_k^* | x_k^{(i)}, x_{k-1}^{(i)}\right)}\right\}$.

    After burn-in points, keep $x_k^{(j)} = x_k^{(i)}$ as new particles for approximating $p\left(x_k \mid y_{1:k}\right)$.

  end

end

Septier *et al.* (2009) discuss some attractive features of genetic algorithms and simulated annealing into the framework of MCMC based particle scheme. One may refer to the reference for details.

4.3 On-line State and Parameter Estimation

The state transition density and the conditional likelihood function depend not only upon the dynamic state x_t, but also on a static parameter vector θ, which will be stressed by use of the notations $f(x_t \mid x_{t-1}, \theta)$ and $g(y_t \mid x_t, \theta)$. Putting the algorithms on-line means to update the parameters and states instantly as new observations coming into the data stream. For Bayesian dynamic models, however, the most natural option consists in treating the unknown parameter θ, using the state-space representation, as a component of the state which lacks dynamic evolution, also referred to

as a static parameter (Cappé *et al.*, 2007). The standard SMC is deficient for on-line parameter estimation. As a result of the successive resampling steps, after a certain time t, the approximation $\hat{p}(\theta \mid y_{1:t})$ will only contain a single unique value for θ. In other words, SMC approximation of the marginalized parameter posterior distribution is represented by a single Dirac delta function. It also causes error accumulation in successive Monte Carlo steps growing exponentially or polynomially in time (Kantas *et al.*, 2009).

In this section, we discuss some methods that estimate combined state and parameter by either jointly estimating the state and parameter or by marginalizing the parameter through sufficient statistics.

4.3.1 Artificial Dynamic Noise

Some methods are trying to solve the posterior distribution $p(\theta \mid y_{1:t})$ by

$$p(\theta \mid y_{1:t}) \propto p(y_{1:t} \mid \theta)p(\theta) \tag{4.30}$$

through maximize the likelihood function without introducing any bias or controlling the bias in states propagation. A pragmatic approach to reduce parameter sample degeneracy and error accumulation in successive MC approximations is to adding an artificial dynamic equation on θ, (Higuchi, 2001; Kitagawa, 1998), which gives

$$\theta_{n+1} = \theta_n + \varepsilon_{n+1}. \tag{4.31}$$

The artificial noise $\varepsilon_{t+1} \sim N(0, W_{t+1})$ is specified by a covariance matrix W_{t+1}. With this noise, SMC can now be applied to approximate $p(x_{1:t}, \theta \mid y_{1:t})$. A related kernel density estimation method proposes a kernel density estimate of the target (Liu and West, 2001)

$$\hat{p}(\theta \mid y_{1:t}) = \frac{1}{N} \sum M\left(\theta - \theta_n^{(i)}\right). \tag{4.32}$$

At time $t + 1$, the samples obtain a new set of particles.

4.3.2 Practical Filtering

A *fixed-lag approach* to filtering and sequential parameter learning was proposed in (Polson *et al.*, 2008). Its key idea is to express the filtering distribution as a mixture of lag-smoothing distributions and to implement it sequentially.

With a fixed-lag l, the state filtering and parameter learning require the sequence of the joint distribution $p(x_t, \theta \mid y_{1:t})$, which implies the desired filtering distribution

$p(x_t \mid y_{1:t})$ being marginalized as

$$p(x_t \mid y_{1:t}) = \int p(x_{t-l+1:t} \mid y_{1:t}) dx_{t-l+1:t-1}, \tag{4.33}$$

and the posterior distribution of the parameter $p(\theta \mid y_{1:t})$. Arguing that the approximation that draws from $p(x_{0:t-l} \mid y_{1:t-1})$ are approximate draws from $p(x_{0:t-l} \mid y_{1:t})$, the state filtering with static parameter θ is

$$\begin{aligned} p(x_{t-l+1:t}, \theta \mid y_{1:t}) &= \int p(x_{t-l+1,t}, \theta \mid x_{0:t-l}, y_{1:t}) dp(x_{0:t-l} \mid y_{1:t}) \\ &\approx \int p(x_{t-l+1,t}, \theta \mid x_{0:t-l}, y_{1:t}) dp(x_{0:t-l} \mid y_{1:t-1}). \end{aligned} \tag{4.34}$$

Therefore we can draw some samples $x_{0:t-l}^{(i)}$ first from $p(x_{0:t-l} \mid y_{1:t-1})$, which is approximately the same as $p(x_{0:t-l} \mid y_{1:t})$ and $i = 1, \ldots, M$. Then, use these samples to estimate states and parameter by

$$x_{t-l+1} \sim p\left(x_{t-l+1} \mid x_{0:t-l}^{(i)}, \theta, y_{t-l+1:t}\right), \tag{4.35}$$

$$\theta \sim p\left(\theta \mid x_{0:t-l}^{(i)}, x_{t-l+1}, y_{t-l+1:t}\right), \tag{4.36}$$

with two-step Gibbs sampler. The algorithm is summarized in the following.

The speed and accuracy of this algorithm depend on the choice of sample size M and the lag l, which is difficult, and there is a non-vanishing bias that is difficult to quantify (Polson *et al.*, 2008; Kantas *et al.*, 2009).

4.3.3 Liu and West's Filter

Particles degeneracy is inevitable in SMC. A method in Section 4.3.1 reduces the degeneracy by adding artificial noise to the parameters, however, that will also lead to the variance of estimates. Liu and West (2001) use a kernel smoothing approximation combined with a neat shrinkage idea to kill over-dispersion.

At time t, suppose we have particles $\left\{x_t^{(i)}\right\}$ and associated weights $\left\{w_t^{(i)}\right\}$, $i = 1, \ldots, N$, Bayes' theorem tells us that approximation to the posterior distribution $p(x_{t+1} \mid y_{1:t+1})$ at time $t+1$ of the state is

$$p(x_{t+1} \mid y_{1:t+1}) \propto \sum_{i=1}^{N} w_t^{(i)} p\left(x_{t+1} \mid x_t^{(i)}\right) p\left(y_{t+1} \mid x_{t+1}\right). \tag{4.37}$$

However, variance increases through over t by the Gaussian mixture. West (1993) uses a smooth kernel density

$$p(\theta \mid y_{1:t}) \approx \sum_{i=1}^{N} w_t^{(i)} N\left(\theta \mid m_t^{(i)}, h^2 V_t\right) \tag{4.38}$$

Algorithm 4.4: Practical Filtering Algorithm

Initialization: Set $\theta^{(i)} = \theta_0$ as initial values, $i = 1, \ldots, N$.
Burn-In: **for** $k = 1, \ldots, l$ **do**
    for $i = 1, \ldots, N$ **do**
        Initialize $\theta = \theta^{(i)}$.
        Generate $x_{0:k} \sim p(x_{0:k} \mid \theta, y_{1:k})$ and $\theta \sim p(\theta \mid x_{0:k}, y_{1:k})$.
        After a few iterations, achieve a set of $\left\{\tilde{x}_{0:k}^{(i)}, \theta^{(i)}\right\}$.
    end
end
Sequential Updating: **for** $k = l+1, \ldots, t$ **do**
    for $i = 1, \ldots, N$ **do**
        initialize $\theta = \theta^{(i)}$.
        Generate $x_{k-l+1:k} \sim p\left(x_{k-l+1:k} \mid \tilde{x}_{k-l}^{(i)}, \theta, y_{k-l+1,k}\right)$ and
        $\theta \sim p\left(\theta \mid \tilde{x}_{0:k-l}^{(i)}, x_{k-l+1:k}, y_{1:k}\right)$.
        Achieve a set of $\left\{\tilde{x}_{k-l+1}^{(i)}, \theta^{(i)}\right\}$ and leave $\tilde{x}_{0:k-l}^{(i)}$ unchanged.
    end
end

to against the sample dispersion. Here, V_t is the Monte Carlo variance matrix of $p(\theta \mid y_{1:t})$. Because $N(\cdot \mid m, C)$ is a multivariate normal density with mean m and covariance matrix C, so the above density (4.38) is a mixture of $N\left(\theta \mid m_t^{(i)}, h^2 V_t\right)$ distributions weighted by the sample weights $w_t^{(i)}$. Without this shrinkage approach, the standard kernel locations would be $m_t^{(i)} = \theta_t^{(i)}$, by which there is an over dispersed kernel density, because of $(1 = h^2)V_t$ is always large than V_t. θ_t indicates that the samples are from the posterior at a specific time t instead of time-varying.

To correct it, the idea of shrinkage kernel is taking

$$m_t^{(i)} = \alpha\theta_t^{(i)} + (1 - \alpha)\bar{\theta}_t, \tag{4.39}$$

where $\alpha = \sqrt{1 - h^2}$ and $h > 0$ is the smoothing parameter. Consequently, the resulting normal mixture retains the mean $\bar{\theta}_t$ and now has the correct covariance V_t, hence the over dispersion is trivially corrected (Liu and West, 2001).

A general algorithm is summarized bellow:

Algorithm 4.5: Liu and West's Filter

for $k = 1, \ldots, t$ **do**
  for $i = 1, \ldots, N$ **do**
    Identify the prior estimation of (x_k, θ) by $(\mu_{k+1}^{(i)}, m_k^{(i)})$, where $\mu_{k+1}^{(i)} = \mathrm{E}(x_{k+1} \mid x_k^{(i)}, \theta_k^{(i)})$, and $m_k^{(i)} = \alpha\theta_k^{(i)} + (1-\alpha)\bar{\theta}_k$.
    Sample an auxiliary integer index I from $\{1, \ldots, N\}$ with probability proportional to $g_{k+1}^{(i)} \propto \tilde{w}_k^{(i)} p(y_{k+1} \mid \mu_{k+1}^{(i)}, m_k^{(i)})$.
    Sample a new parameter vector $\theta_{k+1}^{(I)}$ from $N(\theta_{k+1} \mid m_k^{(I)}, h^2 V_k)$.
    Sample current state vector $x_{k+1}^{(I)}$ from $p(x_{k+1} \mid x_k^{(I)}, \theta_{k+1}^{(I)})$.
    Evaluate weights $w_{k+1}^{(i)} \propto \frac{p(y_{k+1} \mid x_{k+1}^{(I)}, \theta_{k+1}^{(I)})}{p(y_{k+1} \mid \mu_{k+1}^{(I)}, m_k^{(I)})}$
  end
  Normalize weights: $\tilde{w}_{k+1}^{(i)} = \frac{w_{k+1}^{(i)}}{\sum w_{k+1}^{(i)}}$.
end

4.3.4 Storvik Filter

Storvik filter, proposed by Storvik (2002), is assuming that the posterior $p(\theta \mid x_{0:t}, y_{1:t})$ depends on a low dimensional set of sufficient statistics s_t with an associated recursive update via $s_t = S(s_{t-1}, x_t, y_t)$. This approach is based on marginalizing the static parameters out of the posterior distribution, in which only the state vector needs to be considered, and aiming at reducing the particle impoverishment. It can be thought of as an extension of particle filters with additional steps of updating sufficient statistics and sampling parameters sequentially (Lopes and Tsay, 2011). In particular, models for which the underlying process is Gaussian and linear in the parameters can be handled by this approach (Storvik, 2002). Moreover, some observational distributions with unknown parameters can also be handled by this approach but subject to unavailable sufficient statistics.

The Storvik filter is summarized bellow:

4.3.5 Particle Learning

Carvalho *et al.* (2010) propose the *Particle Learning* that uses the similar sufficient statistics as Storvik filter does, in which the set of sufficient statistics is used for parameters estimation only. As an extension to the mixture Kalman filter (Chen and Liu, 2000), Particle Learning allows parameters learning throughout the process and

Algorithm 4.6: Storvik Filter

for $k = 1, \ldots, t$ **do**
  for $i = 1, \ldots, N$ **do**
    Sample $x_k^{(i)}$ from $p\left(x_k \mid x_{k-1}^{(i)}, y_{1:k}, \theta^{(i)}\right)$.
    Calculate weights $w_k \propto p\left(y_k \mid x_k^{(i)}, \theta^{(i)}\right)$ and normalize it by $\tilde{w}_k^{(i)} = \frac{w_k^{(i)}}{\sum w_k^{(i)}}$.
    Resample $\left\{\theta_k^{(i)}, x_k^{(i)}, s_k^{(i)}\right\}$ according to $\tilde{w}_k$.
    Update sufficient statistics $s_k^{(i)} = S\left(s_{k-1}^{(i)}, x_k, y_k\right)$.
    Sample $\theta^{(i)}$ from $p\left(\theta \mid s_k^{(i)}\right)$.
  end
end

utilize a resampling propagate framework together with a set of particles that includes a set of sufficient statistics (if it is available) for the states.

By denoting s_t and s_t^x the sufficient statistics for the parameter and state respectively, the updating rules are satisfied: $s_t = S(s_{t-1}, x_t, y_t)$ and $s_t^x = K\left(s_{t-1}^x, \theta, y_t\right)$, where $K(\cdot)$ is the Kalman filter recursions. In Particle Learning, the prior to sampling from the proposal distribution uses a predictive likelihood and takes y_{t+1} into account (Vieira and Wilkinson, 2016). This algorithm is summarized in the following:

Algorithm 4.7: Particle Learning Algorithm

for $k = 1, \ldots, t$ **do**
  for $i = 1, \ldots, N$ **do**
    Resample $\tilde{z}_k^{(i)} = \left(\tilde{s}_k^{x(i)}, \tilde{s}_k^{(i)}, \tilde{\theta}^{(i)}\right)$ from $z_k^{(i)} = \left(s_k^x, s_k, \theta\right)^{(i)}$ with weight $w_k \propto p\left(y_{k+1} \mid z_t^{(i)}\right)$.
    Draw $x_{k+1}^{(i)}$ from $p\left(x_{k+1} \mid \tilde{z}_t^{(i)}, y_{1:k+1}\right)$.
    Update parameter-sufficient statistics $s_{k+1}^{(i)} = S\left(\tilde{s}_k^{(i)}, x_{k+1}^{(i)}, y_{k+1}\right)$.
    Sample $\theta^{(i)}$ from $p\left(\theta \mid s_{k+1}^{(i)}\right)$.
    Update state-sufficient statistics $s_{k+1}^{x(i)} = K\left(s_k^{x(i)}, \theta^{(i)}, y_{k+1}\right)$.
  end
end

4.3.6 Adaptive Ensemble Kalman Filter

Storvik filter and Particle learning algorithms are efficient in some ways, however, the drawbacks are obvious. One of them is that the sufficient statistics are not always available, or hard to find, for complex models. They are trying to reduce the problem of particle impoverishment, although in practice they did not solve the problem completely (Chopin *et al.*, 2010). A Bayesian adaptive ensemble Kalman filter method was proposed for sequential state and parameter estimation by Stroud *et al.* (2018). This method is fully Bayesian and propagates the joint posterior density of states and parameters through over the process.

The ensemble Kalman filter, which is an extension to the standard Kalman filter, is an approximate filtering method introduced in the geophysics literature by Evensen (1994). Instead of working with the entire distribution, the ensemble Kalman filter stores propagates and updates an ensemble of vectors that approximates the state distribution (Katzfuss *et al.*, 2016).

Recall that an on-line combined parameters and state estimation relies on the decomposition of the joint posterior distribution

$$p(x_{t+1}, \theta \mid y_{1:t+1}) \propto p(x_{t+1} \mid y_{1:t+1}, \theta) p(\theta \mid y_{1:t+1}). \tag{4.40}$$

To implement on-line sequential estimation, the first term on the right side of the above formula should be written in the following recursive form as

$$p(x_{t+1} \mid \theta, y_{1:t+1}) \propto p(y_{t+1} \mid x_{t+1}, \theta) \int p(x_{t+1} \mid x_t, \theta) p(x_t \mid \theta, y_{1:t}) dx_t, \tag{4.41}$$

and the second term in the recursive form is

$$\begin{aligned} p(\theta \mid y_{1:t+1}) &\propto p(y_{1:t+1} \mid \theta) p(\theta) \\ &= p(y_{t+1} \mid \theta, y_{1:t}) p(\theta \mid y_{1:t}). \end{aligned} \tag{4.42}$$

The ensemble Kalman filter is used to find (4.41), which is the state inference. The estimated Kalman gain is

$$\hat{K}_{t+1}(\theta) = F_{t+1}(\theta) \hat{P}^f_{t+1}(\theta) F^\top_{t+1}(\theta) \hat{\Sigma}^{-1}_{t+1}(\theta), \tag{4.43}$$

where F_{t+1} is the observation map. The posterior ensemble at time $t+1$ based on parameter θ is

$$x^{(i)}_{t+1} = x^{f(i)}_{t+1} + \hat{K}_{t+1}(\theta) \left(y_{t+1} + v^{(i)}_{t+1} + F_{t+1}(\theta) x^{f(i)}_{t+1} \right), \tag{4.44}$$

where $\left\{x_t^{(i)}\right\}_1^N$ is an ensemble of states representing the filtering distribution at time t. $x_{t+1}^{f(i)}$ is the forecast ensemble from the forward map by $x_{t+1}^{f(i)} = x_{t+1}^{p(i)} + w_{t+1}^{(i)} = G\left(x_t^{(i)}\right) + w_{t+1}^{(i)}$. For the second term of (4.42), Stroud *et al.* (2018) propose a feasible likelihood approximation by a multivariate Gaussian distribution (Mitchell and Houtekamer, 2000) for high-dimensional states:

$$p(y_{t+1} \mid \theta, y_{1:t}) \propto \left|\hat{\Sigma}_t(\theta)\right|^{-\frac{1}{2}} \exp\left(-\frac{1}{2}\hat{e}_{t+1}(\theta)^\top \hat{\Sigma}_t(\theta)^{-1}\hat{e}_{t+1}(\theta)\right), \tag{4.45}$$

where $\hat{e}_{t+1}(\theta) = y_{t+1} - F_{t+1}(\theta)\hat{a}_{t+1}$, and $\hat{a}_{t+1} = \frac{1}{N}x_{t+1}^{p(i)}$

To find $p(\theta \mid y_{1:t})$, a generic way is using a normal approximation, where the posterior density is given by

$$p(\theta \mid y_{1:t}) \propto \exp\left(-\frac{1}{2}(\theta - m_t)^\top C_t^{-1}(\theta - m_t)\right). \tag{4.46}$$

A grid-based representation is writing the posterior in the way that $p(\theta \mid y_{1:t}) \propto p(y_t \mid \theta, y_{1:t-1})p(\theta \mid y_{1:t-1})$. The recursion weights can be updated by $\pi_{t,k} \propto p(y_t \mid \theta, y_{1:t-1})\pi_{t,k-1}$.

To summarize it up, the complete algorithm is in the following

Algorithm 4.8: Adaptive Ensemble Kalman Filter

```
Initialize samples θ^(i) ~ p(θ) and x_1^(i) ~ N(x_0, P_0), i = 1, ..., N.
for k = 1, ..., t do
    for i = 1, ..., N do
        Propagate. x_k^p(i) = G(x_{k-1}^(i)).
        Approximate likelihood function by (4.45).
        Update the analytical parameter distribution using either use normal
         approximation or grid-based approximation to find (4.42).
        Draw θ^(i) ~ p̂(θ | y_{1:k}).
        Generate forecast ensemble by x_k^f(i) = x_k^p(i) + w_k.
        Draw posterior ensemble using equation (4.44).
    end
end
```

This algorithm works well when θ is small and the parameter in the forward map $G(\cdot)$ is known. If the forward map parameter is not known and has a high correlation with the state, the author suggests that it can be combined with the state augmentation (Anderson, 2001) and this algorithm is still working.

4.3.7 On-line Pseudo-Likelihood Estimation

Bayesian estimation requires the posterior distribution of $p(\theta \mid y_{1:t})$, where the θ is treated as a random variable. By contrast, maximum likelihood estimation is looking for a value $\hat{\theta}$, which maximum the likelihood $p(y_{1:t} \mid \theta)$.

The classical *expectation maximization* (EM) algorithm (Dempster *et al.*, 1977) for maximizing $l(\theta)$ is a two step procedure:

- E-step: Compute $Q(\theta_k, \theta) = \int \ln p_\theta(x_{0:t}, y_{1:t}) p_{\theta_k}(x_{0:t} \mid y_{1:t}) dx_{0:t}$.
- M-step: Update the parameter θ_k by $\theta_{k+1} = \arg\max Q(\theta_k, \theta)$.

Then $\{l(\theta_k)_k\}$ generated by the EM is a non-decreasing sequence.

A straightforward *on-line EM* algorithm uses SMC method to maximize $l(\theta)$. However, it requires estimating sufficient statistics base on joint probability distributions whose dimension is increasing over time and has a computational load of $O(N^2)$ per time step (Kantas *et al.*, 2009). To circumvent this problem, Andrieu *et al.* (2005) propose a pseudo-likelihood function for finite state-space models.

Assuming that the process is stationary, give a time lag $L \geq 1$ and any $k \geq 1$, $x_{1:t}$ and $y_{1:t}$ are sliced to $X_k = x_{kL+1:(k+1)L}$ and $Y_k = y_{kL+1:(k+1)L}$. For example: $X_1 = x_{L+1:2L}$ consisting of L data. Further, the joint distribution of $p(X_k, Y_k)$ is

$$p(X_k, Y_k) = \pi(x_{kL+1}) F(y_{kL+1} \mid x_{xL+1}) \Pi_{n=kL+2}^{(k+1)L} G(x_n \mid x_{n-1}) F(y_n \mid x_n). \tag{4.47}$$

The likelihood of a block Y_k of observations is given by

$$p(Y_k) = \int p\left(X_k, Y_k\right) dX_k, \tag{4.48}$$

and the log pseudo-likelihood for m slices is $\sum_{k=0}^{m-1} \ln p(Y_k)$ (Andrieu *et al.*, 2005).

The advantage of this algorithm is that it only requires an approximation of the fixed dimensional distribution $p(X_k \mid Y_k)$ and don't suffer degeneracy for small L (Kantas *et al.*, 2009). The disadvantage is that it only applies to stationary distribution, and can be observed empirically that the algorithm might converge to incorrect values and even sometimes drift away from the correct values as t increases (Andrieu *et al.*, 2010).

4.4 Simulation Study

In this section, we compare the performance of Liu and West's filter (LW), Storvik filter (St), Particle Learning (PL) and the proposed sequential MCMC Algorithm 5.2

in Section 5.5 by a simple dynamic linear model, see examples in (Liu and West, 2001). Explicitly, the model is

$$\begin{aligned} y_t &= Fx_t + \varepsilon_t, \\ x_t &= \phi x_{t-1} + w_t, \\ x_0 &\sim N(m_0, C_0), \end{aligned} \tag{4.49}$$

where $\varepsilon_t \sim N(0, \sigma^2)$ and $w_t \sim N(0, \tau^2)$, x_t are hidden status and y_t are observations. Assuming that $F = 1$, $\sigma^2 = 1$ and $\tau^2 = 1$. The initial value $x_0 = 0$. $\theta = \phi$ a single static parameter without unobserved state variable.

A length of 897 simulated data set was generated from this $AR(1)$ model at $\phi = 0.8$. First of all, we should find the sufficient statistics for Storvik filter and Particle Learning. For Particle Learning, the sufficient statistics s_t^x for state x and s_t for parameter ϕ are satisfying the updating rules $s_t^x = K\left(s_{t-1}^x, \phi, y_t\right)$ and $s_t = S\left(s_{t-1}, x_t, y_t\right)$ respectively. Because of the assumption, the Kalman observation map is $H_k = 1$ and the variances are normal distributed. Thus, the Kalman gain is $K = 1$. For details, the Particle Learning algorithm runs as :

- Step 1. Resample $\left\{\tilde{z}_t^{(i)}\right\}_{i=1}^N = \left(\tilde{s}_t^{x(i)}, \tilde{s}_t^{(i)}, \tilde{\phi}^{(i)}\right)$ from $p\left(z_t \mid s_t^x, s_t, \phi\right)$ with weight $w \propto p\left(y_{t+1} \mid s_t^x, \phi\right)$. It is found that

$$p\left(y_{t+1} \mid s_t^x, \phi\right) \propto \exp\left(-\frac{1}{2}\left(y_{t+1} - \phi x_t\right)^2\right).$$

- Step 2. Draw $x_{t+1}^{(i)}$ from $p\left(x_{t+1} \mid \tilde{s}_t^x, \tilde{\phi}, y_{1:t+1}\right)$.

$$\begin{aligned} p\left(x_{t+1} \mid \tilde{z}_t^{(i)}, y_{1:t+1}\right) &= p\left(x_{t+1} \mid s_t^x, \phi, y_{1:t+1}\right) \propto p\left(x_{t+1}, y_{1:t+1} \mid s_t^x, \phi\right) \\ &\propto p\left(x_{t+1} \mid s_t^x, \phi\right) p\left(y_{t+1} \mid x_{t+1}, s_t^x, \phi\right) \\ &= N\left(x_{t+1} \mid \phi x_t, 1\right) N\left(y_{t+1} \mid x_{t+1}, 1\right) \\ &= N\left(x_{t+1} \mid \frac{1}{2}\left(y_{t+1} + \phi x_t\right), \frac{1}{\sqrt{2}}\right) \end{aligned}$$

- Step 3. Update sufficient statistics $s_{t+1} = S\left(\tilde{s}_t, x_{t+1}, y_{t+1}\right)$.

$$\begin{aligned} s_{t+1,1} &= x_{t+1} \\ s_{t+1,2} &= x_t x_{t+1} + s_{t,2} = x_t s_{t,1} + s_{t,2} \\ s_{t+1,3} &= x_t^2 + s_{t,3} = s_{t,1}^2 + s_{t,3}. \end{aligned}$$

- Step 4. Sampling ϕ from $p(\phi \mid s_{t+1})$.

$$p(\phi \mid x_{1:t+1}, y_{1:t+1}) \propto p(x_{1:t+1}, y_{1:t+1} \mid \phi)\, p(\phi) \propto p(x_{1:t+1} \mid \phi)\, p(\phi)$$
$$= N\left(\phi \mid \frac{s_{t+1,2}}{s_{t+1,3}}, \frac{1}{s_{t+1,3}}\right).$$

- Step 5. Update from s_t^x to s_{t+1}^x via $s_{t+1}^x = K(s_t^x, \phi, y_{t+1})$.

Notice that the proposed sliding window MCMC algorithm requires using a few data to learn the parameter's mean and variance in the learning phase. Besides, LW, St and PL do not converge at the first few data. Then, to be fair, we take the first 300 data out and use them in the learning phase of the proposed algorithm. In the estimation phase, we use three different strategies: a fixed length of 100, a fixed length of 300 and an expanding length including all the historical data along with time t. In the former three algorithms, we use 5 000 particles to infer state and parameter. In the latter MCMC algorithm, we take 5 000 samples at each time t for $x_t^{(i)}$ and $\phi^{(i)}$, where $i = 1, \ldots, 5\,000$ and $t = 300, \ldots, 897$. Furthermore, we run the comparison for 50 times to check their stabilities.

From Figure 4.1, it can be seen that the former three algorithms converge to the true parameter ϕ at similar speeds along with the time t. LW filter has a larger distance to the true parameter comparing with St and PL filters. The proposed MCMC with 100 length data in estimation phase has the largest variance. By setting a longer length L, the proposed adaptive MCMC becomes stable.

From Figure 4.2, we can see that, by repeatedly running 50 simulations, the proposed MCMC algorithm is more precise in estimating parameter ϕ as it has the lowest standard error (SE) among all the algorithms. However, for the sliding window approaches, the estimate for ϕ shows more variability as more data is incorporated. Nevertheless, this does not affect state inference: the MSE of all the algorithms on estimating x is at a similar level.

The estimates for x_t from $t = 300$ to 897 are very close and the differences are hard to tell visually. See Figure 4.3.

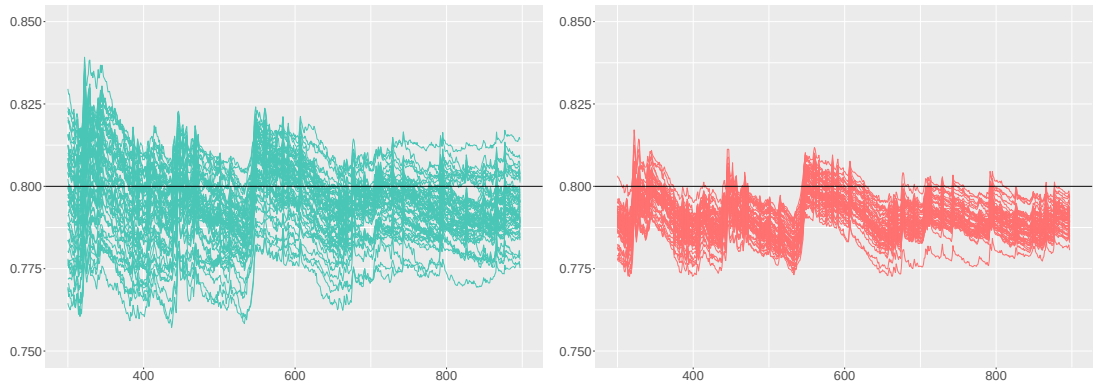

(a) Liu and West's filter

(b) Storvik Filter

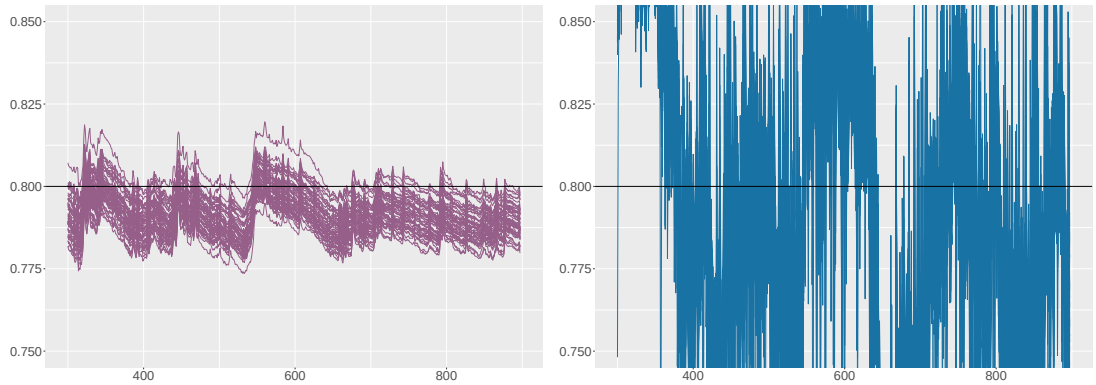

(c) Particle Learning

(d) MCMC with 100-length

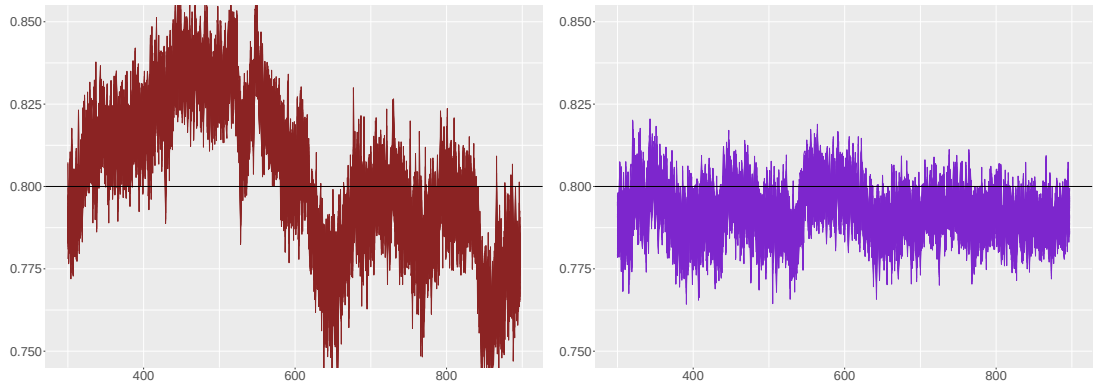

(e) MCMC with 300-length

(f) MCMC with varying-length

Figure 4.1: Plots of the inferred value of ϕ over time; median value shown for filtering methods and mean value shown for MCMC methods. Repeatedly running 50 times with cutting off the first **300** data. It is apparent that all these algorithms converge to the true parameter (black horizontal line) along with time. St, PL and MCMC-vary have a narrower range. MCMC-100 has a higher variability and MCMC-vary has the least. The more data incorporated in the estimation phase the better approximation to be obtained.

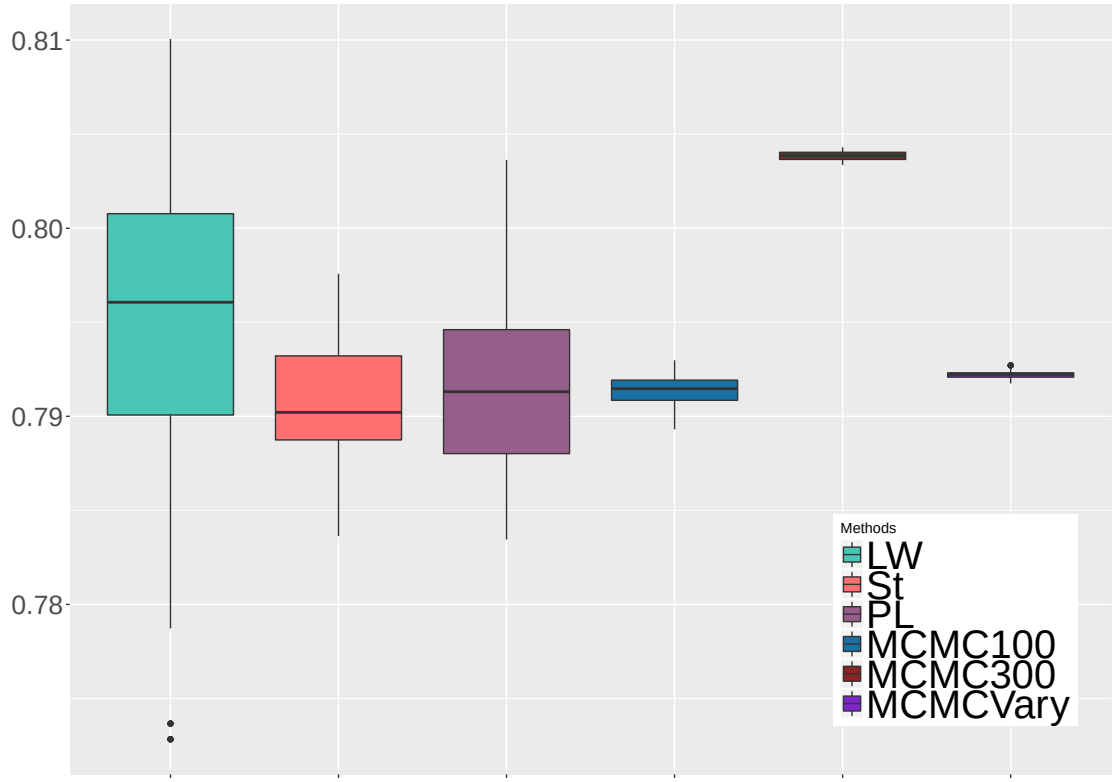

	LW	St	PL	MCMC-100	MCMC-300	MCMC-vary
Mean of $\hat{\phi}$	0.7947	0.7908	0.7918	0.7914	0.8038	0.7922
SE of $\hat{\phi}$ ($\times 10^{-4}$)	13.1000	4.8793	6.2877	1.1388	0.3275	0.27506
$\frac{1}{n}\sum_t(\hat{x}_t - x_t)^2$	0.5745	0.5739	0.5737	0.5875	0.5741	0.5740

Figure 4.2: Box-plots comparison of all the algorithms. The proposed MCMC algorithm is more stable than other filters.

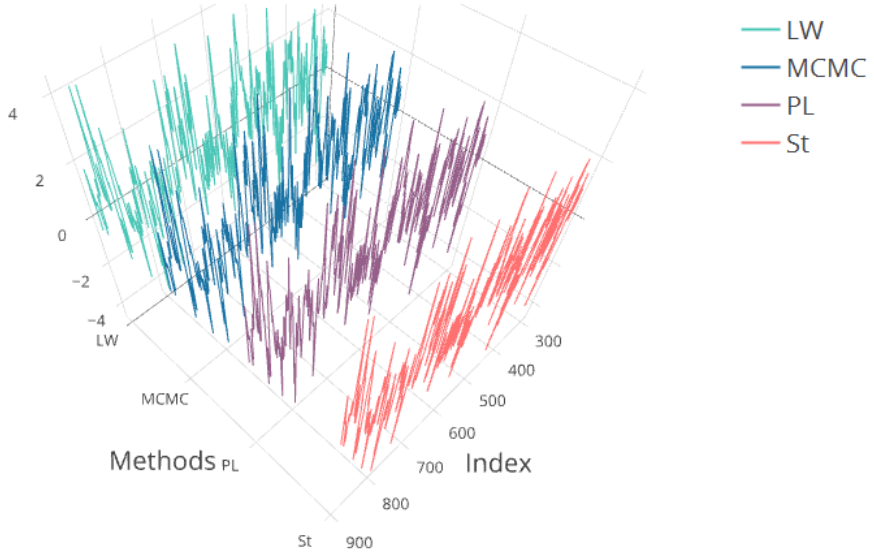

Figure 4.3: Plot of state estimation over time; $\hat{x}_t$ is median value for filtering methods and mean value for MCMC methods. The filtering for $x_{300:897}$ is competitive. The algorithms return very similar estimates. The plots for MCMC-100 and MCMC-300 are hard to distinguish from MCMC-vary.

4.5 Conclusion

In this chapter, we take an overview of existing sequential state estimation methods and combined state and parameter estimation methods. The particle filter is an efficient algorithm for state estimation, although the particles impoverishment is inevitable. Extended to this method, researchers are working on killing particles degeneracy and several accomplishments have been achieved. A new challenge is estimating the unknown parameters. In no doubt, for complex stochastic processes and dynamics, both Bayesian and Frequentist methods are working well. One refer to (Wakefield, 2013) for further discussions between Bayesian and Frequentist methods and implementation.

As a summary, most of the research issues for filtering and parameter estimation focus on

(i) Choices of resampling scheme to kill particles degeneracy, such as Liu and West's filter.

(ii) Exploration of an efficient sampling algorithm, such as Metropolis-Hastings sampler and related sampling algorithms.

(iii) Exploration of accurate estimation with low variances in higher dimensional space.

Subject to pages and time, some algorithms are not included in this chapter. For more information and interests, readers can refer to unscented Kalman filter (Wan and Van Der Merwe, 2000) and its related algorithms for non-linear estimation, particle MCMC (Andrieu *et al.*, 2010) for off-line Bayesian estimation and on-line gradient approach (Poyiadjis *et al.*, 2005) for parameter estimation.

Chapter 5

Adaptive Sequential MCMC for On-line State and Parameter Estimation

5.1 Introduction

Data assimilation is a sequential process, by which the observations are incorporated into a numerical model describing the evolution of this system throughout the whole process. The quality of the numerical model determines the accuracy of this system, which requires sequential combined state and parameter inferences. An enormous literature exists on pure state estimation, however, less research has been carried out on combined state and parameter estimation.

Sequential Monte Carlo (SMC) has been well studied in scientific literature and have been applied in real world applications. It allows us to specify complex, non-linear time series patterns and enables us to perform real-time Bayesian estimations when it is coupled with *Dynamic Generalized Linear Models* (Vieira and Wilkinson, 2016). However, model parameters are unknown in real-world applications and this restricts the usefulness of standard SMC. Extensions to standard SMC have been considered by a number of researchers. Kitagawa (1998) propose a self-organizing filter and augmenting the state vector with unknown parameters. The state and parameter are estimated simultaneously by either a non-Gaussian filter or a particle filter. Liu and West (2001) propose an improved particle filter to kill degeneracy, which is a common issue in static parameter estimation. They use a kernel smoothing approximation, with a correction factor to account for over-dispersion. Alternatively, Storvik (2002)

propose a new filter algorithm by assuming the posterior depends on a set of sufficient statistics, which can be updated recursively. However, this approach only applies to parameters with conjugate priors (Stroud *et al.*, 2018). Unlike Storvik filter, the Particle learning approach, introduced by Carvalho *et al.* (2010), uses sufficient statistics solely to estimate parameters and promises to reduce particle impoverishment. These particle-like methods use more or less sampling and resampling algorithms to update particles recursively.

Stroud *et al.* (2018) propose an SMC algorithm by using ensemble Kalman filter framework for high dimensional space models with observations. Their approach combines information about the parameters from data at different time points in a formal way of Bayesian updating. Polson *et al.* (2008) rely on a fixed-lag length of data approximation to filtering and sequential parameter learning in a general dynamic state-space model. This approach allows for sequential parameter learning where importance sampling has difficulties and avoids degeneracies in particle filtering. A new adaptive MCMC method yields a quick and flexible way for estimating posterior distribution in parameter estimation (Haario *et al.*, 1999). This new adaptive proposal method depends on historical data, is introduced to avoid the difficulties of tunning the proposal distribution in Metropolis-Hastings methods.

A further question is how to find an efficient way to draw samples for θ. There are a few sampling algorithms that have been discussed in literatures, such as importance sampling (Hammersley and Handscomb, 1964; Geweke, 1989), rejection sampling (Casella *et al.*, 2004; Martino and Míguez, 2010), Gibbs sampling (Geman and Geman, 1984), Metropolis-Hastings method (Metropolis *et al.*, 1953; Hastings, 1970) and so on. Finally, delayed acceptance MCMC has been used to speed up computations (Payne and Mallick, 2018; Quiroz *et al.*, 2018). The main idea in delayed acceptance is to avoid computations if there is an indication that the proposed draw will ultimately be rejected.

In this chapter, an adaptive Delayed-Acceptance Metropolis-Hastings algorithm is proposed to estimate the posterior distribution for combined state and parameter with two phases. In the learning phase, a self-tuning random walk Metropolis-Hastings sampler is used to learn the parameter mean and covariance structure. In the estimation phase, the parameter mean and covariance structure informs the proposed mechanism and is also used in a delayed-acceptance algorithm, which greatly improves sampling efficiency. Information on the resulting state of the system is given by a Gaussian mixture. To keep the algorithm a higher computing efficiency for on-line estimation,

it is suggested to cut off historical data and to use a fixed length of data up to the current state, like a window sliding along with time. At the end of this chapter, an application of this algorithm on irregularly sampled GPS time series data is presented.

5.2 Bayesian Inference on Combined State and Parameter

In a general state-space model, a forward map F controls the stochastic evolution of the state x_t and an observation model G connects the observation y_t to the state x_t. The goal of inference is to estimate the state of the system and the parameters of the forward map and the observation model. Given a probability for the initial state, $p(x_1 \mid \theta)$, where θ are the parameters to be estimated, and a prior distribution over the parameters, $p(\theta)$, the general Bayesian filtering problem requires computing the posterior distribution of the current state, $p(x_t \mid y_{1:t})$. If we assume that, given x_{t-1}, x_t is conditionally independent of states at all other times and all observations, then

$$p(x_t \mid y_{1:t}, \theta) = \int p(x_t \mid x_{t-1}, \theta) p(x_{t-1} \mid y_{1:t}, \theta) dx_{t-1}, \tag{5.1}$$

where $y_{1:t} = \{y_1, \ldots, y_t\}$ is the observation information up to time t. Then given the posterior distribution for the parameters at time t, $p(\theta \mid y_{1:t})$, we have

$$p(x_t \mid y_{1:t}) = \int p(x_t \mid y_{1:t}, \theta) p(\theta \mid y_{1:t}) d\theta. \tag{5.2}$$

The approach in equation (5.2) relies on the two terms: (i) a conditional posterior distribution for the states with given parameters and observations; (ii) a marginal posterior distribution for parameter θ. Several methods can be used in finding the second term, such as cross validation, Expectation Maximization algorithm, Gibbs sampling, Metropolis-Hastings algorithm and so on. A Monte Carlo method is popular in research area solving this problem. Monte Carlo method is an algorithm that relies on repeated random sampling to obtain numerical results. To compute an integration of $\int f(x)dx$, one has to sample as many independent x_i, $(i = 1, \ldots, N)$, as possible and numerically to find $\frac{1}{N}\sum_i f(x_i)$ to approximate the target function. In the target function (5.2), we draw samples of θ and use a numerical way to calculate its posterior distribution $p(\theta \mid y_{1:t})$.

Additionally, the marginal posterior distribution for the parameter can be written

in two different ways:

$$p(\theta \mid y_{1:t}) \propto p(y_{1:t} \mid \theta)p(\theta), \tag{5.3}$$

$$p(\theta \mid y_{1:t}) \propto p(y_t \mid y_{1:t-1}, \theta)p(\theta \mid y_{1:t-1}). \tag{5.4}$$

The above formula (5.3) is a standard Bayesian inference requiring a prior distribution $p(\theta)$. It can be used in off-line methods, in which $\hat{\theta}$ is inferred by iterating over a fixed observation record $y_{1:t}$. By contrast, formula (5.4) is defined in a recursive way over time depending on the previous posterior at time $t-1$, which is known as on-line method. $\hat{\theta}$ is estimated sequentially as a new observation y_{t+1} becomes available.

In this chapter, we propose the use of a *linear* state-space model to infer the trajectory of a moving vehicle. Specifically, we suppose that the forward map and the observation model are linear and homogeneous, and the noise is Gaussian. The so-called linear Gaussian state-space model which has been extensively studied in the literature (Durbin and Koopman, 2012). Even in the linear state-space model, parameter and state estimation is difficult. Our goal is to develop a fast and efficient MCMC algorithm for online estimation.

5.2.1 The Posterior Distribution

For sampling θ, we should find its distribution function first from the covariance matrix of the joint $x_{1:t}$ and $y_{1:t}$. Under the assumption that the forward map and the observation model are linear and homogeneous, the joint distribution of the states and observations is

$$\begin{bmatrix} x_{1:t} \\ y_{1:t} \end{bmatrix} \Bigg| \theta \sim N\left(0, \Sigma_t\right), \tag{5.5}$$

where $x_{1:t}$ represents the hidden states $\{x_1, \ldots, x_t\}$, $y_{1:t}$ represents observed $\{y_1, \ldots, y_t\}$ and θ is a set of all known and unknown parameters. The inverse of the covariance matrix Σ_t^{-1} is the precision matrix. In our application, as we will see, it is a block matrix in the form

$$\Sigma_t^{-1} = \begin{bmatrix} A_t & -B_t \\ -B_t^\top & B_t \end{bmatrix}, \tag{5.6}$$

where A_t is a $t \times t$ matrix coming from the forward map, B_t is a $t \times t$ diagonal matrix coming from the observation model. The structure of the matrices, such as bandwidth, sparse density, depends on the details of the model. Then, we may find the covariance

matrix by calculating the inverse of the precision matrix

$$\begin{aligned}\Sigma_t &= \begin{bmatrix} \left(A_t - B_t^\top B_t^{-1} B_t\right)^{-1} & -\left(A_t - B_t^\top B_t^{-1} B_t\right)^{-1} B_t^\top B_t^{-1} \\ -B_t^{-1} B_t \left(A_t - B_t^\top B_t^{-1} B_t\right)^{-1} & \left(B_t - B_t^\top A_t^{-1} B_t\right)^{-1} \end{bmatrix} \\ &= \begin{bmatrix} (A_t - B_t)^{-1} & (A_t - B_t)^{-1} \\ (A_t - B_t)^{-1} & \left(I_t - A_t^{-1} B_t\right)^{-1} B_t^{-1} \end{bmatrix} \\ &\triangleq \begin{bmatrix} \Sigma_{XX} & \Sigma_{XY} \\ \Sigma_{YX} & \Sigma_{YY} \end{bmatrix}. \end{aligned} \tag{5.7}$$

Because of the covariance $\Sigma_{YY} = \left(I_t - A_t^{-1} B_t\right)^{-1} B_t^{-1}$, therefore the inverse is

$$\Sigma_{YY}^{-1} = B_t \left(I_t - A_t^{-1} B_t\right) = B_t A_t^{-1} \Sigma_{XX}^{-1}. \tag{5.8}$$

Given the Choleski decomposition $L_t L_t^\top = A_t$, we have

$$\begin{aligned}\Sigma_{YY}^{-1} &= B_t L_t^{-\top} L_t^{-1} \Sigma_{XX}^{-1} \\ &= \left(L_t^{-1} B_t\right)^\top \left(L_t^{-1} \Sigma_{XX}^{-1}\right) \end{aligned} \tag{5.9}$$

More usefully, by given another Choleski decomposition $R_t R_t^\top = A_t - B_t = \Sigma_{XX}^{-1}$,

$$\begin{aligned} y_{1:t}^\top \Sigma_{YY}^{-1} y_{1:t} &= \left(L_t^{-1} B_t y_{1:t}\right)^\top \left(L_t^{-1} \Sigma_{XX}^{-1} y_{1:t}\right) \\ &\triangleq W_t^\top \left(L_t^{-1} \Sigma_{XX}^{-1} y_{1:t}\right) \end{aligned} \tag{5.10}$$

$$\begin{aligned} \det \Sigma_{YY}^{-1} &= \det B_t \det L_t^{-\top} \det L_t^{-1} \det R_t \det R_t^\top \\ &= \det B_t \left(\det L_t^{-1}\right)^2 \left(\det R_t\right)^2. \end{aligned} \tag{5.11}$$

From the objective function (5.3), the posterior distribution of θ is

$$p\left(\theta \mid y_{1:t}\right) \propto p\left(y_{1:t} \mid \theta\right) p\left(\theta\right) \propto \exp\left(-\frac{1}{2} y_{1:t} \Sigma_{YY}^{-1} y_{1:t}\right) \sqrt{\det \Sigma_{YY}^{-1}}\, p\left(\theta\right). \tag{5.12}$$

Then, by taking natural logarithm on the posterior of θ and by using the useful solutions in equations (5.10) and (5.11), we will have

$$\ln L\left(\theta\right) = -\frac{1}{2} y_{1:t}^\top \Sigma_{YY}^{-1} y_{1:t} + \frac{1}{2} \sum \ln \operatorname{tr}\left(B_t\right) - \sum \ln \operatorname{tr}\left(L_t\right) + \sum \ln \operatorname{tr}\left(R_t\right) + \ln p\left(\theta\right). \tag{5.13}$$

5.2.2 The Forecast Distribution

From equation (5.4), a sequential way for estimating the forecast distribution is needed. Suppose it is

$$y_t \mid y_{1:t-1}, \theta \sim N\left(\bar{\mu}_t, \bar{\sigma}_t\right). \tag{5.14}$$

Look back to the covariance matrices of observations that we found in the previous section

$$\begin{aligned} p(y_{1:t-1},\theta) &= N\left(0,\Sigma_{YY}^{(t-1)}\right), \\ p(y_t,y_{1:t-1},\theta) &= N\left(0,\Sigma_{YY}^{(t)}\right), \end{aligned} \tag{5.15}$$

where the covariance matrix of the joint distribution is $\Sigma_{YY}^{(t)} = (I_t - A_t^{-1}B_t)^{-1}B_t^{-1}$, I_t is a $t \times t$ identity matrix. Then, by taking its inverse, we will get

$$\begin{aligned} \Sigma_{YY}^{(t)(-1)} &= B_t(I_t - A_t^{-1}B_t) \\ &= B_t(B_t^{-1} - A_t^{-1})B_t \\ &\triangleq \begin{bmatrix} B_t & 0 \\ 0 & B_1 \end{bmatrix} \begin{bmatrix} Z_t & b_t \\ b_t^\top & K_t \end{bmatrix} \begin{bmatrix} B_t & 0 \\ 0 & B_1 \end{bmatrix} \end{aligned} \tag{5.16}$$

where Z_t is a $t \times t$ matrix, b_t is a $t \times 1$ matrix and K_t is a 1×1 matrix. Thus, by taking its inverse again, we will get

$$\Sigma_{YY}^{(t)} = \begin{bmatrix} B_t^{-1}\left(Z_t - b_tK_t^{-1}b_t^\top\right)^{-1}B_t^{-1} & -B_t^{-1}Z_t^{-1}b_t\left(K_t - b_t^\top Z_t^{-1}b_t\right)^{-1}B_1^{-1} \\ -B_1^{-1}K_t^{-1}b_t^\top\left(Z_t - b_tK_t^{-1}b_t^\top\right)^{-1}B_t^{-1} & B_1^{-1}\left(K_t - b_t^\top Z_t^{-1}b_t\right)^{-1}B_1^{-1} \end{bmatrix}. \tag{5.17}$$

So, from the above covariance matrix, we can find the mean and variance of $p\left(y_t \mid y_{1:t-1},\theta\right)$ are

$$\bar{\mu}_t = B_1^{-1}K_t^{-1}b_t^\top B_{t-1}^{-1}y_{1:t-1}, \tag{5.18}$$

$$\bar{\sigma}_t^2 = B_1^{-1}K_tB_1^{-1}. \tag{5.19}$$

5.2.3 The Estimation Distribution

From the joint distribution (5.5), one can find the best estimation with a given θ by

$$\begin{aligned} x_{1:t} \mid y_{1:t},\theta &\sim N\left(A_t^{-1}B_ty_{1:t}, A_t^{-1}\right) \\ &\sim N(L_t^{-\top}L_t^{-1}B_ty_{1:t-1}, L^{-\top}L_t^{-1}) \\ &\sim N(L_t^{-\top}W_t, L^{-\top}L_t^{-1}). \end{aligned} \tag{5.20}$$

For sole x_t, its joint distribution with $y_{1:t}$ is

$$x_t, y_{1:t} \mid \theta \sim N\left(0, \begin{bmatrix} C_t^\top(A_t - B_t)^{-1}C_t & C_t^\top(A_t - B_t)^{-1} \\ (A_t - B_t)^{-1}C_t & (I_t - A_t^{-1}B_t)^{-1}B_t^{-1} \end{bmatrix}\right), \tag{5.21}$$

where $C_t^\top = \begin{bmatrix} 0 & \cdots & 0 & 1 \end{bmatrix}$ is $t \times 1$ vector. Thus, the filtering distribution of the state is

$$x_t \mid y_{1:t}, \theta \sim N\left(\mu_t^{(x)}, \mathrm{Var}(x_t)\right), \tag{5.22}$$

where, after simplifying, the mean and variance are

$$\mu_t^{(x)} = C_t^\top A_t^{-1} B_t y_{1:t}, \tag{5.23}$$

$$\mathrm{Var}(x_t) = C_t^\top A_t^{-1} C_t. \tag{5.24}$$

Generally, researchers would like to find the combined estimation for x_t and θ at time t by

$$p(x_t, \theta \mid y_{1:t}) = p(x_t \mid y_{1:t}, \theta) p(\theta \mid y_{1:t}). \tag{5.25}$$

Differently, from the target equation (5.2), the state inference containing N samples is a mixture Gaussian distribution in the following form

$$p(x_t \mid y_{1:t}) = \int p(x_t \mid y_{1:t}, \theta) p(\theta \mid y_{1:t}) d\theta \doteq \frac{1}{N} \sum_{i=1}^{N} p\left(x_t \mid \theta^{(i)}, y_{1:t}\right). \tag{5.26}$$

Suppose $x_t \mid y_{1:t}, \theta_i \sim N\left(\mu_{ti}^{(x)}, \mathrm{Var}(x_{ti})\right)$ is found from equation (5.23) and (5.24) for each θ_i, then its mean is

$$\mu_t^{(x)} = \frac{1}{N} \sum_i \mu_{ti}^{(x)} \tag{5.27}$$

and the unconditional variance of x_t, by law of total variance, is

$$\begin{aligned} \mathrm{Var}(x_t) &= \mathrm{E}[\mathrm{Var}(x_t \mid y_{1:t}, \theta)] + \mathrm{Var}[\mathrm{E}(x_t \mid y_{1:t}, \theta)] \\ &= \frac{1}{N} \sum_i \left(\mu_{ti}^{(x)} \mu_{ti}^{(x)\top} + \mathrm{Var}(x_{ti})\right) - \frac{1}{N^2} \left(\sum_i \mu_{ti}^{(x)}\right) \left(\sum_i \mu_{ti}^{(x)}\right)^\top. \end{aligned} \tag{5.28}$$

5.3 Random Walk Metropolis-Hastings Algorithm

Metropolis-Hastings algorithm is an important class of MCMC algorithms (Smith and Roberts, 1993; Tierney, 1994; Gilks *et al.*, 1995). This algorithm has been used extensively in physics but was little known to others until Müller (1991); Tierney (1994) expound the value of this algorithm to statisticians. The algorithm is extremely powerful and versatile and has been included in a list of "The Top 10 Algorithms" with the greatest influence on the development and practice of science and engineering in the 20th century (Dongarra and Sullivan, 2000; Medova, 2008).

Given essentially a probability distribution $\pi(\cdot)$ (the target distribution), MH algorithm provides a way to generate a Markov chain $x_1, x_2, \ldots, x_t$, who has the target

distribution as a stationary distribution, for the uncertain parameters x requiring only that this density can be calculated at x. Suppose that we can evaluate $\pi(x)$ for any x. The transition probabilities should satisfy the detailed balance condition

$$\pi\left(x^{(t)}\right) q\left(x', x^{(t)}\right) = \pi\left(x'\right) q\left(x^{(t)}, x'\right), \tag{5.29}$$

which means that the transition from the current state $\pi(x^{(t)})$ to the new state $\pi(x')$ has the same probability as that from $\pi(x')$ to $\pi(x^{(t)})$. In sampling method, drawing x_i first and then drawing x_j should have the same probability as drawing x_j and then drawing x_i. However, in most situations, the details balance condition is not satisfied. Therefore we introduce a function $\alpha(x, y)$ satisfying

$$\pi\left(x'\right) q\left(x', x^{(t)}\right) \alpha\left(x', x^{(t)}\right) = \pi\left(x^{(t)}\right) q\left(x^{(t)}, x'\right) \alpha\left(x^{(t)}, x'\right). \tag{5.30}$$

In this way, a tentative new state x' is generated from the proposal density $q\left(x'; x^{(t)}\right)$ and it is accepted or rejected according to acceptance probability

$$\alpha = \frac{\pi\left(x'\right)}{\pi\left(x^{(t)}\right)} \frac{q\left(x^{(t)}, x'\right)}{q\left(x', x^{(t)}\right)}. \tag{5.31}$$

If $\alpha \geq 1$, the new state is accepted. Otherwise, the new state is accepted with probability α.

Here comes an issues of how to choose $q\left(\cdot \mid x^{(t)}\right)$. The most widely used subclass of MCMC algorithms is based on the *random walk Metropolis* (RWM). The RWM updating scheme was first applied by Metropolis *et al.* (1953) and proceeds as follows. Given a current value of the d-dimensional Markov chain $x^{(t)}$, a new value x' is obtained by proposing a jump $\epsilon = |x' - x^{(t)}|$ from the pre-specified Lebesgue density

$$\tilde{\gamma}\left(\epsilon^{\star}; \lambda\right) = \frac{1}{\lambda^d} \gamma\left(\frac{\epsilon^{\star}}{\lambda}\right), \tag{5.32}$$

with $\gamma(\epsilon) = \gamma(-\epsilon)$ for all ϵ. Here, the positive λ governs the overall distance of the proposed jump and plays a crucial role in determining the efficiency of any algorithm. In a random walk, the proposal density function $q(\cdot)$ can be chosen for some suitable normal distribution, and hence $q\left(x' \mid x^{(t)}\right) = N\left(x' \mid x^{(t)}, \epsilon^2\right)$ and $q\left(x^{(t)} \mid x'\right) = N\left(x^{(t)} \mid x', \epsilon^2\right)$ cancel in the above equation (5.31) (Sherlock *et al.*, 2017). To decide whether to accept the new state, we compute the the probability of accepting the new state by

$$\alpha = \min\left\{1, \frac{\pi\left(x'\right) q\left(x^{(t)} \mid x'\right)}{\pi\left(x^{(t)}\right) q\left(x' \mid x^{(t)}\right)}\right\} = \min\left\{1, \frac{\pi\left(x'\right)}{\pi\left(x^{(t)}\right)}\right\}. \tag{5.33}$$

If the proposed value is accepted it becomes the next current value $x^{(t+1)} = x'$; otherwise the current value is left unchanged $x^{(t+1)} = x^{(t)}$ (Sherlock *et al.*, 2010).

5.3.1 The Self-tuning Metropolis-Hastings Algorithm

The self-tuning MH algorithm automatically tunes the step sizes for different parameters by one-variable-at-a-time random walk. Aiming at the target acceptance rates for each parameter, the algorithm efficiently and accurately explore the structure of the d-dimensional parameter space.

By assuming the parameters are independent, the idea of this algorithm is that in each iteration, only one parameter is proposed and the others remain to be changed. After the step, take n samples out of the total amount of iterations N as new sequences. In Figure 5.1, examples of different proposing methods are compared.

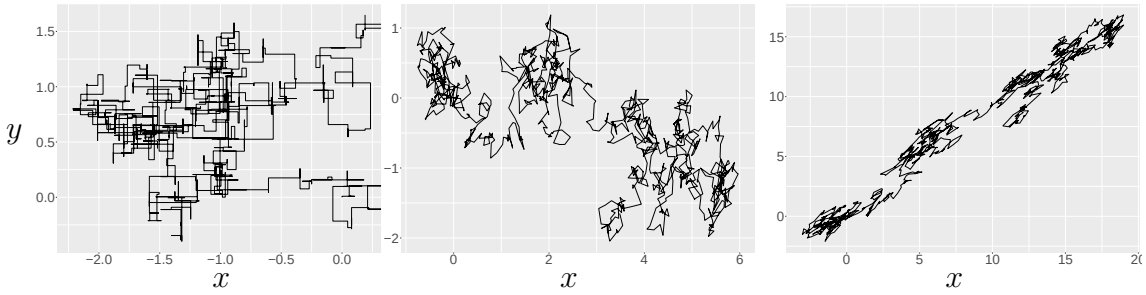

(a) One-variable-at-a-time random walk.

(b) Independent multi-variable-at-a-time random walk.

(c) Correlated multi-variable-at-a-time random walk.

Figure 5.1: Examples of 2-Dimensional random walk Metropolis-Hastings algorithm. Figure 5.1a is the trace of one-variable-at-a-time random walk. At each time, only one variable is changed and the other one stay constant. Figure 5.1b and 5.1c present the traces by multi-variable-at-a-time random walk. In Figure 5.1b, the proposal for each step is independent, but in Figure 5.1c the proposal are proposed correlated.

To gain the target acceptance rates α_i, $(i = 1, \ldots, d)$, the step size s_i for each parameter is tuned automatically. The concept of the algorithm is if the proposal is accepted, we are more confident on the direction and step size that were made. In this scenario, the next moving step should be further. In another word, the step size s_{t+1} in the next step is bigger than s_t. Otherwise, a conservative proposal is made with a shorter distance, which is $s_{t+1} \leq s_t$.

Let a and b be non-negative numbers indicating the distances of a forward movement, the new step size s_{t+1} from current s_t is

$$\ln s_{t+1} = \begin{cases} \ln s_t + a & \text{with probability } \alpha \\ \ln s_t - b & \text{with probability } 1 - \alpha \end{cases}, \tag{5.34}$$

where the logarithm guarantees the step size is positive. By taking its expectation

$$\mathrm{E}[\ln s_{t+1} \mid \ln s_t] = \alpha(\ln s_t + a) + (1-\alpha)(\ln s_t - b), \tag{5.35}$$

and simplifying to

$$\mu = \alpha(\mu + a) + (1-\alpha)(\mu - b), \tag{5.36}$$

one can find that

$$a = \frac{1-\alpha}{\alpha} b. \tag{5.37}$$

Thus, if the proposal is accepted, the step size s_t is tuned to $s_{t+1} = s_t e^a$, otherwise $s_{t+1} = s_t / e^b$.

The complete one-variable-at-a-time MH is summarized in the following:

Algorithm 5.1: Self-tuning Random Walk Metropolis-Hastings Algorithm

1 Initialization: Given an arbitrary positive step size $s_i^{(1)}$ for each parameter. Set up a value for b and find a by using the formula (5.37). Set up a target acceptance rate α_i for each parameter, where $i = 1, \ldots, d$.

2 Run sampling algorithm: **for** *k from 1 to N* **do**

3 Randomly select a parameter $\theta_i^{(k)}$, propose a new one by $\theta_i' \sim N\left(\theta_i^{(k)}, \epsilon s_i^{(k)}\right)$ and leave the rest unchanged.

4 Accept θ_i' with probability $\alpha = \min\left\{1, \frac{\pi(\theta')q\left(\theta^{(k)}, \theta'\right)}{\pi\left(\theta^{(k)}\right)q\left(\theta', \theta^{(k)}\right)}\right\}$.

5 If it is accepted, tune step size to $s_i^{(k+1)} = s_i^{(k)} e^a$, otherwise $s_i^{(k+1)} = s_i^{(k)} / e^b$.

6 Set $k = k + 1$ and move to step 3 until N.

7 Take n samples out from N with equal spaced index for each parameter being a new sequence.

The advantage of the Algorithm 5.1 is that it returns a more accurate estimation for θ and is more reliable to learn the structure of the parameter space. However, if $\pi(\cdot)$ has an singular structure, the algorithm becomes time-consuming and low efficient. To solve the issue, the *Delayed-Acceptance Metropolis-Hastings* (DA MH) algorithm is utilized to speed up the computation.

5.3.2 Adaptive Delayed-Acceptance Metropolis-Hastings Algorithm

The DA MH algorithm proposed in (Christen and Fox, 2005) is a two-stage Metropolis-Hastings algorithm in which, typically, proposed parameter values are accepted or

rejected at the first stage based on a computationally cheap surrogate $\hat{\pi}(x)$ for the likelihood $\pi(x)$. In stage one, the quantity α_1 is found by a standard MH acceptance formula

$$\alpha_1 = \min\left\{1, \frac{\hat{\pi}(x')q\left(x^{(t)}, x'\right)}{\hat{\pi}(x^{(t)})q\left(x', x^{(t)}\right)}\right\}, \tag{5.38}$$

where $\hat{\pi}(\cdot)$ is a cheap estimation for x and a simple form is $\hat{\pi}(\cdot) = N\left(\cdot \mid \hat{x}, \epsilon\right)$. Once α_1 is accepted, the process goes into stage two and the acceptance probability α_2 is

$$\alpha_2 = \min\left\{1, \frac{\pi(x')\hat{\pi}\left(x^{(t)}\right)}{\pi\left(x^{(t)}\right)\hat{\pi}(x')}\right\}, \tag{5.39}$$

where the overall acceptance probability $\alpha_1\alpha_2$ ensures that detailed balance is satisfied with respect to $\pi(\cdot)$; however if a rejection occurs at stage one, the expensive evaluation of $\pi(x)$ at stage two is unnecessary.

For a symmetric proposal density kernel $q\left(x', x^{(t)}\right)$ such as is used in the random walk MH algorithm, the acceptance probability in stage one is simplified to

$$\alpha_1 = \min\left\{1, \frac{\pi(x')}{\pi\left(x^{(t)}\right)}\right\}. \tag{5.40}$$

If the true posterior is available, the delayed-acceptance Metropolis-Hastings algorithm is obtained by substituting this for the unbiased stochastic approximation in (5.39) (Sherlock *et al.*, 2015).

To accelerate the MH algorithm, DA MH requires a cheap approximate estimation $\hat{\pi}(\cdot)$ in formula (5.40). Intuitively, the approximation should be efficient with respect to time and accuracy to the true posterior $\pi(\cdot)$. A sensible option is assuming the parameter distribution at each time t is following a normal distribution with mean m_t and covariance C_t. So the posterior density is given by

$$\hat{\pi}(\theta \mid y_{1:t}) \propto \exp\left(-\frac{1}{2}(\theta - m_t)^\top C_t^{-1}(\theta - m_t)\right). \tag{5.41}$$

A lazy C_t is chosen as an identity matrix, in which way all the parameters are independent. In terms of m_t, in most of circumstances, 0 is not an idea choice. To find an optimal or suboptimal m_t and C_t, several algorithms have been discussed. Stroud *et al.* (2018) use a second-order expansion of $l(\theta)$ at the mode and the mean and covariance become $m_t = \arg\max l(\theta)$ and $C_t = -\left[\frac{\partial l(\theta)}{\partial\theta_i\partial\theta_j}\right]^{-1}_{\theta=m_t}$ respectively. The drawback of this estimation is a global optimum is not guaranteed. Mathew *et al.* (2012) propose a fast adaptive MCMC sampling algorithm, which is a consist of two phases. In the learning phase, they use hybrid Gibbs sampler to learn the covariance structure of the variance

components. In phase two, the covariance structure is used to formulate an effective proposal distribution for a MH algorithm.

Likewise, we are suggesting that use a batch of data with length $L < t$ to learn the parameter space by using self-tuning random walk MH algorithm in the learning phase first. This algorithm tunes each parameter at its own optimal step size and explores the surface in different directions. When the process is done, we have a sense of the surface for $\theta \approx \hat{\theta}$ and its mean $\hat{\mu} \approx m_L$ and covariance $\hat{\Sigma} \approx C_L$ can be estimated. Then, we can move to the second phase: DA MH algorithm. The new θ' is proposed from $N\left(\theta^{(t)} \mid m_L, C_L\right)$, which is in the following form

$$\theta' = \theta^{(t)} + R\epsilon z, \tag{5.42}$$

where $R^\top R = C_L$ is the Cholesky decomposition, ϵ is the tuned step size and $z \sim N(0,1)$ is Gaussian white noise. This proposing method reduces the impact of drawing θ' from a correlation space.

5.3.3 Efficiency of Metropolis-Hastings Algorithm

In equation (5.32), the jump size ϵ determines the efficiency of RWM algorithm. For a general RWM, it is intuitively clear that we can make the algorithm arbitrarily poor by making ϵ either very large or very small (Sherlock *et al.*, 2010). Assuming ϵ is extremely large, the proposal $x' \sim N\left(x^{(t)}, \epsilon\right)$, for example, is taken a further distance from current value $x^{(t)}$. Therefore the algorithm will reject most of its proposed moves and stay where it was for a few iterations. On the other hand, if ϵ is extremely small, the algorithm will keep accepting the proposed x' since α is always approximately be 1 because of the continuity of $\pi(x)$ and $q(\cdot)$ (Roberts and Rosenthal, 2001). Thus, RWM takes a long time to explore the posterior space and converge to its stationary distribution. So, the balance between these two extreme situations must exist. This appropriate step size $\hat{\epsilon}$ is optimal, sometimes is suboptimal, the solution to gain a Markov chain.

Figure 5.2 illustrates the performances of RWM with different ϵ. From these figures, one can see that either too large or too small ϵ causes high correlation chains, indicating bad samples in sampling algorithm. An appropriate ϵ decorrelates samples and returns a stationary chain. That is considered highly efficient.

Plenty of work has been done in determining the efficiency of Metropolis-Hastings algorithm in recent years. Gelman *et al.* (1996) work with algorithms consisting of a single Metropolis move (not multi-variable-at-a-time), and obtain many interesting

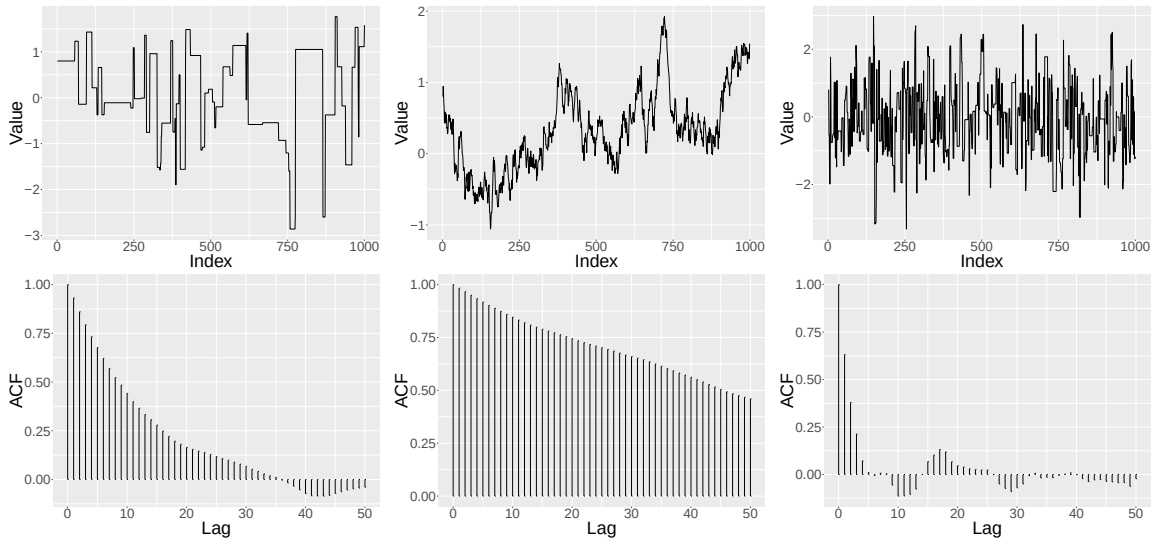

(a) With a large step size (b) With a small step size (c) With a proper step size

Figure 5.2: Metropolis-Hastings sampler for a single parameter with: 5.2a a large step size, 5.2b a small step size, 5.2c an appropriate step size. The upper plots show the sample chains and lower plots indicate the autocorrelation values for each case.

results for the d-dimensional spherical multivariate normal problem with symmetric proposal distributions, including that the optimal scale is approximately $2.4/\sqrt{d}$ times the scale of target distribution, which implies optimal acceptance rates of 0.44 for $d = 1$ and 0.23 for $d \to \infty$ (Gilks *et al.*, 1995). Roberts and Rosenthal (2001) evaluate scalings that are optimal (in the sense of integrated autocorrelation times) asymptotically in the number of components. They find that an acceptance rate of 0.234 is optimal in many random walk Metropolis situations, but their studies are also restricted to algorithms that consist of only a single step in each iteration, and in any case, they conclude that acceptance rates between 0.15 and 0.5 do not cost much efficiency. Other researchers, such as (Gelman *et al.*, 1997; Bédard, 2007; Beskos *et al.*, 2009; Sherlock and Roberts, 2009; Sherlock, 2013), have been tackled for various shapes of target on choosing the optimal scale of the RWM proposal and led to the similar rule: choose the scale so that the acceptance rate is approximately 0.234. Although nearly all of the theoretical results are based upon limiting arguments in high dimension, the rule of thumb appears to be applicable even in relatively low dimensions (Sherlock *et al.*, 2010).

In terms of the step size ϵ, it is pointed out that for a stochastic approximation procedure, its step size sequence $\{\epsilon_i\}$ should satisfy $\sum_{i=1}^{\infty} \epsilon_i = \infty$ and $\sum_{i=1}^{\infty} \epsilon_i^{1+\lambda} < \infty$ for some $\lambda > 0$. The former condition somehow ensures that any point of X can

eventually be reached, while the second condition ensures that the noise is contained and does not prevent convergence (Andrieu and Thoms, 2008). Sherlock *et al.* (2010) tune various algorithms to attain target acceptance rates, and one of the algorithms tunes step sizes of univariate updates to attain the optimal efficiency of Markov chain at the acceptance rates between 0.4 and 0.45. Additionally, Graves (2011) mentions that it is certain that one may use the actual arctangent relationship to try to choose a good ϵ: in the univariate example, if α is the desired acceptance rate, then $\epsilon = 2\sigma/\tan(\pi/2\alpha)$, where σ is the posterior standard deviation, will be obtained. In fact, some explorations infer a linear relationship between acceptance rate and step size, which is $\texttt{logit}(\alpha) \approx 0.76 - 1.12 \ln \epsilon/\sigma$, and the slope of the relationship is nearly equal to the constant -1.12 independently.

However, in multi-variable-at-a-time RWM, one expects that the proper interpretation of σ is not the posterior standard deviation but the average conditional standard deviation, which is presumably more difficult to estimate from a Metropolis algorithm. In a higher d-dimensional space, or propose multi-variable-at-a-time, suppose Σ is known or can be estimated, then X' can be proposed from $q \sim N(X, \epsilon^2\Sigma)$. Thus,the optimal step size ϵ is required. A concessive way of RWM in high dimension is proposing one-variable-at-a-time and treating them as separate one dimensional space individually. In any case, however, the behavior of RWM on a multivariate normal distribution is governed by its covariance matrix Σ, and it performs better than a fixed $N(X, \epsilon^2 I_d)$ distribution (Roberts and Rosenthal, 2001).

To explore the efficiency of a MCMC process, we introduce some notions first. For an arbitrary square integrable function g, Roberts and Rosenthal (2001) define its *integrated autocorrelation time* by

$$\tau_g = 1 + 2\sum_{i=1}^{\infty} \mathrm{Corr}\left(g(X_0), g(X_i)\right), \tag{5.43}$$

where X_0 is assumed to be distributed according to π. Because central limit theorem, the variance of the estimator $\bar{g} = \sum_{i=1}^{n} g(X_i)/n$ for estimating $\mathrm{E}[g(X)]$ is approximately $\mathrm{Var}_\pi[g(X)] \times \tau_g/n$. The variance tells us the accuracy of the estimator $\bar{g}$. The smaller it is, the faster the chain converges. Therefore, they suggest that the efficiency of Markov chains (Eff) can be found by comparing the reciprocal of their integrated autocorrelation time, which is

$$e_g(\sigma) \propto \left(\tau_g \mathrm{Var}_\pi[g(X)]\right)^{-1}. \tag{5.44}$$

However, the disadvantage of their method is that the measurement of efficiency is highly dependent on the function g. Instead, an alternative approach uses *effective*

sample size (ESS) (Kass *et al.*, 1998; Robert, 2004), which is defined in (Gong and Flegal, 2016) in the following form of

$$\text{ESS} = \frac{n}{1 + 2\sum_{k=1}^{\infty} \rho_k(X)} \approx \frac{n}{1 + 2\sum_{k=1}^{k_{\text{cut}}} \rho_k(X)} = \frac{n}{\tau}, \tag{5.45}$$

where n is the amount of samples, $k_{\texttt{cut}}$ is lag of the first $\rho_k < 0.01$ or 0.05 , and τ is the integrated autocorrelation time. Given a Markov chain having n iterations, the ESS measures the size of i.i.d. samples with the same standard error. Moreover, a wide support among both statisticians (Geyer, 1992) and physicists (Sokal, 1997) use the following cost of independent samples to evaluate the performance of MCMC, that is

$$\frac{n}{\text{ESS}} \times \text{cost per step} = \tau \times \text{cost per step}. \tag{5.46}$$

Being inspired by their research, we now define the Efficiency in Unit Time (EffUT) and ESS in Unit Time (ESSUT) as follows:

$$\text{EffUT} = \frac{e_g}{T}, \tag{5.47}$$

$$\text{ESSUT} = \frac{\text{ESS}}{T}, \tag{5.48}$$

where T represents the computation time, which is also known as running time. The computation time is the length of time, in minutes or hours, etc, required to perform a computational process. The best Markov chain with an appropriate step size ϵ should not only have a lower correlation, as illustrated in Figure 5.2, but also have less time-consuming. The standard efficiency e_g and ESS do not depend on the computation time, but EffUT and ESSUT do. The best-tuned step size gains the balance between the size of effective proposed samples and cost of time.

5.4 Simulation Studies

In this section, we consider the model in regular and irregular spaced time difference separately. For an one dimensional state-space model, we consider the hidden state process $\{x_t, t \geq 1\}$ is a stationary and ergodic Markov process and transited by $F(x' \mid x)$. In this paper, we assume that the state of a system has an interpretation as the summary of the past one-step behavior of the system. The states are not observed directly but by another process $\{y_t, t \geq 1\}$, which is assumed depending on $\{x_t\}$ by the process $G(y \mid x)$ only and independent with each other. When observed on discrete

time $T_1, \ldots, T_k$, the model is summarized on the directed acyclic following graph

$$\begin{array}{cccccccccc} \text{State} & x_0 & \to & x_1 & \to \cdots & x_k & \to \cdots & x_t & \to \cdots \\ & & & \downarrow & & \downarrow & & \downarrow & \\ \text{Observation} & & & y_1 & & y_k & & y_t & \\ \text{Time} & & & T_1 & & T_k & & T_t & \end{array} \tag{5.49}$$

We define $\Delta_k = T_k - T_{k-1}$. If Δ_t is constant, we retrieve a standard *AR(1)* model process with regular spaced time steps; if Δ_t is not constant, then the model becomes more complicated with irregular spaced time steps. (Note that we do not consider x_0 below: given an appropriate prior, x_0 can always be integrated out of the model probability.)

5.4.1 Simulation on Regularly Sampled Time Series Data

If the time steps are evenly spaced, the model can be written as a simple linear homogeneous state-space model:

$$\begin{aligned} y_t \mid x_t &\sim N\left(x_t, \sigma^2\right) \\ x_t \mid x_{t-1} &\sim N\left(\phi x_{t-1}, \tau^2\right), \end{aligned} \tag{5.50}$$

where σ and τ are i.i.d. errors occurring in processes and ϕ is a static process parameter in the forward map. An initial value $x_1 \sim N(0, L^2)$.

The joint distribution is $p(x_{1:t}, y_{1:t}) = p(y_t \mid x_t)p(x_t \mid x_{t-1}) \cdots p(y_1 \mid x_1)p(x_1)$. Given the form of the Gaussian density, the joint distribution becomes

$$\left[\begin{array}{c} x \\ y \end{array} \middle| \theta\right] \sim N\left(0, \Sigma\right), \tag{5.51}$$

where $\theta = \{\phi, \sigma, \tau\}$, and the precision matrix Σ^{-1} is

$$\begin{bmatrix}
\frac{1}{L^2}+\frac{\phi^2}{\tau^2}+\frac{1}{\sigma^2} & -\frac{\phi}{\tau^2} & \cdots & 0 & 0 & -\frac{1}{\sigma^2} & 0 & \cdots & 0 & 0 \\
-\frac{\phi}{\tau^2} & \frac{1+\phi^2}{\tau^2}+\frac{1}{\sigma^2} & \cdots & 0 & 0 & 0 & -\frac{1}{\sigma^2} & \cdots & 0 & 0 \\
\vdots & \vdots & \ddots & \vdots & \vdots & \vdots & \vdots & \ddots & \vdots & \vdots \\
0 & 0 & \cdots & \frac{1+\phi^2}{\tau^2}+\frac{1}{\sigma^2} & -\frac{\phi}{\tau^2} & 0 & 0 & \cdots & -\frac{1}{\sigma^2} & 0 \\
0 & 0 & \cdots & -\frac{\phi}{\tau^2} & \frac{1}{\tau^2}+\frac{1}{\sigma^2} & 0 & 0 & \cdots & 0 & -\frac{1}{\sigma^2} \\
-\frac{1}{\sigma^2} & 0 & \cdots & 0 & 0 & \frac{1}{\sigma^2} & 0 & \cdots & 0 & 0 \\
0 & -\frac{1}{\sigma^2} & \cdots & 0 & 0 & 0 & \frac{1}{\sigma^2} & \cdots & 0 & 0 \\
\vdots & \vdots & \ddots & \vdots & \vdots & \vdots & \vdots & \ddots & \vdots & \vdots \\
0 & 0 & \cdots & -\frac{1}{\sigma^2} & 0 & 0 & 0 & \cdots & \frac{1}{\sigma^2} & 0 \\
0 & 0 & \cdots & 0 & -\frac{1}{\sigma^2} & 0 & 0 & \cdots & 0 & \frac{1}{\sigma^2}
\end{bmatrix}, \tag{5.52}$$

and denoted as $\Sigma^{-1} \triangleq \begin{bmatrix} A_t & -B_t \\ -B_t & B_t \end{bmatrix}$, where B_t is a diagonal matrix $\frac{1}{\sigma^2} I$ proportional to an identity matrix.

Parameter Estimation

In the formula (5.3), the parameter posterior is estimated with observation $y_{1:t}$. By using the Algorithm 5.1, although it may take a longer time, we will achieve a precise estimation. Similarly with Section 5.2.1, from the objective function, the posterior distribution of θ is the same as equation (5.12). Then, by taking natural logarithm on the posterior of θ and by using the useful solutions in equations (5.10) and (5.11), we will have the same log-likelihood function (5.13).

In a simple linear case, we are choosing the parameter $\theta = \{\phi = 0.9, \tau^2 = 0.5, \sigma^2 = 1\}$ as the author did in (Lopes and Tsay, 2011) and using $n = 500$ data set, setting initial $L = 0$. Instead of inferring τ and σ, we are estimating $\nu_1 = \ln \tau^2$ and $\nu_2 = \ln \sigma^2$ in the RW-MH to avoid singular proposals. After the process, the parameters can be transformed back to original scale. Therefore the new parameter $\theta^* = \{\phi, \nu_1, \nu_2\} = \{\phi, \ln \tau^2, \ln \sigma^2\}$.

By using Algorithm 5.1 and aiming the optimal acceptance rate at 0.44, after 10 000 iterations we get the acceptance rates for each parameters are $\alpha_\phi = 0.4409, \alpha_{\nu_1} = 0.4289$ and $\alpha_{\nu_2} = 0.4505$, and the estimations are $\phi = 0.8794, \nu_1 = -0.6471$ and $\nu_2 = -0.0639$ respectively. Thus, we have the cheap surrogate $\hat{\pi}(\cdot)$. Keep going to the DA MH with another 10 000 iterations, the algorithm returns the best estimation with $\alpha_1 = 0.1896$ and $\alpha_2 = 0.8782$. In Figure 5.3, the trace plots illustrates that the Markov chain of $\hat{\theta}$

is stably fluctuating around the true θ.

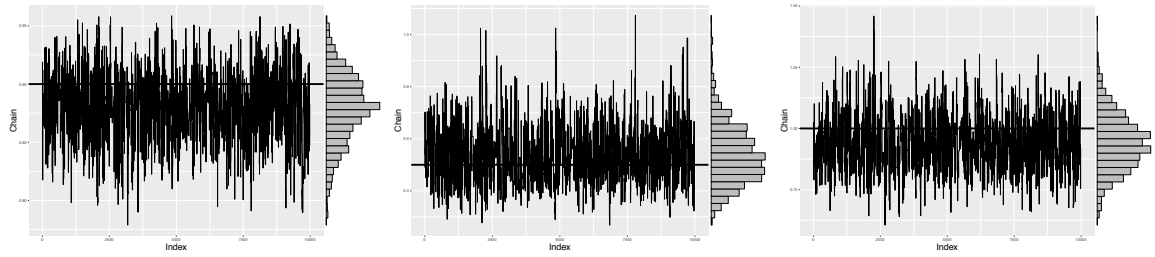

(a) Trace plot of ϕ (b) Trace plot of τ^2 (c) Trace plot of σ^2

Figure 5.3: Linear simulation with true parameter $\theta = \{\phi = 0.9, \tau^2 = 0.5, \sigma^2 = 1\}$. By transforming back to the original scale, the estimation of $\hat{\theta}$ is $\{\phi = 0.8810, \tau^2 = 0.5247, \sigma^2 = 0.9416\}$.

Recursive Forecast Distribution

The calculation of log-posterior of the parameters requires finding out the forecast distribution of $p(y_{1:t} \mid y_{1:t-1}, \theta)$. A general way is to use the joint distribution of y_t and $y_{1:t-1}$, which is $p(y_{1:t} \mid \theta) \sim N(0, \Sigma_{YY})$, and following the procedure in Section 5.2.2 to work out the inverse matrix of a multivariate normal distribution. For example, one may find the inverse of the covariance matrix

$$\Sigma_{YY}^{-1} = B_t(I_t - A_t^{-1}B_t) = \frac{1}{\sigma^4}(\sigma^2 I_t - A_t^{-1}) \triangleq \frac{1}{\sigma^4}\begin{bmatrix} Z_t & b_t \\ b_t^\top & K_t \end{bmatrix}, \tag{5.53}$$

and the original form of this covariance is

$$\Sigma_{YY} = \sigma^4 \begin{bmatrix} \left(Z_t - b_t K_t^{-1} b_t^\top\right)^{-1} & -Z_t^{-1} b_t \left(K_t - b_t^\top Z_t^{-1} b_t\right)^{-1} \\ -K_t^{-1} b_t^\top \left(Z_t - b_t K_t^{-1} b_t^\top\right)^{-1} & \left(K_t - b_t^\top Z_t^{-1} b_t\right)^{-1} \end{bmatrix}. \tag{5.54}$$

By denoting $C_t^\top = \begin{bmatrix} 0 & \cdots & 0 & 1 \end{bmatrix}$ and post-multiplying Σ_{YY}^{-1}, we will have

$$\Sigma_{YY}^{-1} C_t = \frac{1}{\sigma^4}\left(\sigma^2 I_t - A_t^{-1}\right) C_t = \frac{1}{\sigma^4}\begin{bmatrix} b_t \\ K_t \end{bmatrix}. \tag{5.55}$$

A recursive way of calculating b_t and K_t is to use the Sherman-Morrison-Woodbury formula. In the late 1940s and the 1950s, Sherman and Morrison (1950); Woodbury (1950); Bartlett (1951); Bodewig (1959) discovered the following Theorem 8. The original Sherman-Morrison-Woodbury (for short SMW) formula has been used to consider the inverse of matrices (Deng, 2011). In this paper, we will consider the more generalized case.

Theorem 8. *(Sherman-Morrison-Woodbury formula). Let $A \in B(H)$ and $G \in B(K)$ both be invertible, and $Y, Z \in B(K, H)$. Then, $A + YGZ^*$ is invertible if and only if $G^{-1} + ZA^{-1}Y$ is invertible. In which case,*

$$(A + YGZ^*)^{-1} = A^{-1} - A^{-1}Y\left(G^{-1} + ZA^{-1}Y\right)^{-1}ZA^{-1}. \tag{5.56}$$

A simple form of SMW formula is Sherman-Morrison formula represented in the following statement (Bartlett, 1951): Suppose $A \in R^{n\times n}$ is an invertible square matrix and $u, v \in R^n$ are column vectors. Then, $A + uv\top$ is invertible $\iff 1 + u^\top A^{-1}v \neq 0$. If $A + uv\top$ is invertible, then its inverse is given by

$$\left(A + uv^T\right)^{-1} = A^{-1} - \frac{A^{-1}uv^TA^{-1}}{1 + v^TA^{-1}u}. \tag{5.57}$$

By using the formula (5.57), one can update K_t and b_t in such a recursive way

$$K_t = \frac{\sigma^4}{\tau^2 + \sigma^2 + \phi^2(\sigma^2 - K_{t-1})}, \tag{5.58}$$

$$b_t = \begin{bmatrix} \frac{b_{t-1}\phi K_t}{\sigma^2} \\ \frac{K_t(\sigma^2+\tau^2)-\sigma^4}{\phi\sigma^2} \end{bmatrix}. \tag{5.59}$$

With the above formula, the recursive way of updating the mean and covariance is in the following formula:

$$\bar{\mu}_t = \frac{\phi}{\sigma^2}K_{t-1}\bar{\mu}_{t-1} + \phi\left(1 - \frac{K_{t-1}}{\sigma^2}\right)y_{t-1}, \tag{5.60}$$

$$\bar{\Sigma}_t = \sigma^4 K_t^{-1}, \tag{5.61}$$

where $K_1 = \frac{\sigma^4}{\sigma^2+L^2}$. For calculation details, we refer readers to Appendix B.1.

The Estimation Distribution

As discussed in Section 5.2.3, from the joint distribution of $x_{1:t}$ and $y_{1:t}$, one can find the estimation distribution (5.20), a further joint distribution for $x_t, y_{1:t}$ (5.21), and the mixture Gaussian distribution (5.26) with mean (5.27) and variance (5.28). Because of

$$C_t^\top A_t^{-1} = \begin{bmatrix} -b_t^\top & \sigma^2 - K_t \end{bmatrix}, \tag{5.62}$$

thus, for any given θ, we have $x_t \mid y_{1:t}, \theta \sim N\left(\mu_t^{(x)}, \mathrm{Var}(x_t)\right)$, where

$$\mu_t^{(x)} = \frac{K_t\bar{\mu}_t}{\sigma^2} + \left(1 - \frac{K_t}{\sigma^2}\right)y_t \tag{5.63}$$

$$\mathrm{Var}(x_t) = \sigma^2 - K_t. \tag{5.64}$$

By substituting them into the equation (5.27) and (5.28), the estimated x_t is obtained. For calculation details, we refer readers to Appendix B.1.

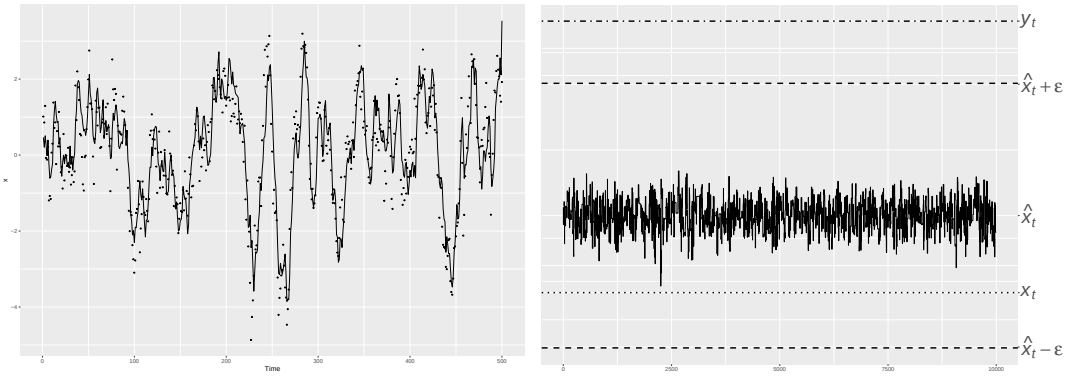

(a) Estimation of $x_{1:t}$ (b) Estimation of a single x_t

Figure 5.4: Linear simulation for $x_{1:t}$ and single x_t. In Figure 5.4a, the black dots are the true $x_{1:t}$ and the solid line is the estimation $\hat{x}_{1:t}$. In Figure 5.4b, the chain of estimation $\hat{x}_t$ is very close to the true x. In fact, the true x falls in the interval $[\hat{x} - \varepsilon, \hat{x} + \varepsilon]$, where ε is the standard deviation of the estimation for x_t.

5.4.2 Simulation on Irregularly Sampled Time Series Data

Irregularly sampled time series data is painful for scientists and researchers. In spatial data analysis, several satellites and buoy networks provide continuous observations of wind speed, sea surface temperature, ocean currents, etc. However, data was recorded with irregular time-step, with generally several data each day but also sometimes gaps of several days without any data. Tandeo *et al.* (2011) adapt a continuous-time state-space model to analyze this kind of irregular time-step data, in which the state is supposed to be an Ornstein-Uhlenbeck process.

The OU process is an adaptation of Brownian Motion, which models the movement of a free particle through a liquid and was first developed by Einstein (1956). By considering the velocity u_t of a Brownian motion at time t, over a small time interval, two factors affect the change in velocity: the frictional resistance of the surrounding medium whose effect is proportional to u_t and the random impact of neighboring particles whose effect can be represented by a standard Wiener process. Thus, because mass times velocity equals force, the process in a differential equation form is

$$mdu_t = -\omega u_t dt + dW_t, \tag{5.65}$$

where $\omega > 0$ is called the friction coefficient and $m > 0$ is the mass. If we define $\gamma = \omega/m$ and $\lambda = 1/m$, we obtain the OU process (Schöbel and Zhu, 1999), which was introduced with the following differential equation:

$$du_t = -\gamma u_t dt + \lambda dW_t. \tag{5.66}$$

The OU process is used to describe the velocity of a particle in a fluid and is encountered in statistical mechanics. It is the model of choice for random movement toward a concentration point. It is sometimes called a continuous-time Gauss Markov process, where a Gauss Markov process is a stochastic process that satisfies the requirements for both a Gaussian process and a Markov process. Because a Wiener process is both a Gaussian process and a Markov process, in addition to being a stationary independent increment process, it can be considered a Gauss-Markov process with independent increments (Kijima, 1997).

To apply OU process on irregularly sampled data, we assume that the latent process $\{x_{1:t}\}$ is a simple OU process, that is a stationary solution of the following stochastic differential equation :

$$dx_t = -\gamma x_t dt + \lambda dW_t, \tag{5.67}$$

where W_t is a standard Brownian motion, $\gamma > 0$ represents the slowly evolving transfer between two neighbor data and λ is the forward transition variability. It is not hard to find the solution of equation (5.67) is

$$x_t = x_{t-1}e^{-\gamma t} + \int_0^t \lambda e^{-\gamma(t-s)} dW_s. \tag{5.68}$$

For any arbitrary time step t, the general form of the process satisfies

$$x_t = x_{t-1}e^{-\gamma \Delta_t} + \tau, \tag{5.69}$$

where $\Delta_t = T_t - T_{t-1}$ is the time difference between two consecutive data points, τ is a Gaussian white noise with mean zero and variances $\frac{\lambda^2}{2\gamma}\left(1 - e^{-2\gamma\Delta_t}\right)$.

The observed $y_{1:t}$ is measured by

$$y_t = Hx_t + \varepsilon, \tag{5.70}$$

where $\varepsilon \sim N(0, \sigma)$ is a Gaussian white noise.

To run the simulations, we generate an irregular time-lag sequence $\{\Delta_t\}$ first from an *Inverse Gamma* distribution with parameters $\alpha = 2, \beta = 0.1$. Then, the following parameters were chosen for the numerical simulation: $\gamma = 0.5$, $\lambda^2 = 0.1$, $\sigma^2 = 1$.

Similarly, we can get the joint distribution for $x_{1:t}$ and $y_{1:t}$ having a similar precision matrix shown in equation (5.4.1), where $\phi_t = e^{-\gamma\Delta_t}, \tau_t^2 = \frac{\lambda^2}{2\gamma}\left(1 - e^{-2\gamma\Delta_t}\right)$, θ represents for the unknown parameters.

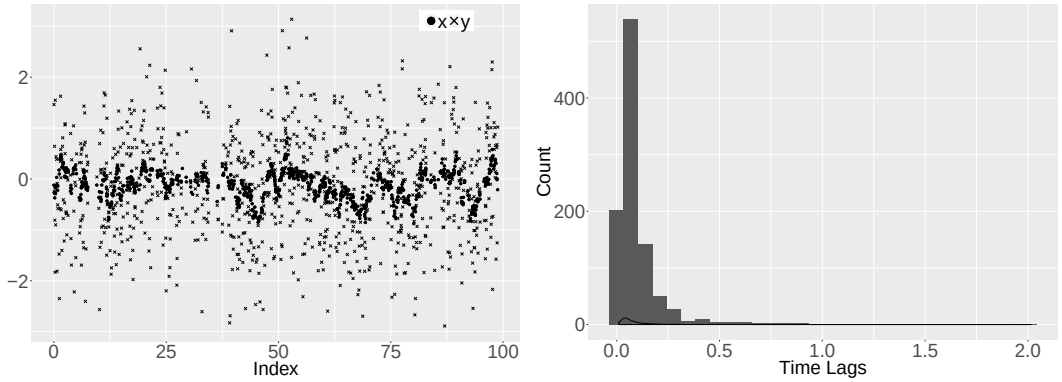

Figure 5.5: Simulated data. The solid dots indicate the true state x and cross dots indicate observation y. Irregular time lag Δ_t are generated from *Inverse Gamma*(2,0.1) distribution.

Parameter Estimation

By implementing he Algorithm 5.1, similarly with Section 5.2.1, from the objective function, the posterior distribution of θ is the same as equation (5.12). By taking natural logarithm on the posterior of θ and by using the useful solutions in equations (5.10) and (5.11), we have the same log-likelihood function (5.13).

Because of all parameters are positive, we are estimating $\nu_1 = \ln \lambda$, $\nu_2 = \ln \gamma^2$ and $\nu_3 = \ln \sigma^2$ instead. When the estimation process is done, we can transform them back to the original scale by taking exponential.

After running the whole process, it gives us the best estimation of $\hat{\theta}$ is $\{\gamma = 0.4841, \lambda^2 = 0.1032, \sigma^2 = 0.9276\}$. In Figure 5.6, we can see that the θ chains are skew to the true value with tails.

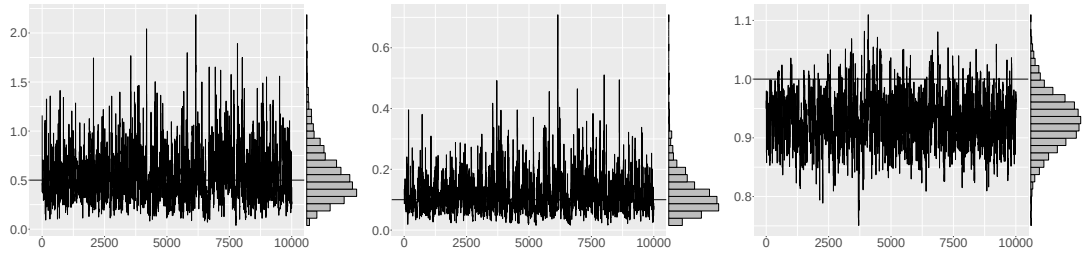

(a) Trace plot of γ (b) Trace plot of λ^2 (c) Trace plot of σ^2

Figure 5.6: Irregular time step OU process simulation. The estimation of $\hat{\theta}$ is $\{\gamma = 0.4841, \lambda^2 = 0.1032, \sigma^2 = 0.9276\}$. In the plots, the horizontal dark lines are the true θ.

Recursive Calculation and State Estimation

Follow the procedure in Section 5.2.2 and do similar calculation with Section 5.4.1, one can find the following recursive way to update K_t and b_t:

$$K_t = \frac{\sigma^4}{\tau_t^2 + \sigma^2 + \phi_t^2(\sigma^2 - K_{t-1})}, \tag{5.71}$$

$$b_t = \begin{bmatrix} \frac{b_{t-1}\phi_t K_t}{\sigma^2} \\ \frac{K_t(\sigma^2+\tau_t^2)-\sigma^4}{\phi_t\sigma^2} \end{bmatrix}. \tag{5.72}$$

With the above formula, the recursive way of updating the mean and covariance are

$$\bar{\mu}_t = \frac{\phi_t}{\sigma^2} K_{t-1}\bar{\mu}_{t-1} + \phi_t \left(1 - \frac{K_{t-1}}{\sigma^2}\right) y_{t-1}, \tag{5.73}$$

$$\bar{\Sigma}_t = \sigma^4 K_t^{-1}, \tag{5.74}$$

where $K_1 = \frac{\sigma^4}{\sigma^2+L^2}$.

With a given θ, the estimation is $x_t \mid y_{1:t}, \theta \sim N\left(\mu_t^{(x)}, \mathrm{Var}(x_t)\right)$, where

$$\mu_t^{(x)} = \frac{K_t\bar{\mu}_t}{\sigma^2} + \left(1 - \frac{K_t}{\sigma^2}\right) y_t \tag{5.75}$$

$$\mathrm{Var}(x_t) = \sigma^2 - K_t. \tag{5.76}$$

By substituting them into the equation (5.27) and (5.28), the estimated x_t is obtained.

Notice that the difference between equations (5.58)(5.59) and equations (5.71) (5.72) is that in the latter ones the parameters are dependent on the time lag Δ_t.

5.5 High Dimensional Ornstein-Uhlenbeck Process Application

Tractors moving on an orchard are mounted with GPS units, which are recording data and transfer to the remote server. This data infers longitude, latitude, bearing, etc, with unevenly spaced time mark. However, one dimensional OU process containing either only position or velocity is not enough to infer a complex movement.

In this section, we are introducing an Ornstein-Uhlenbeck process (OU-process) model combing both position and velocity with the following equations

$$\begin{cases} du_t = -\gamma u_t dt + \lambda dW_t, \\ dx_t = u_t dt + \xi dW_t'. \end{cases} \tag{5.77}$$

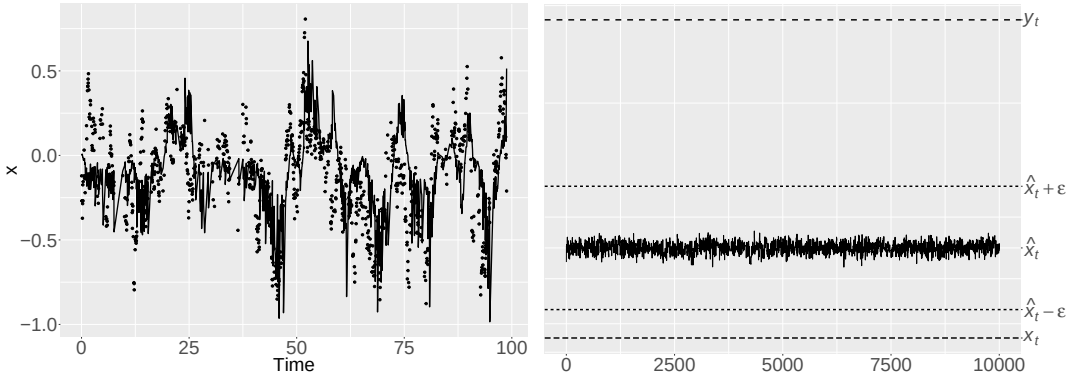

(a) Batch method of estimating $x_{1:t}$ (b) Sequential method of estimating x_t

Figure 5.7: Irregular time step OU process simulation of $x_{1:t}$ and sole x_t. In Figure 5.7a, the dots is the true $x_{1:t}$ and the solid line is the estimation $\hat{x}_{1:t}$. In Figure 5.7b, the chain in solid line is the estimation $\hat{x}_t$; dotted line is the true value of x_t; dot-dash line on top is the observed value y_t; dashed lines represent the standard deviation of the estimation for x_t.

The solution can be found by integrating dt out, that gives us

$$\begin{cases} u_t = u_{t-1}e^{-\gamma t} + \int_0^t \lambda e^{-\gamma(t-s)} dW_s, \\ x_t = x_{t-1} + \frac{u_{t-1}}{\gamma}\left(1 - e^{-\gamma t}\right) + \int_0^t \frac{\lambda}{\gamma} e^{\gamma s}\left(1 - e^{-\gamma t}\right) dW_s + \int_0^t \xi dW'_s. \end{cases} \tag{5.78}$$

As a result, the joint distribution is

$$\begin{bmatrix} x_t \\ u_t \end{bmatrix} \sim N\left(\begin{bmatrix} \mu_t^{(x)} \\ \mu_t^{(u)} \end{bmatrix}, \begin{bmatrix} \sigma_t^{(x)2} & \rho_t \sigma_t^{(x)} \sigma_t^{(u)} \\ \rho_t \sigma_t^{(x)} \sigma_t^{(u)} & \sigma_t^{(u)2} \end{bmatrix} \right), \tag{5.79}$$

where $\mu_t^{(x)}$ and $\mu_t^{(u)}$ are from the forward map process

$$\begin{bmatrix} \mu_t^{(x)} \\ \mu_t^{(u)} \end{bmatrix} = \begin{bmatrix} 1 & \frac{1-e^{-\gamma\Delta_t}}{\gamma} \\ 0 & e^{-\gamma\Delta_t} \end{bmatrix} \begin{bmatrix} x_{t-1}^{(x)} \\ u_{t-1} \end{bmatrix} \triangleq \Phi \begin{bmatrix} x_{t-1}^{(x)} \\ u_{t-1} \end{bmatrix}, \tag{5.80}$$

and

$$\begin{cases} \sigma_t^{(x)2} & = \frac{\lambda^2\left(e^{2\gamma\Delta_t}-1\right)\left(1-e^{-\gamma\Delta_t}\right)^2}{2\gamma^3} + \xi^2\Delta_t \\ \sigma_t^{(u)2} & = \frac{\lambda^2\left(1-e^{-2\gamma\Delta_t}\right)}{2\gamma} \\ \rho_t\sigma_t^{(x)}\sigma_t^{(u)} & = \frac{\lambda^2\left(e^{\gamma\Delta_t}-1\right)\left(1-e^{-2\gamma\Delta_t}\right)}{2\gamma^2} \end{cases} \tag{5.81}$$

In the above equations $\Delta_t = T_t - T_{t-1}$ and initial values are $\Delta_1 = 0$, $x_1 \sim N\left(0, L_x^2\right)$, $u_1 \sim N(0, L_u^2)$, $\rho_t^2 = 1 - \frac{\xi^2\Delta_t}{\sigma_t^{(x)2}}$. To be useful, we use $\frac{1}{1-\rho_t^2} = \frac{\sigma_t^{(x)2}}{\xi^2\Delta_t}$ in the calculation.

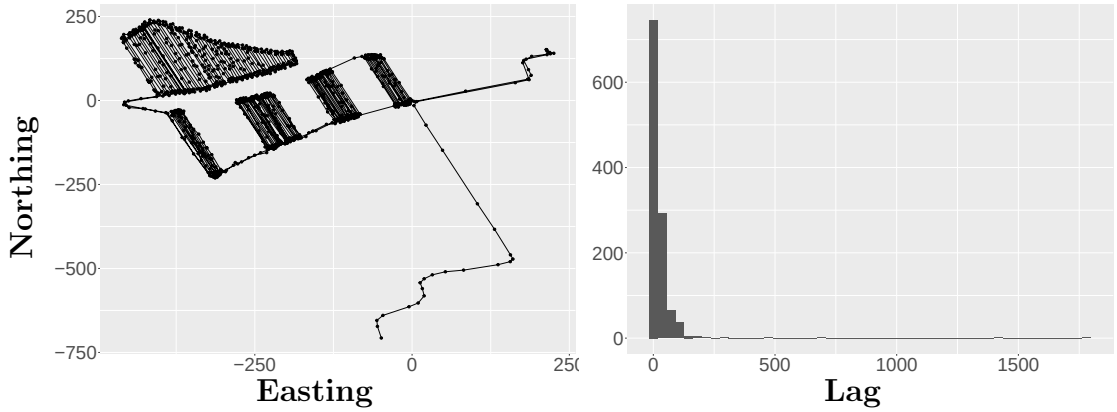

Figure 5.8: Demonstration of line-based trajectory of a moving tractor. The time lags (right side figure) obtained from GPS units are irregular.

Furthermore, the independent observation process is

$$\begin{cases} y_t = x_t + \varepsilon_t, \\ v_t = u_t + \varepsilon'_t, \end{cases} \tag{5.82}$$

where $\varepsilon_t \sim N(0, \sigma), \varepsilon'_t \sim N(0, \tau)$ are normally distributed independent errors. Thus, the joint distribution of observations is

$$\begin{bmatrix} y_t \\ v_t \end{bmatrix} \sim N\left(\begin{bmatrix} x_t \\ u_t \end{bmatrix}, \begin{bmatrix} \sigma^2 & 0 \\ 0 & \tau^2 \end{bmatrix} \right). \tag{5.83}$$

Consequently, the parameter θ of an entire Ornstein-Uhlenbeck process is a set of five parameters from both hidden status and observation process, which is represented as $\theta = \{\gamma, \xi^2, \lambda^2, \sigma^2, \tau^2\}$.

Starting from the joint distribution of $x_{0:t}, u_{0:t}$ and $y_{1:t}, v_{1:t}$ by given θ, it can be found that

$$\begin{bmatrix} \tilde{X} \\ \tilde{Y} \end{bmatrix} \theta \sim N\left(0, \tilde{\Sigma}\right), \tag{5.84}$$

where $\tilde{X}$ represents for the hidden statues $\{x, u\}$, $\tilde{Y}$ represents for observed $\{y, v\}$, θ is the set of five parameters. The inverse of the covariance matrix $\tilde{\Sigma}^{-1}$ is the precision matrix in the form of

$$\tilde{\Sigma}^{-1} = \begin{bmatrix} Q_{xx} & Q_{xu} & -\frac{1}{\sigma^2} I & 0 \\ Q_{ux} & Q_{uu} & 0 & -\frac{1}{\tau^2} I \\ -\frac{1}{\sigma^2} I & 0 & \frac{1}{\sigma^2} I & 0 \\ 0 & -\frac{1}{\tau^2} I & 0 & \frac{1}{\tau^2} I \end{bmatrix}. \tag{5.85}$$

To make the covariance matrix a more beautiful form and convenient computing, $\tilde{X}$, $\tilde{Y}$ and $\tilde{\Sigma}$ can be rearranged in a time series order, that makes $X_{1:t} = \{x_1, u_1, x_2, u_2, \ldots, x_t, u_t\}$, $Y_{1:t} = \{y_1, v_1, y_2, v_2, \ldots, y_t, v_t\}$ and the new precision matrix Σ^{-1} looks like

$$\Sigma^{-1} = \begin{bmatrix} \sigma_{11}^{(x)2} + \frac{1}{\sigma^2} & \sigma_{11}^{(xu)2} & \cdots & \sigma_{1t}^{(x)2} & \sigma_{1t}^{(xu)2} & -\frac{1}{\sigma^2} & 0 & \cdots & 0 & 0 \\ \sigma_{11}^{(ux)2} & \sigma_{11}^{(u)2} + \frac{1}{\tau^2} & \cdots & \sigma_{1t}^{(ux)2} & \sigma_{1t}^{(x)2} & 0 & -\frac{1}{\tau^2} & \cdots & 0 & 0 \\ \vdots & \vdots & \ddots & \vdots & \vdots & \vdots & \vdots & \ddots & \vdots & \vdots \\ \sigma_{t1}^{(x)2} & \sigma_{t1}^{(xu)2} & \cdots & \sigma_{tt}^{(x)2} + \frac{1}{\sigma^2} & \sigma_{tt}^{(xu)2} & 0 & 0 & \cdots & -\frac{1}{\sigma^2} & 0 \\ \sigma_{t1}^{(ux)2} & \sigma_{t1}^{(u)2} & \cdots & \sigma_{tt}^{(ux)2} & \sigma_{tt}^{(u)2} + \frac{1}{\tau^2} & 0 & 0 & \cdots & 0 & -\frac{1}{\tau^2} \\ -\frac{1}{\sigma^2} & 0 & \cdots & 0 & 0 & \frac{1}{\sigma^2} & 0 & \cdots & 0 & 0 \\ 0 & -\frac{1}{\tau^2} & \cdots & 0 & 0 & 0 & \frac{1}{\tau^2} & \cdots & 0 & 0 \\ \vdots & \vdots & \ddots & \vdots & \vdots & \vdots & \vdots & \ddots & \vdots & \vdots \\ 0 & 0 & \cdots & -\frac{1}{\sigma^2} & 0 & 0 & 0 & \cdots & \frac{1}{\sigma^2} & 0 \\ 0 & 0 & \cdots & 0 & -\frac{1}{\tau^2} & 0 & 0 & \cdots & 0 & \frac{1}{\tau^2} \end{bmatrix} \tag{5.86}$$

$$\triangleq \begin{bmatrix} A_t & -B_t \\ -B_t^\top & B_t \end{bmatrix}, \tag{5.87}$$

where B_t is a $2t \times 2t$ diagonal matrix of observation errors at time t in the form of $\begin{bmatrix} \frac{1}{\sigma^2} & \cdot & \cdot & \cdot & \cdot \\ \cdot & \frac{1}{\tau^2} & \cdot & \cdot & \cdot \\ \vdots & \vdots & \ddots & \vdots & \vdots \\ \cdot & \cdot & \cdot & \frac{1}{\sigma^2} & \cdot \\ \cdot & \cdot & \cdot & \cdot & \frac{1}{\tau^2} \end{bmatrix}$. In fact, the matrix A_t is a $2t \times 2t$ bandwidth six sparse matrix at time t in the process. Then, we may find the covariance matrix by calculating the inverse of the precision matrix as

$$\Sigma \triangleq \begin{bmatrix} \Sigma_{XX} & \Sigma_{XY} \\ \Sigma_{YX} & \Sigma_{YY} \end{bmatrix}. \tag{5.88}$$

A detailed structure of the covariance matrix Σ_{XX} is presented in Appendix B.3.

5.5.1 The Posterior Distribution

To find the log-posterior distribution of $X_{1:t}$ and $Y_{1:t}$, we start from the joint distribution. Similarly, the inverse of the covariance matrix is the same as equation (5.8). Additionally, the posterior distribution and log-likelihood function are the same form as equations (5.12) and (5.13).

5.5.2 The Forecast Distribution

It is known that

$$p(Y_{1:t-1}, \theta) = N\left(0, \Sigma_{YY}^{(t-1)}\right) \tag{5.89}$$

$$p(Y_t, Y_{1:t-1}, \theta) = N\left(0, \Sigma_{YY}^{(t)}\right) \tag{5.90}$$

$$p(Y_t \mid Y_{1:t}, \theta) = N\left(\bar{\mu}_t, \bar{\Sigma}_t\right) \tag{5.91}$$

where the covariance matrix of the joint distribution is $\Sigma_{YY}^{(t)} = \left(I_t - A_t^{-1}B_t\right)^{-1} B_t^{-1}$. Then, by taking its inverse, one can obtain

$$\Sigma_{YY}^{(t)(-1)} = B_t(I_t - A_t^{-1}B_t). \tag{5.92}$$

To be clear, the matrix B_t is short for the matrix $B_t(\sigma^2, \tau^2)$, which is $2t \times 2t$ diagonal matrix with elements $\frac{1}{\sigma^2}, \frac{1}{\tau^2}$ repeating for t times on its diagonal. For instance, the very simple $B_1(\sigma^2, \tau^2) = \begin{bmatrix} \frac{1}{\sigma^2} & 0 \\ 0 & \frac{1}{\tau^2} \end{bmatrix}_{2\times 2}$ is a 2×2 matrix.

Because of A_t is symmetric and invertible, B_t is the diagonal matrix defined as above, therefore they have the following property

$$A_t B_t = A_t^\top B_t^\top = (B_t A_t)^\top, \tag{5.93}$$

$$A_t^{-1} B_t = A_t^{-\top} B_t^\top = \left(B_t A_t^{-1}\right)^\top. \tag{5.94}$$

Followed up the form of $\Sigma_{YY}^{(t)(-1)}$, we can define that

$$\Sigma_{YY}^{(t)(-1)} \triangleq \begin{bmatrix} B_{t-1} & 0 \\ 0 & B_1 \end{bmatrix} \begin{bmatrix} Z_t & b_t \\ b_t^\top & K_t \end{bmatrix} \begin{bmatrix} B_{t-1} & 0 \\ 0 & B_1 \end{bmatrix} \tag{5.95}$$

where Z_t is a $2t \times 2t$ matrix, b_t is a $2t \times 2$ matrix and K_t is a 2×2 matrix. Thus,by taking its inverse again, we will get

$$\Sigma_{YY}^{(t)} = \begin{bmatrix} B_{t-1}^{-1}\left(Z_t - b_t K_t^{-1} b_t^\top\right)^{-1} B_{t-1}^{-1} & -B_{t-1}^{-1} Z_t^{-1} b_t \left(K_t - b_t^\top Z_t^{-1} b_t\right)^{-1} B_1^{-1} \\ -B_1^{-1} K_t^{-1} b_t^\top \left(Z_t - b_t K_t^{-1} b_t^\top\right)^{-1} B_{t-1}^{-1} & B_1^{-1}\left(K_t - b_t^\top Z_t^{-1} b_t\right)^{-1} B_1^{-1} \end{bmatrix}. \tag{5.96}$$

It is easy to find the relationship of A_{t-1} and A_t satisfies

$$A_t = \begin{bmatrix} A_{t-1} & \cdot & \cdot \\ \cdot & \frac{1}{\sigma^2} & \cdot \\ \cdot & \cdot & \frac{1}{\tau^2} \end{bmatrix} + U_t U_t^\top \triangleq M_t + U_t U_t^\top, \tag{5.97}$$

where, in fact, $M_t = \begin{bmatrix} A_{t-1} & \cdot & \cdot \\ \cdot & \frac{1}{\sigma^2} & \cdot \\ \cdot & \cdot & \frac{1}{\tau^2} \end{bmatrix} = \begin{bmatrix} A_{t-1} & 0 \\ 0 & B_1 \end{bmatrix}$ and its inverse is $M_t^{-1} = \begin{bmatrix} A_{t-1}^{-1} & 0 \\ 0 & B_1^{-1} \end{bmatrix}$. By using the Sherman-Morrison-Woodbury formula, one can find the inverse of A_t in such a recursive way that

$$A_t^{-1} = \left(M_t + U_t U_t^\top\right)^{-1} = M_t^{-1} - M_t^{-1} U_t \left(I_t + U_t^\top M_t^{-1} U_t\right)^{-1} U_t^\top M_t^{-1}. \tag{5.98}$$

Consequently, after being simplified, it gives us

$$K_t = B_1^{-1} D_t \left(I_t + S_t^\top \left(B_1^{-1} - K_{t-1}\right) S_t + D_t^\top B_1^{-1} D_t\right)^{-1} D_t^\top B_1^{-1}, \tag{5.99}$$

and

$$b_t = \begin{bmatrix} -b_{t-1} \\ B_1^{-1} - K_{t-1} \end{bmatrix} S_t \left(I_t + S_t^\top \left(B_1^{-1} - K_{t-1}\right) S_t + D_t^\top B_1^{-1} D_t\right)^{-1} D_t^\top B_1^{-1}, \tag{5.100}$$

by which, K_t and b_t are updated in a recursive way. As a result, one can obtain the following recursive updating formula for the mean and covariance matrix

$$\begin{aligned} \bar{\mu}_t &= \Phi_t K_{t-1} B_1 \bar{\mu}_{t-1} + \Phi_t \left(I_t - K_{t-1} B_1\right) Y_{t-1} \\ \bar{\Sigma}_t &= \left(B_1 K_t B_1\right)^{-1} \end{aligned} \tag{5.101}$$

The matrix K_t is updated via equation (5.99), or updating its inverse in the following form makes the computation faster, that is

$$K_t^{-1} = B_1 D_t^{-\top} D_t^{-1} B_1 + B_1 \Phi_t \left(B_1^{-1} - K_{t-1}\right) \Phi_t^\top B_1 + B_1, \tag{5.102}$$

$$\bar{\Sigma}_t = D_t^{-\top} D_t^{-1} + \Phi_t \left(B_1^{-1} - K_{t-1}\right) \Phi_t^\top + B_1^{-1} \tag{5.103}$$

and $K_1 = B_1^{-1} - A_1^{-1} = \begin{bmatrix} \frac{\sigma^4}{\sigma^2 + L_x^2} & 0 \\ 0 & \frac{\tau^4}{\tau^2 + L_u^2} \end{bmatrix}$. For calculation details, readers can refer to Appendix B.2.

5.5.3 The Estimation Distribution

Because of the joint distribution (5.84), one can find the estimation with a given θ is in the same form as equation (5.20). Being explicitly, for X_t, the joint distribution with $Y_{1:t}$ updated to time t is

$$X_t, Y_{1:t} \mid \theta \sim N\left(0, \begin{bmatrix} C_t^\top \left(A_t - B_t\right)^{-1} C_t & C_t^\top \left(A_t - B_t\right)^{-1} \\ \left(A_t - B_t\right)^{-1} C_t & \left(I_t - A_t^{-1} B_t\right)^{-1} B_t^{-1} \end{bmatrix}\right), \tag{5.104}$$

where $C_t^\top = \begin{bmatrix} 0 & \cdots & 0 & 1 & 0 \\ 0 & \cdots & 0 & 0 & 1 \end{bmatrix}$ is a $2 \times 2t$ matrix. Thus,

$$X_t \mid Y_{1:t}, \theta \sim N\left(\mu_t^{(X)}, \Sigma_t^{(X)}\right), \tag{5.105}$$

where

$$\mu_t^{(X)} = C_t^\top A_t^{-1} B_t Y_t = C_t^\top L_t^{-\top} W_t, \tag{5.106}$$

$$\Sigma_t^{(X)} = C_t^\top A_t^{-1} C_t = U_t^\top U_t, \tag{5.107}$$

and $U_t = L_t^{-1} C_t$. The recursive updating formula is

$$\mu_t^{(X)} = K_t B_1 \bar{\mu}_t + (I_t - B_1 K_t) Y_t \tag{5.108}$$

$$\Sigma_t^{(X)} = B_1^{-1} - K_t. \tag{5.109}$$

5.5.4 Prior Distribution for Parameters

The well known *Hierarchical Linear Model*, where the parameters vary at more than one level, is first introduced by Lindley and Smith (1972); Smith (1973). Hierarchical Model can be used on data with many levels, although 2-level models are the most common ones. The state-space model in equations (4.1) and (4.2) is one of Hierarchical Linear Model if G_t and F_t are linear, and non-linear model if G_t and F_t are non-linear processes. Researchers have made a few discussions and work on these both linear and non-linear models. In this section, we only discuss on the prior for parameters in these models.

Various informative and non-informative prior distributions have been suggested for scale parameters in hierarchical models. Gelman (2006) give a discussion on prior distributions for variance parameters in hierarchical models. General considerations include using invariance (Jeffries, 1961), maximum entropy (Jaynes, 1983) and agreement with classical estimators (Box and Tiao, 2011). Regarding informative priors, the author suggests to distinguish them into three categories: (i) is traditional informative prior. A prior distribution giving numerical information is crucial to statistical modeling and it can be found from a literature review, an earlier data analysis or the property of the model itself. (ii) is weakly informative prior. This genre prior is not supplying any controversial information but are strong enough to pull the data away from inappropriate inferences that are consistent with the likelihood. Some examples and brief discussions of weakly informative priors for logistic regression models are

given in (Gelman *et al.*, 2008). (iii) is uniform prior, which allows the information from the likelihood to be interpreted probabilistically.

Stroud and Bengtsson (2007) discuss a model with different structures in the errors. The two errors ω_t and ε_t are assumed normally distributed as

$$\omega_t \sim N(0, \alpha Q), \tag{5.110}$$

$$\varepsilon_t \sim N(0, \alpha R), \tag{5.111}$$

where the two matrices R and Q are known and α is an unknown scale factor to be estimated. (Note that the forward map will be deterministic if $Q = 0$.) The density of the Gaussian state-space model therefore becomes

$$p(y_t \mid x_t, \alpha) = N(F(x_t), \alpha R), \tag{5.112}$$

$$p(x_t \mid x_{t-1}, \alpha) = N(G(x_{t-1}), \alpha Q). \tag{5.113}$$

The parameter α is assumed *Inverse Gamma* distribution.

For the priors of all the parameters in an OU-process, shown in equation (5.77) and (5.82), first of all, we should understand what meanings of these parameters are standing for. The reciprocal of γ is typical velocity falling in the reasonable range of 0.1 to 100 m/s. ξ is the error occurs in transition process, σ and τ are errors in the forward map for position and velocity respectively. Generally, the error is a positive finite number. Considering prior distributions for these parameters, before looking at the data, we have an idea of ranges where these parameters are falling in. Conversely, we do not have any assumptions about the true value of λ, which means it can be anywhere. According to this assumption, the prior distributions are

$$\gamma \sim IG(10, 0.5), \tag{5.114}$$

$$\xi^2 \sim IG(5, 2.5), \tag{5.115}$$

$$\sigma^2 \sim IG(5, 2.5), \tag{5.116}$$

where $IG(\alpha, \beta)$ represents the *Inverse Gamma* distribution with two parameters α and β.

5.5.5 Efficiency of Delayed-Acceptance Metropolis-Hastings Algorithm

We have discussed the efficiency of Metropolis-Hastings (MH) algorithm and how it is affected by the step size. To explain it explicitly, here we give an example comparing

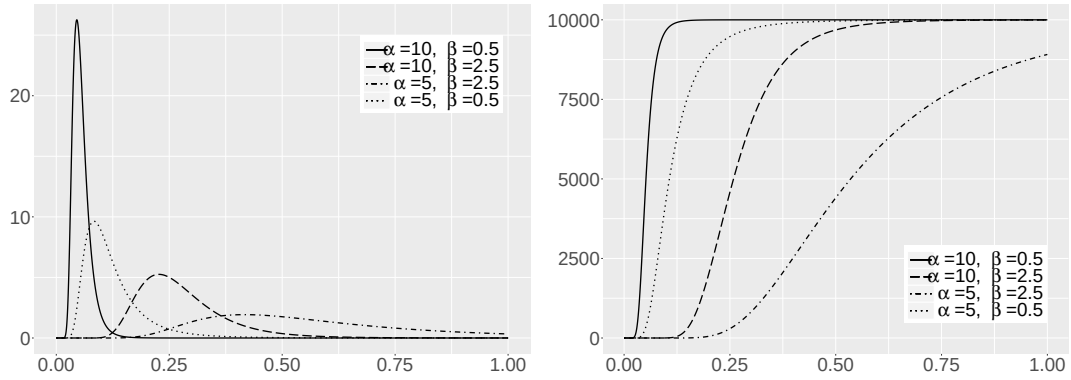

Figure 5.9: Probability density function and cumulative distribution function of *Inverse Gamma* with two parameters α and β.

Eff (efficiency), EffUT (efficiency in unit time), ESS (effective sample size) and ESSUT (effective sample size in unit time), which are calculated by using the data set, which is demonstrated in Figure 5.8, and running 10 000 iterations of DA MH. We are taking a sequence from 0.1 to 4 with equal-space of 0.3, so that $s = \{0.1, \ldots, 4\}$, and to solve criterion formula with each of the value. Table 5.1 and Figure 5.10 show the compares the results of the calculation.

The best step size found by Eff is 1, which is as the same as that found by ESS. Let $s = 1$ and run 1 000 iterations, the DA MH takes 36.35 seconds to get the Markov chain for θ and the acceptance rates α_1 for approximating $\hat{\pi}(\cdot)$ and α_2 for estimating the posterior distribution $\pi(\cdot)$ are 0.3097 and 0.8324 respectively. By using EffUT and ESSUT, the best step size is 2.5, which is bigger. One of the advantages of using this step size is the significant decreasing of the computation time to 5.10 seconds. It is because the surrogate $\hat{\pi}(\cdot)$ takes bad proposals out and only good ones are accepted to pass to the next level. It can be seen from the lower rates α_1 in Table 5.1.

Table 5.1: An example of Eff, EffUT, ESS and ESSUT found by running 10 000 iterations with same data. The computation time is measured in seconds s.

	Values	Time	Step Size	α_1	α_2
Eff	0.0515	36.35	1.0	0.3097	0.8324
EffUT	0.0031	5.10	2.5	0.0360	0.7861
ESS	501.4248	36.35	1.0	0.3097	0.8324
ESSUT	29.8912	5.10	2.5	0.0360	0.7861

On the surface, a bigger step size causes lower acceptance rates α_1 and it might not

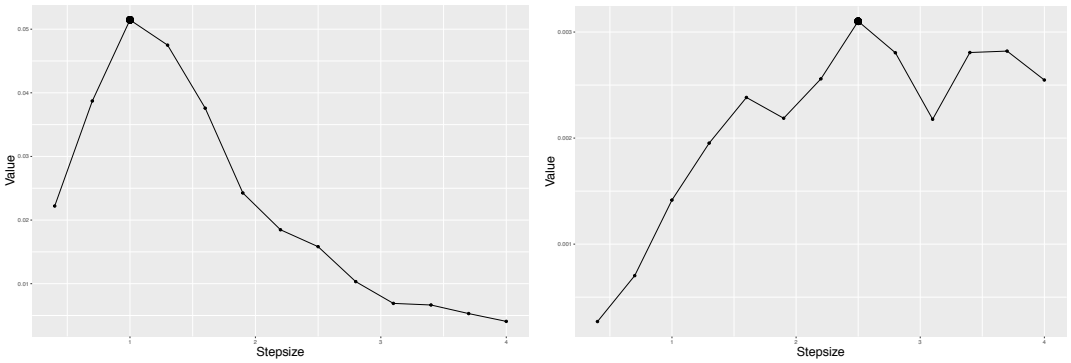

(a) Efficiency against different step sizes (b) EffUT against different step sizes

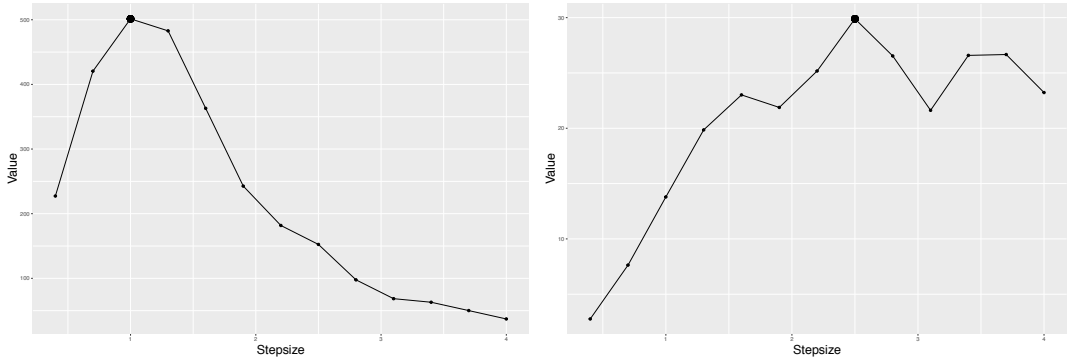

(c) ESS against different step sizes (d) ESSUT against different step sizes

Figure 5.10: Influences of different step sizes on sampling efficiency (Eff), efficiency in unit time (EffUT), effective sample size (ESS) and effective sample size in unit time (ESSUT) found with the same data

be a smart choice. However, on the other hand, one should notice the less time cost. To make it sensible, we are running the DA MH with different step sizes, as presented in Table 5.1, for the same (or similar) amount of time. Because of the bigger step size takes less time than smaller one, so we achieve a longer chain. To be more clear, we take 1 000 samples out from a longer chain, such as 8 500, and calculate Eff, EffUT, ESS and ESSUT separately by the embedded function IAT, (Christen and Fox, 2010), and ESS of the package LaplacesDemon in R and the above formulas . As we can see from the outcomes, by running the similar amount of time, the Markov chain with a bigger step size has a higher efficiency and effective sample size in unit time. More intuitively, the advantage of using larger step size is the sampling algorithm generates more representative samples per second. Figure B.1 is comparing different θ chains found by using different step sizes but running the same amount of time. As we can see that θ with the optimal step size has a lower correlated relationship.

Table 5.2: Comparison of Eff, EffUT, ESS and ESSUT values with different step size. The 1000* means taking 1 000 samples from a longer chain, like 1 000 out of 5 000 sample chain. The computation time is measured in seconds s.

Step Size	Length	Time	Eff	EffUT	ESS	ESSUT
1.0	1 000	3.48	0.0619	0.0178	69.4549	19.9583
1.3	1 400	3.40	0.0547	0.0161	75.3706	22.1678
	1 000*	3.40	0.0813	0.0239	72.5370	21.3344
2.2	5 000	3.31	0.0201	0.0061	96.6623	29.2031
	1 000*	3.31	0.0941	0.0284	94.2254	28.4669
2.5	7 000	3.62	0.0161	0.0044	112.3134	31.0258
	1 000*	3.62	**0.1095**	**0.0302**	**113.4063**	**31.3277**

5.5.6 A Sliding Window State and Parameter Estimation Approach

The length of data used in the algorithm really affects the computation time. The forecast distribution $p(Y_t \mid Y_{1:t-1}, \theta)$ and estimation distribution $p(X_t \mid Y_{1:t}, \theta)$ require finding the inverse of the covariance $\Sigma_{YY}^{(t+1)}$, however, which is time consuming if the sample size is big to generate a large sparse matrix. For a moving vehicle, one is more willing to get the estimation and moving status instantly rather than being delayed. Therefore a compromise solution is the fixed-length sliding window sequential filter. A fixed-lag sequential parameter learning method was proposed by Polson *et al.* (2008) and named as *Practical Filtering*. The authors rely on the approximation of

$$p(x_{0:n-L}, \theta \mid y_{0:n-1}) \approx p(x_{0:n-L}, \theta \mid y_{0:n}) \tag{5.117}$$

for large L. The new observations coming after the nth data has little influence on $x_{0:n-L}$.

Being inspired, we do not use the first 0 to $n-1$ date and ignore the latest nth, on the contrary, use all the latest date with truncating the first few history ones. Suppose we are given a fixed-length L, up to time t ($t > L$), we estimate the x_t by using all the retrospective observations to the point at $t - L + 1$. In another word, the estimation distribution for the current state is

$$p(X_t \mid Y_{t-L+1:t}, \theta), \tag{5.118}$$

where $t > L$. We name this method the *Sliding Window Sequential Parameter Learning Filter*.

The next question is how to choose an appropriate L. The length of data used in MH and DA MH algorithms has an influence on the efficiency and accuracy of parameter learning and state estimation. Being tested on real data set, there is no doubt that the more data be in use, the more accurate the estimation is, and lower efficient is in computation. In Table B.4, one can see the pattern of parameters γ, ξ, τ follow the same trend with the choice of L and σ increases when L decreases. Since estimation bias is inevitable, we are indeed to keep the bias as small as possible, and in the meantime, the higher efficiency and larger effective sample size are bonus items. In Figure 5.11, we can see that the efficiency and effective sample size is not varying along with the sample size used in sampling algorithm, but in unit time, they are decreasing rapidly as data size increases. In addition, from a practical point of view,

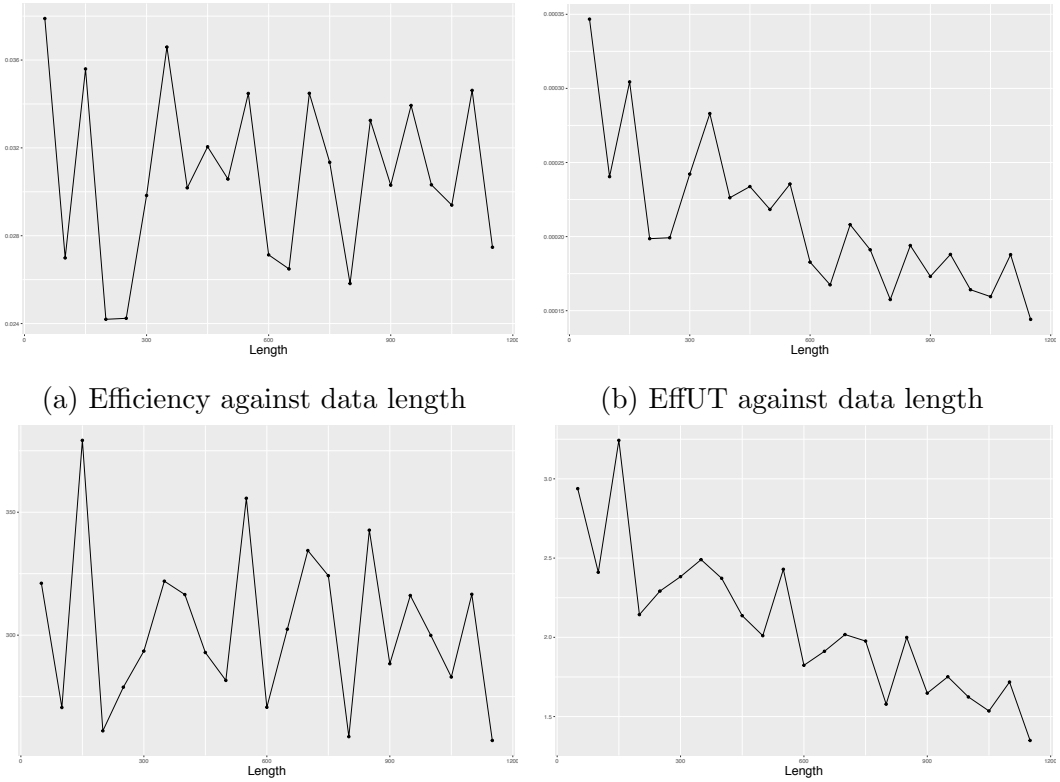

(a) Efficiency against data length

(b) EffUT against data length

(c) ESS against data length

(d) ESSUT against data length

Figure 5.11: Comparison of efficiency (Eff), efficiency in unit time (EffUT), effective sample size (ESS) and effective sample size in unit time (ESSUT) against the different length of data. Increasing data length does not significantly improve the efficiency and ESSUT.

the observation error σ should be kept at a reasonable level, let's say $50cm$, and the computation time should be as less as possible. To reach that level, $L = 100$ is an

appropriate choice. For a one-dimensional linear model, L can be chosen larger and that does not change too much. If the data up to time t is less than or equal to the chosen L, the whole data set is used in learning θ and estimating X_t.

For the true posterior, the algorithm requires a cheap estimation $\hat{\pi}(\cdot)$, which is found by one-variable-at-a-time Metropolis-Hastings algorithm. The advantage is getting a precise estimation of the parameter structure, and disadvantage is, obviously, lower efficiency. Luckily, we find that it is not necessary to run this MH every time when estimate a new state from x_{t-1} to x_t. In fact, in the DA MH process, the cheap $\hat{\pi}$ does not vary too much in the filtering process with new data coming into the data set. We may use this property in the algorithm. First of all, we use all available data from 1 to t with length up to L to learn the structure of θ and find out the cheap approximation $\hat{\pi}$. Then, use DA MH to estimate the true posterior π for θ and x_t. After that, extend data set to $1 : t+1$ if $t \leq L$ or shift the data window to $2 : t+1$ if $t > L$ and run DA MH again to estimate θ and x_{t+1}. From Figures B.3 and B.4, we can see that the main features and parameters in the estimating process between batch method and sliding window method have not significant differences.

To avoid estimation bias, which is caused by sampling degeneracy, we are introducing a *threshold* criterion and a *cutting-off* value. In a certain circumstance, the cheap $\hat{\pi}(\cdot)$ is not accurate and is replaced by a new one $\hat{\pi}_{\text{new}}(\cdot)$. The *cutting-off* procedure stops the algorithm when a large Δ_t occurs in the progress. A large time gap indicates a break of the vehicle at a time point and it causes irregularity and bias. A smart way is to stop the process and to wait for new data coming in. By running testings on real data, the *threshold* is chosen $\alpha_2 < 0.7$ and the *cutting-off* value is set at $\Delta_t \geq 300$. For each time, if the acceptance rate α_2 is less than 0.7, we update the mean of $\hat{\pi}$ and remain the covariance unchanged.

In fact, the mean of the estimation may vary upon the data but the covariance matrix does not change too much, as is shown in Figure B.4. Actually, these two values are on researchers' choices. Figures 5.12 and 5.13 compare the performances of using and not using the *threshold* criterion to update the mean of the parameters. We can see that by using the *threshold* criterion, we effectively avoid estimation bias and obtain more effective samples.

Consequently, a complete form of this algorithm is summarized in the following Algorithm 5.2:

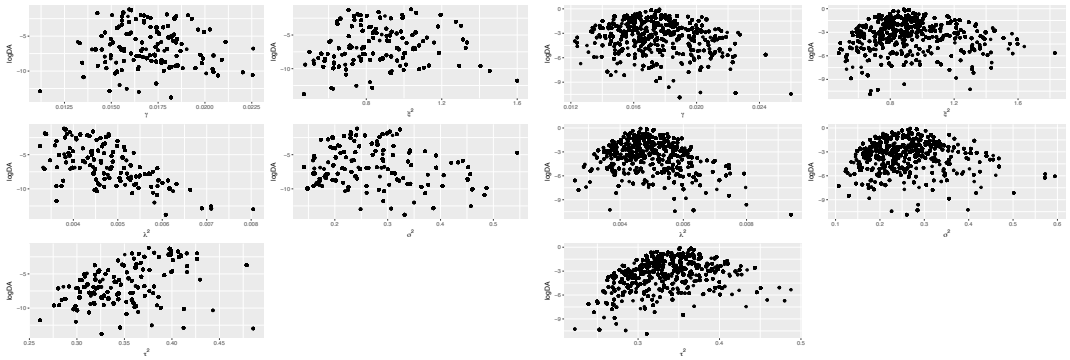

(a) $\ln DA$ surfaces of not-updating-mean

(b) $\ln DA$ surfaces of updating-mean

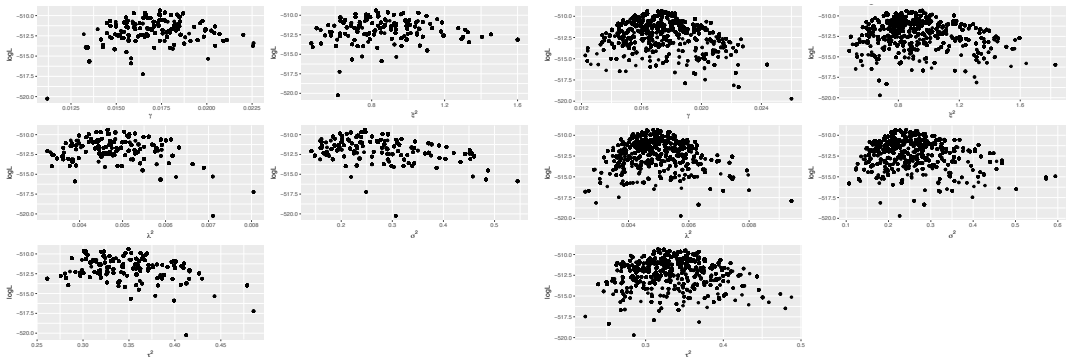

(c) $\ln L$ surfaces of not-updating-mean

(d) $\ln L$ surfaces of updating-mean

Figure 5.12: Comparing $\ln DA$ and $\ln L$ surfaces between not-updating-mean and updating-mean methods. It is obviously that the updating-mean method has higher dense log-surfaces, which contain more effective samples.

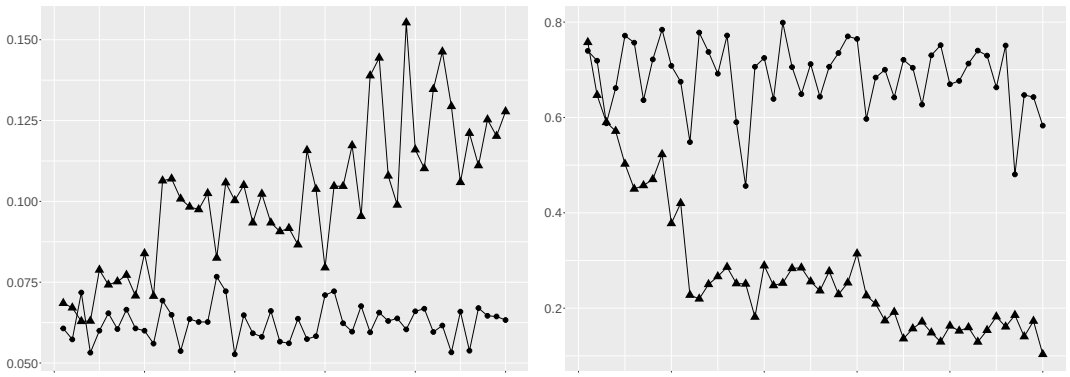

(a) Comparing α_1

(b) Comparing α_2

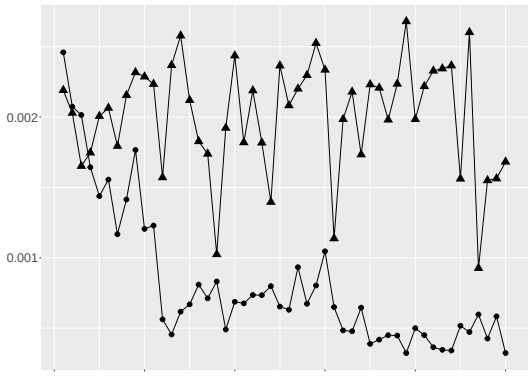

(c) Comparing EffUT

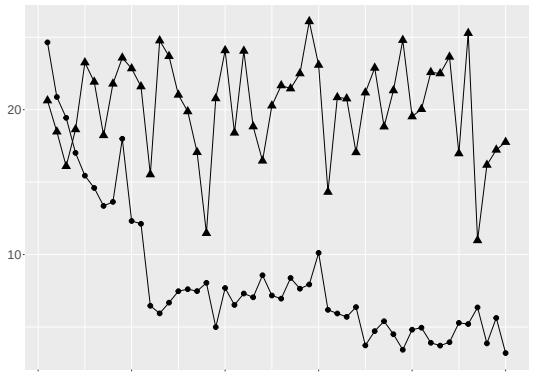

(d) Comparing ESSUT

Figure 5.13: Comparing acceptance rates α_1, α_2, EffUT and ESSUT between not-updating-mean and updating-mean methods. Black solid dots • indicate values obtained from not-updating-mean method and black solid triangular ▲ indicate values obtained from updating-mean method. The acceptance rates of the updating-mean method are more stable and effective samples are larger in unit computation time.

Algorithm 5.2: Sliding Window Adaptive MCMC

1 Initialization: Set up L, *threshold* and *cutting-off* criteria.

2 Learning phase: Estimate θ with $p\left(\theta \mid Y_{1:\min\{t,L\}}\right) \propto p\left(Y_{1:\min\{t,L\}} \mid \theta\right) p\left(\theta\right)$ by one-variable-at-a-time Random Walk Metropolis-Hastings algorithm gaining the target acceptance rates and find out the structure of $\theta \sim N\left(\mu, \Sigma\right)$ and the approximation $\hat{\pi}\left(\cdot\right)$.

3 Estimation phase: draw samples for θ and $X_{\max\{1,t-L+1\}:\min\{t,L\}}$ given $Y_{\max\{1,t-L+1\}:\min\{t,L\}}$: **for** *i from 1 to N* **do**

4 Propose θ_i^* from $N\left(\theta_i \mid \mu, \Sigma\right)$, accept it with probability $\alpha_1 = \min\left\{1, \frac{\hat{\pi}\left(\theta_i^*\right) q\left(\theta_i, \theta_i^*\right)}{\hat{\pi}\left(\theta_i\right) q\left(\theta_i^*, \theta_i\right)}\right\}$ and go to next step; otherwise go to step 4.

5 Accept θ_i^* with probability $\alpha_2 = \min\left\{1, \frac{\pi\left(\theta_i^*\right) \hat{\pi}\left(\theta_i\right)}{\pi\left(\theta_i\right) \hat{\pi}\left(\theta_i^*\right)}\right\}$ and go to next step; otherwise go to step 4.

6 Calculate $\mu_i^{(t)}, \Sigma_i^{(t)}$ for X_t and $\mu_i^{(t+s)}, \Sigma_i^{(t+s)}$ for X_{t+s}.

7 **end**

8 Calculate $\mu_X^{(t)} = \frac{1}{N} \sum_i \mu_i^{(t)}$, $\mathrm{Var}[X^{(t)}] = \frac{1}{N} \sum_i \left(\mu_i^{(t)} \mu_i^{(t)\top} + \Sigma_i\right) - \frac{1}{N^2} \left(\sum_i \mu_i^{(t)}\right) \left(\sum_i \mu_i^{(t)}\right)^\top$ and $\mu_X^{(t+s)}$, $\mathrm{Var}[X^{(t+s)}]$ with the same formula.

9 Check *threshold* and *cutting-off* criteria. **if** *threshold is TRUE* **then**

10 Update $\theta \sim N\left(\mu, \Sigma\right)$

11 **else if** *cutting-off is TRUE* **then**

12 Stop process.

13 **else**

14 Go to next step.

15 **end**

16 Shift the window by setting $t = t + 1$ and go back to step 3.

5.5.7 Application to 2-Dimensional GPS Data

An application of the Algorithm 5.2 is to track the position of a moving tractor on a farm. The original GPS data set is plotted in Figure 1.1. In a 2-dimensional trajectory filtering problem, we use the same parameter $\theta = \{\gamma, \xi^2, \lambda^2, \sigma^2, \tau^2\}$ for both easting and northing directions. The observations on these two directions are denoted as Y_E and Y_N respectively. The hidden states on easting and northing directions are X_E and X_N.

To speed up the estimation, we should get an idea of what the parameter space looks like by running step 2 of the algorithm with a subset of observations. By setting $L = 100$ and running 5 000 iterations, we find 5 000 samples for θ in 59 seconds. For each parameter of θ, we take 1 000 sub-samples out as a new sequence. The new θ^* is representative for the parameter space. Then the traces and correlation are derived from θ^*. Meanwhile, the acceptance rates for each parameter are $\alpha_\gamma = 0.453, \alpha_{\xi^2} = 0.433, \alpha_{\lambda^2} = 0.435, \alpha_{\sigma^2} = 0.414, \alpha_{\tau^2} = 0.4490$ respectively. Hence, the structure of $\hat{\theta} \sim N(m_t, C_t)$, which is depicted in Figure 5.14, is obtained.

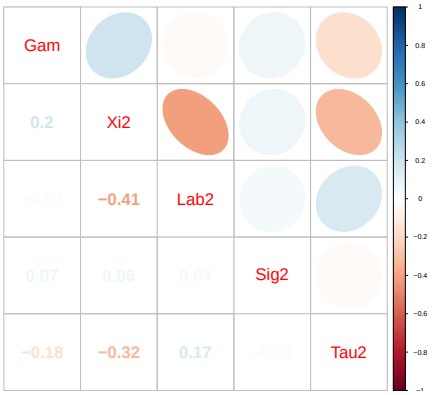

Figure 5.14: Visualization of the parameters correlation matrix, which is found in the learning phase. Diagonal labels represent for γ, ξ^2, λ^2, σ^2 and τ^2.

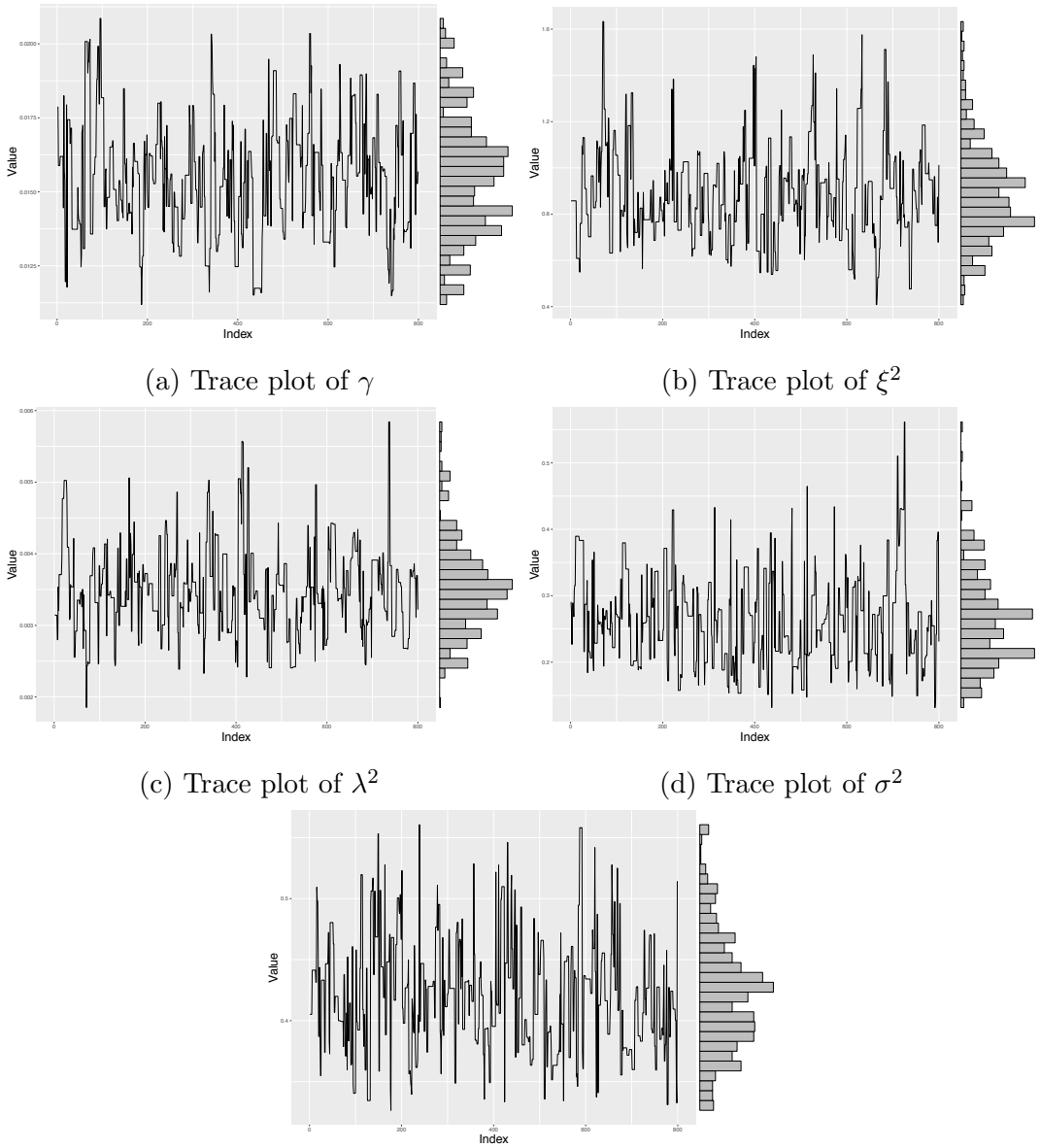

(a) Trace plot of γ

(b) Trace plot of ξ^2

(c) Trace plot of λ^2

(d) Trace plot of σ^2

(e) Trace plot of τ^2

Figure 5.15: Trace plots of θ after taking 1 000 burn-in samples out from 5 000 from the learning phase.

Since a cheap surrogate $\hat{\pi}(\cdot)$ for the true $\pi(\cdot)$ is found in step 2 (the learning phase), it is time to move on to the estimation phase. Algorithm 5.2 takes fixed L length data from $\{Y_E, Y_N\}_{1:L}$ to $\{Y_E, Y_N\}_{t-L+1:t}$ until an irregular large time lag meets the cutting-off criterion. In the implementation, the first cutting-off occurs after the 648-th point. The first 100 estimates $\{X_E, X_N\}_{1:100}$ were found in the learning phase and $\{X_E, X_N\}_{101:648}$ were found sequentially in the estimation phase with approximate 9 seconds per 10 000 iterations for each $\{X_E, X_N\}_s, s \in [101, 648]$. The outcome is depicted in Figure 5.16.

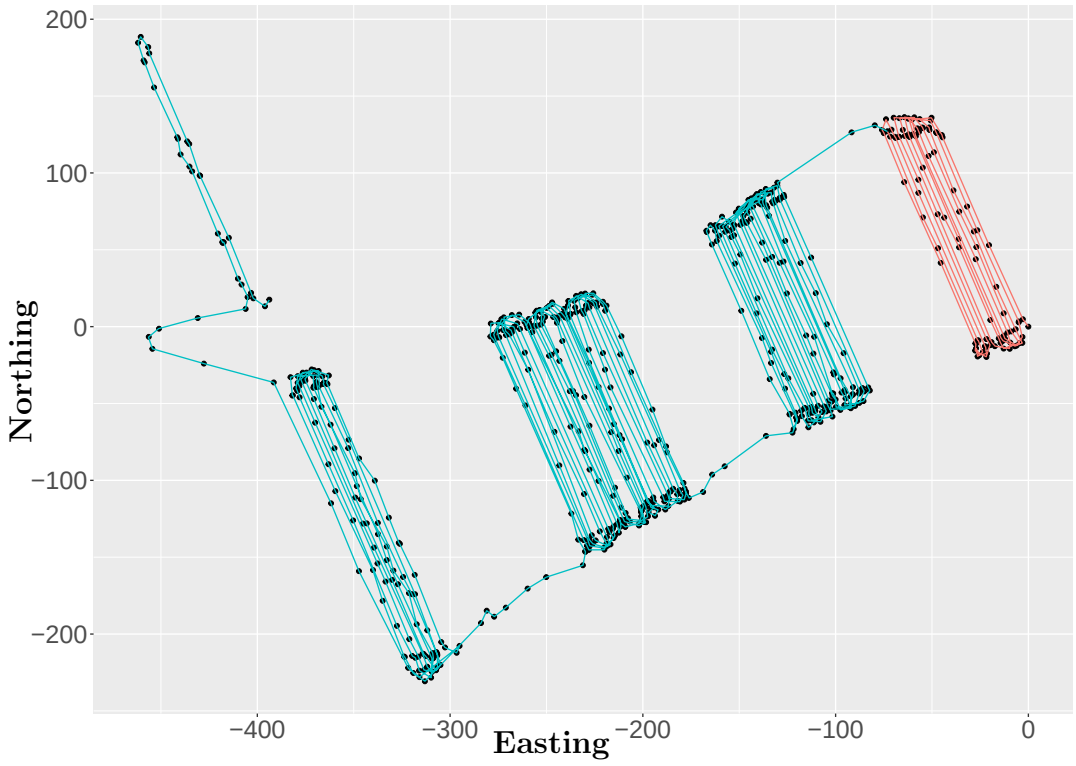

Figure 5.16: Estimations of Z found by combined batch and sequential methods. The red line is the estimation by batch method and the green line is the sequential MCMC filtering estimation. Black dots are the measurements.

The means of uncertainties in the estimation for each direction are about 0.5 meters. Figure 5.17 depicts uncertainties of the estimation before the first cutting-off procedure activated. The shaded blue filling indicates that there are larger uncertainties at turning points. In the estimation phase, Algorithm 5.2 is able to estimate X_t and to predict X_{t+s}. However, when s goes along time t, the uncertainty becomes larger. When a new observation X_{t+1} comes into the data stream, the uncertainty shrinks.

After a cutting-off procedure is activated, the adaptive MCMC algorithm goes

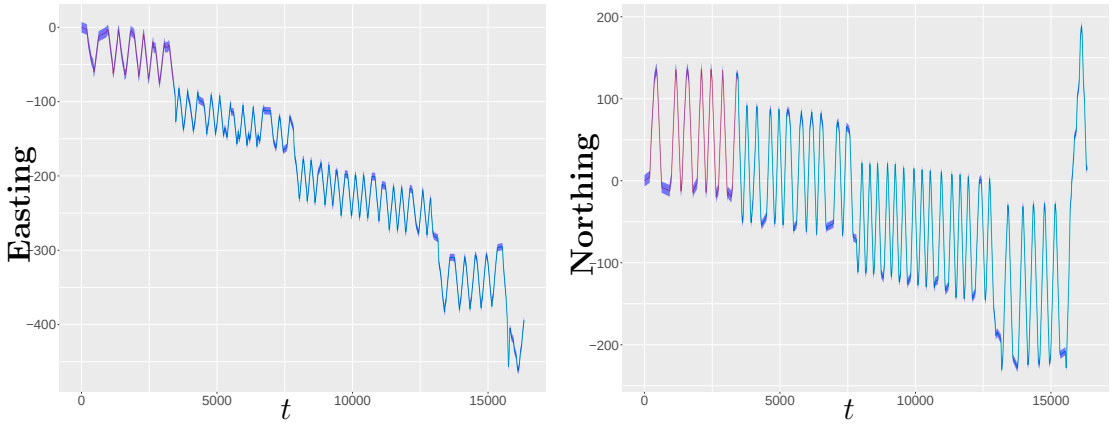

Figure 5.17: Uncertainties on easting and northing directions before the first cutting-off procedure. The means of uncertainties on each direction are about 0.5 meters.

off-line and accumulates measurements until there are enough, for example 100, for continued estimation [1]. In the application, we can see that the first 100 observations are used for parameter estimation in the learning phase. Once this step is done, the sequential estimation phase goes on-line for filtering calculation. Because there is a large time lag between the 648-th and 649-th points, the algorithm goes off-line again to accumulate data in the learning phase, and then goes back to on-line for filtering estimation.

Figure 5.18 gives the whole estimated trajectory by the proposed sliding window MCMC algorithm. There are two main learning phase occur on the entire data set. The first learning phase uses the first 100 data and the second learning phase uses the data from 649 to 748. With the information obtained from the learning phase, two sequential estimation phases estimate the data from 101 to 648 and from 749 to 1121 respectively. However, when the third large time lag occurs after the 1121-th point, the algorithm has insufficient observations to run a third learning phase. In this figure, the on-line/off-line switching points are colored in yellow.

5.6 Discussion and Future Work

In this chapter, an adaptive MCMC algorithm is proposed for estimating combined state and parameter in a homogeneous linear state-space model. The whole process is split into two phases: learning phase and estimation phase. In the learning phase, a

[1] Alternatively, a "hot start" is possible in which the priors are the posteriors of the previous estimation phase and no learning phase is required.

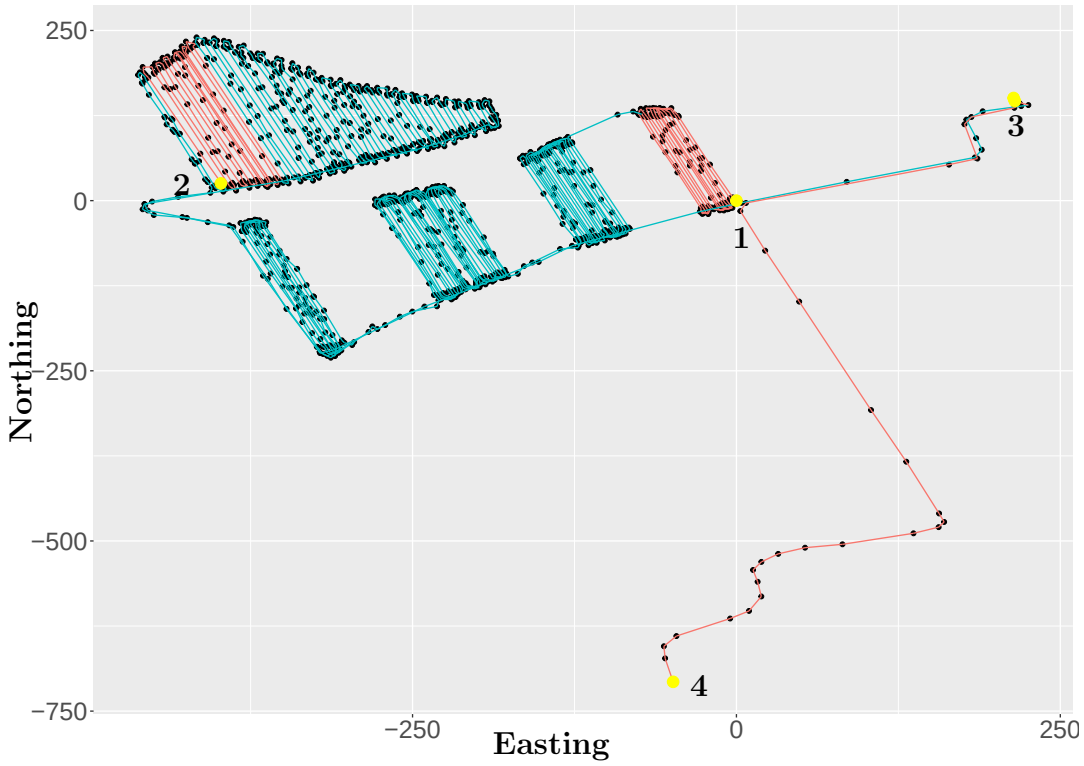

Figure 5.18: Two learning phases are colored by red and two sequential estimation phases are colored by green. The algorithm is not able to estimate the data from 1121 till the end because of the lack of observations. Point 1 is the first point of the data stream. Points 2 and 3 are the switching points. Point 4 is the last point of the data stream.

self-tuning one-variable-at-a-time random walk Metropolis-Hastings algorithm is used to learn the structure of the parameter space. After getting a cheap surrogate for the expensive posterior distribution, it is then used in a delayed-acceptance algorithm in the estimation phase.

Note that in the learning phase, we determine an approximation for the posterior distribution to be used in the delayed-acceptance MH algorithm. This is quite different to population MCMC (Laskey and Myers, 2003), in which multiple chains are used to determine a better proposal distribution. This does, however, suggest that multiple chains can be used to improve the learning phase.

In on-line mode, the algorithm is adaptive to maintain sampling efficiency and uses a sliding window approach to maintain sampling speed. At the end of this chapter, the algorithm is applied to on-line estimation on a 2-dimensional GPS data set.

The advantage of this algorithm is that it is easy to understand and to implement

in practice. In contrast, Particle Learning algorithm is highly efficient, however, the sufficient statistics are not available at all times.

The sliding window adaptive MCMC algorithm should be contrasted with the V-spline algorithm proposed in Chapter 2. The sliding window adaptive MCMC algorithm is a filtering algorithm that is designed for fast estimation. The V-spline is a smoothing algorithm that uses all the data for entire trajectory estimation and parameter optimization can be time consuming. On the other hand, the V-spline has piecewise continuous second derivatives, whereas the forward map (5.77) built into our sliding window adaptive MCMC algorithm implies sample paths are not twice differentiable.

The gradient boosting V-spline, discussed in Chapter 6, is potentially a much faster algorithm that also will be employed in on-line mode. Like the V-spline, the forward map in the adaptive MCMC algorithm can also incorporate vehicle operating characteristics. However, it would be important to maintain the efficiency of the MCMC sampler in higher dimensions.

Chapter 6

Future Work

In this thesis, two main practical algorithms are proposed: the adaptive V-spline and the adaptive sequential MCMC algorithm. The first algorithm is appropriate for batch estimation and the second for on-line estimation, and we have seen that both algorithms have good performance in practice. Nevertheless, there are a number of areas in which further improvements can be made.

Gradient Boosting V-Spline

V-spline is an advanced smoothing spline algorithm returning least true mean squared errors. However, to implement this algorithm on-line needs feasible solutions. One of them probably is combining spline method and gradient boosting algorithm.

In machine learning application, it is best to build a non-parametric regression or classification model from the data itself. A connection between the statistical framework and machine learning is the gradient-descent based formulation of boosting methods, which was derived by Freund and Schapire (1995); Friedman (2001). The gradient boosting algorithm is a powerful machine-learning technique that has shown considerable success in a wide range of practical applications, particularly in machine learning competitions on *Kaggle*.

The motivation of gradient boosting algorithms is combining weak learners together as a strong leaner, which keeps minimizing the target loss function. It has highly customizable application to meet particular needs, like being learned with respect to different loss functions. For example, for a continuous response $y \in R$, the loss function can be chosen as a Gaussian L_2 loss function. Hence, the squared error L_2 loss function is

$$L_2(y, f(t)) = \frac{1}{2}\left(y - f(t)\right)^2, \tag{6.1}$$

and the best trained f^* is

$$f^* = \arg_f \min E_{t,y}[L_2(y, f)]. \tag{6.2}$$

To find f^*, it is reducing the loss $\tilde{y}_i = y_i - F_{m-1}(t_i)$ recursively. Consequently, the

$$f_m(t) = f_{m-1}(t) + \rho_m h(t, \alpha_m), \tag{6.3}$$

is the sum of some basic learners $h_m(t, \alpha)$. $m = 1, \ldots, M$ determines the complexity of the solution.

On-line boosting algorithms are given by Babenko *et al.* (2009); Beygelzimer *et al.* (2015). It is assumed that the loss over the entire training data can be expressed as a sum of the loss for each point t_i, that is $L(f(t, y)) = \sum_i L(f(t_i, y_i))$. Instead of computing the gradient of the entire loss, the gradient is computed with respect to just one data point. Furthermore, by adding additional regularization term will help to smooth the final learned weights to avoid over-fitting in a penalized regression problem (Chen and Guestrin, 2016).

Accordingly, the V-spline $f^*(t)$ is a sum of several weak learners $f_m(t)$, each of which has $2N$ parameters $\theta_m = \left\{\theta_m^{(1)}, \ldots, \theta_m^{(2N)}\right\}$. The optimal θ^* is found by

$$\theta^* = \sum_{m=0}^{M} \theta_m, \tag{6.4}$$

where θ_m is computed via $\theta_m = -\rho_m \frac{\partial L(\theta)}{\partial \theta}$.

As a result, after M iterations, θ^* is convergence and $f^*(t, y, \theta^*)$ is obtained.

Directional Dependent OU-Process

In the usual formulation of an OU-process, we have

$$dv_t = -\gamma v_t + \lambda dW_t, \tag{6.5}$$

where $v_t = \begin{bmatrix} v_t^x \\ v_t^y \end{bmatrix}$, $W_t = \begin{bmatrix} W_t^x \\ W_t^y \end{bmatrix}$ are vectors in $\mathbb{R}^2$. In particular, W_t^x and W_t^y are independent Wiener processes. However, we can imagine that the stochastic term has independent components in the directions parallel and perpendicular to the velocity. Let $\{n_t, m_t\}$ be an orthonormal frame in $\mathbb{R}^2$, where $n_t = \frac{v_t}{|v_t|}$ is the direction of the velocity. The proposal is that λdW_t can be replaced with $\lambda_\parallel n_t dW_t^\parallel + \lambda_\perp m_t dW_t^\perp$, where $W_t^\parallel$ and $W_t^\perp$ are independent Wiener processes.

Grid-based MCMC

In several references, Grid-based methods have been proved that it provides an optimal recursion of the filtered density $p(x_t \mid y_{1:t})$ if the state-space is discrete and consists of a finite number of states (Ristic *et al.*, 2004; Stroud *et al.*, 2018; Arulampalam *et al.*, 2002; Hartmann *et al.*, 2016).

In the application of real time series data set, the model is supposed as an OU-process containing five unknown parameters. With the idea of grid-based algorithm, the 5-dimension parameter space $\mathbb{R}^5$ can be initialized by spanning $\theta_0^{(i)}$ with equal weights $w_0 = \left\{\frac{1}{N}, \frac{1}{N}, \frac{1}{N}, \frac{1}{N}, \frac{1}{N}\right\}$ at time $t = 0$, where $i = 1, \ldots, N$. When a new observation $Y_t = \{y_t, v_t\}$ comes into the system, the weights for each parameter in each subspace are updated via $w_t \propto p(Y_t \mid \theta, Y_{1:t-1}) w_{t-1}$.

However, the grid-based MCMC may not be practical for a higher n-dimensional space, which requires $\mathrm{O}\left(N^n\right)$ computation cost per MCMC step.

Parallel MCMC

Parallel computing is a type of computation in which many calculations or the execution of processes are carried out simultaneously on multi-core processors (Asanovic *et al.*, 2006). A master process controls the strategy on how to split large, expensive computation into smaller slave processes and solved concurrently on each separate processor (Almasi and Gottlieb, 1994). After computing, slave processes pass results back to the master process, in which the final result is generated.

The parallel MCMC uses this technology to deploy the computation and run samplers on multi-core CPU. Approaches for parallel MCMC are either by implementing parallelization within a single chain or by running multiple chains (Wu *et al.*, 2012). It is useful for computing complex Bayesian models, which do not only lead to a dramatic speedup in computing but can also be used to optimize model parameters in complex Bayesian models.

A simple parallel Monte Carlo estimation of $\mathrm{E}[p(\theta)]$ proceeds in the following way (Kontoghiorghes, 2005). Suppose there amount to k CPU cores to generate N samples. Thus, on each CPU there are $m = N/k$ samples on average. A master process passes m to each slave process i, $i = 1, \ldots, k$. At each slave process, it generates m samples for $\theta_i^{(m)}$ and passes middle-result S_i back to the master process. At last, the master process computes the final result by

$$\mathrm{E}[p(\theta)] = \frac{\sum_i S_i}{N}. \tag{6.6}$$

The parallel MCMC uses MCMC sampler scheme to draw samples on multi-cores simultaneously. A naive yet natural approach to parallel MCMC is simply to generate several independent Markov chains on different processors and then combine the results appropriately (Bradford and Thomas, 1996; Gelman and Rubin, 1992). Or, alternatively, develop parallelism within a single chain. Suppose there are k CPU cores. Give initial values $\theta_i^{(0)}$ for each core. Concurrently update θ chains by a predetermined MCMC sampler with $p(\theta \mid y_{1:t})$ on each slave process. Computes summary statistics for the updated $\theta_i^{(0:N)}$ and passes back to the master process. Finally, achieve a sequence of θ of length kN (Wu *et al.*, 2012).

A further weighted parallel MCMC and parallelization approach to the Gibbs sampler is proposed by VanDerwerken and Schmidler (2013).

Consequently, the parallel MCMC is a potential alternative approach of sliding window MCMC in Chapter 5 to improve the computation speed in high dimensional space.

Chapter 7

Summary

Inference and characterization of planar trajectories have long been the focus of scientific and commercial research. Efficient algorithms for both precise and efficient trajectory reconstruction remain in high demand in a wide variety of applications. In this thesis, an off-line method named V-spline is proposed to reconstruct the whole trajectory and an on-line adaptive MCMC algorithm is used to update and track unknown state and parameter instantly.

In Chapter 2, the proposed V-spline is built up by new basis functions consisting of Hermite splines. For n paired time series data $\{t_i, y_i, v_i\}_{i=1}^n$, the amount of basis functions is $2n$. In the new objective function (2.4), V-spline incorporates both location and velocity information but penalizes excessive accelerations. It is not only minimizing the squared residuals of $|y_i - f(t_i)|^2$ but also reducing the squared residuals of $|v_i - f'(t_i)|^2$, for $i = 1, \ldots, n$, with a new parameter γ.

In the objective function of a conventional smoothing spline, the penalty parameter λ is a constant number that controls the trade-off between interpolations ($\lambda \to 0$) and a straight line ($\lambda \to \infty$). Instead, the penalty parameter $\lambda(t)$ of a V-spline is a piecewise constant function, which is varying on each interval $[t_i, t_{i+1})$, $i = 1, \ldots, n-1$. Hence, in the objective function of V-splines, there are overall n parameters, including $n-1$ λs and γ, to be estimated. Additionally, to handle unexpected curvatures in the reconstruction, an adjusted penalty term $\frac{(\Delta t_i)^3}{(\Delta d_i)^2}$ adapts to more complicated curvature status. The idea behind this term is that either velocity and acceleration goes to zero, the penalty value λ should be large enough to enforce a straight line.

It is proved that, with improper priors, smoothing splines are corresponding to Bayes estimates. In particular, smoothing splines can be interpreted by Gaussian process regression in a certain reproducing kernel Hilbert space. This property extends

smoothing splines to more flexible and general applications. Similarly, if a V-spline is equipped with an appropriate inner product (3.23) if $\lambda(t)$ is constant, or an inner product (3.44) if $\lambda(t)$ is piecewise constant, it is corresponding to the posterior mean of the Bayes estimates in the reproducing kernel Hilbert space $\mathcal{C}^{(2)}_{\text{p.w.}}[0,1]$. This result is discussed in Chapter 3. Recall the property of V-splines that if and only if $\lambda(t)$ is constant and $\gamma = 0$ would the second derivatives be continuous on the entire interval. Otherwise, the second derivatives may not be continuous at the knots but are linear in each interval.

To find the best parameters, an extended leave-one-out cross-validation technique is proposed in Chapter 2 to find the smoothing parameters of interest. This method uses observations to tune the parameters to the optimal level. Accordingly, V-spline is a data-driven nonparametric regression solution to handle paired time series data consisting of position and velocity information. However, for data with correlated errors, the generalized cross-validation algorithm is more effective. Being modified a generic GCV, in Chapter 3, an extended GCV is used for finding the optimal parameters for V-spline and its Bayes estimate containing correlated errors. Suppose the solution of a V-spline and its first derivative are in the form of $f = S(\lambda,\gamma)y + \gamma T(\lambda,\gamma)v$ and $f' = U(\lambda,\gamma)y + \gamma V(\lambda,\gamma)v$, the GCV calculates the trace of matrices S, T, U and V. It is much faster than calculating the sum of the single element in each matrix in LOOCV.

Simulation studies are given to compare the performances of V-spline and other methods, such as Wavelet algorithms and penalized B-spline, in Chapter 2. It is obvious that these algorithms are competitive on reconstructing trajectories. By contrast, only the proposed V-spline returns the least true mean squared errors. At the end of this chapter, a numeric simulation is presented to demonstrate the effectiveness of V-spline. Being applied to a real GPS data set, the parameter λ is classified by λ_u and λ_d representing for two operating status of a mechanic boom. λ_u is a set of $\{\lambda_i\}$ in the intervals where the boom is not operating and, by contrast, λ_d is a set of $\{\lambda_i\}$ in the intervals where the boom is operating. The reconstruction from V-spline can be treated as the real trajectory of a moving vehicle with confidence.

Without loss of generality, $\lambda(t)$ can be classified into more groups to adapt to complex maneuver system and V-spline is flexible to be applied on higher dimensional cases.

However, subject to the property that smoothing splines require the solution of a global problem that involves the entire set of points to be interpolated, it might

not be suitable for on-line estimation. Hence, Chapter 4 give an overview of existing filtering and estimation algorithms. Some popular algorithms, such as Particle filter, are concentrating on inferring the unknown state but assuming the parameters known. Moreover, the sample impoverishment has never been solved properly. Liu and West's filter tries to kill particle degeneracy by incorporating with a shrinkage kernel and estimates the unknown parameters simultaneously. Storvik filter and Particle learning algorithms marginalize out the parameters through sufficient statistics to obtain a better outcome. In some way, they are advanced algorithms but not practicable at any time. In most circumstances, sufficient statistics are not available or hard to find. More flexible and easy-implement methods are in demand.

An adaptive sequential MCMC algorithm is proposed in Chapter 5. The adaptive sequential MCMC is dealing with paired time series data set including both position and velocity information.

In the case of a linear state-space model and starting with a joint distribution over state x, observation y and parameter θ, an MCMC sampler is implemented in two phases. In the learning phase, a self-tuning sampler utilizes one-variable-at-a-time random walk Metropolis-Hastings algorithm to learn the mean and covariance structure of the parameter space with aiming at a target acceptance rate for each parameter. After exploring the parameter space, the information is used in the subsequent phase — the estimation phase — to inform the proposed mechanism and is also used in a delayed-acceptance algorithm.

Suppose the mean and covariance matrix of θ are m and $C = L^\top L$ respectively, where L is the Cholesky decomposition. The proposal $\theta^* = \theta + \epsilon LZ$, where $Z \sim N(0, I)$ and ϵ is the step size. The effect of L is to reduce the correlation of proposals and move to the next step on purpose. The step size ϵ makes the proposal process more efficient. Rather than focusing on the criteria of efficiency (Eff) and effective sample size (ESS), the Eff in unit time (EffUT) and ESS in unit time (ESSUT) are the new criteria to determine the optimal step size. By running the same amount of time, the optimal step size found by EffUT and ESSUT helps sampler in generating more effective and representative samples.

Further, the delayed-acceptance algorithm uses a cheap surrogate $p(\theta \mid m, C)$ to the true posterior $p(\theta \mid y)$ in the first line of defense to keep not-good samples outside. Only good proposals would pass the first line and move forward to the additional expensive calculation. This strategy greatly improves sampling efficiency.

Information on the resulting state of the system is indicated by a Gaussian mixture.

For each sample of $\theta^{(i)}$, it matches an $x^{(i)} \sim N\left(\mu^{(i)}, \sigma^{(i)}\right)$. Consequently, the final estimation of x is given by a set of Gaussian mixture.

In the on-line mode, the algorithm is adaptive and uses a sliding window approach by cutting off historical data to accelerate sampling speed and to maintain appropriate acceptance rates. In a simple one parameter simulation in Chapter 4, the proposed adaptive MCMC shows a stable feature comparing with other filters. In Chapter 5, this algorithm shows an advantage in estimating irregularly sampled time series data.

At the end of Chapter 5, the proposed algorithm is applied to combined state and parameter estimation in the case of irregularly sampled time series GPS data. Suppose that the model is a four-dimensional linear Ornstein-Uhlenbeck (OU) process containing observed positions and velocities on both easting and northing directions, denoted as $Y_E = \{y_E, v_E\}$ and $Y_N = \{y_N, v_N\}$. The hidden states on the two directions are $X_E = \{x_E, u_E\}$ and $X_N = \{x_N, u_N\}$. The same parameter $\theta = \{\gamma, \xi^2, \lambda^2, \sigma^2, \tau^2\}$ is shared by the two directions. The proposed algorithm efficiently infers the state X_E and X_N along with time t returning approximate 50 centimeter uncertainties.

As a conclusion, the proposed algorithms in this thesis contribute to related areas, nevertheless, are not perfect. V-spline may not be appropriate for on-line estimation and the sliding window adaptive MCMC algorithm dose not use the entire data set that might lose some information. Future work and deeper research are required to improve their performances.

Appendices

Appendix A

Proofs and Figures of V-Spline Theorems

A.1 Penalty Matrix in (2.16)

The i-th $\Omega^{(i)}$ is a $2n \times 2n$ bandwidth four symmetric matrix and its non-zero elements on the upper triangular are

$$\Omega^{(i)}_{2i-1,2i-1} = \int_{t_i}^{t_{i+1}} \frac{d^2 h^{(i)}_{00}(t)}{dt^2} \frac{d^2 h^{(i)}_{00}(t)}{dt^2} dt = \frac{12}{\Delta_i^3} \tag{A.1.1}$$

$$\Omega^{(i)}_{2i-1,2i} = \int_{t_i}^{t_{i+1}} \frac{d^2 h^{(i)}_{00}(t)}{dt^2} \frac{d^2 h^{(i)}_{10}(t)}{dt^2} dt = \frac{6}{\Delta_i^2} \tag{A.1.2}$$

$$\Omega^{(i)}_{2i-1,2i+1} = \int_{t_i}^{t_{i+1}} \frac{d^2 h^{(i)}_{00}(t)}{dt^2} \frac{d^2 h^{(i)}_{01}(t)}{dt^2} dt = \frac{-12}{\Delta_i^3} \tag{A.1.3}$$

$$\Omega^{(i)}_{2i-1,2i+2} = \int_{t_i}^{t_{i+1}} \frac{d^2 h^{(i)}_{00}(t)}{dt^2} \frac{d^2 h^{(i)}_{11}(t)}{dt^2} dt = \frac{6}{\Delta_i^2} \tag{A.1.4}$$

$$\Omega^{(i)}_{2i,2i} = \int_{t_i}^{t_{i+1}} \frac{d^2 h^{(i)}_{10}(t)}{dt^2} \frac{d^2 h^{(i)}_{10}(t)}{dt^2} dt = \frac{4}{\Delta_i} \tag{A.1.5}$$

$$\Omega^{(i)}_{2i,2i+1} = \int_{t_i}^{t_{i+1}} \frac{d^2 h^{(i)}_{10}(t)}{dt^2} \frac{d^2 h^{(i)}_{01}(t)}{dt^2} dt = \frac{-6}{\Delta_i^2} \tag{A.1.6}$$

$$\Omega^{(i)}_{2i,2i+2} = \int_{t_i}^{t_{i+1}} \frac{d^2 h^{(i)}_{10}(t)}{dt^2} \frac{d^2 h^{(i)}_{11}(t)}{dt^2} dt = \frac{2}{\Delta_i} \tag{A.1.7}$$

$$\Omega^{(i)}_{2i+1,2i+1} = \int_{t_i}^{t_{i+1}} \frac{d^2 h^{(i)}_{01}(t)}{dt^2} \frac{d^2 h^{(i)}_{01}(t)}{dt^2} dt = \frac{12}{\Delta_i^3} \tag{A.1.8}$$

$$\Omega^{(i)}_{2i+1,2i+2} = \int_{t_i}^{t_{i+1}} \frac{d^2 h^{(i)}_{01}(t)}{dt^2} \frac{d^2 h^{(i)}_{11}(t)}{dt^2} dt = \frac{-6}{\Delta_i^2} \tag{A.1.9}$$

$$\Omega^{(i)}_{2i+2,2i+2} = \int_{t_i}^{t_{i+1}} \frac{d^2 h^{(i)}_{11}(t)}{dt^2} \frac{d^2 h^{(i)}_{11}(t)}{dt^2} dt = \frac{4}{\Delta_i} \tag{A.1.10}$$

where $\Delta_i = t_{i+1} - t_i$ and $i = 1, 2, \ldots, n-1$. Then

$$\mathbf{\Omega} = \sum_{i=1}^{n-1} \lambda_i \Omega^{(i)}$$

A.2 Proof of Theorem 1

Proof. If $g : [a, b] \mapsto \mathbb{R}$ is a proposed minimizer, construct a cubic spline $f(t)$ that agrees with $g(t)$ and its first derivatives at $t_1, \ldots, t_n$, and is component-wise linear on $[a, t_1]$ and $[t_n, b]$. Let $h(t) = g(t) - f(t)$. Then, for $i = 1, \ldots, n-1$,

$$\begin{aligned}
\int_{t_i}^{t_{i+1}} f''(t)h''(t)dt &= f''(t)h'(t)\Big|_{t_i}^{t_{i+1}} - \int_{t_i}^{t_{i+1}} f'''(t)h'(t)dt \\
&= 0 - f'''\left(t_i^+\right) \int_{t_i}^{t_{i+1}} h'(t)dt \\
&= -f'''\left(t_i^+\right) \left(h(t_{i+1}) - h(t_i)\right) \\
&= 0.
\end{aligned}$$

Additionally, $\int_a^{t_1} f''(t)h''(t)dt = \int_{t_n}^{b} f''(t)h''(t)dt = 0$, since $f(t)$ is assumed linear outside the knots. Thus, for $i = 0, \ldots, n$,

$$\begin{aligned}
\int_{t_i}^{t_{i+1}} |g''(t)|^2 dt &= \int_{t_i}^{t_{i+1}} |f''(t) + h''(t)|^2 dt \\
&= \int_{t_i}^{t_{i+1}} |f''(t)|^2 dt + 2\int_{t_i}^{t_{i+1}} f''(t)h''(t)dt + \int_{t_i}^{t_{i+1}} |h''(t)|^2 dt \\
&= \int_{t_i}^{t_{i+1}} |f''(t)|^2 dt + \int_{t_i}^{t_{i+1}} |h''(t)|^2 dt \\
&\geq \int_{t_i}^{t_{i+1}} |f''(t)|^2 dt.
\end{aligned}$$

The result $J[f] \leq J[g]$ follows since $\lambda_i > 0$.

Furthermore, equality of the curvature penalty term only holds if $g(t) = f(t)$. On $[t_1, t_n]$, we require $h''(t) = 0$ but since $h(t_i) = h'(t_i) = 0$ for $i = 1, \ldots, n$, this means $h(t) = 0$. Meanwhile on $[a, t_1]$ and $[t_n, b]$, $f''(t) = 0$ so that equality requires $g''(t) = 0$. Since $f(t)$ agrees with $g(t)$ and its first derivatives at t_1 and t_n, equality is forced on both intervals. □

A.3 Proof of Corollary 1

Proof. By setting $\gamma \to 0$, the velocity information v is taken away. The degrees of freedom of parameters decreases from $2n$ to n. Hence, there exists an $n \times 2n$ matrix

Q_λ restricting n degrees of freedom of $\hat{\theta}$ and satisfying $Q_\lambda \hat{\theta} = 0$.

The matrices B and C have the following property:

$$BB^\top = CC^\top = I_n,$$
$$C^\top CB^\top = B^\top BC^\top = 0.$$

Denoting $G = B^\top B + \gamma C^\top C + n\Omega_\lambda$ and giving $\hat{\theta} = (B^\top B + \gamma C^\top C + n\Omega_\lambda)^{-1}(B^\top y + \gamma C^\top v)$, we will have $G\hat{\theta} = B^\top y + \gamma C^\top v$ and

$$BG\hat{\theta} = y + \gamma BC^\top v$$
$$CG\hat{\theta} = CB^\top y + \gamma v.$$

Further, $C^\top CG\hat{\theta} = C^\top(CB^\top y + \gamma v) = \gamma C^\top v$. If by setting $\gamma = 0$, one will get $Q_\lambda = C^\top CG$, which consists of the even rows of Ω_λ.

By integrating by parts and using properties of the basis functions at the knots, one can get the even rows of $\Omega^{(i)}$, which are

$$\begin{aligned}
\Omega^{(i)}_{2i,2i-1} &= N''_{2i-1}\left(t_i^-\right) - N''_{2i-1}\left(t_i^+\right) \\
\Omega^{(i)}_{2i,2i} &= N''_{2i}\left(t_i^-\right) - N''_{2i}\left(t_i^+\right) \\
\Omega^{(i)}_{2i,2i+1} &= N''_{2i+1}\left(t_i^-\right) - N''_{2i+1}\left(t_i^+\right) \\
\Omega^{(i)}_{2i,2i+2} &= N''_{2i+2}\left(t_i^-\right) - N''_{2i+2}\left(t_i^+\right) \\
\Omega^{(i)}_{2i+2,2i-1} &= N''_{2i-1}\left(t_{i+1}^-\right) - N''_{2i-1}\left(t_{i+1}^+\right) \\
\Omega^{(i)}_{2i+2,2i} &= N''_{2i}\left(t_{i+1}^-\right) - N''_{2i}\left(t_{i+1}^+\right) \\
\Omega^{(i)}_{2i+2,2i+1} &= N''_{2i+1}\left(t_{i+1}^-\right) - N''_{2i+1}\left(t_{i+1}^+\right) \\
\Omega^{(i)}_{2i+2,2i+2} &= N''_{2i+2}\left(t_{i+1}^-\right) - N''_{2i+2}\left(t_i^+\right)
\end{aligned}$$

Thus

$$Q_\lambda = nC^\top C\Omega_\lambda = nC^\top C\sum_i \lambda_i \Omega^{(i)}.$$

Consequently, if and only if λ is constant, $Q_\lambda\hat{\theta} = -\lambda\left(f''\left(t_i^+\right) - f''\left(t_i^-\right)\right) = 0$, for $i = 1, \ldots, n$, otherwise $Q_\lambda\theta = 0$ is true but does not represent $f''\left(t_i^+\right) - f''\left(t_i^-\right)$.

As a result, $f''(t)$ is continuous at the knots t_i if $\lambda(t)$ is constant and $\gamma = 0$.

□

A.4 Proof of Lemma 2

Proof. For any smooth curve f with $\mathbf{y}^*$, we have

$$\begin{aligned}
&\frac{1}{n}\sum_{j=1}^{n}\left(y_j^*-f(t_j)\right)^2+\frac{\gamma}{n}\sum_{j=1}^{n}\left(v_j^*-f'(t_j)\right)^2+\sum_{j=1}^{n}\lambda_j\int_{t_j}^{t_{j+1}}f''^2dt\\
\geq&\frac{1}{n}\sum_{j\neq i}\left(y_j^*-f(t_j)\right)^2+\frac{\gamma}{n}\sum_{j\neq i}\left(v_j^*-f'(t_j)\right)^2+\sum_{j=1}^{n}\lambda_j\int_{t_j}^{t_{j+1}}f''^2dt\\
\geq&\frac{1}{n}\sum_{j\neq i}\left(y_j^*-\hat{f}^{(-i)}(t_j)\right)^2+\frac{\gamma}{n}\sum_{j\neq i}\left(v_j^*-\hat{f}'^{(-i)}(t_j)\right)^2+\sum_{j=1}^{n}\lambda_j\int_{t_j}^{t_{j+1}}\left(\hat{f}''^{(-i)}\right)^2dt\\
=&\frac{1}{n}\sum_{j=1}^{n}\left(y_j^*-\hat{f}^{(-i)}(t_j)\right)^2+\frac{\gamma}{n}\sum_{j=1}^{n}\left(v_j^*-\hat{f}'^{(-i)}(t_j)\right)^2+\sum_{j=1}^{n}\lambda_j\int_{t_j}^{t_{j+1}}\left(\hat{f}''^{(-i)}\right)^2dt
\end{aligned}$$

by the definition of $\hat{\mathbf{f}}^{(-i)}$, $\hat{\mathbf{f}}'^{(-i)}$ and the fact that $y_i^*=\hat{f}^{(-i)}(t_i)$, $v_i^*=\hat{f}'^{(-i)}(t_i)$. It follows that $\hat{f}^{(-i)}$ is the minimizer of the objective function (2.4), so that

$$\begin{aligned}
\hat{\mathbf{f}}^{(-i)}&=S\mathbf{y}^*+\gamma T\mathbf{v}^*\\
\hat{\mathbf{f}}'^{(-i)}&=U\mathbf{y}^*+\gamma V\mathbf{v}^*
\end{aligned}$$

as required. □

A.5 Proof of Theorem 2

Proof.

$$\begin{aligned}
\hat{f}^{(-i)}(t_i)-y_i=&\sum_{j=1}^{n}S_{ij}y_j^*+\gamma\sum_{j=1}^{n}T_{ij}v_j^*-y_i^*\\
=&\sum_{j\neq i}^{n}S_{ij}y_j+\gamma\sum_{j\neq i}^{n}T_{ij}v_j+S_{ii}\hat{f}^{(-i)}(t_i)+\gamma T_{ii}\hat{f}'^{(-i)}(t_i)-y_i\\
=&\sum_{j=1}^{n}S_{ij}y_j+\gamma\sum_{j=1}^{n}T_{ij}v_j+S_{ii}\left(\hat{f}^{(-i)}(t_i)-y_i\right)+\gamma T_{ii}\left(\hat{f}'^{(-i)}(t_i)-v_i\right)-y_i\\
=&\left(\hat{f}(t_i)-y_i\right)+S_{ii}\left(\hat{f}^{(-i)}(t_i)-y_i\right)+\gamma T_{ii}\left(\hat{f}'^{(-i)}(t_i)-v_i\right).
\end{aligned}\tag{A.5.1}$$

Additionally,

$$\begin{aligned}
\hat{f}'^{(-i)}(t_i) - v_i &= \sum_{j=1}^{n} U_{ij} y_j^* + \gamma \sum_{j=1}^{n} V_{ij} v_j^* - v_i^* \\
&= \sum_{j\neq i}^{n} U_{ij} y_j + \gamma \sum_{j\neq i}^{n} V_{ij} v_j + U_{ii} \hat{f}^{(-i)}(t_i) + \gamma V_{ii} \hat{f}'^{(-i)}(t_i) - v_i \\
&= \sum_{j=1}^{n} U_{ij} y_j + \gamma \sum_{j=1}^{n} V_{ij} v_j + U_{ii} \left(\hat{f}^{(-i)}(t_i) - y_i \right) + \gamma V_{ii} \left(\hat{f}'^{(-i)}(t_i) - v_i \right) - v_i \\
&= \left(\hat{f}'(t_i) - v_i \right) + U_{ii} \left(\hat{f}^{(-i)}(t_i) - y_i \right) + \gamma V_{ii} \left(\hat{f}'^{(-i)}(t_i) - v_i \right).
\end{aligned} \tag{A.5.2}$$

Thus

$$\hat{f}'^{(-i)}(t_i) - v_i = \frac{\hat{f}'(t_i) - v_i}{1 - \gamma V_{ii}} + \frac{U_{ii} \left(\hat{f}^{(-i)}(t_i) - y_i \right)}{1 - \gamma V_{ii}}. \tag{A.5.3}$$

By substituting equation (A.5.3) to (A.5.1), we get

$$\hat{f}^{(-i)}(t_i) - y_i = \frac{\hat{f}(t_i) - y_i + \gamma \frac{T_{ii}}{1-\gamma V_{ii}} \left(\hat{f}'(t_i) - v_i \right)}{1 - S_{ii} - \gamma \frac{T_{ii}}{1-\gamma V_{ii}} U_{ii}}.$$

Consequently,

$$CV(\lambda, \gamma) = \frac{1}{n} \sum_{i=1}^{n} \left(\frac{\hat{f}(t_i) - y_i + \gamma \frac{T_{ii}}{1-\gamma V_{ii}} \left(\hat{f}'(t_i) - v_i \right)}{1 - S_{ii} - \gamma \frac{T_{ii}}{1-\gamma V_{ii}} U_{ii}} \right)^2.$$

□

A.6 Reconstructions at SNR=3

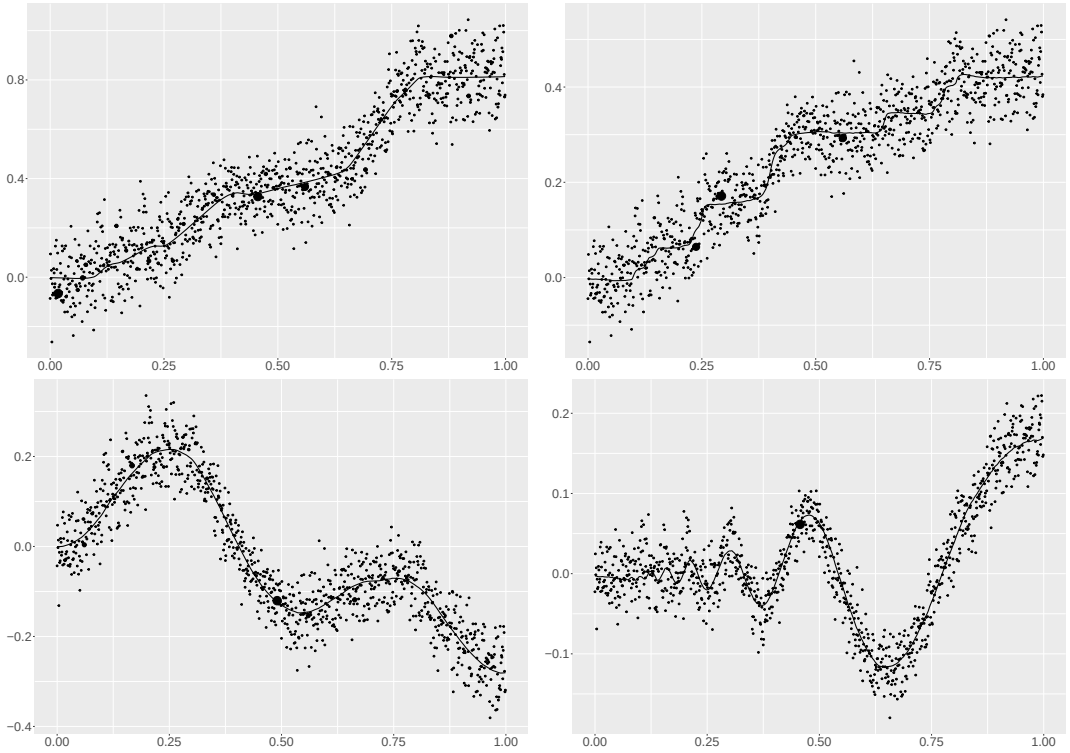

Figure A.1: Reconstructions of generated *Blocks*, *Bumps*, *HeaviSine* and *Doppler* functions by V-spline at SNR=3. The penalty values $\lambda(t)$ in V-spline are projected into reconstructions. The blacks dots are the measurements. The bigger blacks dots indicate the larger penalty values.

A.7 Residual Analysis of Simulations

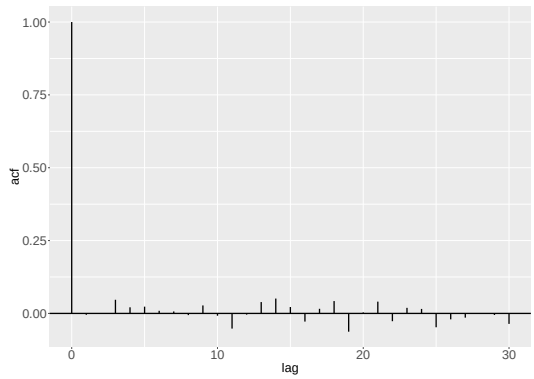

(a) ACF of residuals from *Blocks*

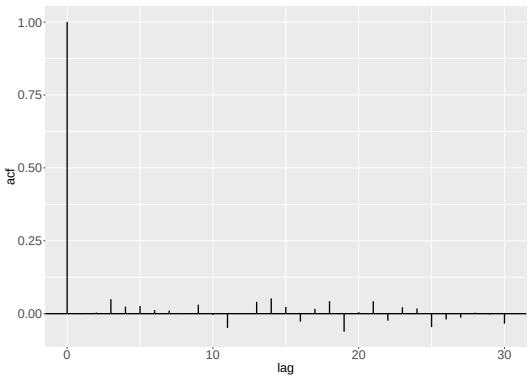

(b) ACF of residuals from *Bumps*

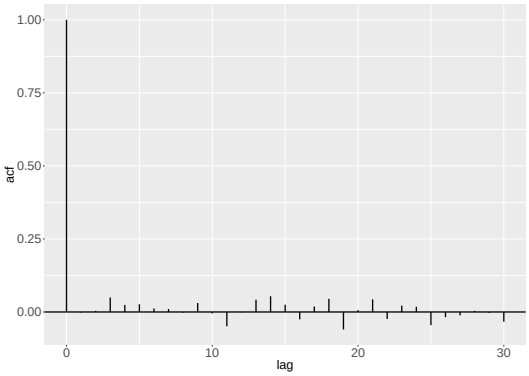

(c) ACF of residuals from *HeaviSine*

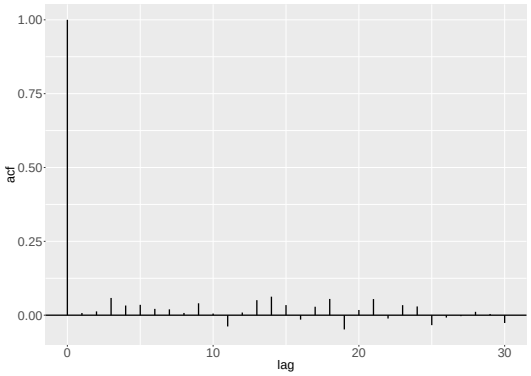

(d) ACF of residuals from *Doppler*

Figure A.2: ACF of residuals at SNR level of 7.

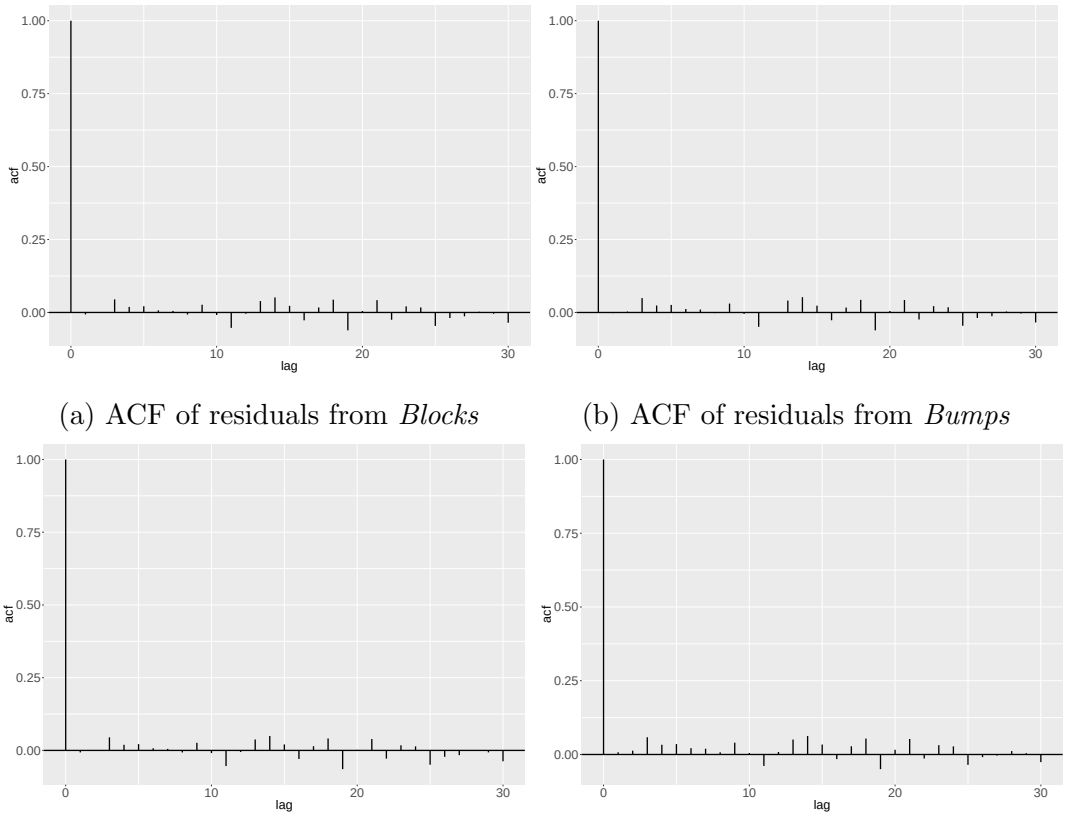

(a) ACF of residuals from *Blocks*

(b) ACF of residuals from *Bumps*

(c) ACF of residuals from *HeaviSine*

(d) ACF of residuals from *Doppler*

Figure A.3: ACF of residuals at SNR level of 3.

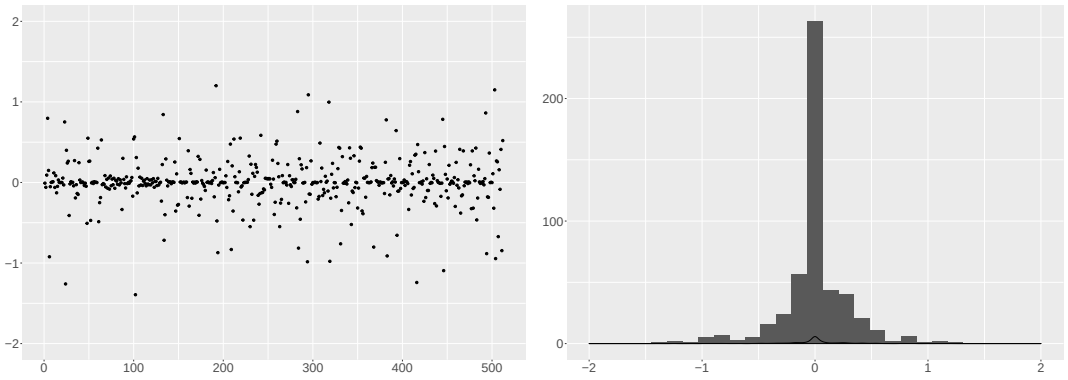

(a) residuals of x

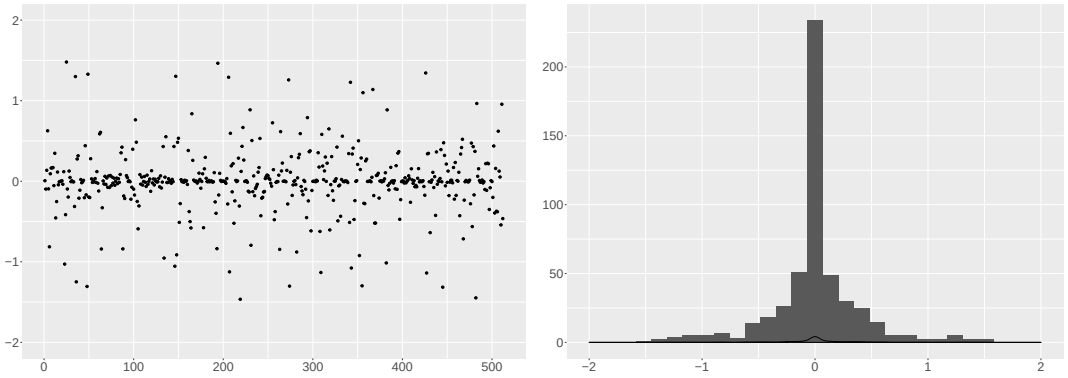

(b) residuals of y

Figure A.4: Residuals of 2-dimensional real data reconstruction

Appendix B

Calculations and Figures of Adaptive Sequential MCMC

B.1 Linear Simulation Calculations

The Forecast Distribution

Calculating the log-posterior of parameters requires finding out the forecast distribution of $p\left(y_{1:t} \mid y_{1:t-1}, \theta\right)$. A general way is to use the joint distribution of y_t and $y_{1:t-1}$, which is $p\left(y_{1:t} \mid \theta\right) = N\left(0, \Sigma_{YY}\right)$ and following the procedure in Section 5.2.2 to work out the inverse matrix of a multivariate normal distribution. For example, one may find the inverse of the covariance matrix

$$\Sigma_{YY}^{-1} = B\left(I_t - A_t^{-1} B_t\right) = \frac{1}{\sigma^4}\left(\sigma^2 I_t - A_t^{-1}\right) \triangleq \frac{1}{\sigma^4}\begin{bmatrix} Z_t & b_t \\ b_t^\top & K_t \end{bmatrix}.$$

Therefore the original form of this covariance is

$$\Sigma_{YY} = \sigma^4 \begin{bmatrix} \left(Z_t - b_t K_t^{-1} b_t^\top\right)^{-1} & -Z_t^{-1} b_t \left(K_t - b_t^\top Z_t^{-1} b_t\right)^{-1} \\ -K_t^{-1} b_t^\top \left(Z_t - b_t K_t^{-1} b_t^\top\right)^{-1} & \left(K_t - b_t^\top Z_t^{-1} b_t\right)^{-1} \end{bmatrix}.$$

For sake of simplicity, Z_t is a $t \times t$ matrix, b_t is a $t \times 1$ vector and K_t is a 1×1 constant number. By denoting $C_t^\top = \begin{bmatrix} 0 & \cdots & 0 & 1 \end{bmatrix}$, a $1 \times t$ vector, and post-multiplying Σ_{YY}^{-1}, it gives us

$$\Sigma_{YY}^{-1} C_t = \frac{1}{\sigma^4}\left(\sigma^2 I_t - A_t^{-1}\right) C_t = \frac{1}{\sigma^4}\begin{bmatrix} b_t \\ K_t \end{bmatrix}. \tag{B.1.1}$$

By using the formula, one can find a recursive way to update K_t and b_{t-1}, which

are

$$K_t = \frac{\sigma^4}{\tau^2 + \sigma^2 + \phi^2\left(\sigma^2 - K_{t-1}\right)}, \tag{B.1.2}$$

$$b_t = \begin{bmatrix} \frac{b_{t-1}\phi K_t}{\sigma^2} \\ \frac{K_t\left(\sigma^2+\tau^2\right)-\sigma^4}{\phi\sigma^2} \end{bmatrix}. \tag{B.1.3}$$

With the above formula, the recursive way of updating the mean and covariance are

$$\bar{\mu}_t = \frac{\phi}{\sigma^2} K_{t-1}\bar{\mu}_{t-1} + \phi\left(1 - \frac{K_{t-1}}{\sigma^2}\right) y_{t-1}, \tag{B.1.4}$$

$$\bar{\Sigma}_t = \sigma^4 K_t^{-1}, \tag{B.1.5}$$

where $K_1 = \frac{\sigma^4}{\sigma^2+L^2}$.

By using the formula again, one term of equation (5.55) becomes

$$A_t^{-1}C_t = \left(I - \frac{M_t^{-1}u_t u_t^\top}{1 + u_t^\top M_t^{-1} u_t}\right) M_t^{-1} C_t, \tag{B.1.6}$$

in which

$$M_t^{-1}C_t = \begin{bmatrix} A_{t-1}^{-1} & 0 \\ 0 & \sigma^2 \end{bmatrix} C_t = \sigma^2 C_t,$$

$$u_t^\top C_t = \begin{bmatrix} 0 & \cdots & 0 & \frac{-\phi}{\tau} & \frac{1}{\tau} \end{bmatrix} \begin{bmatrix} 0 \\ \vdots \\ 0 \\ 1 \end{bmatrix} = \frac{1}{\tau}.$$

Then the above equation becomes

$$A_t^{-1}C_t = \sigma^2 C_t - \frac{M_t^{-1}u_t\frac{\sigma^2}{\tau}}{1 + u^\top M_t^{-1} u}. \tag{B.1.7}$$

Moreover,

$$M_t^{-1}u_t = \begin{bmatrix} A_{t-1}^{-1} & 0 \\ 0 & \sigma^2 \end{bmatrix} \begin{bmatrix} 0 \\ \vdots \\ 0 \\ -\frac{\phi}{\tau} \\ \frac{1}{\tau} \end{bmatrix} = \begin{bmatrix} A_{t-1}^{-1} & 0 \\ 0 & \sigma^2 \end{bmatrix} \begin{bmatrix} -\frac{\phi}{\tau}C_{t-1} \\ \frac{1}{\tau} \end{bmatrix} = \begin{bmatrix} -\frac{\phi}{\tau}A_{t-1}^{-1}C_{t-1} \\ \frac{\sigma^2}{\tau} \end{bmatrix},$$

$$u^\top M_t^{-1}u = \begin{bmatrix} 0 & \cdots & 0 & -\frac{\phi}{\tau} & \frac{1}{\tau} \end{bmatrix} \begin{bmatrix} -\frac{\phi}{\tau}A_{t-1}^{-1}C_{t-1} \\ \frac{\sigma^2}{\tau} \end{bmatrix} = \begin{bmatrix} -\frac{\phi}{\tau}C_{t-1}^\top & \frac{1}{\tau} \end{bmatrix} \begin{bmatrix} -\frac{\phi}{\tau}A_{t-1}^{-1}C_{t-1} \\ \frac{\sigma^2}{\tau} \end{bmatrix}$$

$$= \frac{\phi^2}{\tau^2} C_{t-1}^\top A_{t-1}^{-1} C_{t-1} + \frac{\sigma^2}{\tau^2}.$$

Thus

$$A_t^{-1}C_t = \begin{bmatrix} -b_t \\ \sigma^2 - K_t \end{bmatrix} = \sigma^2 C_t - \frac{1}{1 + \frac{\phi^2}{\tau^2} C_{t-1}^\top A_{t-1}^{-1} C_{t-1} + \frac{\sigma^2}{\tau^2}} \begin{bmatrix} -\frac{\phi\sigma^2}{\tau^2} A_{t-1}^{-1} C_{t-1} \\ \frac{\sigma^4}{\tau^2} \end{bmatrix}$$
$$= \sigma^2 C_t - \frac{1}{\tau^2 + \phi^2 C_{t-1}^\top A_{t-1}^{-1} C_{t-1} + \sigma^2} \begin{bmatrix} -\phi\sigma^2 A_{t-1}^{-1} C_{t-1} \\ \sigma^4 \end{bmatrix} \tag{B.1.8}$$

and

$$\sigma^2 - K_t = \sigma^2 - \frac{\sigma^4}{\tau^2 + \phi^2 C_{t-1}^\top A_{t-1}^{-1} C_{t-1} + \sigma^2}$$
$$= \sigma^2 - \frac{\sigma^4}{\tau^2 + \sigma^2 + \phi^2 \left(\sigma^2 - K_{t-1}\right)}.$$

Hence,

$$K_t = \frac{\sigma^4}{\tau^2 + \sigma^2 + \phi^2 \left(\sigma^2 - K_{t-1}\right)}, \tag{B.1.9}$$

and

$$b_t = \begin{bmatrix} \frac{b_{t-1}\phi K_t}{\sigma^2} \\ \frac{K_t\left(\sigma^2+\tau^2\right) - \sigma^4}{\phi\sigma^2} \end{bmatrix},$$

$$\begin{aligned}
\bar{\mu}_t &= 0 - \sigma^4 K_t^{-1} b_t^\top \left(Z_t - b_t K_t^{-1} b_t^\top\right)^{-1} \sigma^{-4} \left(Z_t - b_t K_t^{-1} b_t^\top\right) y_{1:t-1} \\
&= -K_t^{-1} b_t^\top y_{1:t-1} \\
&= \frac{\phi}{\sigma^2} K_{t-1} \bar{\mu}_{t-1} + \phi \left(1 - \frac{K_{t-1}}{\sigma^2}\right) y_{t-1}, \\
\bar{\Sigma}_t &= \sigma^4 \left(K_t - b_t^\top Z_t^{-1} b_t\right)^{-1} \\
&\quad - \sigma^4 K_t^{-1} b_t^\top \left(Z_t - b_t K_t^{-1} b_t^\top\right)^{-1} \left(Z_t - b_t K_t^{-1} b_t^\top\right) Z_t^{-1} b_t \left(K_t - b_t^\top Z_t^{-1} b_t\right)^{-1} \\
&= \sigma^4 \left(I_t - K_t^{-1} b_t^\top Z_t^{-1} b_t\right) \left(K_t - b_t^\top Z_t^{-1} b_t\right)^{-1} \\
&= \sigma^4 K_t^{-1},
\end{aligned}$$

where $K_1 = \frac{\sigma^4}{\sigma^2 + L^2}$.

The Estimation Distribution

As discussed before, $p\left(x_t \mid y_{1:t}\right)$ is a mixture Gaussian distribution with given θ and its mean and variance can be found by

$$\mu_x^{(t)} = \frac{1}{N}\sum_i \mu_i \tag{B.1.10}$$

$$\begin{aligned}\mathrm{Var}[x^{(t)}] &= \mathrm{E}[\mathrm{Var}\left(x \mid y, \theta\right)] + \mathrm{Var}[\mathrm{E}\left(x \mid y, \theta\right)] \\ &= \frac{1}{N}\sum_i \left(\mu_i\mu_i^\top + \Sigma_i\right) - \frac{1}{N^2}\left(\sum_i \mu_i\right)\left(\sum_i \mu_i\right)^\top .\end{aligned} \tag{B.1.11}$$

To find μ_i and Σ_i, we will use the joint distribution of x_t and $y_{1:t}$, which is $p\left(x_t, y_{1:t} \mid \theta\right) = N\left(0, \Gamma\right)$ and

$$\Gamma = \begin{bmatrix} C_t^\top \left(A_t - B_t\right)^{-1} C_t & C_t^\top \left(A_t - B_t\right)^{-1} \\ \left(A_t - B_t\right)^{-1} C_t & \left(I_t - A_t^{-1}B_t\right)^{-1} B_t^{-1} \end{bmatrix}.$$

Because of

$$C_t^\top A_t^{-1} = \begin{bmatrix} -b_t^\top & \sigma^2 - K_t \end{bmatrix},$$

thus, for any given θ_i, $x_t \mid y_{1:t}, \theta_i \sim N\left(\mu_t^{(x)}, \sigma_t^{(x)2}\right)$, where

$$\begin{aligned}\mu_i &= \phi x_{t-1} + C_t^\top \left(A_t - B_t\right)^{-1} B_t \left(I_t - A_t^{-1}B_t\right) y_{1:t} \\ &= \phi x_{t-1} + C_t^\top A_t^{-1} B_t y_{1:t} \\ &= \phi x_{t-1} + \frac{1}{\sigma^2} C_t^\top A_t^{-1} y_{1:t} \\ &= 0 + \frac{1}{\sigma^2}\begin{bmatrix} -b_t^\top & \sigma^2 - K_t \end{bmatrix}\begin{bmatrix} y_{1:t-1} \\ y_t \end{bmatrix} \\ &= -\frac{1}{\sigma^2} b_{t-1}^\top y_{1:t-1} + \left(1 - \frac{K_t}{\sigma^2}\right) y_t \\ &= \frac{K_t \bar{\mu}_t}{\sigma^2} + \left(1 - \frac{K_t}{\sigma^2}\right) y_t \\ \Sigma_i &= C_t^\top \left(A_t - B_t\right)^{-1} C_t - C_t^\top \left(A_t - B_t\right)^{-1} B_t \left(I_t - A_t^{-1}B_t\right)\left(A_t - B_t\right)^{-1} C_t \\ &= C_t^\top \left(A_t - B_t\right)^{-1} C_t - C_t^\top A_t^{-1} B_t \left(A_t - B_t\right)^{-1} C_t \\ &= C_t^\top A_t^{-1} C_t \\ &= \sigma^2 - K_t.\end{aligned}$$

By substituting them into the equation (5.27) and (5.28), the estimated x_t is obtained.

B.2 OU-Process Calculation

The Forecast Distribution

We are now using the capital letter Y to represent the joint $\{y, v\}$ and $Y_{1:t} = \{y_1, v_1, y_2, v_2, \cdots, y_t, v_t\}$, $Y_{t+1} = \{y_{t+1}, v_{t+1}\}$. It is known that

$$\begin{aligned} p\left(Y_{1:t}, \theta\right) &= N\left(0, \Sigma_{YY}^{(t)}\right) \\ p\left(Y_{t+1}, Y_{1:t}, \theta\right) &= N\left(0, \Sigma_{YY}^{(t+1)}\right) \\ p\left(Y_{t+1} \mid Y_{1:t}, \theta\right) &= N\left(\bar{\mu}_{t+1}, \bar{\Sigma}_{t+1}\right) \end{aligned}$$

where the covariance matrix of the joint distribution is $\Sigma_{YY}^{(t+1)} = \left(I_{t+1} - A_{t+1}^{-1} B_{t+1}\right)^{-1} B_{t+1}^{-1}$. Then, by taking its inverse, we will get

$$\Sigma_{YY}^{(t+1)(-1)} = B_{t+1}\left(I_{t+1} - A_{t+1}^{-1} B_{t+1}\right).$$

To be clear, the matrix B_t is short for the matrix $B_t\left(\sigma^2, \tau^2\right)$, which is $2t \times 2t$ diagonal matrix with elements $\frac{1}{\sigma^2}, \frac{1}{\tau^2}$ repeating for t times on its diagonal. For instance, the very simple $B_1\left(\sigma^2, \tau^2\right) = \begin{bmatrix} \frac{1}{\sigma^2} & 0 \\ 0 & \frac{1}{\tau^2} \end{bmatrix}_{2\times 2}$ is a 2×2 matrix.

Because of A is symmetric and invertible, B is the diagonal matrix defined as above, then they have the following property

$$\begin{aligned} AB &= A^\top B^\top = (BA)^\top, \\ A^{-1}B &= A^{-\top} B^\top = \left(BA^{-1}\right)^\top. \end{aligned}$$

Followed up the form of $\Sigma_{YY}^{(t+1)(-1)}$, we can find out that

$$\begin{aligned} \Sigma_{YY}^{(t+1)(-1)} &= B_{t+1}\left(I_{t+1} - A_{t+1}^{-1} B_{t+1}\right) \\ &= B_{t+1}\left(B_{t+1}^{-1} - A_{t+1}^{-1}\right) B_{t+1} \\ &\triangleq \begin{bmatrix} B_t & 0 \\ 0 & B_1 \end{bmatrix} \begin{bmatrix} Z_{t+1} & b_{t+1} \\ b_{t+1}^\top & K_{t+1} \end{bmatrix} \begin{bmatrix} B_t & 0 \\ 0 & B_1 \end{bmatrix} \end{aligned}$$

where Z_{t+1} is a $2t \times 2t$ matrix, b_{t+1} is a $2t \times 2$ matrix and K_{t+1} is a 2×2 matrix. Thus by taking its inverse again, we will get

$$\Sigma_{YY}^{(t+1)} = \begin{bmatrix} B_t^{-1}\left(Z_{t+1} - b_{t+1} K_{t+1}^{-1} b_{t+1}^\top\right)^{-1} B_t^{-1} & -B_t^{-1} Z_{t+1}^{-1} b_{t+1}\left(K_{t+1} - b_{t+1}^\top Z_{t+1}^{-1} b_{t+1}\right)^{-1} B_1^{-1} \\ -B_1^{-1} K_{t+1}^{-1} b_{t+1}^\top\left(Z_{t+1} - b_{t+1} K_{t+1}^{-1} b_{t+1}^\top\right)^{-1} B_t^{-1} & B_1^{-1}\left(K_{t+1} - b_{t+1}^\top Z_{t+1}^{-1} b_{t+1}\right)^{-1} B_1^{-1} \end{bmatrix}.$$

It is easy to find the relationship between A_{t+1} and A_t in the Sherman-Morrison-Woodbury form, which is

$$A_{t+1} = \begin{bmatrix} A_t & \cdot & \cdot \\ \cdot & \frac{1}{\sigma^2} & \cdot \\ \cdot & \cdot & \frac{1}{\tau^2} \end{bmatrix} + U_{t+1}U_{t+1}^\top \triangleq M_{t+1} + U_{t+1}U_{t+1}^\top,$$

where $M_{t+1} = \begin{bmatrix} A_t & \cdot & \cdot \\ \cdot & \frac{1}{\sigma^2} & \cdot \\ \cdot & \cdot & \frac{1}{\tau^2} \end{bmatrix} = \begin{bmatrix} A_t & 0 \\ 0 & B_1 \end{bmatrix}$ and its inverse is $M_{t+1}^{-1} = \begin{bmatrix} A_t^{-1} & 0 \\ 0 & B_1^{-1} \end{bmatrix}$.
Additionallly, U is a $2t+2 \times 2$ matrix in the following form

$$U_{t+1} = \frac{1}{\sqrt{1-\rho_{t+1}^2}} \begin{bmatrix} \mathbf{0}_{2t-2} & \mathbf{0}_{2t-2} \\ \frac{1}{\sigma_{t+1}^{(x)}} & 0 \\ \frac{1-e^{-\gamma\Delta_{t+1}}}{\gamma\sigma_{t+1}^{(x)}} - \frac{\rho_{t+1}e^{-\gamma\Delta_{t+1}}}{\sigma_{t+1}^{(u)}} & \frac{\sqrt{1-\rho_{t+1}^2}e^{-\gamma\Delta_{t+1}}}{\sigma_{t+1}^{(u)}} \\ -\frac{1}{\sigma_{t+1}^{(x)}} & 0 \\ \frac{\rho_{t+1}}{\sigma_{t+1}^{(u)}} & -\frac{\sqrt{1-\rho_{t+1}^2}}{\sigma_{t+1}^{(u)}} \end{bmatrix} \triangleq \begin{bmatrix} C_t S_{t+1} \\ D_{t+1} \end{bmatrix},$$

where $S_{t+1} = \frac{1}{\sqrt{1-\rho_{t+1}^2}} \begin{bmatrix} \frac{1}{\sigma_{t+1}^{(x)}} & 0 \\ \frac{1-e^{-\gamma\Delta_{t+1}}}{\gamma\sigma_{t+1}^{(x)}} - \frac{\rho_{t+1}e^{-\gamma\Delta_{t+1}}}{\sigma_{t+1}^{(u)}} & \frac{\sqrt{1-\rho_{t+1}^2}e^{-\gamma\Delta_{t+1}}}{\sigma_{t+1}^{(u)}} \end{bmatrix}$,

$D_{t+1} = \frac{1}{\sqrt{1-\rho_{t+1}^2}} \begin{bmatrix} -\frac{1}{\sigma_{t+1}^{(x)}} & 0 \\ \frac{\rho_{t+1}}{\sigma_{t+1}^{(u)}} & -\frac{\sqrt{1-\rho_{t+1}^2}}{\sigma_{t+1}^{(u)}} \end{bmatrix}$ and $C_{t+1} = \begin{bmatrix} 0 & 0 \\ \vdots & \vdots \\ 0 & 0 \\ 1 & 0 \\ 0 & 1 \end{bmatrix} = \begin{bmatrix} \mathbf{0}_t \\ I_2 \end{bmatrix}$.

By post-multiplying $\Sigma_{YY}^{(t+1)(-1)}$ with C_{t+1}, it gives us

$$\begin{aligned} \Sigma_{YY}^{(t+1)(-1)} C_{t+1} &= B_{t+1}\left(I_{t+1} - A_{t+1}^{-1}B_{t+1}\right)C_{t+1} \\ &= \begin{bmatrix} B_t & 0 \\ 0 & B_1 \end{bmatrix} \left(\begin{bmatrix} B_t^{-1} & 0 \\ 0 & B_1^{-1} \end{bmatrix} - A_{t+1}^{-1} \right) \begin{bmatrix} B_t & 0 \\ 0 & B_1 \end{bmatrix} C_{t+1} \\ &= \begin{bmatrix} B_t & 0 \\ 0 & B_1 \end{bmatrix} \begin{bmatrix} Z_{t+1} & b_{t+1} \\ b_{t+1}^\top & K_{t+1} \end{bmatrix} \begin{bmatrix} B_t & 0 \\ 0 & B_1 \end{bmatrix} C_{t+1} \\ &= \begin{bmatrix} B_t & 0 \\ 0 & B_1 \end{bmatrix} \begin{bmatrix} b_{t+1}B_1 \\ K_{t+1}B_1 \end{bmatrix}. \end{aligned}$$

and the property of A_{t+1}^{-1} is

$$A_{t+1}^{-1}C_{t+1} = \begin{bmatrix} -b_{t+1} \\ B_1^{-1} - K_{t+1} \end{bmatrix}.$$

Moreover, by pre-multiplying $C_{t+1}^\top$ on the left side of the above equation, we will have

$$C_{t+1}^\top A_{t+1}^{-1} C_{t+1} = B_1^{-1} - K_{t+1}, \tag{B.2.1}$$

$$K_{t+1} = B_1^{-1} - C_{t+1}^\top A_{t+1}^{-1} C_{t+1}. \tag{B.2.2}$$

We may use Sherman-Morrison-Woodbury formula to find the inverse of A_{t+1} in a recursive way, which is

$$A_{t+1}^{-1} = \left(M_{t+1} + U_{t+1}U_{t+1}^\top\right)^{-1} = M_{t+1}^{-1} - M_{t+1}^{-1}U_{t+1}\left(I + U_{t+1}^\top M_{t+1}^{-1}U_{t+1}\right)^{-1}U_{t+1}^\top M_{t+1}^{-1}. \tag{B.2.3}$$

Consequently, it is easy to find that $M_{t+1}^{-1}C_{t+1} = \begin{bmatrix} 0 \\ B_1^{-1} \end{bmatrix}$ and

$$\begin{aligned}
A_{t+1}^{-1}C_{t+1} &= \begin{bmatrix} 0 \\ B_1^{-1} \end{bmatrix} - \begin{bmatrix} A_t^{-1} & 0 \\ 0 & B_1^{-1} \end{bmatrix} \begin{bmatrix} C_t S_{t+1} \\ D_{t+1} \end{bmatrix} \left(I + U_{t+1}^\top M_{t+1}^{-1} U_{t+1}\right)^{-1} \begin{bmatrix} S_{t+1}^\top C_t^\top & D_{t+1}^\top \end{bmatrix} \begin{bmatrix} 0 \\ B_1^{-1} \end{bmatrix} \\
&= \begin{bmatrix} 0 \\ B_1^{-1} \end{bmatrix} - \begin{bmatrix} A_t^{-1}C_t S_{t+1} \\ B_1^{-1} D_{t+1} \end{bmatrix} \left(I + U_{t+1}^\top M_{t+1}^{-1} U_{t+1}\right)^{-1} D_{t+1}^\top B_1^{-1} \\
&= \begin{bmatrix} 0 \\ B_1^{-1} \end{bmatrix} - \begin{bmatrix} A_t^{-1}C_t S_{t+1} \\ B_1^{-1} D_{t+1} \end{bmatrix} \left(I + S_{t+1}^\top C_t^\top A_t^{-1} C_t S_{t+1} + D_{t+1}^\top B_1^{-1} D_{t+1}\right)^{-1} D_{t+1}^\top B_1^{-1} \\
&= \begin{bmatrix} 0 \\ B_1^{-1} \end{bmatrix} - \begin{bmatrix} A_t^{-1}C_t S_{t+1} \\ B_1^{-1} D_{t+1} \end{bmatrix} \left(I + S_{t+1}^\top \left(B_1^{-1} - K_t\right) S_{t+1} + D_{t+1}^\top B_1^{-1} D_{t+1}\right)^{-1} D_{t+1}^\top B_1^{-1}.
\end{aligned}$$

Thus, by using the equation (B.2.2), we will get

$$K_{t+1} = B_1^{-1} D_{t+1} \left(I + S_{t+1}^\top \left(B_1^{-1} - K_t\right) S_{t+1} + D_{t+1}^\top B_1^{-1} D_{t+1}\right)^{-1} D_{t+1}^\top B_1^{-1}, \tag{B.2.4}$$

and

$$\begin{aligned}
b_{t+1} &= A_t^{-1} C_t S_{t+1} \left(I + S_{t+1}^\top \left(B_1^{-1} - K_t\right) S_{t+1} + D_{t+1}^\top B_1^{-1} D_{t+1}\right)^{-1} D_{t+1}^\top B_1^{-1} \\
&= \begin{bmatrix} -b_t \\ B_1^{-1} - K_t \end{bmatrix} S_{t+1} \left(I + S_{t+1}^\top \left(B_1^{-1} - K_t\right) S_{t+1} + D_{t+1}^\top B_1^{-1} D_{t+1}\right)^{-1} D_{t+1}^\top B_1^{-1}.
\end{aligned}$$

To achieve the recursive updating formula, we need to find the form of $b_{t+1}^\top B_t Y_{1:t}$ first.

In fact, it is

$$
\begin{aligned}
b_{t+1}^{\top} B_t Y_{1:t} &= B_1^{-\top} D_{t+1} \left(I + S_{t+1}^{\top} \left(B_1^{-1} - K_t\right) S_{t+1} + D_{t+1}^{\top} B_1^{-1} D_{t+1}\right)^{-\top} S_{t+1}^{\top} \begin{bmatrix} -b_t^{\top} & B_1^{-1} - K_t \end{bmatrix} B_t \begin{bmatrix} Y_{1:t-1} \\ Y_t \end{bmatrix} \\
&= B_1^{-\top} D_{t+1} \left(I + S_{t+1}^{\top} \left(B_1^{-1} - K_t\right) S_{t+1} + D_{t+1}^{\top} B_1^{-1} D_{t+1}\right)^{-\top} S_{t+1}^{\top} \\
&\left(-b_t^{\top} B_{t-1} Y_{1:t-1} + \left(B_1^{-1} - K_t\right) B_1 Y_t\right) \\
&= B_1^{-\top} D_{t+1} \left(I + S_{t+1}^{\top} \left(B_1^{-1} - K_t\right) S_{t+1} + D_{t+1}^{\top} B_1^{-1} D_{t+1}\right)^{-\top} S_{t+1}^{\top} \left(K_t B_1 \bar{\mu}_t + \left(I - K_t B_1\right) Y_t\right).
\end{aligned}
$$

By using equation (B.2.4) and simplifying the above equation, one can achieve a recursive updating form of the mean, which is

$$
\begin{aligned}
\bar{\mu}_{t+1} &= -B_1 K_{t+1}^{-1} b_{t+1}^{\top} B_t Y_{1:t} \\
&= -D_{t+1}^{-\top} S_{t+1}^{\top} \left(K_t B_1 \bar{\mu}_t + \left(I - K_t B_1\right) Y_t\right) \\
&= -D_{t+1}^{-\top} S_{t+1}^{\top} \left(Y_t + K_t B_1 \left(\bar{\mu}_t - Y_t\right)\right),
\end{aligned}
$$

where by simplifying $D_{t+1}^{-\top} S_{t+1}^{\top}$, one may find

$$
D_{t+1}^{-\top} S_{t+1}^{\top} = \begin{bmatrix} -1 & -\frac{1-e^{-\gamma \Delta_{t+1}}}{\gamma} \\ 0 & -e^{-\gamma \Delta_{t+1}} \end{bmatrix} = -\Phi_{t+1},
$$

which is the negative of forward process. Then the final form of recursive updating formula are

$$
\begin{cases} \bar{\mu}_{t+1} = \Phi_{t+1} K_t B_1 \bar{\mu}_t + \Phi_{t+1} \left(I - K_t B_1\right) Y_t \\ \bar{\Sigma}_{t+1} = \left(B_1 K_{t+1} B_1\right)^{-1} \end{cases}. \tag{B.2.5}
$$

The matrix K_{t+1} is updated via

$$
K_{t+1} = B_1^{-1} D_{t+1} \left(I + S_{t+1}^{\top} \left(B_1^{-1} - K_t\right) S_{t+1} + D_{t+1}^{\top} B_1^{-1} D_{t+1}\right)^{-1} D_{t+1}^{\top} B_1^{-1}, \tag{B.2.6}
$$

or updating its inverse in the following form makes the computation faster, that is

$$
\begin{cases} K_{t+1}^{-1} = B_1 D_{t+1}^{-\top} D_{t+1}^{-1} B_1 + B_1 \Phi_{t+1} \left(B_1^{-1} - K_t\right) \Phi_{t+1}^{\top} B_1 + B_1, \\ \bar{\Sigma}_{t+1} = D_{t+1}^{-\top} D_{t+1}^{-1} + \Phi_{t+1} \left(B_1^{-1} - K_t\right) \Phi_{t+1}^{\top} + B_1^{-1} \end{cases}
$$

and $K_1 = B_1^{-1} - A_1^{-1} = \begin{bmatrix} \frac{\sigma^4}{\sigma^2 + L_x^2} & 0 \\ 0 & \frac{\tau^4}{\tau^2 + L_u^2} \end{bmatrix}$.

The Estimation Distribution

Because of the joint distribution (5.84), one can find the best estimation with a given θ by

$$\begin{aligned} X_t \mid Y_{1:t}, \theta &\sim N\left(A_t^{-1} B_t Y_{1:t}, A_t^{-1}\right) \\ &\sim N\left(L_t^{-\top} L_t^{-1} B_t Y_{1:t}, L_t^{-\top} L_t^{-1}\right) \\ &\sim N\left(L_t^{-\top} W_t, L_t^{-\top} L_t^{-1}\right). \end{aligned}$$

For X_{t+1}, the joint distribution with $Y_{1:t+1}$ updated to stage $t+1$ is

$$X_{t+1}, Y_{1:t+1} \mid \theta \sim N\left(0, \begin{bmatrix} C_{t+1}^{\top} \left(A_{t+1} - B_{t+1}\right)^{-1} C_{t+1} & C_{t+1}^{\top} \left(A_{t+1} - B_{t+1}\right)^{-1} \\ \left(A_{t+1} - B_{t+1}\right)^{-1} C_{t+1} & \left(I - A_{t+1}^{-1} B_{t+1}\right)^{-1} B_{t+1}^{-1} \end{bmatrix}\right),$$

where $C_{t+1}^{\top} = \begin{bmatrix} 0 & \cdots & 0 & 1 & 0 \\ 0 & \cdots & 0 & 0 & 1 \end{bmatrix}$ is a $2 \times 2\,(t+1)$ matrix. Thus

$$X_{t+1} \mid Y_{1:t+1}, \theta \sim N\left(\bar{\mu}_{t+1}^{(X)}, \bar{\Sigma}_{t+1}^{(X)}\right),$$

where

$$\begin{aligned} \bar{\mu}_{t+1}^{(X)} &= C_{t+1}^{\top} A_{t+1}^{-1} B_{t+1} Y_{1:t+1} = C_{t+1}^{\top} L_{t+1}^{-\top} W_{t+1}, \\ \bar{\Sigma}_{t+1}^{(X)} &= C_{t+1}^{\top} A_{t+1}^{-1} C_{t+1} = U_{t+1}^{\top} U_{t+1}, \end{aligned}$$

and $U_{t+1} = L_{t+1}^{-1} C_{t+1}$.

The filtering distribution of the state with given parameters is $p\left(X_{t+1} \mid Y_{1:t+1}, \theta\right)$. To find its form, one can use the joint distribution of X_{t+1} and $Y_{1:t+1}$, which is $p\left(X_{t+1}, Y_{1:t+1} \mid \theta\right) = N\left(0, \Gamma\right)$, where

$$\Gamma = \begin{bmatrix} C_{t+1}^{\top} \left(A_{t+1} - B_{t+1}\right)^{-1} C_{t+1} & C_{t+1}^{\top} \left(A_{t+1} - B_{t+1}\right)^{-1} \\ \left(A_{t+1} - B_{t+1}\right)^{-1} C_{t+1} & \left(I - A_{t+1}^{-1} B_{t+1}\right)^{-1} B_{t+1}^{-1} \end{bmatrix}.$$

Because of

$$C_{t+1}^{\top} A_{t+1}^{-1} = \begin{bmatrix} -b_{t+1}^{\top} & B_1^{-1} - K_{t+1} \end{bmatrix},$$

then $X_{t+1} \mid Y_{1:t+1}, \theta \sim N\left(\bar{\mu}_{t+1}^{(X)}, \bar{\sigma}_{t+1}^{(X)2}\right)$, where

$$\begin{aligned}
\bar{\mu}_{t+1}^{(X)} &= \Phi\hat{x}_t + C_{t+1}^{\top}\left(A_{t+1} - B_{t+1}\right)^{-1} B_{t+1}\left(I - A_{t+1}^{-1}B_{t+1}\right) Y_{1:t+1} \\
&= \Phi\hat{x}_t + C_{t+1}^{\top}A_{t+1}^{-1}B_{t+1}Y_{1:t+1} \\
&= 0 + \begin{bmatrix} -b_{t+1}^{\top} & B_1^{-1} - K_{t+1} \end{bmatrix} \begin{bmatrix} B_{t+1} & 0 \\ 0 & B_1 \end{bmatrix} \begin{bmatrix} Y_{1:t} \\ Y_{y+1} \end{bmatrix} \\
&= -b^{\top}B_{t+1}Y_{1:t} + \left(I - B_1K_{t+1}\right) Y_{t+1} \\
&= K_{t+1}B_1\bar{\mu}_{t+1} + \left(I - B_1K_{t+1}\right) Y_{t+1} \\
\bar{\sigma}_{t+1}^{(X)2} &= C_{t+1}^{\top}\left(A_{t+1} - B_{t+1}\right)^{-1} C_{t+1} - C_{t+1}^{\top}A_{t+1}^{-1}B_{t+1}\left(A_{t+1} - B_{t+1}\right)^{-1} C_{t+1} \\
&= C_{t+1}^{\top}A_{t+1}^{-1}C_{t+1} \\
&= B_1^{-1} - K_{t+1}.
\end{aligned}$$

B.3 Covariance Matrix in Details

$$\begin{aligned}
\Sigma_t &= \begin{bmatrix} \sigma_t^{(x)2} & \rho_t\sigma_t^{(x)}\sigma_t^{(u)} \\ \rho_t\sigma_t^{(x)}\sigma_t^{(u)} & \sigma_t^{(u)2} \end{bmatrix} \\
\Sigma_t^{-1} &= \frac{1}{1-\rho_t^2} \begin{bmatrix} \frac{1}{\sigma_t^{(x)2}} & -\frac{\rho_t}{\sigma_t^{(x)}\sigma_t^{(u)}} \\ -\frac{\rho_t}{\sigma_t^{(x)}\sigma_t^{(u)}} & \frac{1}{\sigma_t^{(u)2}} \end{bmatrix} \\
M_t^{\top} &= \begin{bmatrix} 1 & 0 \\ \frac{1-e^{-\gamma\Delta_t}}{\gamma} & e^{-\gamma\Delta_t} \end{bmatrix} \\
z_t &= \begin{bmatrix} x_t \\ u_t \end{bmatrix}
\end{aligned}$$

$$M_t^{\top}\Sigma_t^{-1} = \frac{1}{1-\rho_t^2} \begin{bmatrix} \frac{1}{\sigma_t^{(x)2}} & -\frac{\rho_t}{\sigma_t^{(x)}\sigma_t^{(u)}} \\ \frac{1-e^{-\gamma\Delta_t}}{\gamma\sigma_t^{(x)2}} - \frac{\rho_t e^{-\gamma\Delta_t}}{\sigma_t^{(x)}\sigma_t^{(u)}} & -\frac{\rho_t\left(1-e^{-\gamma\Delta_t}\right)}{\gamma\sigma_t^{(x)}\sigma_t^{(u)}} + \frac{e^{-\gamma\Delta_t}}{\sigma_t^{(u)2}} \end{bmatrix}$$

$$M_t^{\top}\Sigma_t^{-1}M_t = \frac{1}{1-\rho_t^2} \begin{bmatrix} \frac{1}{\sigma_t^{(x)2}} & \frac{1-e^{-\gamma\Delta_t}}{\gamma\sigma_t^{(x)2}} - \frac{\rho_t e^{-\gamma\Delta_t}}{\sigma_t^{(x)}\sigma_t^{(u)}} \\ \frac{1-e^{-\gamma\Delta_t}}{\gamma\sigma_t^{(x)2}} - \frac{\rho_t e^{-\gamma\Delta_t}}{\sigma_t^{(x)}\sigma_t^{(u)}} & \frac{\left(1-e^{-\gamma\Delta_t}\right)^2}{\gamma^2\sigma_t^{(x)2}} - \frac{2\rho_t e^{-\gamma\Delta_t}\left(1-e^{-\gamma\Delta_t}\right)}{\gamma\sigma_t^{(x)}\sigma_t^{(u)}} + \frac{e^{-2\gamma\Delta_t}}{\sigma_t^{(u)2}} \end{bmatrix}$$

$$\Sigma_4^{(X)-1} = \frac{1}{1-\rho_t^2}\begin{bmatrix}
\frac{1-\rho_t^2}{L_x^2}+\frac{1}{\sigma_2^{(x)2}} & -\frac{1}{\sigma_2^{(x)2}} & 0 & 0 & \frac{1-e^{-\gamma\Delta_2}}{\gamma\sigma_2^{(x)2}}-\frac{\rho_t e^{-\gamma\Delta_2}}{\sigma_2^{(x)}\sigma_2^{(u)}} & \frac{\rho_t}{\sigma_2^{(x)}\sigma_2^{(u)}} & 0 & 0\\
-\frac{1}{\sigma_2^{(x)2}} & \frac{1}{\sigma_2^{(x)2}}+\frac{1}{\sigma_3^{(x)2}} & -\frac{1}{\sigma_3^{(x)2}} & 0 & -\frac{1-e^{-\gamma\Delta_2}}{\gamma\sigma_2^{(x)2}}+\frac{\rho_t e^{-\gamma\Delta_2}}{\sigma_2^{(x)}\sigma_2^{(u)}} & \frac{1-e^{-\gamma\Delta_3}}{\gamma\sigma_3^{(x)2}}-\frac{\rho_t e^{-\gamma\Delta_3}}{\sigma_3^{(x)}\sigma_3^{(u)}}-\frac{\rho_t}{\sigma_2^{(x)}\sigma_2^{(u)}} & \frac{\rho_t}{\sigma_3^{(x)}\sigma_3^{(u)}} & 0\\
0 & -\frac{1}{\sigma_3^{(x)2}} & \frac{1}{\sigma_3^{(x)2}}+\frac{1}{\sigma_4^{(x)2}} & -\frac{1}{\sigma_4^{(x)2}} & 0 & -\frac{1-e^{-\gamma\Delta_3}}{\gamma\sigma_3^{(x)2}}+\frac{\rho_t e^{-\gamma\Delta_3}}{\sigma_3^{(x)}\sigma_3^{(u)}} & \frac{1-e^{-\gamma\Delta_4}}{\gamma\sigma_4^{(x)2}}-\frac{\rho_t e^{-\gamma\Delta_4}}{\sigma_4^{(x)}\sigma_4^{(u)}}-\frac{\rho_t}{\sigma_3^{(x)}\sigma_3^{(u)}} & \frac{\rho_t}{\sigma_4^{(x)}\sigma_4^{(u)}}\\
0 & 0 & -\frac{1}{\sigma_4^{(x)2}} & \frac{1}{\sigma_4^{(x)2}} & 0 & 0 & -\frac{1-e^{-\gamma\Delta_4}}{\gamma\sigma_4^{(x)2}}+\frac{\rho_t e^{-\gamma\Delta_4}}{\sigma_4^{(x)}\sigma_4^{(u)}} & -\frac{\rho_t}{\sigma_4^{(x)}\sigma_4^{(u)}}\\
\top & \top & 0 & 0 & \frac{1-\rho_t^2}{L_u^2}+C_2 & -\frac{e^{-\gamma\Delta_2}}{\sigma_2^{(u)2}}+\frac{\rho_t\left(1-e^{-\gamma\Delta_2}\right)}{\gamma\sigma_2^{(x)}\sigma_2^{(u)}} & 0 & 0\\
\top & \top & \top & 0 & -\frac{e^{-\gamma\Delta_2}}{\sigma_2^{(u)2}}+\frac{\rho_t\left(1-e^{-\gamma\Delta_2}\right)}{\gamma\sigma_2^{(x)}\sigma_2^{(u)}} & \frac{1}{\sigma_2^{(u)2}}+C_3 & -\frac{e^{-\gamma\Delta_3}}{\sigma_3^{(u)2}}+\frac{\rho_t\left(1-e^{-\gamma\Delta_3}\right)}{\gamma\sigma_3^{(x)2}\sigma_3^{(u)}} & 0\\
0 & \top & \top & \top & 0 & -\frac{e^{-\gamma\Delta_3}}{\sigma_3^{(u)2}}+\frac{\rho_t\left(1-e^{-\gamma\Delta_3}\right)}{\gamma\sigma_3^{(x)}\sigma_3^{(u)}} & \frac{1}{\sigma_3^{(u)2}}+C_4 & -\frac{e^{-\gamma\Delta_4}}{\sigma_4^{(u)2}}+\frac{\rho_t\left(1-e^{-\gamma\Delta_4}\right)}{\gamma\sigma_4^{(x)}\sigma_4^{(u)}}\\
0 & 0 & \top & \top & 0 & 0 & -\frac{e^{-\gamma\Delta_4}}{\sigma_4^{(u)2}}+\frac{\rho_t\left(1-e^{-\gamma\Delta_4}\right)}{\gamma\sigma_4^{(x)}\sigma_4^{(u)}} & \frac{1}{\sigma_4^{(u)2}}
\end{bmatrix}$$

where $C_t = \frac{\left(1-e^{-\gamma\Delta_t}\right)^2}{\gamma^2\sigma_t^{(x)2}} + \frac{e^{-2\gamma\Delta_t}}{\sigma_t^{(u)2}} - \frac{2\rho_t e^{-\gamma\Delta_t}\left(1-e^{-\gamma\Delta_t}\right)}{\gamma\sigma_t^{(x)}\sigma_t^{(u)}}$, $\Delta_t = T_t - T_{t-1}$. Symbol $\top$ indicates the transpose term in the matrix.

B.4 Real Data Implementation

Efficiency Plots

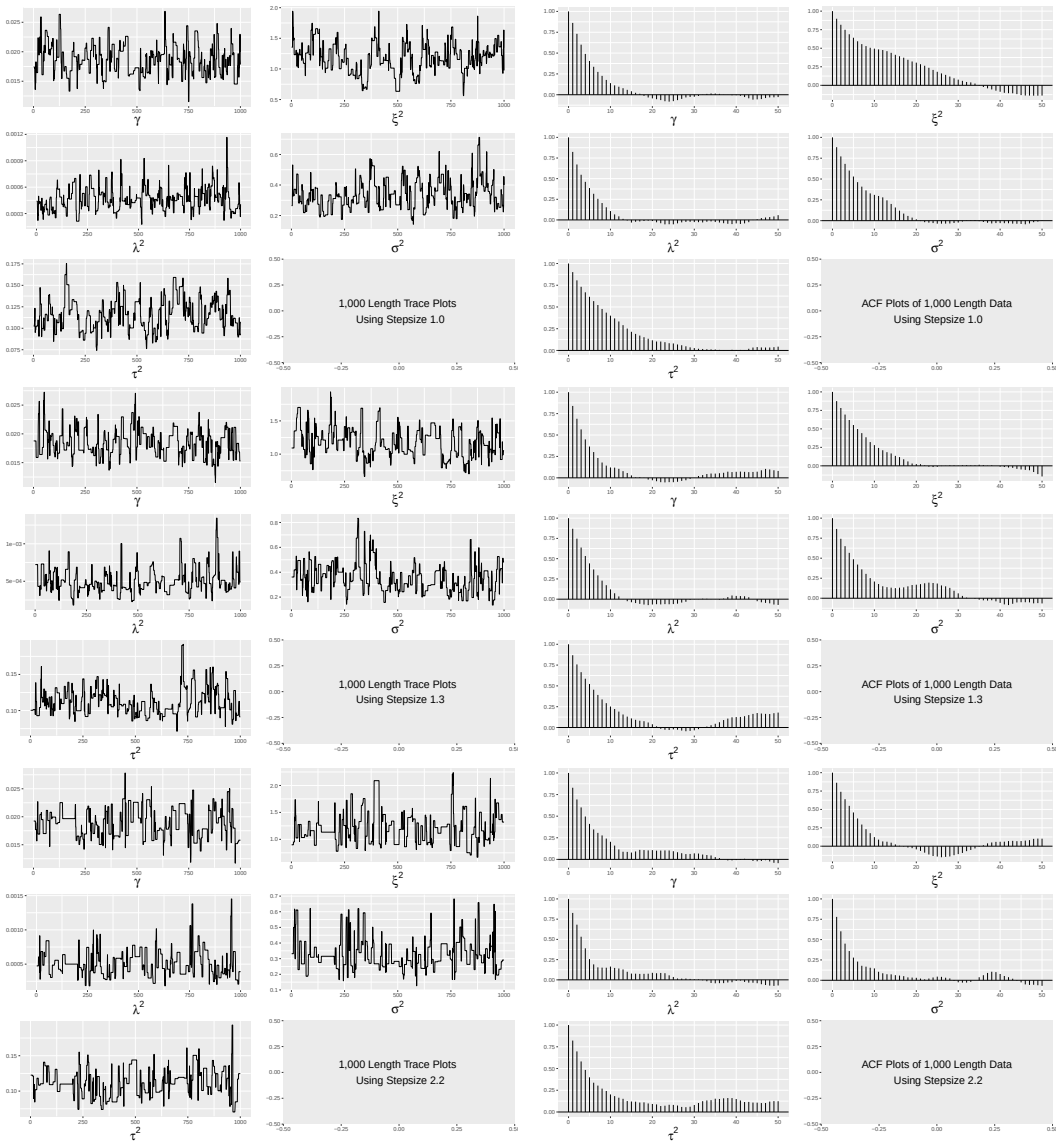

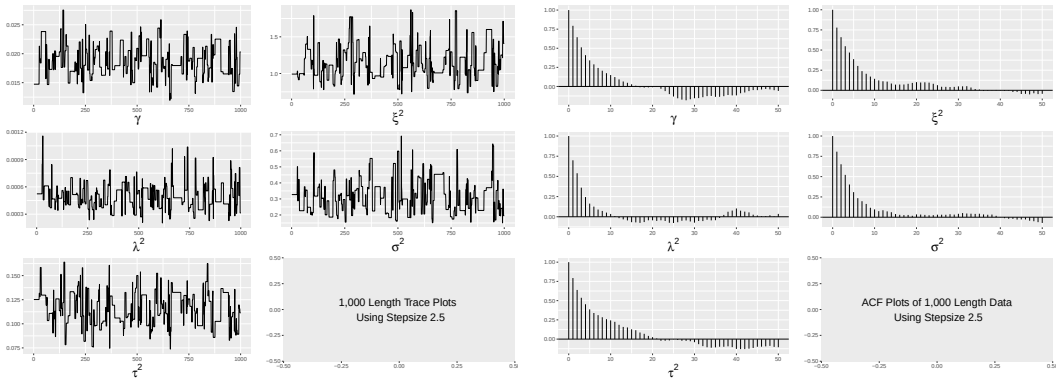

Figure B.1: Running the same amount of time and taking the same length of data, the step size $\epsilon = 2.5$ returns the highest ESSUT value and generates more effective samples in a lower correlated relationship.

Comparing Estimation with Different Length of Data

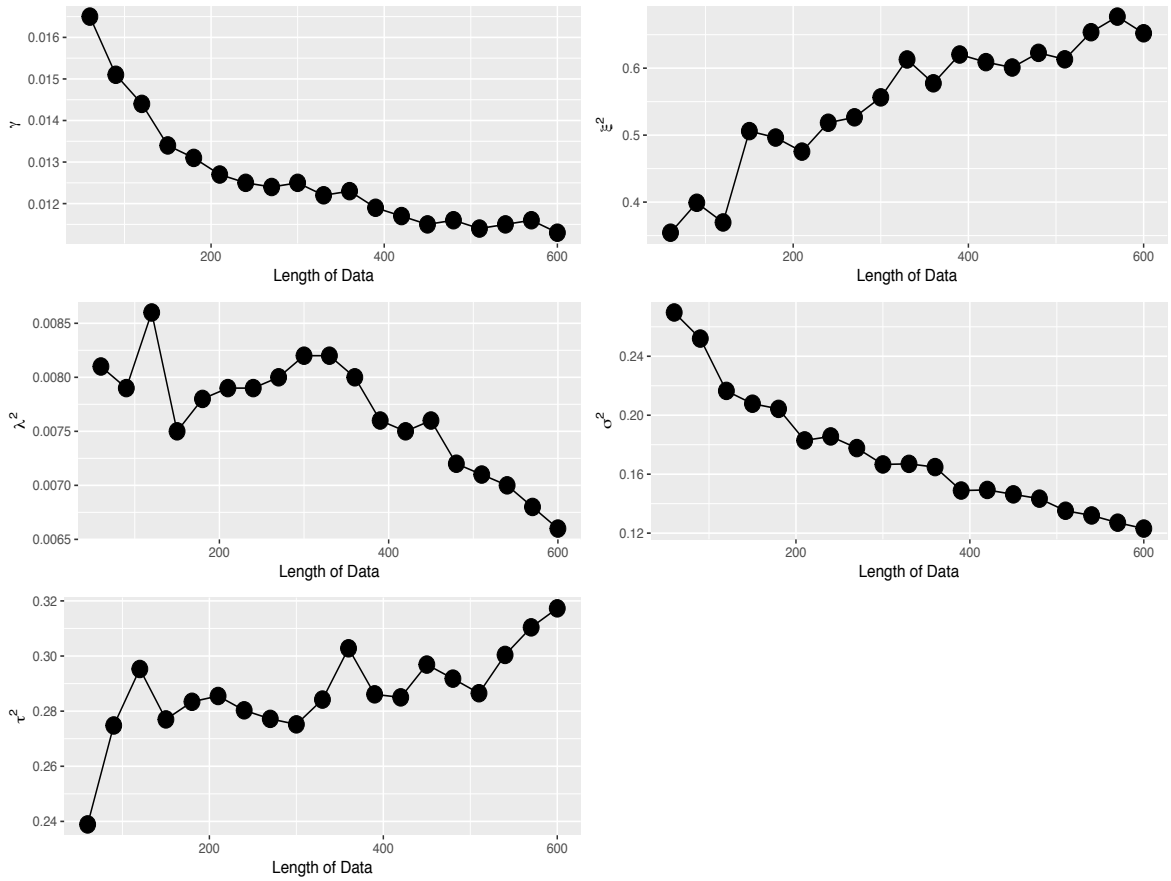

Figure B.2: Impacts of data length on optimal parameter. There is an obvious trend on the estimation against length of data in the estimation process.

Table B.1: Parameter estimation by running the whole surface learning and DA MH processes with different length of data

Length	**Time**	γ	ξ^2	λ^2	σ^2	τ^2	α_1	α_2	x	u	y	v
Obs	-	-	-	-	-	-	-	-	-339.0569	0.0413	-100.2065	1.1825
600	85.96	0.0113	0.6521	0.0066	0.1231	0.3173	0.0536	0.7873	-339.0868	0.4331	-100.1498	-0.7498
570	85.72	0.0116	0.6770	0.0068	0.1271	0.3104	0.0542	0.7638	-339.0872	0.4292	-100.1476	-0.7356
540	84.25	0.0115	0.6537	0.0070	0.1320	0.3004	0.0662	0.7553	-339.0889	0.4326	-100.1435	-0.7375
510	85.13	0.0114	0.6132	0.0071	0.1352	0.2865	0.0684	0.7310	-339.0907	0.4376	-100.1387	-0.7425
480	81.23	0.0116	0.6229	0.0072	0.1434	0.2918	0.0534	0.8127	-339.0921	0.4368	-100.1359	-0.7408
450	81.57	0.0115	0.6010	0.0076	0.1463	0.2969	0.0580	0.7931	-339.0924	0.4432	-100.1348	-0.7521
420	80.31	0.0117	0.6090	0.0075	0.1493	0.2850	0.0626	0.7636	-339.0938	0.4392	-100.1310	-0.7397
390	78.84	0.0119	0.6204	0.0076	0.1489	0.2861	0.0620	0.7581	-339.0931	0.4373	-100.1320	-0.7354
360	76.66	0.0123	0.5774	0.0080	0.1648	0.3028	0.0554	0.7762	-339.0971	0.4457	-100.1248	-0.7563
330	76.38	0.0122	0.6130	0.0082	0.1670	0.2842	0.0636	0.7830	-339.0969	0.4403	-100.1220	-0.7336
300	73.27	0.0125	0.5564	0.0082	0.1666	0.2752	0.0548	0.8212	-339.0989	0.4457	-100.1174	-0.7443
270	73.68	0.0124	0.5266	0.0080	0.1777	0.2772	0.0636	0.6698	-339.1027	0.4489	-100.1104	-0.7546
240	71.85	0.0125	0.5185	0.0079	0.1856	0.2803	0.0548	0.7336	-339.1050	0.4495	-100.1067	-0.7590
210	71.26	0.0127	0.4754	0.0079	0.1829	0.2855	0.0656	0.7561	-339.1057	0.4559	-100.1065	-0.7754
180	70.25	0.0131	0.4964	0.0078	0.2043	0.2834	0.0566	0.7880	-339.1107	0.4498	-100.0955	-0.7620
150	70.87	0.0134	0.5060	0.0075	0.2078	0.2770	0.0582	0.7801	-339.1129	0.4436	-100.0916	-0.7507
120	68.38	0.0144	0.3696	0.0086	0.2165	0.2953	0.0570	0.7754	-339.1168	0.4705	-100.0825	-0.8057
90	65.73	0.0151	0.3990	0.0079	0.2520	0.2748	0.0552	0.8188	-339.1296	0.4550	-100.0556	-0.7740
60	68.81	0.0165	0.3543	0.0081	0.2697	0.2389	0.0694	0.7176	-339.1412	0.4527	-100.0204	-0.7573

B.5 Comparison Between Batch and Sliding Window Methods

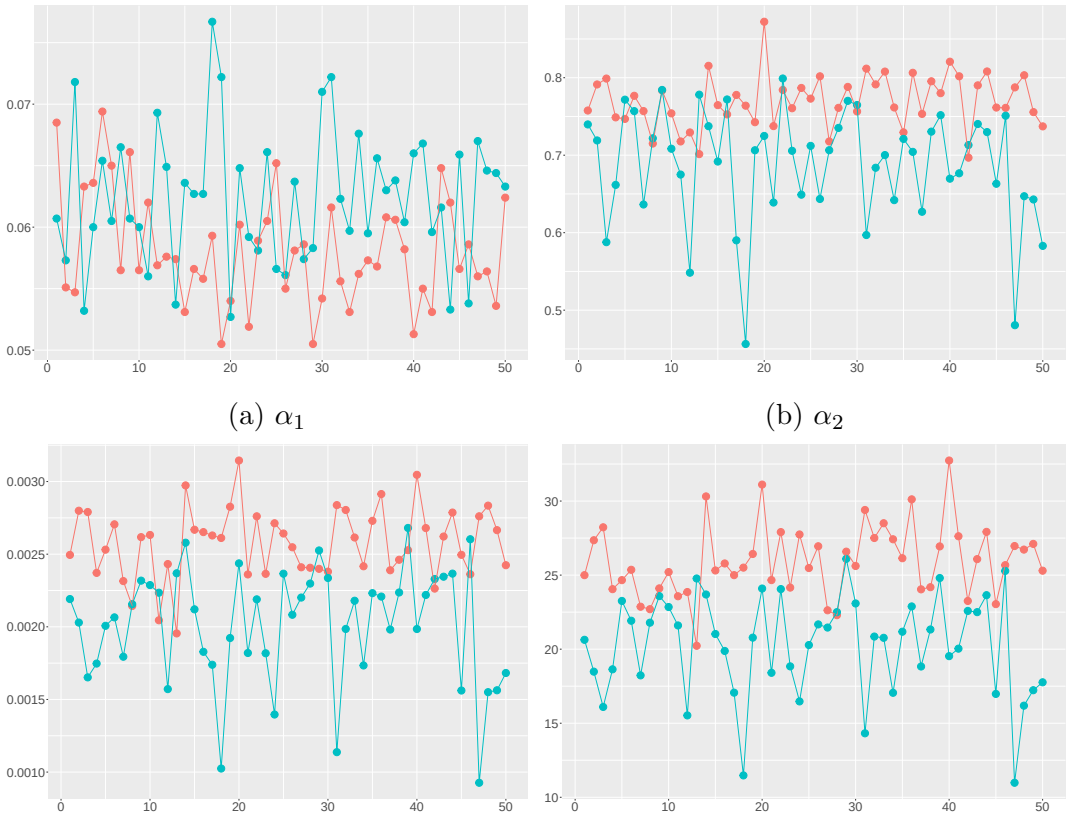

(a) α_1 (b) α_2

(c) EffUT (d) ESSUT

Figure B.3: Comparison of α_1, α_2, EffUT and ESSUT between batch MCMC (orange) and sliding window MCMC (green).

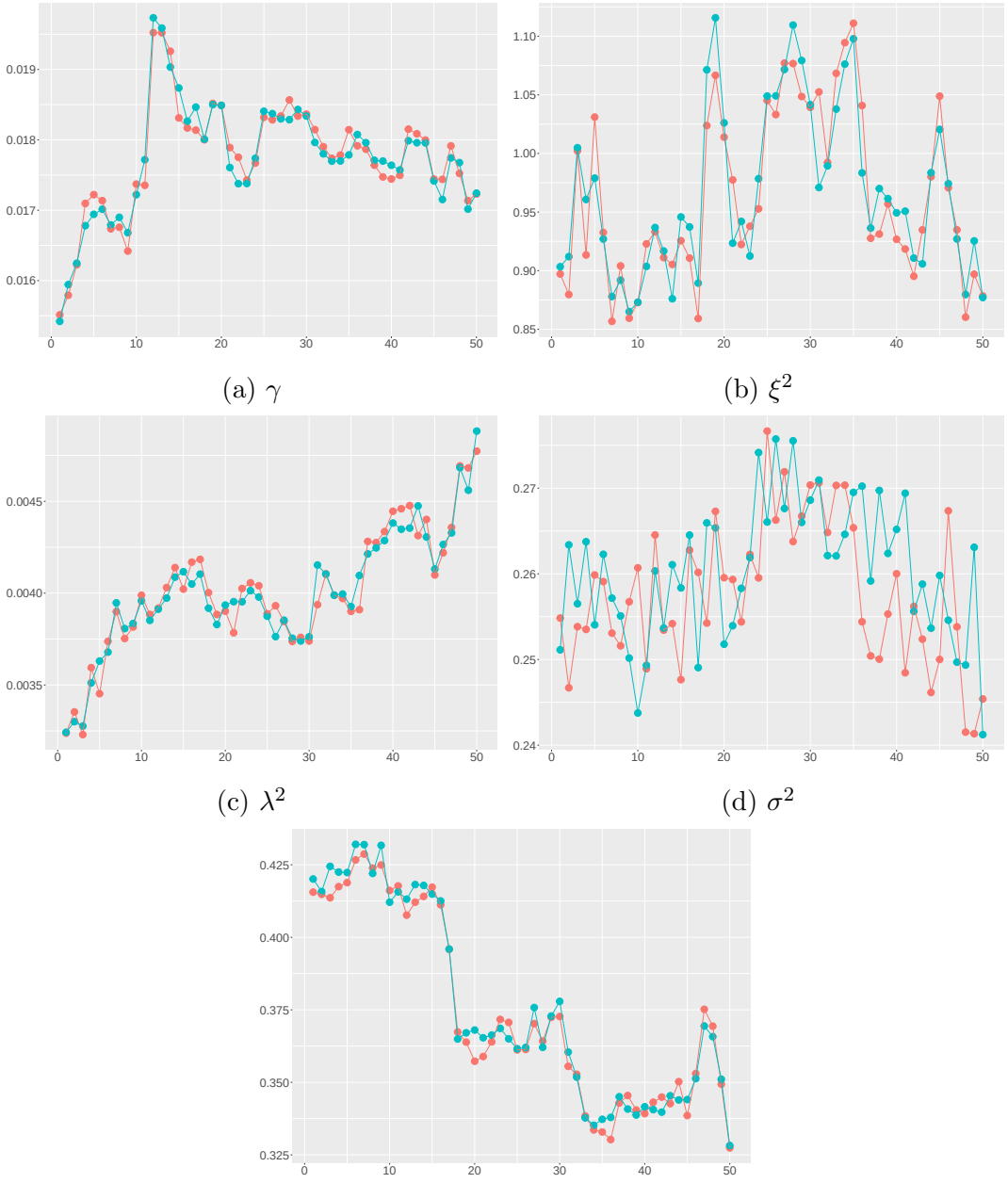

(a) γ (b) ξ^2

(c) λ^2 (d) σ^2

(e) τ^2

Figure B.4: Comparison of parameters estimation between batch MCMC (orange) and sliding window MCMC (green).

B.6 Parameter Evolution Visualization

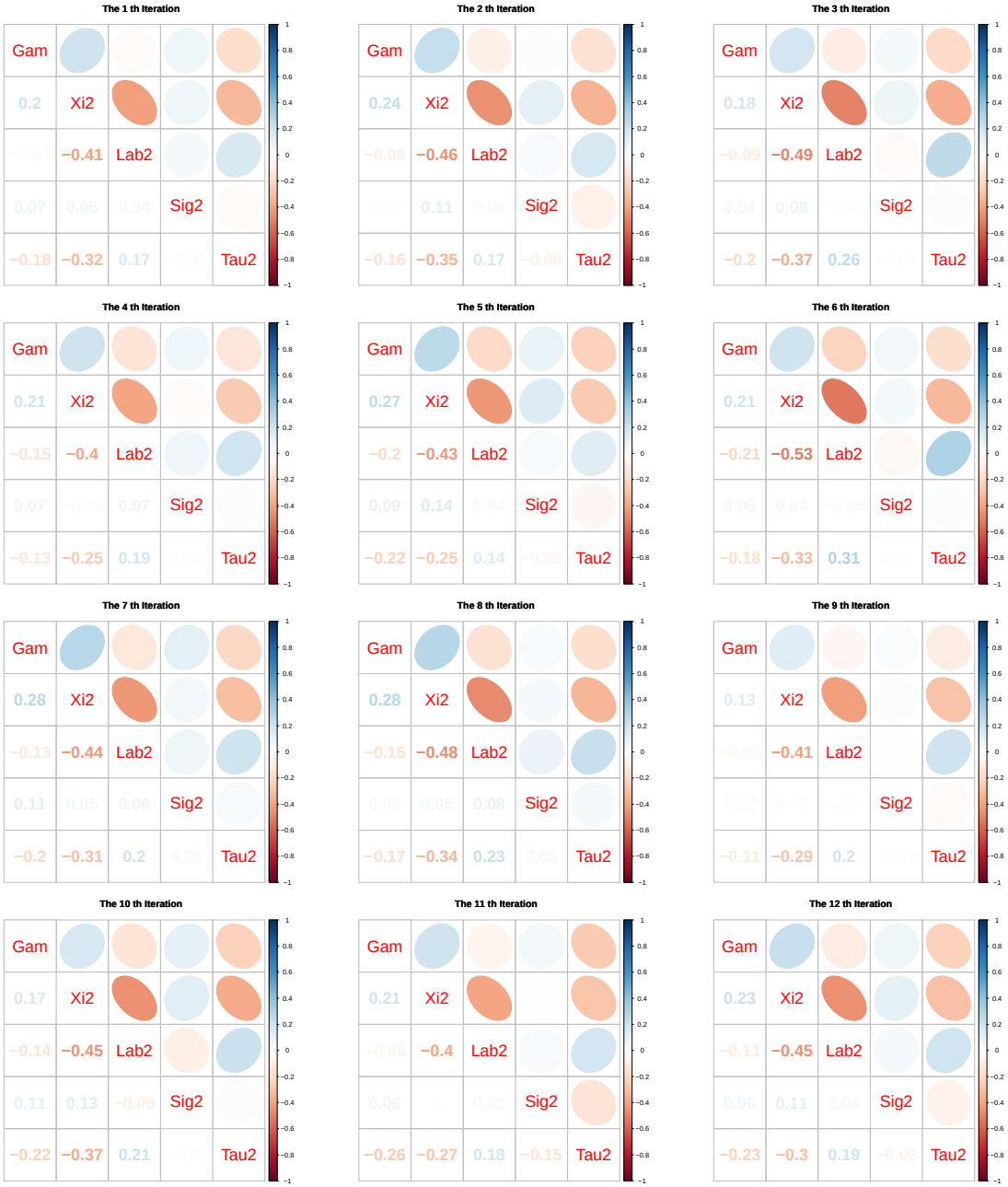


The 13 th Iteration
Gam
0.15 Xi2
−0.08 −0.42 Lab2
0.06 0.13 0.06 Sig2
−0.15 −0.35 0.23 −0.06 Tau2
The 14 th Iteration
Gam
0.27 Xi2
−0.2 −0.56 Lab2
0.03 0.12 −0.04 Sig2
−0.21 −0.38 0.31 −0.03 Tau2
The 15 th Iteration
Gam
0.23 Xi2
−0.13 −0.4 Lab2
0.1 0.16 −0.08 Sig2
−0.16 −0.31 0.18 −0.09 Tau2
The 16 th Iteration
Gam
0.3 Xi2
−0.19 −0.46 Lab2
0.03 0.08 0.04 Sig2
−0.26 −0.43 0.31 −0.05 Tau2
The 17 th Iteration
Gam
0.31 Xi2
−0.18 −0.47 Lab2
0.06 0.1 0.06 Sig2
−0.29 −0.39 0.21 −0.13 Tau2
The 18 th Iteration
Gam
0.19 Xi2
−0.05 −0.55 Lab2
0.11 0.18 0.07 Sig2
−0.14 −0.43 0.36 −0.1 Tau2
The 19 th Iteration
Gam
0.17 Xi2
−0.09 −0.47 Lab2
0.07 0.04 0.1 Sig2
−0.17 −0.35 0.24 −0.07 Tau2
The 20 th Iteration
Gam
0.15 Xi2
−0.08 −0.5 Lab2
0.06 0.07 0.03 Sig2
−0.11 −0.38 0.21 −0.13 Tau2
The 21 th Iteration
Gam
0.19 Xi2
−0.08 −0.44 Lab2
0.07 0.03 0.11 Sig2
−0.22 −0.32 0.13 −0.06 Tau2
The 22 th Iteration
Gam
0.12 Xi2
−0.03 −0.44 Lab2
0.12 0.09 0.01 Sig2
−0.07 −0.38 0.27 0.06 Tau2
The 23 th Iteration
Gam
0.2 Xi2
−0.12 −0.48 Lab2
0.09 0.05 0.03 Sig2
−0.16 −0.39 0.21 −0.15 Tau2
The 24 th Iteration
Gam
0.16 Xi2
−0.09 −0.56 Lab2
0.06 0.08 −0.05 Sig2
−0.12 −0.37 0.34 −0.08 Tau2


The 25 th Iteration
Gam
0.13 Xi2
−0.08 −0.44 Lab2
0.06 0.11 Sig2
−0.13 −0.35 0.18 −0.06 Tau2
The 26 th Iteration
Gam
0.07 Xi2
−0.1 −0.45 Lab2
0.07 Sig2
−0.06 −0.27 0.12 Tau2
The 27 th Iteration
Gam
0.11 Xi2
−0.1 −0.36 Lab2
0.07 Sig2
−0.14 −0.35 0.18 −0.12 Tau2
The 28 th Iteration
Gam
0.13 Xi2
−0.1 −0.49 Lab2
Sig2
−0.17 −0.33 0.18 −0.11 Tau2
The 29 th Iteration
Gam
0.19 Xi2
−0.06 −0.51 Lab2
0.1 Sig2
−0.15 −0.48 0.26 Tau2
The 30 th Iteration
Gam
0.16 Xi2
−0.41 Lab2
Sig2
−0.15 −0.36 0.18 −0.15 Tau2
The 31 th Iteration
Gam
0.09 Xi2
−0.5 Lab2
0.07 Sig2
−0.3 0.19 Tau2
The 32 th Iteration
Gam
0.18 Xi2
−0.09 −0.43 Lab2
Sig2
−0.1 −0.31 0.21 Tau2
The 33 th Iteration
Gam
0.11 Xi2
−0.41 Lab2
Sig2
−0.45 0.25 Tau2
The 34 th Iteration
Gam
0.11 Xi2
−0.48 Lab2
0.07 Sig2
−0.32 0.17 Tau2
The 35 th Iteration
Gam
Xi2
−0.48 Lab2
Sig2
−0.38 0.3 Tau2
The 36 th Iteration
Gam
0.16 Xi2
−0.42 Lab2
0.1 Sig2
−0.43 0.24 Tau2

Figure B.4: Parameter Evolution Visualization. The correlation among parameters does not change two much. The parameters are considered static.

Appendix C

A Spin-off Outcome: Data Simplification Method

C.1 Introduction

GPS devices are widely used in orchard planting and maintenance. This location-based system allows orchardist to check trajectory of tractors. The trajectory is a connection by a time series successive positions recorded by GPS devices. A classical GPS device records skeleton information, including time mark, latitude, longitude, number of available satellites, etc. Recently, researchers try to enrich trajectory (called Semantic Trajectory) by adding background geographic information to discover meaningful pattern (Ying *et al.*, 2011).

Normally GPS units record more data than necessary and cause more errors due to weak signals or shelter from branches. To obtain a more accurate observation data set and to save local storage space, several data simplification methods were proposed and are focusing on simplifying data set by making either a local or global decision.

A local simplification algorithm focuses on a couple of particular consecutive points. By analyzing the relationship between these points, a decision is made that which point can be deleted or retained. Distance threshold algorithm is one of these algorithms. All points, whose distance to the preceding track point is less than a predetermined threshold, are deleted. Direction changing algorithm is another one. The point is retained if the change in direction is greater than a predetermined threshold (Ivanov, 2012).

Alternatively, global simplification algorithms have an overview of all tracked points. After analyzing the relationships among these points, a decision will be made about

which one or more points to delete or to retain. The Douglas-Peucker algorithm is the most popular one (Douglas and Peucker, 1973). A proposed simplification method, represented by Chen *et al.* (2009), consider both the skeleton information and semantic meanings of a trajectory when performing simplification.

Intuitively, the global simplification algorithms can be applied on off-line data analyses and local simplification algorithms will perform better on on-line or real-time track simplification. However, a pertinent algorithm is required in our case.

In our case, a GPS log is a sequence time series points $p_i \in P$, $P = \{p_1, p_2, \ldots, p_n\}$. Each GPS point p_i contains information of time mark, latitude, longitude and semantic information of velocity, heading direction and boom status, which can be written in form of

$$T = \{p_t = [x_t, y_t, v_t, \theta_t, b_t] \mid t \in \mathbb{R}\}. \tag{C.1.1}$$

Sequentially connect these points will give us a trajectory of a moving vehicle. Particularly, a tractor working on an orchard generates two kinds of boom status information: operating and not-operating. This information is recorded by GPS units and is indicated by $b = 1$ for operating and $b = 0$ for not-operating.

To move further, here are two concepts that will be useful to understand the simplification scheme.

- **Segment** A segment is a part of the consecutive trajectory. Regarding the status of the boom, the trajectory can be simply divided into two kinds of the segment in our data set, one is boom-operating, the other is boom-not-operating.

- **Direction**. Direction θ denotes the heading direction of a tractor at a specific point location. This parameter uses north direction as a basis, in which way $0° \leq \theta < 360°$.

C.2 Simplification Algorithm

The first two steps are designed to reduce some errors caused by misoperation and GPS units bugs.

- Merging Phase. If the length of a segment composed of consecutive boom operating or not-operating points is less than a threshold, merge this one into its backward segment.

- Removing Phase. If two or more data points have duplicated time mark, remove the latter ones.

Now only two types of segment points are left in GPS log, boom operating, and not-operating and the length of each segment are greater than the predetermined threshold.

The following algorithm is based on the relationship between a candidate point p_i and its neighboring points p_{i-1} and p_{i+1}, and the importance of the p_i in the segment where it belongs to, $i = 2, \ldots, n-1$.

- Rule 1. The candidate point p_i is retained if it is not linear predictable or cannot be used for linear predicting. With the velocity information v_{i-1}, v_i at point p_{i-1}, p_i and time differences $\Delta t_{i-1} = |t_i - t_{i-1}|, \Delta t_i = |t_{i+1} - t_i|$, an estimated position can be calculated by $\hat{p}_i = \Delta t_{i-1} p_{i-1}$, $\hat{p}_{i+1} = \Delta t_i p_i$. If the distance $|\hat{p}_i - p_i|$ or $|\hat{p}_{i+1} - p_{i+1}|$ is less than a threshold, then the point p_i is not linear predictable or cannot be used for linear predicting.
- Rule 2. Select a candidate point p_i. Retain this point if the distance between p_i and p_{i-1} is greater than the threshold d, where d is the mean distances of these points $p_{i-1}, p_i, \ldots, p_{i+k}$ with same boom status $b_{i-1} = b_i = \cdots = b_{i+k}$.
- Rule 3. Neighbor Heading Changing. The candidate point p_i belongs to the track if $|\theta_i - \theta_{i-1}| + |\theta_i - \theta_{i+1}| > \theta$, where $|\theta_i - \theta_{i-1}|$ and $|\theta_i - \theta_{i+1}|$ are the direction changes between points p_i and p_{i-1} and between points p_i and p_{i+1}, θ is predefined threshold.
- Rule 4. The candidate point p_i belongs to the track if the boom status $b_i \neq b_{i-1}$.

Finally, the point p_i belongs to the track if Rule 1 = TRUE or Rule 2 = TRUE or Rule 3 = TRUE or Rule 4 = TRUE.

C.3 Evaluation

Errors are measured by Synchronized Euclidean Distance (Lawson *et al.*, 2011). SED measures the distances between the original and compressed trace at the same time. As shown in Figure C.1, the green points $P_{t1}, \ldots, P_{t5}$ are original positions. After simplification, the points P_{t2}, P_{t3} and P_{t4} are removed. The black curve is the original trajectory and the gray dash-dot line is the simplified trajectory. The blue points P'_{t2},P'_{t3} and P'_{t4} on simplified trajectory have the same time difference as the point P_{t2}, P_{t3} and P_{t4} on original trajectory did. For instance, the time difference between P_{t2} and P_{t3} is the same as that between P'_{t2} and P'_{t3}. Further, the distances between P_{t2} and P'_{t2}, P_{t3} and P'_{t3} and P_{t4}, P'_{t4} can be calculated.

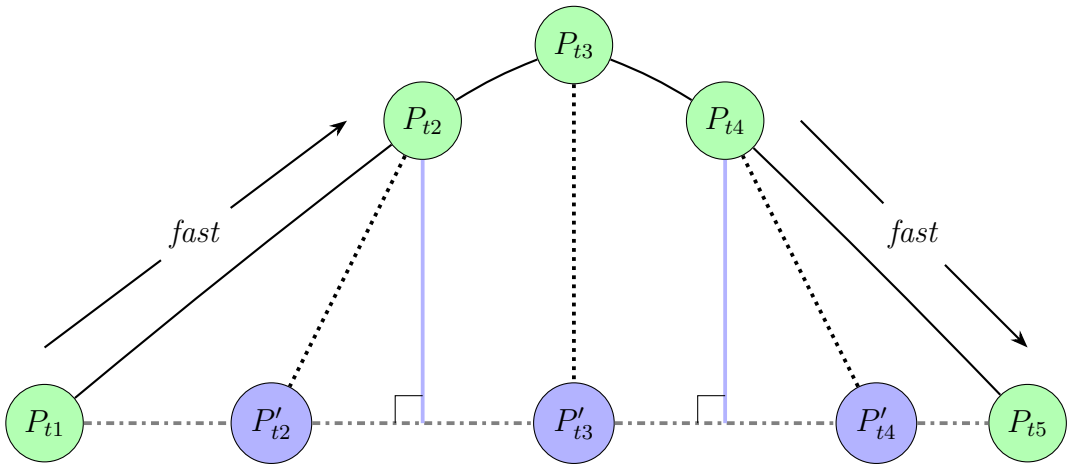

Figure C.1: Synchronized Euclidean Distance

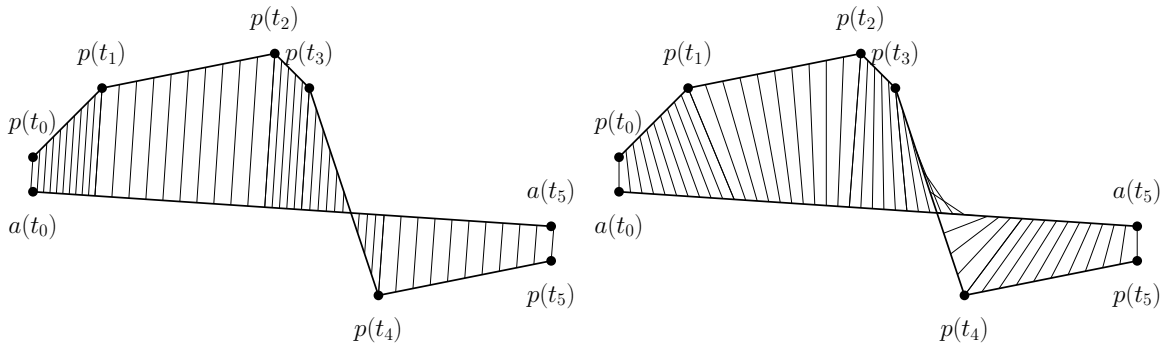

(a) perpendicular distance chords

(b) time-synchronous distance chords

Figure C.2: C.2a indicates that the errors are measured at fixed sampling rate as sum of perpendicular distance chords. C.2b indicates that the errors are measured at fixed sampling rates as sum of time-synchronous distance chords.

Another way to calculate the difference between a GPS trace and its compressed version is to measure the perpendicular distance. This algorithm ignores the temporal component and uses simple perpendicular distance (Meratnia and Rolf, 2004). The Figure C.2 expresses these differences clearly.

C.4 Numerical Study

In the numerical simulation study, we use *Kalman filter* (KF) to fit the trajectory after data simplification. The KF equations describe the prediction step in such a

Table C.1: Comparison between raw data and simplified data

	Original Data	**DP Algorithm**	**Proposed Algorithm**
Remaining Points	1021	847	847
Tracked Distances(m)	74041.31	74038.33	74012.56
SED (m)	NA	1316.715	607.9587

following way:

$$\hat{x}_k^- = A\hat{x}_{k-1} + Bu_k$$
$$P_k^- = AP_{k-1}A^\top + Q$$

where $\hat{x}_k^-$ is a priori state estimate, $\hat{x}_k$ is a posteriori state estimate, A is status transition matrix, P_k^- is a priori estimate for error covariance, u_k is an input parameter and Q is process noise covariance. When a new observation comes into the data stream, KF update and corrects its estimation by:

$$K_k = P_k^- H^\top \left(HP_k^- H^\top + R\right)^{-1}$$
$$\hat{x}_k = \hat{x}_k^- + K_k\left(z_k - H\hat{x}_k^-\right)$$
$$P_k = (I - K_k H)P_k^-$$

where K_k is the Kalman gain matrix, z_k is the observed data.

The original data set contains 1 021 rows, including latitude, longitude, velocity, bearing (heading direction) and boom status. Douglas-Peucker Algorithm, with distance threshold 0.205m, retained 847 points. The proposed algorithm, given a predictable distance 5m and heading direction changing threshold 30°, returns the same amount of simplified points. Under the same circumstance, we calculated SED and other information.

Table C.1 describes the results after being simplified by DP algorithm and the proposed algorithm. Figure C.3 demonstrates the simplified raw data and Figure C.4 is the fitted trajectories by KF.

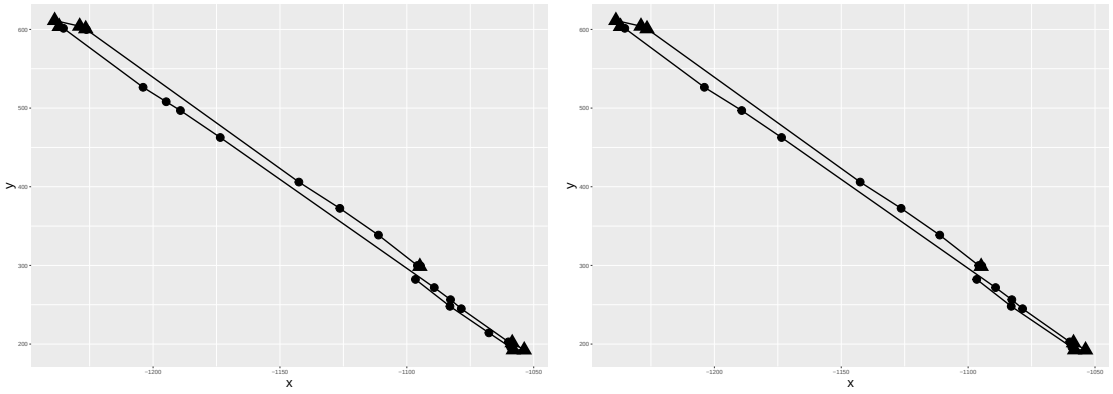

(a) Raw trajectory

(b) Simplified trajectory by DP

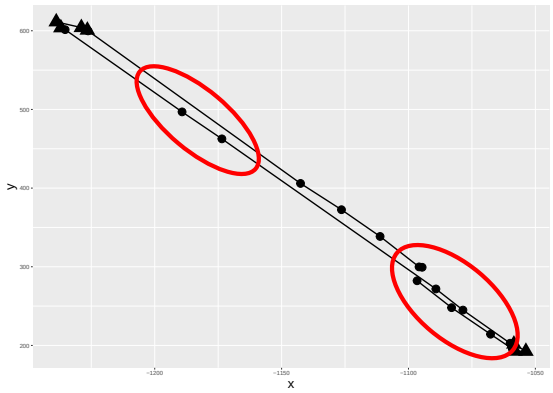

(c) Simplified trajectory by proposed algorithm

Figure C.3: A segment start from time $t = 2\,000$ to $3\,000$, recorded by GPS units. ▲ indicates that the boom is not operating. • indicates that the boom is operating. Figure C.3a, the trajectory connected by raw data with 27 points. Figure C.3b, the trajectory connected by simplified data with Douglas-Peucker algorithm with 24 points. Figure C.3c, the trajectory connected by simplified data with proposed simplification algorithm with 23 points.

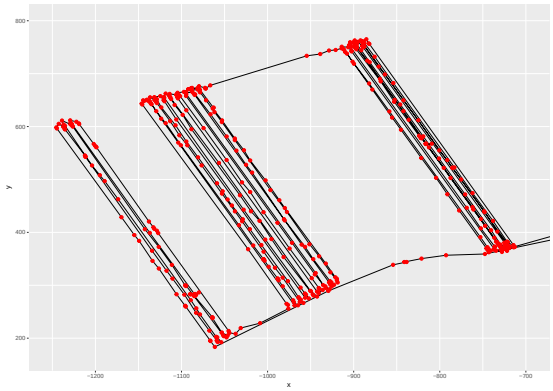

(a) Fitted Kalman filter with raw data

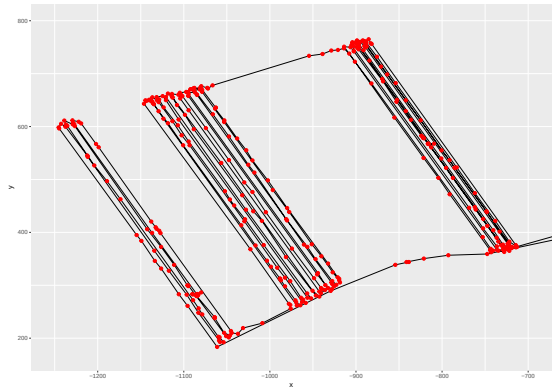

(b) Fitted Kalman filter with simplified data by DP

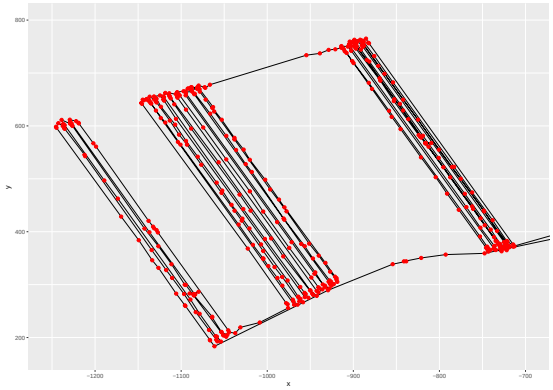

(c) Fitted Kalman filter with simplified data by proposed algorithm

Figure C.4: Trajectory fitted by Kalman filter. The mean squared errors of raw data, DP and proposed algorithm are 26.8922, 23.9788 and 23.9710 respectively.

C.5 Conclusion

The data simplification algorithm is originally proposed to solve the over-fitting and wiggle-construction problems. Duplicated and short-distance points cause reconstruction issues in spline fitting. The advantage of data simplification algorithm is that less data points potentially increase computation efficiency and save storage space without of losing information for reconstructing.

References

Abramovich, F., Sapatinas, T., and Silverman, B. W. (1998). Wavelet thresholding via a Bayesian approach. *Journal of the Royal Statistical Society: Series B (Statistical Methodology)*, *60*(4), 725–749.

Agarwal, P. K., Arge, L., and Erickson, J. (2003). Indexing moving points. *Journal of Computer and System Sciences*, *66*(1), 207–243.

Agrawal, D. P. and Zeng, Q.-A. (2015). *Introduction to wireless and mobile systems*. Cengage learning.

Almasi, G. S. and Gottlieb, A. (1994). *Highly parallel computing* (Second ed.). Redwood City, CA, USA: Benjamin-Cummings Publishing Co., Inc.

Anderson, B. D. O. and Moore, J. B. (1979). Optimal filtering. *Englewood Cliffs*, *21*, 22–95.

Anderson, J. L. (2001). An ensemble adjustment Kalman filter for data assimilation. *Monthly Weather Review*, *129*(12), 2884–2903.

Andrieu, C., De Freitas, N., and Doucet, A. (1999). Sequential MCMC for Bayesian model selection. In *Higher-Order Statistics, 1999. Proceedings of the IEEE Signal Processing Workshop on*, 130–134. IEEE.

Andrieu, C., Djurić, P. M., and Doucet, A. (2001). Model selection by MCMC computation. *Signal Processing*, *81*(1), 19–37.

Andrieu, C., Doucet, A., and Holenstein, R. (2010). Particle Markov chain Monte Carlo methods. *Journal of the Royal Statistical Society: Series B (Statistical Methodology)*, *72*(3), 269–342.

Andrieu, C., Doucet, A., and Tadic, V. B. (2005). On-line parameter estimation in general state-space models. In *Proceedings of the 44th IEEE Conference on Decision and Control*, 332–337. IEEE.

Andrieu, C. and Thoms, J. (2008). A tutorial on adaptive MCMC. *Statistics and Computing*, *18*(4), 343–373.

Arlot, S. and Celisse, A. (2010). A survey of cross-validation procedures for model selection. *Statistics Surveys*, *4*, 40–79.

Aronszajn, N. (1950). Theory of reproducing kernels. *Transactions of the American Mathematical Society*, *68*(3), 337–404.

Arulampalam, M. S., Maskell, S., Gordon, N., and Clapp, T. (2002). A tutorial on particle filters for online nonlinear/non-Gaussian Bayesian tracking. *IEEE Transactions on Signal Processing*, *50*(2), 174–188.

Asanovic, K., Bodik, R., Catanzaro, B. C., Gebis, J. J., Husbands, P., Keutzer, K., Patterson, D. A., Plishker, W. L., Shalf, J., Williams, S. W., and Yelick, K. A. (2006). The landscape of parallel computing research: a view from berkeley. Technical Report No. UCB/EECS-2006-183, EECS Department University of California, Berkeley.

Atchade, Y., Fort, G., Moulines, E., and Priouret, P. (2009). Adaptive Markov chain Monte Carlo: theory and methods. Technical report, Department of Statistics at the University of Michigan.

Aydın, D., Memmedli, M., and Omay, R. E. (2013). Smoothing parameter selection for nonparametric regression using smoothing spline. *European Journal of Pure and Applied Mathematics*, *6*(2), 222–238.

Aydin, D. and Tuzemen, M. S. (2012). Smoothing parameter selection problem in nonparametric regression based on smoothing spline: a simulation study. *Journal of Applied Sciences*, *12*(7), 636.

Babenko, B., Yang, M.-H., and Belongie, S. (2009). A family of online boosting algorithms. In *2009 IEEE 12th International Conference on Computer Vision Workshops, ICCV Workshops*, 1346–1353. IEEE.

Bajaj, R., Ranaweera, S. L., and Agrawal, D. P. (2002). GPS: location-tracking technology. *Computer*, *35*(4), 92–94.

Bar-Shalom, Y. and Li, X.-R. (1996). Estimation and tracking-principles, techniques, and software. *IEEE Antennas and Propagation Magazine*, *38*(1), 62.

Bartlett, M. S. (1951). An inverse matrix adjustment arising in discriminant analysis. *The Annals of Mathematical Statistics*, *22*(1), 107–111.

Bédard, M. (2007). Weak convergence of Metropolis algorithms for non-iid target distributions. *The Annals of Applied Probability*, *17*(4), 1222–1244.

Ben-Arieh, D., Chang, S., Rys, M., and Zhang, G. (2004). Geometric modeling of highways using global positioning system data and B-spline approximation. *Journal of Transportation Engineering*, *130*(5), 632–636.

Berlinet, A. and Thomas-Agnan, C. (2011). *Reproducing kernel Hilbert spaces in probability and statistics*. Springer Science & Business Media.

Berzuini, C., Best, N. G., Gilks, W. R., and Larizza, C. (1997). Dynamic conditional independence models and Markov chain Monte Carlo methods. *Journal of the American Statistical Association*, *92*(440), 1403–1412.

Beskos, A., Roberts, G., and Stuart, A. (2009). Optimal scalings for local Metropolis-Hastings chains on nonproduct targets in high dimensions. *Annals of Applied Probability*, *19*(3), 863–898.

Betancourt, M. (2017). A conceptual introduction to Hamiltonian Monte Carlo. *arXiv preprint*, *arXiv:1701.02434*.

Beygelzimer, A., Hazan, E., Kale, S., and Luo, H. (2015). Online gradient boosting. In *Advances in Neural Information Processing Systems*, 2458–2466.

Biagiotti, L. and Melchiorri, C. (2013). Online trajectory planning and filtering for robotic applications via B-spline smoothing filters. In *2013 IEEE/RSJ International Conference on Intelligent Robots and Systems*, 5668–5673. IEEE.

Bierkens, J. and Duncan, A. (2017). Limit theorems for the Zig-Zag process. *Advances in Applied Probability*, *49*(3), 791–825.

Bierkens, J. and Roberts, G. (2016). A piecewise deterministic scaling limit of lifted Metropolis-Hastings in the Curie-Weiss model. *The Annals of Applied Probability*, *27*(2), 846–882.

Bishop, G. and Welch, G. (2001). An introduction to the Kalman filter. *Proc of SIGGRAPH, Course*, *8*(27599-23175), 41.

Blaauw, M. and Christen, J. A. (2011). Flexible paleoclimate age-depth models using an autoregressive gamma process. *Bayesian Analysis*, *6*(3), 457–474.

Bodewig, E. (1959). *Matrix calculus 3rd edition* (Third ed.). North-Holland.

Box, G. E. P. and Tiao, G. C. (2011). *Bayesian inference in statistical analysis*, Volume 40. John Wiley & Sons.

Bradford, R. and Thomas, A. (1996). Markov chain Monte Carlo methods for family trees using a parallel processor. *Statistics and Computing*, *6*(1), 67–75.

Branson, Z., Rischard, M., Bornn, L., and Miratrix, L. (2017). A non-parametric Bayesian methodology for regression discontinuity designs. *arXiv preprint*, *arXiv:1704.04858*.

Cantoni, E. and Ronchetti, E. (2001). Resistant selection of the smoothing parameter for smoothing splines. *Statistics and Computing*, *11*(2), 141–146.

Cappé, O., Godsill, S. J., and Moulines, E. (2007). An overview of existing methods and recent advances in sequential Monte Carlo. *Proceedings of the IEEE*, *95*(5), 899–924.

Cappé, O., Moulines, E., and Rydén, T. (2009). Inference in hidden markov models. In *Proceedings of EUSFLAT Conference*, 14–16.

Cargnoni, C., Müller, P., and West, M. (1997). Bayesian forecasting of multinomial time series through conditionally Gaussian dynamic models. *Journal of the American Statistical Association*, *92*(438), 640–647.

Carlin, B. P., Polson, N. G., and Stoffer, D. S. (1992). A Monte Carlo approach to nonnormal and nonlinear state-space modeling. *Journal of the American Statistical Association*, *87*(418), 493–500.

Carpenter, J., Clifford, P., and Fearnhead, P. (1999). Improved particle filter for nonlinear problems. *IEE Proceedings-Radar, Sonar and Navigation*, *146*(1), 2–7.

Carvalho, C. M., Johannes, M. S., Lopes, H. F., and Polson, N. G. (2010). Particle learning and smoothing. *Statistical Science*, *25*(1), 88–106.

Casella, G., Robert, C. P., and Wells, M. T. (2004). Generalized accept-reject sampling schemes. *Lecture Notes-Monograph Series*, *45*, 342–347.

Castro, M., Iglesias, L., Rodríguez-Solano, R., and Sánchez, J. A. (2006). Geometric modelling of highways using global positioning system (GPS) data and spline approximation. *Transportation Research Part C: Emerging Technologies*, *14*(4), 233–243.

Chadil, N., Russameesawang, A., and Keeratiwintakorn, P. (2008). Real-time tracking management system using GPS, GPRS and Google earth. In *2008 5th International Conference on Electrical Engineering/Electronics, Computer, Telecommunications and Information Technology*, Volume 1, 393–396. IEEE.

Chandrasekar, J., Ridley, A. J., and Bernstein, D. S. (2007). A comparison of the extended and unscented Kalman filters for discrete-time systems with nondifferentiable dynamics. In *American Control Conference, 2007. ACC'07*, 4431–4436. IEEE.

Chen, M.-H., Shao, Q.-M., and Ibrahim, J. G. (2012). *Monte Carlo methods in Bayesian computation*. Springer Science & Business Media.

Chen, R. and Liu, J. S. (2000). Mixture Kalman filters. *Journal of the Royal Statistical Society: Series B (Statistical Methodology)*, *62*(3), 493–508.

Chen, T. and Guestrin, C. (2016). Xgboost: a scalable tree boosting system. In *Proceedings of the 22nd acm sigkdd international conference on knowledge discovery and data mining*, 785–794. ACM.

Chen, W.-K. (2017). *Feedback, nonlinear, and distributed circuits* (Third ed.). The Circuits and Filters Handbook. CRC Press.

Chen, Y., Jiang, K., Zheng, Y., Li, C., and Yu, N. (2009). Trajectory simplification method for location-based social networking services. In *Proceedings of the 2009 International Workshop on Location Based Social Networks*, 33–40. ACM.

Chen, Z. (2003). Bayesian filtering: from Kalman filters to particle filters, and beyond. *Statistics*, *182*(1), 1–69.

Chopin, N. (2002). A sequential particle filter method for static models. *Biometrika*, *89*(3), 539–552.

Chopin, N., Iacobucci, A., Marin, J.-M., Mengersen, K., Robert, C. P., Ryder, R., and Schäfer, C. (2010). On particle learning. *arXiv preprint*, *arXiv:1006.0554*.

Christen, J. A. and Fox, C. (2005). Markov chain Monte Carlo using an approximation. *Journal of Computational and Graphical Statistics*, *14*(4), 795–810.

Christen, J. A. and Fox, C. (2010). A general purpose sampling algorithm for continuous distributions (the t-walk). *Bayesian Analysis*, *5*(2), 263–281.

Cox, D. D. (1993). An analysis of Bayesian inference for nonparametric regression. *The Annals of Statistics*, *21*(2), 903–923.

Cox, M. G. (1982). Practical spline approximation. In P. R. Turner (Ed.), *Topics in Numerical Analysis*, Berlin, Heidelberg, 79–112. Springer Berlin Heidelberg.

Craven, P. and Wahba, G. (1978). Smoothing noisy data with spline functions. *Numerische Mathematik*, *31*(4), 377–403.

De Boor, C., De Boor, C., Mathématicien, E.-U., De Boor, C., and De Boor, C. (1978). *A practical guide to splines*, Volume 27. Springer-Verlag New York.

De Jong, P. (1988). The likelihood for a state space model. *Biometrika*, *75*, 165–169.

Dempster, A. P., Laird, N. M., and Rubin, D. B. (1977). Maximum likelihood from incomplete data via the EM algorithm. *Journal of the Royal Statistical Society. Series B (Methodological)*, *39*, 1–38.

Deng, C. Y. (2011). A generalization of the Sherman-Morrison-Woodbury formula. *Applied Mathematics Letters*, *24*(9), 1561–1564.

Dierckx, P. (1995). *Curve and surface fitting with splines*. Oxford University Press.

Dieudonné, J. (2013). *Foundations of modern analysis*. Read Books Ltd.

Diggle, P. J. and Hutchinson, M. F. (1989). On spline smoothing with autocorrelated errors. *Australian & New Zealand Journal of Statistics*, *31*(1), 166–182.

Dongarra, J. and Sullivan, F. (2000). Guest editors' introduction: the top 10 algorithms. *Computing in Science & Engineering*, *2*(1), 22–23.

Donoho, D. L. and Johnstone, I. M. (1995). Adapting to unknown smoothness via wavelet shrinkage. *Journal of the American Statistical Association*, *90*(432), 1200–1224.

Donoho, D. L., Johnstone, I. M., Kerkyacharian, G., and Picard, D. (1995). Wavelet shrinkage: asymptopia? *Journal of the Royal Statistical Society. Series B (Methodological)*, *57*, 301–369.

Donoho, D. L. and Johnstone, J. M. (1994). Ideal spatial adaptation by wavelet shrinkage. *Biometrika*, *81*(3), 425–455.

Doucet, A., de Freitas, N., and Gordon, N. (2011). *Sequential Monte Carlo pethods in practice*. Springer-Verlag New York.

Doucet, A., De Freitas, N., Murphy, K., and Russell, S. (2000). Rao-Blackwellised particle filtering for dynamic Bayesian networks. In *Proceedings of the 16th Conference on Uncertainty in Artificial Intelligence*, Number 8 in UAI '00, San Francisco, CA, USA, 176–183. Morgan Kaufmann Publishers Inc.: Morgan Kaufmann Publishers Inc.

Doucet, A., Godsill, S., and Andrieu, C. (2000). On sequential Monte Carlo sampling methods for Bayesian filtering. *Statistics and Computing*, *10*(3), 197–208.

Doucet, A. and Johansen, A. M. (2009). A tutorial on particle filtering and smoothing: fifteen years later. *Handbook of Nonlinear Filtering*, *12*(656-704), 3.

Douglas, D. H. and Peucker, T. K. (1973). Algorithms for the reduction of the number of points required to represent a digitized line or its caricature. *Cartographica: The International Journal for Geographic Information and Geovisualization*, *10*(2), 112–122.

Duane, S., Kennedy, A. D., Pendleton, B. J., and Roweth, D. (1987). Hybrid Monte Carlo. *Physics letters B*, *195*(2), 216–222.

Dubins, L. E. (1957). On curves of minimal length with a constraint on average curvature, and with prescribed initial and terminal positions and tangents. *American Journal of mathematics*, *79*(3), 497–516.

Durbin, J. and Koopman, S. J. (2012). *Time series analysis by state space methods*, Volume 38. OUP Oxford.

Eilers, P. H. C. and Marx, B. D. (1996). Flexible smoothing with B-splines and penalties. *Statistical Science*, *11*, 89–102.

Einstein, A. (1956). *Investigations on the theory of the Brownian movement*, Volume 17. Dover Publications.

Elliott, R. J., Aggoun, L., and Moore, J. B. (1995). *Hidden Markov models: estimation and control* (First ed.), Volume 29 of *0172-4568*. Springer-Verlag New York.

Ellis, D., Sommerlade, E., and Reid, I. (2009). Modelling pedestrian trajectory patterns with gaussian processes. In *2009 IEEE 12th International Conference on Computer Vision Workshops, ICCV Workshops*, 1229–1234. IEEE.

Erkorkmaz, K. and Altintas, Y. (2001). High speed CNC system design. part I: jerk limited trajectory generation and quintic spline interpolation. *International Journal of Machine Tools and Manufacture*, *41*(9), 1323–1345.

Eubank, R. L. (2004). A simple smoothing spline, III. *Computational Statistics*, *19*(2), 227–241.

Evensen, G. (1994). Sequential data assimilation with a nonlinear quasi-geostrophic model using Monte Carlo methods to forecast error statistics. *Journal of Geophysical Research: Oceans*, *99*(C5), 10143–10162.

Fearnhead, P. (2002). Markov chain Monte Carlo, sufficient statistics, and particle filters. *Journal of Computational and Graphical Statistics*, *11*(4), 848–862.

Freund, Y. and Schapire, R. E. (1995). A desicion-theoretic generalization of on-line learning and an application to boosting. In *European conference on computational learning theory*, 23–37. Springer.

Friedman, J. H. (2001). Greedy function approximation: a gradient boosting machine. *Annals of Statistics*, *29*, 1189–1232.

Gasparetto, A. and Zanotto, V. (2007). A new method for smooth trajectory planning of robot manipulators. *Mechanism and Machine Theory*, *42*(4), 455–471.

Gelb, A. (1974). *Applied optimal estimation*. MIT press.

Gelman, A. (2006). Prior distributions for variance parameters in hierarchical models (comment on article by Browne and Draper). *Bayesian Analysis*, *1*(3), 515–534.

Gelman, A., Gilks, W. R., and Roberts, G. O. (1997). Weak convergence and optimal scaling of random walk Metropolis algorithms. *The Annals of Applied Statistics*, *7*(1), 110–120.

Gelman, A., Jakulin, A., Pittau, M. G., and Su, Y.-S. (2008). A weakly informative default prior distribution for logistic and other regression models. *The Annals of Applied Statistics*, *2*, 1360–1383.

Gelman, A., Roberts, G. O., and Gilks, W. R. (1996). Efficient Metropolis jumping rules. *Bayesian Statistics*, *5*(599-608), 42.

Gelman, A. and Rubin, D. B. (1992). Inference from iterative simulation using multiple sequences. *Statistical Science*, *7*, 457–472.

Geman, S. and Geman, D. (1984). Stochastic relaxation, Gibbs distributions, and the Bayesian restoration of images. *IEEE Transactions on Pattern Analysis and Machine Intelligence*, *6*(6), 721–741.

Geweke, J. (1989). Bayesian inference in econometric models using Monte Carlo integration. *Econometrica: Journal of the Econometric Society*, *57*, 1317–1339.

Geyer, C. J. (1992). Practical Markov chain Monte Carlo. *Statistical Science*, *7*, 473–483.

Gilks, W. R., Richardson, S., and Spiegelhalter, D. (1995). *Markov chain Monte Carlo in practice*. CRC press.

Girolami, M. and Calderhead, B. (2011). Riemann manifold langevin and hamiltonian Monte Carlo methods. *Journal of the Royal Statistical Society: Series B (Statistical Methodology)*, *73*(2), 123–214.

Gloderer, M. and Hertle, A. (2010). Spline-based trajectory optimization for autonomous vehicles with Ackerman drive. http://ais.informatik.uni-freiburg.de/teaching/ws09/robotics2/projects/mr2-p6-paper.pdf.

Godsill, S., Doucet, A., and West, M. (2001). Maximum a posteriori sequence estimation using Monte Carlo particle filters. *Annals of the Institute of Statistical Mathematics*, *53*(1), 82–96.

Godsill, S. J., Doucet, A., and West, M. (2000). Methodology for Monte Carlo smoothing with application to time-varying autoregressions. In *International Symposium on Frontiers of Time Series Modeling*.

Golightly, A. and Wilkinson, D. J. (2006). Bayesian sequential inference for nonlinear multivariate diffusions. *Statistics and Computing*, *16*(4), 323–338.

Gong, L. and Flegal, J. M. (2016). A practical sequential stopping rule for high-dimensional Markov chain Monte Carlo. *Journal of Computational and Graphical Statistics*, *25*(3), 684–700.

Gordon, N. J., Salmond, D. J., and Smith, A. F. M. (1993). Novel approach to nonlinear/non-Gaussian Bayesian state estimation. In *IEE Proceedings F (Radar and Signal Processing)*, Volume 140, 107–113. IET.

Graves, T. L. (2011). Automatic step size selection in random walk Metropolis algorithms. *arXiv preprint*, *arXiv:1103.5986*.

Green, P. J. (1995). Reversible jump Markov chain Monte Carlo computation and Bayesian model determination. *Biometrika*, *82*(4), 711–732.

Green, P. J. and Silverman, B. W. (1993). *Nonparametric regression and generalized linear models: a roughness penalty approach*. CRC Press.

Gu, C. (1998). Model indexing and smoothing parameter selection in nonparametric function estimation. *Statistica Sinica*, *8*, 607–623.

Gu, C. (2013). *Smoothing spline ANOVA models*, Volume 297. Springer Science & Business Media.

Gu, C. and Wahba, G. (1991). Minimizing GCV/GML scores with multiple smoothing parameters via the Newton method. *SIAM Journal on Scientific and Statistical Computing*, *12*(2), 383–398.

Guzzi, R. (2016). *Data assimilation: mathematical concepts and instructive examples*. Springer.

György, K., Kelemen, A., and Dávid, L. (2014). Unscented Kalman filters and particle filter methods for nonlinear state estimation. *Procedia Technology*, *12*, 65–74.

Haario, H., Saksman, E., and Tamminen, J. (1999). Adaptive proposal distribution for random walk Metropolis algorithm. *Computational Statistics*, *14*(3), 375–396.

Haario, H., Saksman, E., and Tamminen, J. (2001). An adaptive Metropolis algorithm. *Bernoulli*, *7*(2), 223–242.

Hammersley, J. M. and Handscomb, D. C. (1964). Percolation processes. In *Monte Carlo Methods*, 134–141. Springer.

Handschin, J. E. (1970). Monte Carlo techniques for prediction and filtering of non-linear stochastic processes. *Automatica*, *6*(4), 555–563.

Handschin, J. E. and Mayne, D. Q. (1969). Monte Carlo techniques to estimate the conditional expectation in multi-stage non-linear filtering. *International Journal of Control*, *9*(5), 547–559.

Hangos, K. M., Bokor, J., and Szederkényi, G. (2006). *Analysis and control of nonlinear process systems*. Springer Science & Business Media.

Härdle, W. (1990). *Applied nonparametric regression*. 19. Cambridge university press.

Härdle, W., Hall, P., and Marron, J. S. (1988). How far are automatically chosen regression smoothing parameters from their optimum? *Journal of the American Statistical Association*, *83*(401), 86–95.

Hartmann, M., Nowak, T., Pfandenhauer, O., Thielecke, J., and Heuberger, A. (2016). A grid-based filter for tracking bats applying field strength measurements. In *2016 12th Annual Conference on Wireless On-demand Network Systems and Services (WONS)*, 1–8. IEEE.

Hastie, T., Tibshirani, R., and Friedman, J. (2009). *The elements of statistical learning: data mining, inference, and prediction.* (Second ed.). Springer-Verlag.

Hastie, T. J. and Tibshirani, R. J. (1990). *Generalized additive models*, Volume 43. CRC Press.

Hastings, W. K. (1970). Monte Carlo sampling methods using Markov chains and their applications. *Biometrika*, *57*(1), 97–109.

Haykin, S. S. (2001). *Kalman filtering and neural networks*. John Wiley & Sons.

Heckman, N. E. and Woodroofe, M. (1991). Minimax Bayes estimation in nonparametric regression. *The Annals of Statistics*, *19*, 2003–2014.

Hermite, C. (1863). *Remarque sur le développement de comptes rendus de i'académie des sciences.*, Volume 57. Elsevier of behalf of the French Academy of Sciences (France).

Hightower, J. and Borriello, G. (2001). Location systems for ubiquitous computing. *Computer*, *34*(8), 57–66.

Higuchi, T. (2001). Self-organizing time series model. In *Sequential Monte Carlo Methods in Practice*, 429–444. Springer.

Hintzen, N. T., Piet, G. J., and Brunel, T. (2010). Improved estimation of trawling tracks using cubic Hermite spline interpolation of position registration data. *Fisheries Research*, *101*(1), 108–115.

Hurvich, C. M., Simonoff, J. S., and Tsai, C.-L. (1998). Smoothing parameter selection in nonparametric regression using an improved Akaike information criterion. *Journal of the Royal Statistical Society: Series B (Statistical Methodology)*, *60*(2), 271–293.

Ivanov, R. (2012). Real-time GPS track simplification algorithm for outdoor navigation of visually impaired. *Journal of Network and Computer Applications*, *35*(5), 1559–1567.

Jauch, J., Bleimund, F., Rhode, S., and Gauterin, F. (2017). Recursive B-spline approximation using the Kalman filter. *Engineering Science and Technology, an International Journal*, *20*(1), 28–34.

Jaynes, E. T. (1983). *E. T. Jaynes: papers on probability, statistics and statistical physics*, Volume 158. Springer Netherlands.

Jeffries, H. (1961). *Theory of probability*. Clarendon Press, Oxford.

Johansen, A. M. and Doucet, A. (2008). A note on auxiliary particle filters. *Statistics & Probability Letters*, *78*(12), 1498 – 1504.

Johnson, R. A. and Wichern, D. W. (1992). *Applied multivariate statistical analysis.* (Third ed.). Englewood Cliffs (N.J.): Prentice-Hall.

Judd, K. L. (1998). *Numerical methods in economics*. MIT press.

Kailath, T. (1981). *Lectures on Wiener and Kalman filtering*. International Centre for Mechanical Sciences. Springer.

Kalman, R. E. (1960). A new approach to linear filtering and prediction problems. *Journal of Basic Engineering*, *82*(1), 35–45.

Kalos, M. H. and Whitlock, P. A. (2008). *Monte Carlo methods*. John Wiley & Sons.

Kantas, N., Doucet, A., Singh, S. S., and Maciejowski, J. M. (2009). An overview of sequential Monte Carlo methods for parameter estimation in General State-Space Models. In *The 15th IFAC Symposium on System Identification*. Citeseer.

Kaplan, E. and Hegarty, C. (2005). *Understanding GPS: principles and applications*. Artech house.

Kass, R. E., Carlin, B. P., Gelman, A., and Neal, R. M. (1998). Markov chain Monte Carlo in practice: a roundtable discussion. *The American Statistician*, *52*(2), 93–100.

Katzfuss, M., Stroud, J. R., and Wikle, C. K. (2016). Understanding the ensemble Kalman filter. *The American Statistician*, *70*(4), 350–357.

Khan, Z., Balch, T., and Dellaert, F. (2005). MCMC-based particle filtering for tracking a variable number of interacting targets. *IEEE Transactions on Pattern Analysis and Machine Intelligence*, *27*(11), 1805–1819.

Kijima, M. (1997). *Markov processes for stochastic modeling*, Volume 6. CRC Press.

Kim, Y.-J. and Gu, C. (2004). Smoothing spline Gaussian regression: more scalable computation via efficient approximation. *Journal of the Royal Statistical Society: Series B (Statistical Methodology)*, *66*(2), 337–356.

Kimeldorf, G. and Wahba, G. (1971). Some results on tchebycheffian spline functions. *Journal of Mathematical Analysis and Applications*, *33*(1), 82–95.

Kimeldorf, G. S. and Wahba, G. (1970). A correspondence between Bayesian estimation on stochastic processes and smoothing by splines. *The Annals of Mathematical Statistics*, *41*(2), 495–502.

Kitagawa, G. (1998). A self-organizing state-space model. *Journal of the American Statistical Association*, *93*(443), 1203–1215.

Kloek, T. and Van Dijk, H. K. (1978). Bayesian estimates of equation system parameters: an application of integration by Monte Carlo. *Econometrica: Journal of the Econometric Society*, *46*, 1–19.

Kohn, R., Ansley, C. F., and Wong, C.-M. (1992). Nonparametric spline regression with autoregressive moving average errors. *Biometrika*, *79*(2), 335–346.

Kokkala, J. (2016). *Particle and Sigma-point methods for state and parameter estimation in nonlinear dynamic systems; Partikkeli- ja sigmapistemenetelmiä epälineaaristen dynaamisten systeemien tila- ja parametriestimointiin.* G5 artikkeliväitöskirja, Aalto University.

Komoriya, K. and Tanie, K. (1989). Trajectory design and control of a wheel-type mobile robot using B-spline curve. In *IEEE/RSJ International Workshop on Intelligent Robots and Systems '. (IROS '89) 'The Autonomous Mobile Robots and Its Applications*, 398–405. IEEE.

Kong, A., Liu, J. S., and Wong, W. H. (1994). Sequential imputations and Bayesian missing data problems. *Journal of the American Statistical Association*, *89*(425), 278–288.

Kontoghiorghes, E. J. (2005). *Handbook of parallel computing and statistics.* CRC Press.

Krivobokova, T., Crainiceanu, C. M., and Kauermann, G. (2008). Fast adaptive penalized splines. *Journal of Computational and Graphical Statistics*, *17*(1), 1–20.

Larson, S. C. (1931). The shrinkage of the coefficient of multiple correlation. *Journal of Educational Psychology*, *22*(1), 45.

Laskey, K. B. and Myers, J. W. (2003). Population Markov chain Monte Carlo. *Machine Learning*, *50*(1-2), 175–196.

LaViola, J. J. (2003). A comparison of unscented and extended Kalman filtering for estimating quaternion motion. In *American Control Conference, 2003. Proceedings of the 2003*, Volume 3, 2435–2440. IEEE.

Lawson, C. T., Ravi, S. S., and Hwang, J.-H. (2011). Compression and mining of GPS trace data: new techniques and applications. Technical report, Technical Report. Region II University Transportation Research Center.

Lindley, D. V. and Smith, A. F. M. (1972). Bayes estimates for the linear model. *Journal of the Royal Statistical Society. Series B (Methodological)*, *34*, 1–41.

Liu, J. and West, M. (2001). Combined parameter and state estimation in simulation-based filtering. In *Sequential Monte Carlo methods in practice*, 197–223. Springer.

Liu, J. S. (2008). *Monte Carlo strategies in scientific computing*. Springer Science & Business Media.

Liu, J. S., Liang, F., and Wong, W. H. (2000). The multiple-try method and local optimization in Metropolis sampling. *Journal of the American Statistical Association*, *95*(449), 121–134.

Liu, Y., Suo, J., Karimi, H. R., and Liu, X. (2014). A filtering algorithm for maneuvering target tracking based on smoothing spline fitting. In *Abstract and Applied Analysis*, Volume 2014. Hindawi Publishing Corporation.

Liu, Z. and Guo, W. (2010). Data driven adaptive spline smoothing. *Statistica Sinica*, *20*, 1143–1163.

Lopes, H. F. and Tsay, R. S. (2011). Particle filters and Bayesian inference in financial econometrics. *Journal of Forecasting*, *30*(1), 168–209.

Magid, E., Keren, D., Rivlin, E., and Yavneh, I. (2006). Spline-based robot navigation. In *2006 IEEE/RSJ International Conference on Intelligent Robots and Systems*, 2296–2301. IEEE.

Mahendran, N., Wang, Z., Hamze, F., and De Freitas, N. (2012). Adaptive MCMC with Bayesian optimization. In *Artificial Intelligence and Statistics*, 751–760.

Martino, L. and Míguez, J. (2010). Generalized rejection sampling schemes and applications in signal processing. *Signal Processing*, *90*(11), 2981–2995.

Mathew, B., Bauer, A. M., Koistinen, P., Reetz, T. C., Léon, J., and Sillanpää, M. J. (2012). Bayesian adaptive Markov chain Monte Carlo estimation of genetic parameters. *Heredity*, *109*(4), 235.

McDonald, M. (2006). *Intelligent transport systems in Europe: opportunities for future research*. World Scientific.

Medova, E. (2008). *Bayesian analysis and Markov chain Monte Carlo simulation*. Wiley Online Library.

Meratnia, N. and Rolf, A. (2004). Spatiotemporal compression techniques for moving point objects. In *Advances in Database Technology-EDBT 2004*, 765–782. Springer.

Metropolis, N., Rosenbluth, A. W., Rosenbluth, M. N., Teller, A. H., and Teller, E. (1953). Equation of state calculations by fast computing machines. *The Journal of Chemical Physics*, *21*(6), 1087–1092.

Mitchell, H. L. and Houtekamer, P. L. (2000). An adaptive ensemble Kalman filter. *Monthly Weather Review*, *128*(2), 416–433.

Müller, P. (1991). *A generic approach to posterior integration and Gibbs sampling*. Purdue University, Department of Statistics.

Nason, G. (2010). *Wavelet methods in statistics with R*. Springer Science & Business Media.

Neal, R. M. (2011). MCMC using Hamiltonian dynamics. *Handbook of Markov chain Monte Carlo*, *2*(11), 113–162.

Nelder, J. A. and Mead, R. (1965). A simplex method for function minimization. *The Computer Journal*, *7*(4), 308–313.

Opsomer, J., Wang, Y., and Yang, Y. (2001). Nonparametric regression with correlated errors. *Statistical Science*, *16*, 134–153.

Oussalah, M. and De Schutter, J. (2001). Adaptive Kalman filter for noise identification. In *Proceedings of the International Seminar on Modal Analysis*, Volume 3, 1225–1232. KU Leuven; 1998.

Pang, S. K., Li, J., and Godsill, S. J. (2008). Models and algorithms for detection and tracking of coordinated groups. In *Aerospace Conference, 2008 IEEE*, 1–17. IEEE.

Payne, R. D. and Mallick, B. K. (2018). Two-stage Metropolis-Hastings for tall data. *Journal of Classification*, *35*(1), 29–51.

Petris, G., Petrone, S., and Campagnoli, P. (2009). *Dynamic linear models with R*. Springer.

Pham, H. D., Drieberg, M., and Nguyen, C. C. (2013). Development of vehicle tracking system using GPS and GSM modem. In *2013 IEEE Conference on Open Systems (ICOS)*, 89–94. IEEE.

Pitt, M. K. and Shephard, N. (1999). Filtering via simulation: auxiliary particle filters. *Journal of the American Statistical Association*, *94*(446), 590–599.

Polson, N. G., Stroud, J. R., and Müller, P. (2008). Practical filtering with sequential parameter learning. *Journal of the Royal Statistical Society: Series B (Statistical Methodology)*, *70*(2), 413–428.

Poyiadjis, G., Doucet, A., and Singh, S. S. (2005). Maximum likelihood parameter estimation in general state-space models using particle methods. In *Proc of the American Stat. Assoc*. Citeseer.

Quiroz, M., Tran, M.-N., Villani, M., and Kohn, R. (2018). Speeding up MCMC by delayed acceptance and data subsampling. *Journal of Computational and Graphical Statistics*, *27*(1), 12–22.

Ran, C. and Deng, Z. (2010). Self-tuning weighted measurement fusion Kalman filter and its convergence. *Journal of Control Theory and Applications*, *8*(4), 435–440.

Rasmussen, C. E. and Williams, C. K. I. (2006). *Gaussian processes for machine learning*, Volume 1. MIT press Cambridge.

Rhodes, I. (1971). A tutorial introduction to estimation and filtering. *IEEE Transactions on Automatic Control*, *16*(6), 688–706.

Ristic, B., Arulampalam, S., and Gordon, N. (2004). Beyond the Kalman filter. *IEEE Aerospace and Electronic Systems Magazine*, *19*(7), 37–38.

Robert, C. P. (2004). *Monte Carlo methods*. Wiley Online Library.

Roberts, G. O. and Rosenthal, J. S. (2001). Optimal scaling for various Metropolis-Hastings algorithms. *Statistical Science*, *16*(4), 351–367.

Roberts, G. O. and Rosenthal, J. S. (2009). Examples of adaptive MCMC. *Journal of Computational and Graphical Statistics*, *18*(2), 349–367.

Rubin, D. B. (2004). *Multiple imputation for nonresponse in surveys*, Volume 81. John Wiley & Sons.

Ruppert, D., Wand, M. P., and Carroll, R. J. (2003). *Semiparametric regression*. 12. Cambridge university press.

Särkkä, S. (2013). *Bayesian filtering and smoothing*, Volume 3. Cambridge University Press.

Schöbel, R. and Zhu, J. (1999). Stochastic volatility with an Ornstein-Uhlenbeck process: an extension. *Review of Finance*, *3*(1), 23–46.

Schoenberg, I. J. (1964). Spline functions and the problem of graduation. *Proceedings of the National Academy of Sciences*, *52*(4), 947–950.

Schwarz, K.-P. (2012). *Geodesy beyond 2000: the challenges of the first decade, IAG general assembly Birmingham, July 19–30, 1999*, Volume 121. Springer Science & Business Media.

Sealfon, C., Verde, L., and Jimenez, R. (2005). Smoothing spline primordial power spectrum reconstruction. *Physical Review D*, *72*(10), 103520.

Septier, F., Carmi, A., Pang, S. K., and Godsill, S. J. (2009). Multiple object tracking using evolutionary and hybrid MCMC-based particle algorithms. In *15th IFAC Symposium on System Identification, 2009*, Volume 15. IFAC.

Septier, F., Pang, S. K., Carmi, A., and Godsill, S. (2009). On MCMC-based particle methods for Bayesian filtering: application to multitarget tracking. In *2009 3rd IEEE International Workshop on Computational Advances in Multi-Sensor Adaptive Processing (CAMSAP)*, 360–363. IEEE.

Sherlock, C. (2013). Optimal scaling of the random walk Metropolis: general criteria for the 0.234 acceptance rule. *Journal of Applied Probability*, *50*(1), 1–15.

Sherlock, C., Fearnhead, P., and Roberts, G. O. (2010). The random walk Metropolis: linking theory and practice through a case study. *Statistical Science*, *25*, 172–190.

Sherlock, C., Golightly, A., and Henderson, D. A. (2017). Adaptive, delayed-acceptance MCMC for targets with expensive likelihoods. *Journal of Computational and Graphical Statistics*, *26*(2), 434–444.

Sherlock, C. and Roberts, G. (2009). Optimal scaling of the random walk Metropolis on elliptically symmetric unimodal targets. *Bernoulli*, *15*(3), 774–798.

Sherlock, C., Thiery, A., and Golightly, A. (2015). Efficiency of delayed-acceptance random walk Metropolis algorithms. *arXiv preprint*, *arXiv:1506.08155*.

Sherman, J. and Morrison, W. J. (1950). Adjustment of an inverse matrix corresponding to a change in one element of a given matrix. *The Annals of Mathematical Statistics*, *21*(1), 124–127.

Silverman, B. W. (1985). Some aspects of the spline smoothing approach to non-parametric regression curve fitting. *Journal of the Royal Statistical Society. Series B (Methodological)*, *47*, 1–52.

Smith, A. F. M. (1973). A general Bayesian linear model. *Journal of the Royal Statistical Society. Series B (Methodological)*, *35*, 67–75.

Smith, A. F. M. and Roberts, G. O. (1993). Bayesian computation via the Gibbs sampler and related Markov chain Monte Carlo methods. *Journal of the Royal Statistical Society. Series B (Methodological)*, *55*, 3–23.

Sokal, A. (1997). Monte Carlo methods in statistical mechanics: foundations and new algorithms. In *Functional integration*, 131–192. Springer.

Sorenson, H. W. (1985). *Kalman filtering: theory and application* (First ed.). IEEE Press.

Speckman, P. L. and Sun, D. (2003). Fully Bayesian spline smoothing and intrinsic autoregressive priors. *Biometrika*, *90*(2), 289–302.

St-Pierre, M. and Gingras, D. (2004). Comparison between the unscented Kalman filter and the extended Kalman filter for the position estimation module of an integrated navigation information system. In *Intelligent Vehicles Symposium, 2004 IEEE*, 831–835. IEEE.

Stavropoulos, P. and Titterington, D. M. (2001). Improved particle filters and smoothing. In *Sequential Monte Carlo Methods in Practice*, 295–317. Springer.

Storvik, G. (2002). Particle filters for state-space models with the presence of unknown static parameters. *IEEE Transactions on Signal Processing*, *50*(2), 281–289.

Stroud, J. R. and Bengtsson, T. (2007). Sequential state and variance estimation within the ensemble Kalman filter. *Monthly Weather Review*, *135*(9), 3194–3208.

Stroud, J. R., Katzfuss, M., and Wikle, C. K. (2018). A Bayesian adaptive ensemble Kalman filter for sequential state and parameter estimation. *Monthly Weather Review*, *146*(1), 373–386.

Syed, A. R. (2011). A review of cross validation and adaptive model selection. Master's thesis, Georgia State University, Arlanta, GA.

Tandeo, P., Ailliot, P., and Autret, E. (2011). Linear Gaussian state-space model with irregular sampling: application to sea surface temperature. *Stochastic Environmental Research and Risk Assessment*, *25*(6), 793–804.

Tanner, M. A. and Wong, W. H. (1987). The calculation of posterior distributions by data augmentation. *Journal of the American statistical Association*, *82*(398), 528–540.

Tierney, L. (1994). Markov chains for exploring posterior distributions. *the Annals of Statistics*, *22*, 1701–1728.

Tierney, L. and Mira, A. (1999). Some adaptive Monte Carlo methods for Bayesian inference. *Statistics in Medicine*, *18*(1718), 2507–2515.

Toloei, A. and Niazi, S. (2014). State estimation for target tracking problems with nonlinear Kalman filter algorithms. *International Journal of Computer Applications*, *98*(17), 30–36. Full text available.

Turitsyn, K. S., Chertkov, M., and Vucelja, M. (2011). Irreversible Monte Carlo algorithms for efficient sampling. *Physica D: Nonlinear Phenomena*, *240*(4), 410–414.

Tusell, F. (2011). Kalman filtering in R. *Journal of Statistical Software*, *39*(2), 1–27.

VanDerwerken, D. N. and Schmidler, S. C. (2013). Parallel Markov chain Monte Carlo. *arXiv preprint*, *arXiv:1312.7479*.

Vieira, R. and Wilkinson, D. J. (2016). Online state and parameter estimation in dynamic generalised linear models. *arXiv preprint*, *arXiv:1608.08666*.

Wahba, G. (1978). Improper priors, spline smoothing and the problem of guarding against model errors in regression. *Journal of the Royal Statistical Society. Series B (Methodological)*, *40*, 364–372.

Wahba, G. (1985). A comparison of GCV and GML for choosing the smoothing parameter in the generalized spline smoothing problem. *The Annals of Statistics*, *13*, 1378–1402.

Wahba, G. (1990). *Spline models for observational data*, Volume 59. Siam.

Wahba, G. and Wang, Y. (1990). When is the optimal regularization parameter insensitive to the choice of the loss function? *Communications in Statistics-Theory and Methods*, *19*(5), 1685–1700.

Wahba, G. and Wold, S. (1975). A completely automatic french curve: fitting spline functions by cross validation. *Communications in Statistics-Theory and Methods*, *4*(1), 1–17.

Wakefield, J. (2013). *Bayesian and frequentist regression methods*. Springer Science & Business Media.

Wan, E. A. and Van Der Merwe, R. (2000). The unscented Kalman filter for nonlinear estimation. In *Adaptive Systems for Signal Processing, Communications, and Control Symposium 2000. AS-SPCC. The IEEE 2000*, 153–158. Ieee.

Wand, M. P. and Gutierrez, R. G. (1997). Exact risk approaches to smoothing parameter selection. *Journal of Nonparametric Statistics*, *8*(4), 337–354.

Wang, X., Jiang, P., Li, D., and Sun, T. (2017). Curvature continuous and bounded path planning for fixed-wing UAVs. *Sensors*, *17*(9), 2155.

Wang, Y. (1998). Smoothing spline models with correlated random errors. *Journal of the American Statistical Association*, *93*(441), 341–348.

Wecker, W. E. and Ansley, C. F. (1983). The signal extraction approach to nonlinear regression and spline smoothing. *Journal of the American Statistical Association*, *78*(381), 81–89.

West, M. (1993). Mixture models, Monte Carlo, Bayesian updating, and dynamic models. *Computing Science and Statistics*, *25*, 325.

Whittaker, E. T. (1922). On a new method of graduation. *Proceedings of the Edinburgh Mathematical Society*, *41*, 63–75.

Wolberg, G. (1988). Cubic spline interpolation: a review. Technical report, Department of Computer Science, Columbia University.

Woodbury, M. A. (1950). Inverting modified matrices. *Memorandum Report*, *42*(106), 336.

Wu, X.-L., Sun, C., Beissinger, T. M., Rosa, G. J. M., Weigel, K. A., de Leon Gatti, N., and Gianola, D. (2012). Parallel Markov chain Monte Carlo-bridging the gap to high-performance Bayesian computation in animal breeding and genetics. *Genetics Selection Evolution*, *44*(1), 29.

Yang, K. and Sukkarieh, S. (2010). An analytical continuous-curvature path-smoothing algorithm. *Robotics, IEEE Transactions on*, *26*(3), 561–568.

Yao, F., Müller, H.-G., and Wang, J.-L. (2005). Functional linear regression analysis for longitudinal data. *The Annals of Statistics*, *33*(6), 2873–2903.

Ying, J. J.-C., Lee, W.-C., Weng, T.-C., and Tseng, V. S. (2011). Semantic trajectory mining for location prediction. In *Proceedings of the 19th ACM SIGSPATIAL International Conference on Advances in Geographic Information Systems*, 34–43. ACM.

Yu, B., Kim, S. H., Bailey, T., and Gamboa, R. (2004). Curve-based representation of moving object trajectories. In *Database Engineering and Applications Symposium, 2004. IDEAS'04. Proceedings. International*, 419–425. IEEE.

Zhang, K., Guo, J.-X., and Gao, X.-S. (2013). Cubic spline trajectory generation with axis jerk and tracking error constraints. *International Journal of Precision Engineering and Manufacturing*, *14*(7), 1141–1146.